Book B:

*Title:*Phases I and III Data Review report
Vol. I • Data Report
ISBN 0-921095-46-5
Spine width: 3/8" (0.375")
Front Matter: 18 pages
Numbered pages: pp1-168
Add 2 blank pages at end of book: (pp 169,170)
Total Pages: 188
Insert 3 blank pages: ppB-4; B-169; B-170
Pages on disk: pp. B-5 to B-8

CANLEX

THE CANADIAN LIQUEFACTION EXPERIMENT

PHASES I and III DATA REVIEW REPORT

Volume I • Data Report

C.E.WRIDE

P.K.ROBERTSON

The CANadian
CANLEX
Liquefaction EXperiment

All rights reserved.

Information contained in this work has been obtained by BiTech Publishers Ltd. from sources believed to be reliable. However, neither BiTech Publishers nor its authors guarantees the accuracy or completeness of any information published herein, and neither BiTech Publishers nor its authors shall be responsible for any errors, omissions, or damages arising out of use of this information. This work is published with the understanding that BiTech Publishers and its authors are supplying information but are not attempting to render engineering or other professional services. If such services are requires, the assistance of an appropriate professional shall be sought.

No part of this book may be reproduced, stored in a retrieval system or transmitted in any form whatsoever or by any means without written permission from the publisher. Requests for permission should be addressed to BiTech Publishers Ltd., 173-11860 Hammersmith Way, Richmond, B.C. Canada V7A 5G1

Published by:
BiTech Publishers Ltd.
173-11860 Hammersmith Way
Richmond, B.C. Canada V7A 5G1

Printed in Canada, 1999

ISBN for complete set of 5 volumes: 0-921095-45-7

ISBN for this volume 0-921095-47-3

CANLEX

The CANADIAN LIQUEFACTION EXPERIMENT

1993-1997

B-4 - Blank

Canadian Liquefaction Experiment
CANLEX

1993-1997

Characterization of Sand for Dynamic and Static Liquefaction

"The CANLEX Project was awarded the Association of Professional Engineers, Geologists and Geophysicists of Alberta (APEGGA) Project Achievement Award in 1998. This award recognizes a project which demonstrates engineering, geological or geophysical skills and represents a substantial contribution to a technical progress and the betterment of society".

Introduction

The Canadian geotechnical engineering community has completed a major collaborative research project entitled the Canadian Liquefaction Experiment (CANLEX). The phenomenon of soil liquefaction can occur in saturated sandy soils and is characterized by a large loss of strength or stiffness resulting in substantial deformation. In many areas of Canada, large structures are constructed on or comprised of sandy soils. Examples of such structures are tailings impoundments developed by the mining industry and some major earth dams used for hydro-electricity.

The behaviour of loose sandy soils can be difficult to predict, but can have a significant financial impact on these types of engineering structures. The characterization of loose sandy soils is an area of uncertainty in geotechnical engineering. Unlike clay soils, it is almost impossible to obtain undisturbed samples of loose sandy soils, especially at depth, using conventional methods. Hence, in-situ testing techniques have become standard practice for sand characterization and the evaluation of liquefaction potential.

The objectives of the CANLEX Project were:

- develop test sites to study sand characterization
- develop and evaluate undisturbed sampling techniques
- calibrate and evaluate in-situ testing techniques
- obtain an improved understanding of the phenomenon of soil liquefaction

CANLEX participants at test site in Syncrude Canada, Alberta

Project Participants

CANLEX was a collaborative project with participation from industry, engineering consultants and universities. The participants were, as follows:

Industry:

Syncrude Canada Ltd.
Suncor Inc.
Hydro Quebec
Kennecott Corporation, USA
Highland Valley Copper

Engineering Consultants:

AGRA Earth and Environmental Ltd.
ERA Consultants Ltd.
Golder Associated Ltd.
Klohn-Crippen Consultants Ltd.
Thurber Engineering Ltd.

Universities

University of Alberta
University of Briti~h Columbia
Université de Laval
Carleton University

Others

Canadian Geological Survey (CGS)
B.C. Min. of Highways (BC MOTH)
ConeTec Investigations Ltd.
Hughes In-situ Engineering Inc.

Summary of Progress

The CANLEX Project was carried out from February, 1993 to December, 1997. The Project was divided into Phases with each Phase representing essentially a new site and/or research objective. A total of five (5) project Phases were carried out over the approximately 5 year period. Each project Phase was subdivided into a series of activities, with each activity assigned an activity leader and group of participants.

Three main soil types were tested, each located in different regions. Phases I and III were carried out at the Syncrude Canada Ltd. site located north of Fort McMurray in Alberta. The Syncrude soil was a tailings sand resulting from oil extraction from the oil sand deposits. This was a natural sand which had been processed to remove the oil and then hydraulically placed in impoundments.

Phase I was located in the existing Mildred Lake Settling Basin, whereas Phase III was located in freshly deposited tailings placed in an old overburden pit, referred to as J-Pit. Phase II was carried out in the Fraser River delta region near Vancouver, B.C. Two sites were selected for Phase II and consisted of natural deposits of Fraser River sand. Phase IV was carried out at the Highland Valley Copper Mine in central British Columbia, south of Kamloops, B.C. Two sites were selected for Phase IV and consisted of tail-

Laboratory Testing

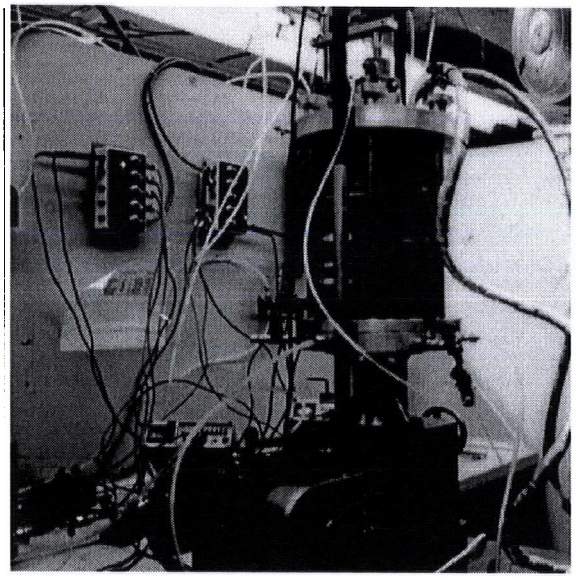

Monotonic Triaxial Testing

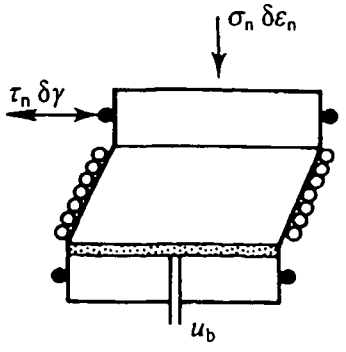

Cyclic Simple Shear Testing

ings sand from the hard rock mining operations of Highland Valley Copper. One site was located in an older tailings storage facility referred to as Highmont Dam. The other site was located in a currently used tailings storage facility referred to as LL Dam.

Phase III included the construction of a full scale embankment in an effort to simulate a flow liquefaction slide. Phase V was located at the site of the Phase III embankment at the Syncrude site in J-Pit and included several controlled blasting experiments in an effort to simulate earthquake loading within the loose saturated tailings sand deposit.

Each Phase (except Phase V) involved the following basic activities:

- site selection to determine the preferred site location.
- site characterization to perform drilling and in-situ testing, which included standard penetration testing (SPT), cone penetration testing (CPT), seismic CPT, self-boring pressuremeter testing (SBPMT) and geophysical logging.
- sampling, which included ground freezing to obtain undisturbed samples, large diameter piston sampling and conventional sampling using a fixed piston thin walled sampler.
- laboratory testing, which included testing on reconstituted samples as well as undisturbed samples. Laboratory testing was carried out to evaluate the response of the soil to both monotonic and cyclic loading.

Undisturbed sampling using large diameter (200mm)CRREI, sampler in sand frozen using liquid nitrogen.

Summary of Results

In general, all of the major objectives of the project have been achieved. The following is a summary of the major achievements:

- a consistent set of definitions for liquefaction phenomena was developed and accepted by the participants.
- six (6) test sites were located and fully characterized; each site has unique features related to grain characteristics, mineralogy, age, depth, density and variability.
- a new technique was developed and evaluated to obtain high quality undisturbed samples using ground freezing techniques.
- the application of the Laval large diameter piston sampler was evaluated.
- the application of high quality conventional fixed piston sampling was evaluated.
- improvements were made to undisturbed sample handling procedures.
- in-situ testing techniques were evaluated and calibrated against response from undisturbed samples.
- a thaw consolidation procedure was developed and evaluated for frozen samples.

- geophysical logging methods were evaluated, including a new radio-isotope CPT.
- the importance of consolidating samples in the laboratory under in-situ stresses (i.e. Ko consolidation) was identified and evaluated.
- the importance of direction of loading on the response of sand was identified and quantified.
- the importance of strain compatible analyses to evaluate ground deformations was identified.
- improvements were made in the understanding of the response of sand to different types of loading.
- improvements were made in the understanding of the density and variability of sand deposits.

The following are the non technical achievements:

- Improved understanding of the safety of structures involving sand deposits.
- Enhanced communication between industrial partners.
- Enhanced knowledge and reputation of consultants.
- Immediate technology transfer.
- Optimization of national geotechnical resources.

Collaboration

The CANLEX Project has been the largest collaborative research project within the Canadian geotechnical community. In general, the collaboration has been excellent. Expertise exists in all segments of the project (i.e. industry, consultants and universities) and participants have shared ideas and comments freely and openly.

Summary

The Canadian geotechnical engineering community has completed a major collaborative research project entitled the Canadian Liquefaction Experiment (CANLEX) with participation from industry, engineering consultants and universities. The project involved a total expenditure of $1,690,000 with approximately $2,246,000 of additional in-kind contributions. The CANLEX project has achieved all of its major objectives.

The results of the CANLEX Project have been published in a series of 70 internal reports, 5 newsletters, 31 conference papers, 5 news articles, 10 journal publications and 13 graduate students theses. Further journal and conference papers are planned as well as some remaining graduate student theses. Further research work has been identified and a future workshop as well as a possible international conference are planned.

CANLEX

THE CANADIAN LIQUEFACTION EXPERIMENT

PHASES I and III
DATA REVIEW REPORT

Mildred Lake and J-Pit Sites

Volume I • Data Report

October • 1997

CANLEX

Phases I and III Data Review Report (Mildred Lake and J-pit Sites, Syncrude Canada Ltd.)

Volume I – Data Report

Prepared by:

C.E. (Fear) Wride and P.K. Robertson
Dept. of Civil & Environmental Engineering
University of Alberta
Edmonton, Alberta
T6G 2G7

Telephone: (403) 492-2176
Fax: (403) 492-8198

OCTOBER 15, 1997

TABLE OF CONTENTS

Page

List of Tables

Page

List of Figures

Page

List of Appendices (contained in Volume II of this report)

Phase I (Mildred Lake Site)

Appendix A	SPT Results (Campanella, 1994)
Appendix B	CPT Results (Campanella, 1994)
Appendix C	Shear Wave Velocity Results (Campanella, 1994)
Appendix D	Geophysical Results (Küpper, 1994)
Appendix E	Pressuremeter Results (Hughes, 1994)
Appendix F	UBC Laboratory Testing Results (Vaid et al., 1996)
Appendix G	Laval Laboratory Testing Results (Konrad and Saint-Laurent, 1995)
Appendix H	U. of A. Laboratory Testing Results (Cunning, 1994; Ayoubian, 1996; Hofmann, 1997; and cyclic triaxial tests)
Appendix I	Industry Laboratory Testing Results: Klohn-Crippen and C-CORE

Phase III (J-pit Site)

Appendix J	SPT Results (Iravani et al., 1995)
Appendix K	CPT Results (Iravani et al., 1995; after ConeTec, 1995)
Appendix L	Shear Wave Velocity Results (Iravani et al., 1995; after ConeTec, 1995)
Appendix M	Geophysical Results (Iravani et al., 1995; after Skirrow, 1995)
Appendix N	Pressuremeter Results (Hughes, 1996)
Appendix O	UBC Laboratory Testing Results (Vaid et al., 1996)

Computer Aided Modelling (CAM)

Appendix P
a) A copy of a paper entitled "Strain Level and Uncertainty of Liquefaction Related Index Tests" (Roy et al., 1996)
b) A copy of a paper entitled "A simple understanding of the liquefaction potential of sands from self-boring pressuremeter tests" (Hughes et al., 1997)

Phase III Full Scale Liquefaction Field Test

Appendix Q
a) A copy of a paper entitled "CANLEX Phase III full scale flow liquefaction test: planning, objectives and conclusions" (Robertson et al., 1996)
b) A copy of a paper entitled "CANLEX Phase III full scale flow liquefaction test: site characterization" (Hofmann et al., 1996a)
c) A copy of a paper entitled "CANLEX Phase III full scale flow liquefaction test: instrumentation and construction" (Hofmann et al., 1996b)
d) A copy of a paper entitled "Analysis of CANLEX liquefaction embankments: prototype and centrifuge models" (Puebla et al., 1996)
e) A copy of a paper entitled "Numerical analysis of the CANLEX Phase III field event" (Soroush et al., 1996)

EXECUTIVE SUMMARY

This report is the third in a series of technical reports arising from the CANLEX Project data review activity. The intent of the report is to synthesize and analyze the large amounts of field and laboratory data obtained from two sites (the Mildred Lake and J-pit sites) at Syncrude Canada Ltd. during Phases I and III of the CANLEX Project. The data are evaluated based on both flow liquefaction and cyclic softening considerations. The terminology and methods used to evaluate and compare the field and laboratory data from the two sites are described in detail in the first report in this series, entitled the Introductory Data Review Report. The interpretation of the Phase I and III data, as presented here, will be compared with the results from the other phases of the CANLEX Project in the final report of this series, in the form of a summary data review report.

1. OBJECTIVES

The primary objectives of this report are to synthesize and analyze the large amounts of field and laboratory data that were produced during Phases I and III of the CANLEX Project, which consisted of two sites (Mildred Lake and J-pit, respectively) at Syncrude Canada Ltd. Various methods of evaluating the potential for both flow liquefaction and cyclic softening (liquefaction) and estimating the associated undrained response are applied to the Phase I and III data. These methods are described in detail in the CANLEX Introductory Data Review Report (Wride and Robertson, 1997).

Frozen samples of Syncrude sand were obtained from a 10 m thick target zone at the Phase I site (Hofmann and Sego, 1994) and a 4 m thick target zone at the Phase III site (Hofmann and Sego, 1995). The target zones were located from approximately 27 to 37 m at Phase I and from 3 to 7 m at Phase III. Cone penetration tests (CPT), standard penetration tests (SPT), shear wave velocity (V_S) measurements, geophysical logging, and pressuremeter testing were conducted in the target zone at each site. Details of SPT, CPT and V_s investigations at the Phase I site are contained in a report by Campanella (1994). Details of geophysical logging and pressuremeter investigations at the Phase I site are contained in reports by Küpper (1994) and Hughes (1994), respectively. Details of SPT, CPT, V_s and geophysical logging investigations at the Phase III site are contained in an in-situ testing summary report by Iravani et al. (1995). The report by Iravani et al. (1995) includes copies of reports submitted to the CANLEX Project by ConeTec (1995) and Skirrow (1995). Details of the pressuremeter investigation at the Phase III site are contained in a report by Hughes (1996). This data review report strives to compare the results of in-situ testing in the target zone with the frozen ("undisturbed") samples in terms of soil state, response to undrained monotonic loading and response to undrained cyclic loading. The results of testing some reconstituted samples are also examined.

2. SOIL PARAMETERS

2.1 Soil Behaviour Type

Figure 1(a) presents the Phase I site CPT data in the target zone (27 to 37 m) on a soil classification chart using the method by Robertson (1990), as outlined in the Introductory Data Review Report; further details regarding the CPT results at the Phase I site are given later in this report. The data have an average Q of 32.0 (SD=7.8) and an average F of 0.727 (SD=0.150). The majority of the data falls into Zone 5 (having an average soil behaviour type index, I_c, of 2.254; SD=0.112) and would be classified as a sand mixture, ranging from a silty sand to a sandy silt, (see the Introductory Data Review Report[1]).

However, since the Phase I target zone is located from 27 m to 37 m and the groundwater table is located, on average, at a depth of 21 m, the in-situ effective stresses in the Phase I target zone are significantly higher than 100 kPa. As a result, the normalization used to calculate the normalized cone tip resistance becomes very important. Olsen and Malone (1988) correctly proposed that the exponent used to normalize cone tip resistance should be a function of the soil behaviour type; however, this method requires an iterative approach to plotting CPT data on a soil classification chart. As a simplified approach, this report suggests that if CPT data fall in zones 2, 3 or 4 (i.e. $I_c > 2.6$, clayey soils) when plotted in terms of Q and F, the linear normalization of cone tip resistance (Q) should continue to be used. However, if CPT data fall in zones 5, 6 or 7 (i.e. $I_c < 2.6$, sandy soils) when plotted in terms of Q and F, the normalization using an exponent of 0.5 (i.e. q_{c1N}) should be used to re-plot the data on the soil classification chart. If, when replotted, any of these data then plot with $I_c > 2.6$, a normalization similar to the definition of q_{c1N}, but using an exponent of 0.75 should be used to re-plot such data on the soil classification chart.

[1] I_c <1.31: gravelly sand; 1.31< I_c <2.05: sands – clean sand to silty sand; 2.05< I_c <2.60: sand mixtures – silty sand to sandy silt; 2.60< I_c <2.95: silt mixtures – clayey silt to silty clay; 2.95< I_c <3.60: clays; I_c >3.6: organic soils – peat.

Figure 1(b) re-plots the Phase I target zone CPT data on the soil classification chart following the method described above. The modified data have an average normalized cone tip resistance of 73.8 (SD=16.7) and an average F of 0.727 (SD=0.150). The majority of the data falls into Zone 6 (having an average soil behaviour type index, I_c, of 1.942; SD=0.105) and would be classified as a sand, ranging from a clean sand to a silty sand. Some data fall into Zone 5 and would be classified as a sand mixture, ranging from a silty sand to a sandy silt. The data fall in the region considered to correspond to normally consolidated soils. Based on where the data plot on the soil classification chart in Figure 1(b) (i.e. F > 0.5 % for most of the data), it would be expected that the soil contains a certain amount of fines. This will be expanded upon in a later section of this report. Note that the data fall within a fairly small range of normalized friction ratio (F).

Figure 2(a) presents the CPT data from the target zone (3 to 7 m) at the Phase III Site on the Robertson (1990) soil classification chart; further details regarding the CPT results at the Phase III site are given later in this report. The data have an average Q of 31.0 (SD=23.9) and an average F of 0.872 (SD=0.331). The majority of the data falls into Zone 5 (having an average I_c of 2.34; SD=0.26) and would be classified as a sand mixture, ranging from a silty sand to a sandy silt (see the Introductory Data Review Report). Some of the data fall into Zones 6, 4 and 3 and would be classified as a sand (ranging from a clean sand to a silty sand), a silt mixture (ranging from a clayey silt to a silty clay), and a clay, respectively. The data fall along, but slightly to the left of the region considered to correspond to normally consolidated soils. Based on where the data plot on the soil classification chart in Figure 2(a) (i.e. F > 0.5 % for most of the data), it would be expected that the soil contains a certain amount of fines. This will be expanded upon in a later section of this report. Note that the data fall within a fairly large range of normalized friction ratio (F).

Since the Phase III target zone is located from 3 m to 7 m and the groundwater table is located, on average, at a depth of 0.5 m, the in-situ effective stresses in the Phase III

target zone are lower than 100 kPa. As a result, the normalization used to calculate the normalized cone tip resistance can become important. To investigate the effect of the choice of normalization, Figure 2(b) re-plots the Phase III target zone CPT data on the soil classification chart following the method described above. The data have an average normalized cone tip resistance of 25.5 (SD=16.5) and an average F of 0.872 (SD=0.331). The majority of the data falls into Zone 5 (having an average soil behaviour type index, I_c, of 2.431; SD=0.369) and would be classified as a sand mixture, ranging from a silty sand to a sandy silt. Some of the data fall into Zones 6, 4 and 3 and would be classified as a sand (ranging from a clean sand to a silty sand), a silt mixture (ranging from a clayey silt to a silty clay), and a clay, respectively. Comparing Figure 2(a) and Figure 2(b), it can be seen that in the target zone at the Phase III site, the choice of normalization does not have a large effect. There are certainly some differences between the two plots, but they are not as significant as the differences between the two plots for the Phase I site.

At first, when comparing Figure 1(a) with either Figure 2(a) or Figure 2(b), it seems that the majority of the soil at each of the Phase I and Phase III sites is similar in nature, in terms of soil behaviour type (a sand mixture (Zone 5), with similar average values of Q and F). However, when Figure 1(b) is compared with either Figure 2(a) or Figure 2(b), it appears that the two soils are actually somewhat different, with the Phase III soil (mostly Zone 5) being siltier than the Phase I soil (mostly Zone 6). Figure 3(a) and Figure 3(b) present copies of scanning electron microscope photographs of in-situ frozen soil samples from the Phase I and Phase III site target zones, respectively. Note that, at each site, the sand particles appear to be somewhat subrounded to subangular and that there appear to be aligned clay mineral platelets present in the soil matrix.

2.2 Index Parameters

Index parameters for the Phase I and Phase III sites are given in Table 1 and can be compared with those for Ticino sand, which are also given in Table 1. The Phase I and Phase III sites, which consist of artificially placed sand deposits as a result of the oilsand industry, are significantly younger than the deposits at the Phase II sites (natural sand

deposits in the Fraser River Delta of B.C.), but are similar in age to the deposits at the Phase IV sites (artificially placed sand deposits as a result of the hardrock mining industry). The Phase III deposit was less than a month old at the time of the site investigation, while the Phase I deposit was approximately 30 years old. The Phase I and Phase III index parameters will be compared with those for the other CANLEX sites in subsequent data review reports.

2.3 Choice of Reference Ultimate State Line (USL)

Prior to testing undisturbed samples from the Phase I and Phase III sites, Cunning (1994) conducted monotonic triaxial compression tests on isotropically consolidated samples of reconstituted (moist tamped) Syncrude sand. The sand was obtained as a bulk sample from the beach surface of the Phase I site. The index parameters for this sand (D_{50}=0.17 mm, average FC=12.4%, G_s=2.62, e_{max}=1.04 and e_{min}=0.61) are similar to those for the Phase I site target zone. Drained and undrained tests were performed. By plotting the end-of-test points from all of the tests on an e-p' plot, the Phase I reference USL was estimated, as shown in Figure 4(a). The USL was found to be bi-linear in nature, with a break at approximately p'=373 kPa and associated values of Γ and λ_{ln}, as given in Table 2. This is consistent with non-linear USLs reported in the literature for other sands, as summarized by Sasitharan et al. (1994), as shown in Figure 4(b).

Figure 5(a) presents all of the results of testing reconstituted, isotropically consolidated samples of Phase I sand, in terms of the end-of-test state of each sample on an e-p' plot. These data are based on results from U.B.C. (Vaid et al., 1996), Laval (Konrad and St. Laurent , 1995), U. of A. (Cunning, 1994) and C-CORE. Complete stress-strain curves for the various laboratory tests are presented in Appendices F to I. The laboratory testing results are discussed in greater detail later in this report. Superimposed on Figure 5(a) is the selected Phase I reference USL which agrees fairly well with the test results from U. of A. and U.B.C., but not as well with the results from Laval and C-CORE.

Figure 5(b) presents the results of testing anisotropically consolidated reconstituted and

undisturbed samples of Phase I sand, in terms of the end-of-test state of each sample on an e-p' plot. These data are based on results from U.B.C. (Vaid et al., 1996), Laval (Konrad and St. Laurent, 1995) and U. of A. (Ayoubian, 1996; Hofmann, 1997). Complete stress-strain curves for these various laboratory tests are presented in Appendices F to H. The laboratory testing results are discussed in greater detail later in this report. Superimposed on Figure 5(b) is the selected Phase I reference USL, which appears to agree with the data fairly well.

Figure 6 presents all of the results of testing anisotropically consolidated undisturbed samples of Phase III sand, in terms of the end-of-test state of each sample on an e-p' plot. These data are based on results from U.B.C. (Vaid et al., 1996). No triaxial tests were performed on reconstituted Phase III sand. Complete stress-strain curves for the various laboratory tests are presented in Appendix O. The laboratory testing results are discussed in greater detail later in this report. Superimposed on Figure 6 is the selected Phase I reference USL. At first, it appears that the Phase III samples do not match the selected Phase I reference USL very well. However, it is important to note that most of the samples were still dilating at the end-of-test point and that several samples experienced problems with either cavitation or necking towards the end of the test. In addition, there are no other data (e.g. tests on very loose reconstituted samples of Phase III sand) available to accurately determine if the Phase III sand should have a significantly different reference USL than the Phase I sand. It is likely that the two USLs may be at least slightly different (note some differences between the two sites in terms of parameters such as fines content, e_{max} and e_{min}, etc. listed in Table 1, and in terms of the soil behaviour type classification described above – see Figure 1 and Figure 2); however, for the purpose of this report, the same reference USL will be used for both the Phase I and Phase III sites and will be herein referred to as the Syncrude reference USL.

Figure 7(a) presents the quasi-steady-state (QSS) conditions on an e-p' plot for the Phase I samples shown in Figure 5(b) that experienced a QSS. Figure 7(b) presents the quasi-steady-state (QSS) conditions on an e-p' plot for the Phase III samples shown in

Figure 6 that experienced a QSS. In Phase I, only two undisturbed samples tested in triaxial extension experienced a true QSS; the undisturbed samples tested in triaxial compression tended to continuously dilate throughout a test. In Phase III three undisturbed samples tested in triaxial extension and two undisturbed samples tested in triaxial compression experienced a true QSS; the other samples tended to continuously dilate throughout a test. The quasi-steady-state points for each of Phase I and Phase III appear to follow a band which is essentially sub-parallel to the selected reference USL. The data are limited; however, the data from the two sites do appear to follow a similar trend, suggesting that soil fabric at the two sites may be similar. The scatter of data around the approximate QSSL is to be expected, based on the findings by Ishihara (1993).

2.4 Grain Characteristic Parameters

Based on the discussion in the above section, the grain characteristic parameters defining the reference USL (Γ and λ_{10}) for the Phase I and Phase III sites are presented in Table 2.

As described in the Introductory Data Review Report, one method of estimating void ratio from in-situ testing is to make use of an empirical link between void ratio (e) and corrected shear wave velocity (V_{s1}). This method requires the input of the parameters A and B (the intercept and slope, respectively, of the V_{s1}-e relationship). These values for the Phase I and Phase III sites are also presented in Table 2. No correction for aging has been applied to the parameter A because both sites (Phase III in particular) are relatively recent deposits. The parameter A is discussed in more detail later in this report.

The Phase I and Phase III grain characteristic parameters will be compared with those for the other CANLEX sites in subsequent data review reports.

3. FLOW LIQUEFACTION – PHASE I (MILDRED LAKE SITE)

3.1 Site Description

The Phase I site is situated in Cell 24 of the Mildred Lake Settling Basin at Syncrude Canada Ltd. (see Figure 8). The Phase I site consists of artificially deposited sands that are approximately 30 years old and was initially selected as a result of the CANLEX Phase I site selection activity (Robertson et al., 1993). The target zone for undisturbed sampling and in-situ testing was selected from 27 to 37 m depth, based on initial site screening (Robertson et al., 1993). The groundwater table at the site is located, on average, at a depth of approximately 21 m. Figure 9 shows a detailed site plan of the testing area, indicating the locations of the various in-situ tests relative to the freezepipe and sampling boreholes.

Two SPTs, identified as PI9406 and PI9407, were conducted through the target zone at the Phase I site (Campanella, 1994). Detailed SPT logs are given in Appendix A. Both SPTs were carried out by Elgin Explorations Ltd. in mud-rotary advanced boreholes using a rubber tired Acker drill rig, with a 4.5 inch tricone bit and AW drill rods (Campanella, 1994). The SPTs were conducted using two different safety hammers (Hammer 1 and Hammer 2) together with a rope and cathead system. Both hammers were reported as having been recently weighed and adhering to the standard weight of 63.5 kg (140 lb). In SPT PI9406, Hammer 1 was used for measurements at depths less than 36 m, while Hammer 2 was used for greater depths. In SPT PI9407, Hammer 2 was used for measurements at depths less than 36 m, while Hammer 1 was used for greater depths. Energy measurements were carried out for both PI9406 and PI9407.

Four CPTs, identified as PI9402 through to PI9405, were conducted through the target zone at the Phase I site (Campanella, 1994). Figure 9 also shows a fifth CPT, identified as CPT PI9401. According to Campanella (1994), CPT PI9401 was an initial sounding that "was pushed from the ground surface to determine if the heavy vehicle would be able

to attain the target zone ... without the need for pre-drilling". However, CPT PI9401 met refusal at a depth of 20.4 m (i.e. well above the location of the target zone); consequently CPTs PI9402 to PI9405 were pre-bored to a starting depth near the top of the target zone. Detailed CPT logs are contained in Appendix B. All of the CPT work was carried out using the UBC in-situ testing vehicle.

All of the CPTs in the target zone were seismic CPTs and thus, four shear wave velocity logs, identified as PI9402 through to PI9405, were conducted at the Phase I site (Campanella, 1994). PI9403, PI9404 and PI9405 pass through the entire target zone. For some unknown reason, PI9402 starts approximately midway through the specified target zone. Detailed shear wave velocity logs are given in Appendix C.

Four geophysical logs, identified as CORE1, CORE2, FPS1 and FPS2, were conducted through the target zone at the Phase I site (Küpper, 1994). CORE1 and CORE2 were carried out in boreholes drilled for continuous core sampling using the Christensen core barrel. FPS1 and FPS2 were carried out in boreholes drilled for fixed piston sampling. Each geophysical hole was logged three to six times with each of two geophysical tools (9072A and 9036A from Century Geophysical Corporation). The data from Tool 9036A were processed in detail by Küpper (1994) and are presented here. Readings were taken every 2 cm; however, in order to reduce "noise", the data were processed using smoothing filters. The average interpreted void ratios from the three runs in each borehole were used in this report. Detailed geophysical logs are given in Appendix D.

Pressuremeter testing was also carried out in the target zone at the Phase I site (Hughes, 1994). Initially, a total of five non-selfbored pressuremeter tests were performed with a high-pressure pressuremeter at depths ranging from 20 m to 32 m. Three of these tests were located at depths within the target zone. Only two of these tests were successful; the deepest test was in an oversized hole and, consequently, the membrane failed upon expansion. At a later date, five self-boring pressuremeter tests were also performed at depths within the target zone. Four of these tests were performed

one after the other without withdrawing the pressuremeter between tests; the last three of these tests gave very consistent results when compared with each other. The interpreted results for these three self-bored pressuremeter tests as well as the results of the non-selfbored pressuremeter tests are given in Appendix E. The interpretation of the non-selfbored pressuremeter results by Hughes (1994) suggests an average K_o in the target zone of about 0.6, while the interpretation of the self-boring pressuremeter test results by Hughes (1994) suggests an average K_o in the target zone of about 0.4. However, there was some uncertainty in the two interpretations. This report adopted an average K_o of 0.5 for interpretation of the Phase I Site.

3.2 Estimation of In-situ State

a) Void ratio

i) Direct methods

Undisturbed samples

Successful ground freezing and sampling was carried out at the Phase I site (Hofmann and Sego, 1994), resulting in 20 m of undisturbed sandy soil core (Hofmann, 1997). Samples of different dimensions were trimmed from these cores in order to produce samples for both triaxial testing and simple shear testing. The void ratio of each sample was calculated at U. of A. using volume calculations (Hofmann, 1995) prior to sending the samples out to the various laboratories to be tested. Successful fixed piston tube sampling was also carried out at the Phase I site (Plewes, 1993), resulting in twenty-two samples of sandy soil. Plewes (1993) indicated that 14 of these fixed piston samples could be considered to be high quality samples (referred to as Types I and II).

In addition, as reported by Plewes (1993), a total of 24.55 m of tailings was cored using the Christensen double-tube core sampler. A total of 15.86 m of core was recovered, representing an average total core recovery of 65%. A total of 9.8 m of core was

preserved in the PVC core liner for inspection and testing. Coring the tailings was hampered by the tendency of the core barrel to meet refusal in frequent dense tailings layers which have q_t values above 20 MPa. Refusal was caused by the high penetration resistance of the dense sand layers and the tendency for the dilative sand to jam in the core shoe. The core samples were disturbed due to handling within the PVC tube.

Figure 10 summarizes the void ratios for all samples. The solid dots represent the void ratios of Quality I frozen samples, the open dots represent the void ratios of Quality II frozen samples, and the solid squares represent the void ratios of Quality III frozen samples. Details of the sampling and quality assessment are given in Hoffman (1997). The void ratios for the undisturbed ground freezing samples are summarized in Table 3. Also shown in Figure 10 are open triangles, which represent the void ratios of Type I and Type II samples obtained using the fixed piston tube sampler (Plewes, 1993). Based on the results shown in Figure 10, it appears that at the Phase I site, the fixed piston tube samples have void ratios which underpredict those of the ground freezing samples. Note that void ratio axis in Figure 10 has been plotted from 0.65 to 0.95, corresponding approximately to e_{min} and e_{max} for the sand at the Phase I site (see Table 1). Thus, approximate relative densities (D_r) for the soil samples can be computed directly from Figure 10. The thick horizontal lines at 27 m and 37 m in this figure and in subsequent figures, indicate the extent of the target zone at the Phase I site.

For the Quality I and II ground freezing samples shown in Figure 10, the average void ratio is 0.768 (SD=0.040) ($D_r \approx 66\%$; SD=15.2%). For the Quality III ground freezing samples shown in Figure 10, the average void ratio is 0.748 (SD=0.038). For the fixed piston samples, the average void ratio is 0.694 (SD = 0.034) ($D_r \approx 91\%$; SD = 11.8%). Hence, it appears that the high quality fixed piston samples have an average relative density approximately 40% larger than the average relative density of the samples obtained using ground freezing.

The thick semi-vertical line superimposed on Figure 10 represents void ratios

corresponding to the selected Syncrude reference USL (see Figure 5 and Table 2) at the effective stresses present over the depth of the target zone, based on a K_o of 0.5. This line corresponds to a relative density (D_r) of approximately 40%. Almost all of the undisturbed samples that were trimmed for testing have void ratios significantly less than this line (i.e. $D_r >> 40\%$), although three samples have void ratios higher than the reference USL (i.e. $D_r < 40\%$) and two samples have void ratios close to the reference USL (i.e. $D_r \approx 40\%$).

Figure 11 presents a comparison between the estimated in-situ void ratios calculated at U. of A. before sending the undisturbed samples out for testing (Hofmann, 1995) and those back-calculated by the individual testing laboratories other than U. of A. (Laval - Konrad and St. Laurent, 1995; U.B.C. - Vaid et al., 1996). Note that U. of A. used G_s=2.66, U.B.C. used G_s=2.62 and Laval used G_s=2.63. In general, the U. of A. values tend to be lower than the values calculated by U.B.C., but higher than those calculated by Laval. For the remainder of this report, the void ratios calculated by Hofmann (1995) will be used as the estimated in-situ void ratios; however, these void ratios should be considered to be accurate to only approximately $\pm$ 0.01.

Geophysical logging

Figure 12 presents the results of the void ratio interpretation of the geophysical logs as given by Küpper (1994). The interpretation of the geophysical results was based on a G_S of 2.63. Superimposed on Figure 12 are the void ratios shown in Figure 10 for the Quality I and II undisturbed frozen samples (G_s=2.66). The void ratio axis in Figure 12 has been plotted from 0.65 to 0.95, corresponding approximately to e_{min} and e_{max} for the sand at Phase I and the thick semi-vertical line represents the reference USL ($D_r \approx 40\%$).

In general, the interpreted void ratio profiles from the geophysical logs seem to slightly overpredict the overall trend and range of the frozen sample void ratios in the target zone at Phase I, predicting an average void ratio of 0.788 (SD=0.053). This is slightly higher

than the average void ratio (e = 0.768) of the undisturbed frozen samples trimmed for testing. The largest differences between the void ratios from frozen samples and the geophysical predicted void ratios appears to occur between approximately 29.5 and 31 m, at which depths the geophysical method predicts significantly higher void ratios. The four geophysical profiles are generally consistent, but indicate a rapid variation in void ratio with depth at the site.

ii) Indirect methods

In-situ test profiles

Figure 13(a) to Figure 13(c) present the in-situ test signatures, corrected for effective overburden stress (and energy effects, in the case of the SPT profiles), for each of the SPTs, CPTs, and shear wave velocity logs at the Phase I site. In Figure 13(a), the SPT profiles are shown as discrete points with attached bars, corresponding to the midpoint and range, respectively, of the 30 cm over which the value of N was measured. In Figure 13(b), the CPT profiles are shown as continuous profiles, since measurements were taken every few centimetres. In Figure 13(c), the shear wave velocity profiles are shown as step functions, indicating that the shear wave velocity was measured (using a method of differences), as an average value over a given interval (typically about 1 m).

The four q_{c1} profiles are consistent with little scatter. The four V_{s1} profiles are less consistent with more scatter. The two $(N_1)_{60}$ profiles are fairly consistent, although, within the target zone, PI9406 has more scatter than PI9407. The CPT profiles, however, do show that there is some variability in the deposit. In the target zone, the overall average measured values and standard deviations (SD) are as follows: V_{s1}=156.4 m/s (SD=20.1 m/s), q_{c1}=7.38 MPa (SD=1.67 MPa), and $(N_1)_{60}$=18.2 (SD=3.0).

Figure 14(a) to Figure 14(c) present the estimated void ratio profiles at Phase I, based on relative density (D_r) based interpretations of the SPT and CPT, and interpretations of the

shear wave velocity measurements. These interpretations are discussed in more detail below. The void ratios of the undisturbed frozen samples (Quality I and II) are superimposed on the plots for comparison. Again, the void ratio axes have been plotted from 0.65 to 0.95, corresponding approximately to e_{min} and e_{max} for the sand at the Phase I site, and the thick semi-vertical lines represent the reference USL ($D_r \approx 40\%$). Figure 14(d) presents the interpretations of the geophysical logs for comparison. The interpreted void ratio profiles from the geophysical logs seem to best capture the overall trend and range of the frozen sample void ratios in the target zone at the Phase I site.

SPT

Figure 14(a) presents the results of the D_r-based void ratio interpretation of the SPT, based on the method by Skempton (1986), as outlined in the Introductory Data Review Report. A value of 40 was used for the constant in the Skempton (1986) equation relating D_r to $(N_1)_{60}$. This should be fairly reasonable for a medium dense sand with some fines. In general, the D_r-based interpretation of the SPT at Phase I appears to predict the average void ratio of the Quality I and II undisturbed samples fairly well, giving an average void ratio in the target zone of 0.763 (SD=0.016), but underpredict the overall range.

CPT

Figure 14(b) presents the results of the D_r-based void ratio interpretation of the CPT, based on the method by Baldi et al. (1986), as outlined in the Introductory Data Review Report. In order to apply this method, it was assumed that the Phase I sand has grain characteristics similar enough to Ticino sand. Thus, the Ticino sand values for the material constants C_0, C_1, and C_2 could be used in the equation developed by Baldi et al. (1986) relating tip resistance to D_r. This is not a very good assumption, based on the comparison between index parameters for Ticino sand and Phase I sand shown in Table 1. Consequently, the interpretations of void ratio based on the D_r-based method of interpreting the CPT at Phase I overpredict the average and do not fully capture the range

of void ratios for the Quality I and II frozen samples. The overall predicted average void ratio in the target zone using this method is 0.812 (SD = 0.028).

Shear wave velocity

Figure 14(c) presents the results of the void ratio interpretation of the shear wave velocity, as outlined in the Introductory Data Review Report and the values of A and B for Phase I sand given in Table 2. The scatter in the V_{s1} profile converts to more significant scatter in the void ratio profile predicted by shear wave velocity, due to the sensitivity of the method. Nevertheless, in general, the interpreted void ratio profiles from the shear wave velocity measurements capture the trend and range of the frozen sample void ratios fairly well over most of the Phase I target zone. However, towards the bottom of the target zone (i.e. at depths greater than 34 m), the shear wave velocity predictions tend to underestimate the void ratios of the Quality I and II frozen samples. Overall, the interpretation of the shear wave velocity logs predicts an average void ratio of 0.747 (SD=0.117) in the target zone. Note that the value of A used in the V_{s1}-e relationship was not adjusted from the value measured in the laboratory on young reconstituted Syncrude sand because the Phase I deposit is relatively young. A small adjustment to the value of A might be appropriate due to the 30 year age of the deposit.

iii) Correlations between in-situ tests

In order to compare the CPT and the SPT, the closest pairs of test types were determined by examining the detailed site plan (see Figure 9). SPT PI9406 and CPT PI9404 were paired together, as were SPT PI9407 and CPT PI9402. The comparisons between SPT and CPT were performed following the method outlined in the Introductory Data Review Report. Based on the comparison between the two pairs of tests, Figure 15(a) shows that the value of $q_{c1}/(N_1)_{60}$ is fairly scattered in the target zone, but has an average value of 0.44 (SD=0.15). This value is within the historical range for a sand. The scatter is predominantly due to the scatter in the SPT $(N_1)_{60}$ values (see Figure 13(c)).

Comparing the CPT and shear wave velocity measurements was straightforward because each CPT and shear wave velocity pair were conducted in the same hole and are directly comparable. The comparisons between CPT and shear wave velocity were performed following the method outlined in the Introductory Data Review Report. At Phase I, as shown in Figure 15(b), the value of Y was fairly scattered, with an average value of 95.6 (SD=12.1) in the target zone. This corresponds to a moderately incompressible sand. In general, the value of Y appears to gradually increase with depth within the target zone. Robertson et al. (1995) suggested that Y should increase with age for a given sand type.

In order to compare the SPT and shear wave velocity, the closest pairs of test types were determined by examining the detailed site plan (see Figure 9). SPT PI9406 and seismic CPT PI9404 were paired together, as were SPT PI9407 and seismic CPT PI9402. Comparisons between SPT and shear wave velocity were performed following the method outlined in the Introductory Data Review Report. Based on the two pairs of tests, Figure 15(c) shows that the value of X in the target zone is scattered, but has an average value of 74.8 (SD=9.0). The scatter is due to scatter in both SPT $(N_1)_{60}$ and V_{s1} values.

Note that one would expect the values of $q_{c1}/(N_1)_{60}$ and X to be less reliable than the values of Y, since each profile of either $q_{c1}/(N_1)_{60}$ or X is determined from pairing an SPT borehole with a seismic CPT borehole, whereas each profile of Y is determined within a single seismic CPT borehole.

iv) Shear wave velocity (V_S) based method of interpreting the SPT and CPT

Figure 16(a) to Figure 16(d) compare the V_S-based methods of interpreting void ratio from the SPT and the CPT with the interpretations of void ratio from the shear wave velocity logs and the geophysical logs at Phase I. The V_S-based interpretations of both the SPT and CPT follow the methods outlined in the Introductory Data Review Report. Borehole-specific average values of X in the target zone were used to interpret the SPT

profiles and borehole-specific average values of Y in the target zone were used to interpret the CPT profiles. As a result, void ratio estimations outside of the target zone may not be reliable. However, it is only within the target zone that frozen samples are available for comparison. To be absolutely correct (particularly if applying this method for design purposes), even within the target zone, values of X and Y that vary with depth should be used to interpret the SPT and CPT using the V_S-based method. However, this report has used average (although borehole-specific) values of both X and Y in the target zone, for ease of calculation. The values of A and B that were used for the V_S-based interpretations of void ratio from the SPT and CPT are given in Table 2. In Figure 16, as in Figure 14, the void ratios of the Quality I and II undisturbed frozen samples are shown, for comparison, and the reference USL ($D_r \approx 40\%$) is also indicated.

Comparing Figure 16(a) with Figure 14(a), it appears that the V_s-based method appears to be slightly better than the D_r-based method at predicting the range of void ratios in the Phase I target zone. The V_S-based method of interpreting the SPT predicts an average void ratio of 0.755 (SD=0.043) in the target zone.

Comparing Figure 16(b) with Figure 14(b), the V_S-based method of interpreting the CPT appears to be better than the D_r-based method at capturing the range of void ratios over most of the target zone at the Phase I site. The V_S-based method of interpreting the CPT predicts an average void ratio of 0.749 (SD=0.056) in the target zone.

b) State parameter

i) Direct methods

CPT

Sladen and Hewitt (1989)

Based on values of e_{max}, e_{min}, G_s, average FC, D_{50} and D_{10} (see Table 1), Syncrude sand

at the Phase I site initially appears to be somewhat similar to Nerlerk and Ukalerk (sometimes called Erksak; Sladen and Hewitt, 1989) sands (see soil descriptions in the Introductory Data Review Report). These sands were used to develop the field observation based relationship outlined in the Introductory Data Review Report that was proposed by Sladen and Hewitt (1989) to determine whether or not Nerlerk or Ukalerk (Erksak) sands were susceptible to flow liquefaction. Consequently, it would seem reasonable to apply the Sladen and Hewitt (1989) dividing line directly to the CPT data from the target zone at the Phase I site. However, as outlined in the Introductory Data Review Report, the best method of estimating if the response of two sands will be similar is to examine their USLs. The selected reference USL for Syncrude sand was presented in Figure 5. The USLs for Nerlerk sand and Ukalerk (Erksak) sand were described in the Introductory Data Review Report. The three USLs are compared in Figure 17(a). At low stresses ($p'<200$ kPa), although the USL for each sand has a similar slope, λ_{ln} (0.0152 for Syncrude; 0.014 for Nerlerk; 0.013 for Ukalerk/Erksak), the value of Γ is different (0.919 for Syncrude; 0.885 for Nerlerk; 0.82 for Ukalerk/Erksak), with the result being that the Syncrude USL would be located at higher void ratios than either the Nerlerk or Ukalerk/Erksak USLs on an e-p' plot (see Figure 17(a)).

Based on a groundwater table at a depth of 21 m and unit weights of soil as given in Table 1, the Sladen and Hewitt (1989) relationship given in the Introductory Data Review Report can be converted to a liquefaction/non-liquefaction dividing line in terms of q_c versus depth. This dividing line is shown superimposed over CPT data from the target zone at the Phase I site in Figure 17(b). In the target zone (27 to 37 m), the field observation method by Sladen and Hewitt (1989) for Nerlerk and Ukalerk (Erksak) sands, when applied directly to the Phase I Site, would predict that, on average, the material could be range from being considered borderline to being susceptible to flow liquefaction.

However, the USL for Syncrude sand is different than that for Nerlerk sand. Figure 17(a) clearly indicates that to move either the Nerlerk USL or the Ukalerk/Erksak USL to the Syncrude USL on an e-p' plot would require an upward shift in void ratio. This would

translate into a shift to the left in the Sladen and Hewitt (1989) dividing line shown in Figure 17(b), resulting in a different evaluation of flow liquefaction potential in the Phase I site target zone. Although the exact size of the corresponding shift is not clear at this point, it is likely to be large enough that the target zone would be predicted to have no flow liquefaction potential, with perhaps some zones being considered as borderline.

Been and Jefferies (1992)

Superimposed over CPT data from the Phase I target zone, Figure 18 presents the dividing line (Ψ=0) determined for Syncrude sand using the method proposed by Been and Jefferies (1992). This method is based on correlating CPT results with state parameter for various soils, as outlined in the Introductory Data Review Report. The dividing line was determined using the equations given in the Introductory Data Review Report, assuming $B_q \approx 0$ in sandy deposits. The measured CPT profiles confirm that B_q was generally small (see Appendix B). M was assigned a value of 1.59, the approximate average laboratory measured value for triaxial compression tests (M_C) on undisturbed samples from the Phase I site, as presented later in this report. The corresponding ultimate state friction angle, ϕ'_{us}, is approximately 39°, based on the equation relating M_C and ϕ'_{us} given in the Introductory Data Review Report.

Since the range of effective stresses in the target zone at Phase I falls just below the effective stress level associated with the breakpoint in the selected Syncrude USL, the flatter part of the bi-linear reference USL can be used to estimate the state dividing line. This part of the USL has a λ_{ln} of 0.0152 (see Table 2) which corresponds to a λ_{log} of 0.035. Combining the five equations given in the Introductory Data Review Report, using the groundwater table depth and unit weights given in Table 1, and setting $\Psi = 0$ results in the dividing line in terms of q_c versus depth as indicated in Figure 18. Also shown in Figure 18 are lines for Ψ= - 0.05 and Ψ= -0.1.

In the target zone (27 to 37 m), the Been and Jefferies (1992) method would predict that

most of the sand could not experience flow liquefaction because most of the deposit is denser than the Ψ=0 dividing line. The average predicted state is Ψ = -0.006 (SD=0.021). Based on the Quality I and II undisturbed samples from the Phase I site (see Table 3), the estimated mean in-situ state parameter is Ψ= -0.064 (SD=0.040), corresponding to a denser state than that predicted by the Been and Jefferies (1992) approach.

Plewes et al. (1992)

Figure 19 shows CPT data from the Phase I target zone (27 to 37 m) plotted on the soil classification chart after Jefferies and Davies (1991), as proposed by Plewes et al. (1992) for estimating contours of state parameter. The method outlined in the Introductory Data Review Report with its associated assumptions was followed to produce the plot. On this soil classification chart, the material in the target plots straddling the border between Zone 6 and Zone 5 would be classified as approximately half a sand (ranging from a clean sand to a silty sand) and half a sand mixture (ranging from silty sand to a sandy silt).

Figure 20 presents the Plewes et al. (1992) interpretation of the CPT data in the form of estimated profiles of Ψ at the Phase I site. In order to produce the profiles of Ψ, M was assigned a value of 1.59, the approximate average laboratory measured value for triaxial compression tests (M_C) on undisturbed samples from the Phase I site. Note that this differs slightly from the M of 1.2 that Plewes et al. (1992) assumed in order to produce the contours of Ψ on their soil classification chart, as shown in Figure 19. Superimposed on Figure 20 is a thick vertical line representing the Ψ=0 state. By examining either Figure 19 or Figure 20, one can see that the method by Plewes et al. (1992) predicts an approximate average state of Ψ = - 0.063 (SD=0.023) in the Phase I target zone. This would suggest that the material in the target zone at the Phase I site is dense of ultimate state and would not be susceptible to flow liquefaction.

This conclusion does not agree well with the prediction using the Been and Jefferies (1992) methodology, even though the Plewes et al. (1992) method draws on earlier work

by Been and Jefferies, as explained in the Introductory Data Review Report. Application of the method by Plewes et al. (1992) allows for variability in compressibility within the soil deposit (since the slope of the USL is estimated from F) whereas, in order to apply the method by Been and Jefferies (1992), a single USL slope needs to be assumed. This report uses a bi-linear USL; however, in reality, as shown by Ishihara (1993), the USL is likely a continuous curve, having a constantly increasing slope with increasing p'. Since the average effective stresses in the Phase I target zone are close to the level at which the breakpoint in the bi-linear USL occurs, it is likely that the true slope of the USL at this stress level falls in between the slopes of the two parts of the bi-linear USL. If such a slope were used in the Been and Jefferies (1992) method, the results would be more similar to those from the Plewes et al. (1992) method.

The calculated values of Ψ for the Quality I and II undisturbed frozen samples from the Phase I site target zone are also shown on Figure 20 for comparison. Compared to the undisturbed frozen samples (having an average Ψ= - 0.064; SD=0.040), the Plewes et al. (1992) method predicts the average state parameter well, but slightly underpredicts the overall range of state parameter within the target zone.

With vertical effective stresses ranging from approximately 450 kPa to 540 kPa and a K_o of 0.5, the Phase I target zone has an approximate range in mean normal effective stress, p', from 300 kPa to 360 kPa. Given that the reference USL in this stress range has been defined by Γ=0.919 and λ_{ln}=0.0152, the profiles of Ψ predicted using the method by Plewes et al. (1992) can be converted into profiles of void ratio, as shown in Figure 21. The void ratios of the undisturbed frozen samples are also shown for comparison. Comparing the void ratio profiles estimated from the in-situ tests with the void ratios of the undisturbed samples in Figure 21 is the same as comparing Ψ estimated from the in-situ tests with Ψ of the undisturbed samples in Figure 20, because the same relationship between Ψ and void ratio was used for both the in-situ testing and the undisturbed samples. The Plewes et al. (1992) interpretation predicts an average void ratio of 0.769 (SD=0.023). This predicts the average Quality I and II undisturbed sample

void ratio well, but slightly underestimates the range of void ratios of the undisturbed samples (having an average void ratio of 0.768; SD=0.040).

Self-boring pressuremeter tests (SBPMT)

The results of the three most reliable self-boring pressuremeter tests in the target zone at the Phase I site (performed at depths of 35.0 m, 35.8 m and 36.6 m) (Hughes, 1994) can be used to estimate state parameter, following the methods by Yu (1994) and/or Yu et al. (1996), as described in the Introductory Data Review Report. An interpretation of the Phase I pressuremeter results using the method by Yu (1994) was not available.

Yu et al. (1996) proposed combining pressuremeter data and CPT data to estimate state parameter (see Figure 22(a)). The average effective pressuremeter limit pressure from the three tests in the target zone at Phase I is approximately 2070 kPa (see Appendix E). Note that in sandy soils, it is difficult to determine a limit pressure from a pressuremeter test, since the pressuremeter response curve does not always level off, but often continues to rise; therefore, for the analysis presented here, the end of the expansion part of the pressuremeter curve was taken as the limit pressure. The average measured cone tip resistance (q_c) associated with the depth ranges of the pressuremeter testing is approximately 16 040 kPa. With the average initial pore pressure in the depth ranges of the pressuremeter testing being approximately 145 kPa, the average effective cone tip resistance is approximately 15 900 kPa. Figure 22(b) shows that, when the effective pressuremeter and cone data are combined as a ratio (having a value of about 7.7), an average state parameter of Ψ = - 0.146 is predicted in the Phase I site target zone. This underestimates the state of the Quality I and II frozen samples.

Included in Appendix P is a copy of a paper by Hughes et al. (1997) which provides a "broad-brush" interpretation of the state of the sand in the Phase I target zone based on the self-boring pressuremeter testing results. The paper concludes that "it is clear that at the Cell 24 ... additional energy over and above that required to shear the sand under

constant volume ... is necessary to shear the soil"; i.e. the sand is in a stable state.

ii) Indirect methods

When combined with the reference USL for Syncrude sand, at the appropriate stress level, any of the methods used above to estimate void ratio at the Phase I site can also be used to estimate state parameter. As explained above, with vertical effective stresses ranging from approximately 450 kPa to 540 kPa and a K_o of 0.5, the Phase I site target zone has an approximate range in mean normal effective stress, p', from 300 kPa to 360 kPa. Given that the reference USL in this stress range has been defined by Γ=0.919 and λ_{10}=0.0152, the interpreted ranges in void ratio based on the SPT, CPT, V_s measurements and geophysical logs can be converted into ranges in state parameter.

Figure 23(a) to (d) present estimated profiles of state parameter in the target zone at the Phase I site from the V_s-based interpretations of void ratio from the SPT and CPT and the void ratio interpretations of the shear wave velocity and geophysical logs, as shown previously in Figure 16(a) to (d). In the target zone, the V_s-based interpretation of the SPT predicts an average Ψ = -0.076 (SD=0.043), the V_s-based interpretation of the CPT predicts an average Ψ = -0.082 (SD=0.056), the interpretation of the shear wave velocity logs predicts an average Ψ = -0.084 (SD=0.117) and the interpretation of the geophysical logs predicts an average Ψ = -0.043 (SD=0.053).

Superimposed on Figure 23(a) to (d) are the calculated values of state parameter for the Quality I and II undisturbed samples, based on the selected reference USL for Syncrude sand. The thick semi-vertical line represents the reference USL (i.e. Ψ=0). Comparing the Ψ profiles estimated from the in-situ tests with the Ψ of the undisturbed samples in Figure 23 is the same as comparing void ratios estimated from the in-situ tests with void ratios of the undisturbed samples in Figure 16, because void ratio was converted to Ψ using the same method for both in-situ testing and the undisturbed samples. Therefore, as for the void ratio comparison in Figure 16, the range in undisturbed sample Ψ seems to be

captured by all of the methods, but the CPT (interpreted using the shear-wave velocity based method) and the geophysical logging appear to best capture the detailed variability of Ψ in the target zone at the Phase I site. Although there are definitely a few regions in the target zone where $\Psi > 0$ would be estimated, the undisturbed samples tested to date seem to indicate that over a large portion of the target zone, the in-situ Ψ is generally less than zero. Based on the Quality I and II undisturbed samples alone, the average estimated in-situ state parameter is $\Psi = -0.064$ (SD=0.040).

3.3 In-situ Response to Undrained Loading

a) Direct methods

Figure 24 presents an enlarged version of Figure 10. Different symbols are used in Figure 24 for each undisturbed frozen sample (FS) indicating to which laboratory it was sent and the type of test that was performed. One triaxial compression test (TC) was carried out on an undisturbed sample with a void ratio greater than the reference USL by U. of A.. One simple shear test (which is more difficult to interpret) was carried out on an undisturbed sample with a void ratio close to the reference USL by U.B.C. The other samples which were tested had void ratios significantly lower than the reference USL. The label "D" for four of the samples tested by UBC (two TC and two TE) indicates a drained test. The rest of the triaxial tests were undrained. Figure 24 does not show the TC test performed by Ayoubian (1996) because documentation as to which undisturbed sample was used was not available. Note that the cyclic triaxial tests at U. of A. were performed on Quality III frozen samples.

The complete stress-strain response curves for all of the laboratory tests are presented in Appendices F (tests by U.B.C.), G (tests by Laval), H (tests by U. of A.), and I (tests by Klohn-Crippen and C-CORE). Results from triaxial (compression and extension), simple shear and cyclic triaxial tests on undisturbed samples of Syncrude sand from the Phase I site are presented. In addition, the results of testing reconstituted (isotropically and anisotropically consolidated) samples of Syncrude sand by Vaid et al. (1996) at U.B.C.,

Ayoubian (1996) at U. of A., Konrad and St. Laurent (1995) at Laval, Plewes (1995) at Klohn-Crippen and C-CORE (1993) are included. Note that the tests on anisotropically consolidated reconstituted samples are directly relevant to field conditions, while the tests on isotropically consolidated reconstituted samples are not.

i) Undisturbed triaxial samples

Table 4 summarizes the anisotropically consolidated undrained triaxial compression and extension test results for undisturbed samples of Syncrude sand from the Phase I site (Vaid et al., 1996; Konrad and St. Laurent, 1995; Ayoubian, 1996; and Hofmann, 1997). The two undisturbed samples that were tested by Klohn-Crippen (see Appendix I) were isotropically consolidated and are, therefore, not included here; both of these samples were strain-hardening in triaxial compression. The tests are identified by the laboratory that conducted the testing as well as the sampling identification number assigned by Hofmann (1995). The results of testing each sample in undrained monotonic loading are broken down into the individual components of response, as outlined in the Introductory Data Review Report. Based on the definitions of monotonic undrained response given in the Introductory Data Review Report, each undrained TC and TE stress-strain curve (see Appendices F to H) has been divided into four main points: (A) initial state, (B) peak (or yield) state, (C) minimum state and (D) ultimate state.

Initial state

The initial state of each sample is defined by its void ratio after thaw and consolidation (e_c) and the vertical and horizontal effective stresses (σ'_{vi} and σ'_{hi}) placed on it. The values of e_c, σ'_{vi} and σ'_{hi} for the samples are those that were reported by the laboratories that conducted the testing. For a given sample, the value of e_c is generally less than the void ratio in-situ (see Table 3), as estimated by Hofmann (1995), as a result of small volume changes that occur during thaw and consolidation. The difference between the in-situ void ratio and e_c will be discussed later in this report.

Stress-strain response

None of the Phase I undisturbed samples that were tested strain-softened directly to their ultimate state during a triaxial test. All of the samples strain-hardened towards their ultimate state. However, two out of four of the undisturbed samples that were subjected to triaxial extension tests demonstrated limited strain-softening in that they strain-softened to a quasi-steady-state (QSS) before eventually, at large enough strains, strain-hardening towards ultimate state (see Appendices F to H).

For samples that strain-hardened to their ultimate state without demonstrating any limited strain-softening (all of the triaxial compression tests and two of the triaxial extension tests), the peak and minimum values of p' and q were taken as equal to the end-of-test values of p' and q. Consequently, the peak and minimum strengths were taken as equal to the end-of-test strength (which can be generally considered to be close to the ultimate state strength). These samples responded to undrained loading in a non-brittle manner and were assigned I_B=0 (see the Introductory Data Review Report). These samples were also assigned an axial strain during minimum strength of zero because there was no minimum condition during the stress-strain curve.

For two of the four samples that were tested in triaxial extension, a QSS point occurred. The corresponding stress-strain curves (see Appendices F to H) had distinct peak, minimum and ultimate points since the samples demonstrated limited strain-softening. For each test, the values of p' and q (and, hence, the values of strength) were determined for each of the three individual points along the stress-strain curve. The values of I_B for these samples were still small (≈ 0.02) because the samples were anisotropically consolidated to approximate the level ground in-situ stress state and were therefore preloaded in compression. Significant unloading had to occur before the samples experienced limited strain-softening. Axial strains that occurred while at the QSS point (i.e. during the point of minimum strength) were also fairly small, ranging from

approximately 3% to 5%. The minimum strengths of these samples were significantly smaller than the end-of-test strengths ($S_{min} \approx 0.30$ of S_f).

ii) Reconstituted triaxial samples

Initial state

Included in Table 4 are results from Ayoubian (1996) for tests (one TC and one TE) on anisotropically consolidated (K_o=0.5) reconstituted samples of Syncrude sand from the Phase I site (prepared by moist tamping) and results from Vaid et al. (1996) for tests (four TC and four TE) on anisotropically (K_o=0.5 except for one with K_o=0.67) consolidated reconstituted samples of Syncrude sand (prepared by water pluviation). The other reconstituted samples of Syncrude sand tested by Vaid et al. (1996) and those tested by Cunning (1994), Konrad and St. Laurent (1995), Klohn-Crippen and C-CORE are not included here because they were isotropically consolidated. Anisotropically consolidated reconstituted samples (with $K_o \approx 0.5$) more closely represent the in-situ stress state and, as discussed previously, produce a response that can be directly linked with the expected in-situ response under level ground conditions, as well as the test results for undisturbed samples. The anisotropically consolidated reconstituted samples can be thought of as being preloaded in compression.

Moist tamping allows for a much looser initial state to be reached than water pluviation. Thus, the combination of moist tamped and water pluviated reconstituted samples span a large range of initial state and would be expected to span a large range in observed response to undrained loading. The moist tamped samples prepared by Ayoubian (1996) had much looser initial states than the water pluviated samples prepared by Vaid et al. (1996).

Stress-strain response

Two of the triaxial compression tests and all of the extension tests on anisotropically

consolidated reconstituted samples by Vaid et al. (1996) experienced a QSS and demonstrated limited strain softening with little brittleness; however, the two TC tests were more brittle than the TE tests. At the QSS point of each test, fairly small axial strains occurred, ranging from approximately 3% to 5%.

Both the triaxial compression test and the triaxial extension test by Ayoubian (1996) strain-softened directly to ultimate state. The triaxial compression test required very little additional load to trigger the strain-softening response; consequently, the response was very brittle, with I_B=5.3. In addition, the axial strain during minimum (ultimate) strength was large, accumulating to approximately 25% by the end of the test. The triaxial extension test was much less brittle (I_B=0.2) and had an accumulated axial strain during minimum (ultimate) strength of approximately 18%. The differences in brittleness between the TC and TE tests illustrates the effects of preloading a sample in compression as it could be under level ground conditions in-situ.

iii) Undisturbed simple shear samples

Table 5 summarizes the undrained monotonic simple shear test results for undisturbed samples of Syncrude sand from the Phase I site. The individual tests are identified by the sampling identification number assigned by Hofmann (1995). All of the testing was conducted by U.B.C. (Vaid et al., 1996). The results of testing each sample are broken down into individual components of response, similar to the triaxial test results. Note, however, that the various components of simple shear response have been defined in terms of the applied shear stress on the horizontal plane, τ, and the measured vertical effective stress. Brittleness index is defined in terms of only the peak and minimum values of applied shear because all of the tests had an initial applied shear of zero. The initial value of vertical effective stress, σ'_{vi}, can be converted to an initial value of mean normal effective stress, p'_i, if an assumption is made about the initial value of K_o. A value of initial K_o=0.5 would be reasonable. Each undrained stress-strain curve (see Appendix F) has been divided into four main points: (A) initial state, (B) peak (or yield)

state, (C) minimum state and (D) ultimate state.

It is interesting to note that, of the eight samples that were tested under simple shear (see stress-strain curves in Appendix F), five samples demonstrated strain-hardening while three samples (one from a depth of 29.8 m and two from a depth of 31.1 m) demonstrated limited strain-softening (one more significantly than the other two).

b) Indirect methods

i) Self-boring pressuremeter tests (SBPMT)

Computer aided modelling results were not available for pressuremeter testing at the Phase I site.

ii) Link with in-situ state

Void ratio

Figure 25 and Figure 26 present the various components of response of all of the undrained triaxial tests on anisotropically consolidated undisturbed Phase I samples and reconstituted Syncrude sand samples tested to date in terms of the individual laboratory void ratio of each sample. In addition, Figure 25(a) presents the initial conditions of each sample relative to the selected Syncrude reference USL and Figure 26(a) presents the end-of-test conditions of each sample relative to the same USL. The undisturbed samples were tested at an average initial p' of about 340 kPa which is approximately equal to the average in-situ p' in the target zone at the Phase I site. The reconstituted samples were tested over a range of initial values of p' (having an average value of approximately 280 kPa) but with similar values of K_o (≈ 0.5).

Figure 25 and Figure 26 present the components of response as follows: brittleness index (I_B), minimum strength ratio (S_{min}/p'_i), axial strain during minimum strength (ε_a),

end-of-test strength ratio (S_f/p'_i), peak stress ratio (M_p) and end-of-test stress ratio (M_f). Definitions of each of these terms are given in the Introductory Data Review Report. With the exception of some samples, for a given direction of loading (i.e. TC or TE) each component of response appears to be generally a function of void ratio. However, some samples do not fit the trends between undrained response and void ratio suggested in Figure 25 and Figure 26 because of the wide range in initial stress level.

Relative density

The graphs in Figure 25 and Figure 26 have been plotted with the laboratory void ratio axes ranging from 0.65 to 0.95, corresponding approximately to e_{min} and e_{max} for the sand at the Phase I site (see Table 1). Thus, approximate relative densities (D_r) can be computed directly from Figure 25 and Figure 26. Hence, similar conclusions can be drawn about the trends between the various components of response and D_r as were drawn above about the trends between the various components of response and void ratio. Although normalizing test data with respect to a soil's individual values of e_{min} and e_{max} may account for some differences between various soils with different USLs, the trends between undrained response and relative density suggested in Figure 25 and Figure 26 are still not unique since the data are for a range in initial stress level.

State parameter

The graphs in Figure 25 and Figure 26 are replotted in Figure 27 and Figure 28 in terms of the individual laboratory state parameter of each sample. When examining the response of a sample in the laboratory, it is important to define Ψ for the sample based on e_c and the laboratory applied stresses. This combination defines the state of the sample immediately prior to testing and influences how it will respond to undrained loading. For most of the samples, the value of Ψ is defined relative to the flat section of the bi-linear reference USL, since the initial values of p' fall in the stress range corresponding to this portion of the USL. However, for two of the undisturbed samples and three of the

reconstituted samples, the value of Ψ is defined relative to the steep section of the bi-linear reference USL, since the initial values of p' for these samples fall in the stress range corresponding to this portion of the USL.

For a given direction of loading (i.e. TC or TE), Ψ appears to provide a better link with each component of response for Phase I samples than did void ratio.

Reference state ratio (RSR)

Undrained triaxial response

The graphs in Figure 27 and Figure 28 are replotted in Figure 29 and Figure 30 in terms of the individual laboratory reference state ratio (RSR) of each sample. When examining the response of a sample in the laboratory, it is important to define RSR for the sample based on e_c and the laboratory applied stresses. This combination defines the state of the sample immediately prior to testing and influences how it will respond to undrained loading. RSR is defined relative to the appropriate section of the bi-linear reference USL shown in Figure 5 (see Table 2), depending on the value of e_c (i.e. whether it is greater than or less than the breakpoint void ratio of 0.979). For a given direction of loading (i.e. TC or TE) each component of response appears to be a function of RSR.

Note that Figure 30(d) presents the end-of-test values of M (which can be considered approximately equal to the ultimate values since the samples were all dilating towards or at ultimate state when the tests were stopped) versus RSR. Despite some scatter, over a large range of RSR, the triaxial compression tests (undisturbed and reconstituted) almost all resulted in similar values of M_C. With the exception of one sample (the reconstituted sample tested by U. of A.) which had an unusually high value of M_C=2.6, the triaxial compression samples (undisturbed and reconstituted) had an average M_C of 1.59 (SD=0.13). Likewise, over a range of RSR, most of the triaxial extension tests (undisturbed and reconstituted) generally resulted in similar values of M_E. With the exception of one sample (the reconstituted sample tested by U. of A.) which had an

higher value of M_E=1.3, the triaxial extension samples had an average M_E of 0.76 (SD=0.16). However, examining these tests more closely, it can be seen that the remaining reconstituted samples (tested by U.B.C.) tend to have lower values of M_E than the undisturbed samples. If only the undisturbed samples tested in triaxial extension are considered, the average M_E is 0.91 (SD=0.13). Using the equations given in the Introductory Data Review Report, the average M_C (undisturbed and reconstituted) correlates to an average friction angle, ϕ'_{us}, of 39.0° (SD=3.0°) and the observed M_E (undisturbed and reconstituted) correlates to an average friction angle, ϕ'_{us}, of 26.3° (SD=7.3°). Therefore, the triaxial compression and triaxial extension tests appear to result in different ultimate state friction angles, although there is considerable scatter in the triaxial extension tests. If only the undisturbed samples tested in triaxial extension are considered, the average M_E correlates to an average friction angle, ϕ'_{us}, of 32.6° (SD=6.5°), which is closer to the average value for the triaxial compression tests.

Undrained simple shear response

Figure 31 and Figure 32 present the simple shear test data from Table 5 in terms of the individual laboratory reference state ratio (RSR) of each sample, in a similar fashion as Figure 29 and Figure 30 presented the triaxial test data. Note, as explained previously, that the various components of simple shear response have been defined in terms of the applied shear stress on the horizontal plane, τ, and the measured vertical effective stress. Brittleness index is defined in terms of only the peak and minimum values of applied shear because all of the tests had an initial applied shear of zero. The initial value of vertical effective stress, σ'_{vi}, can be converted to an initial value of mean normal effective stress, p'_i, if an assumption is made about the initial value of K_o. A value of initial K_o=0.5 would be reasonable.

RSR profiles in-situ

Figure 33(a) to (d) present estimated profiles of RSR based on the SPT, CPT, shear wave velocity measurements and geophysical logging. These profiles were determined from

combining the void ratio profiles in Figure 16(a) to (d) with the reference USL, as explained in the Introductory Data Review Report. Note that Figure 16 used the V_s-based method of estimating void ratio from the SPT and CPT. This method was selected for illustrative purposes only. Any method to estimate state (either void ratio or state parameter) could be used. The value of RSR was referenced to either the flat or steep portion of the Syncrude reference USL shown in Figure 5 (see values of Γ and λ_{ln} in Table 2), depending on whether the estimated void ratio at any given depth was above or below the void ratio defining the breakpoint in the reference USL. Since the average (although borehole specific) values of X and Y in the target zone were used to estimate the void ratio profiles from the SPT and CPT, respectively, the RSR estimations outside of the target zone are not reliable. Note that RSR in Figure 33(a) to (d) is plotted on a scale from 0.01 to 100. Relative to the flat portion of the Syncrude sand reference USL (i.e. λ_{ln}=0.0152), this would correspond to a range in state parameter of Ψ= - 0.070 to Ψ= + 0.070. However, the estimated void ratio is generally less than the breakpoint void ratio and therefore RSR is referenced to the steep portion of the reference USL.

Superimposed on Figure 33(a) to (d) are solid dots representing the in-situ RSR values of the Quality I and II undisturbed frozen samples obtained at the Phase I site (see Table 3). The RSR values of the samples were determined by combining the estimates of in-situ void ratio for each sample (Hofmann, 1995) with the estimated in-situ stresses and the reference USL. The values of RSR were referenced to either the flat or steep portion of the Syncrude sand reference USL shown in Figure 5 (see values of Γ and λ_{ln} in Table 2), depending on whether the estimated void ratio of a particular sample was above or below the void ratio defining the breakpoint in the reference USL.

Comparing the RSR profiles estimated from the in-situ tests with the RSR of the undisturbed samples in Figure 33 is the same as comparing the void ratio estimated from the in-situ tests with the void ratio of the undisturbed samples in Figure 16, because void ratio was converted to RSR using the same method for both in-situ testing and the undisturbed samples. Therefore, as for the void ratio comparison in Figure 16, the range

in undisturbed sample RSR seems to be captured by all of the methods, but the CPT (interpreted using the shear-wave velocity based method) appears to best capture the detailed variability of RSR in the target zone at the Phase I site. Although there are definitely regions in the target zone where RSR > 1 would be estimated, the Quality I and II undisturbed samples that were trimmed for testing seem to indicate that over most of the target zone, the in-situ RSR ranges between approximately 0.3 and 0.9. The interpretations of the in-situ testing predict a similar conclusion.

Link between field and laboratory data

The undrained response observed in the laboratory is linked to the RSR of the sample immediately prior to shearing; i.e. at the void ratio after thaw and consolidation and under the anisotropic stress state imposed in the laboratory. Based on the relationships between response and state (RSR) in the laboratory, the true in-situ response at the depth at which the sample was obtained would only be equal to the response of the sample if the in-situ state (RSR) were the same as the laboratory state (RSR) of the sample. Figure 34(a) compares the estimated in-situ void ratio of each undisturbed sample that was subjected to monotonic loading (Hofmann, 1995) with the void ratio immediately before testing in the laboratory (as reported by each laboratory that tested samples). Figure 34(b) compares the estimated in-situ RSR of each of these undisturbed samples with the RSR immediately before testing in the laboratory. Both the laboratory and estimated field values of void ratio and RSR for each sample are summarized in Table 3. Note that a comparison can not be made for the TC test performed by Ayoubian (1996) because documentation as to which undisturbed sample was used was not available.

Figure 34(a) shows that most of the undisturbed samples subjected to monotonic loading experienced fairly large changes in void ratio during thaw and consolidation, with the void ratio immediately prior to testing ($e_{lab} = e_c$) being smaller than the estimated in-situ void ratio (e_{field}). In general, the triaxial samples tested by U. of A. appear to have experienced smaller changes in void ratio during thaw and consolidation than the triaxial

samples tested by U.B.C., which in turn experienced smaller changes than those tested by Laval. In general, the UBC simple shear samples appear to have experienced smaller changes in void ratio during thaw and consolidation than did the UBC triaxial samples.

Figure 34(b) shows that for all of the undisturbed triaxial samples, the RSR immediately prior to testing (RSR_{lab}) was generally close to, but smaller than the estimated in-situ RSR (RSR_{field}). It is important to note that the relationship between RSR_{lab} and RSR_{field} for any given sample is not directly equivalent to the relationship between e_{lab} and e_{field} for the same sample because RSR is influenced by both void ratio and mean normal effective stress state. The mean normal effective stresses placed on the sample in the laboratory (used to calculate RSR_{lab}) may not have been exactly the same as those estimated in-situ when estimating RSR_{field}, although, in general, the laboratories attempted to simulate the in-situ stresses quite closely. For void ratios less than the breakpoint value (i.e. most of the undisturbed samples), for which RSR is referenced to the steeper portion of the USL, differences in void ratio can be larger before resulting in significant differences in RSR.

Based on the above observations, it is reasonable to conclude that the response of most of the undisturbed samples in the laboratory would differ slightly from the in-situ material located at the same depths from which the undisturbed samples were obtained. Since there is a change in "state" between the in-situ condition of the sample and the laboratory condition after thaw and consolidation, it can be difficult to conclude precisely the in-situ response to loading based only on the laboratory results. However, constitutive modelling, as described in the Introductory Data Review Report, can be used to aid in the interpolation and extrapolation of the laboratory data into the in-situ range of soil state. This will be discussed in the final data review report.

3.4 Conclusions

Overall, the Syncrude sand in the target zone at Phase I appears to be generally strain-hardening in undrained triaxial compression and only slightly strain-softening in

undrained triaxial extension and simple shear. On average, it appears that in monotonic loading, the sand would strain harden to high strength ratios under undrained triaxial compression, but would demonstrate limited strain softening in undrained triaxial extension and simple shear, reaching a low strength ratio temporarily before strain hardening to a high strength ratio. Axial strains while at the low strength ratio (i.e. QSS) would be expected to be less than 5%, on average. On average, based on triaxial compression tests, the material appears to have an ultimate friction angle of 39°.

Therefore, on average, the material in the target zone would likely not be susceptible to flow liquefaction, given a suitable trigger mechanism. However, it is often not the average properties of a soil mass that govern the overall response; the presence of a particular weak layer may provide the weak-link-in-the-chain that controls the response. However, the six CPTs show little or no evidence of a continuous loose sand layer within the target zone of the small test area (having a diameter of approximately 10 m).

4. FLOW LIQUEFACTION – PHASE III SITE

4.1 Site Description

The Phase III site is situated in J-pit (an old borrow pit) at Syncrude Canada Ltd. (see Figure 35), which is located just beyond the northwest corner of the Mildred Lake Settling Basin (see Figure 8). At the time of the site investigation, the Phase III site consisted of artificially deposited sand that was less than one month old. The sand was deposited in J-pit, as part of the CANLEX project, in order to create a loose sand deposit. Following the detailed site characterization, an impoundment was built on top of this loose sand deposit and was rapidly filled in order to attempt to conduct a full scale liquefaction field test. The J-pit site was initially selected as a result of the CANLEX full scale field test planning activity (Byrne et al., 1994). An extensive seismic CPT investigation was carried out over a large area of the Phase III site, after the sand was deposited. Based on these results, the location of the specific area for detailed in-situ testing and ground freezing and sampling was selected. The target zone for undisturbed sampling and in-situ testing in this area was selected from 3 to 7 m depth, based on the initial site screening. The groundwater table at the site is located, on average, at a depth of approximately 0.5 m. Figure 36(a) shows the location of the specific testing area relative to the embankment and the rest of the CPT investigation across the J-pit site. Figure 36(b) shows a detailed site plan of the testing area, indicating the locations of the various in-situ tests relative to the freezepipe and sampling boreholes.

Three SPTs, identified as SPT1, SPT2 and SPT3, were conducted through the target zone at the Phase III site (Iravani et al., 1995). Detailed SPT logs are given in Appendix J. All of the SPTs were carried out by Mobile Augers and Research Ltd. in mud-rotary advanced boreholes using an 82.6 mm carbide bit and AW drill rods. All of the SPTs were conducted using a standard 63.5 kg (140 lb) safety hammer that was dropped 760 mm (30 inches) using an electric winch. Energy measurements were not carried out for these three SPTs. Therefore, a fourth SPT (SPT4) with energy measurements was

conducted nearby at a later date. The same set-up was used as for the first three SPTs and, therefore, the average energy ratio calculated from SPT4 (ER = 49.6%) was assumed to be applicable as the average energy ratio for SPT1, SPT2 and SPT3.

Four CPTs (CPT20 through to CPT23), were conducted through the target zone in the detailed testing area of the Phase III site (Iravani et al., 1995; after ConeTec, 1995). Since none of these CPTs were seismic CPTs, the results of the two closest seismic CPTs (CPT26 and CPT27) that were carried out as part of the initial site screening (see Figure 36(a)) have also been included in this data review. Detailed CPT logs are contained in Appendix K. All of the CPT work was carried out by ConeTec Investigation Ltd.

As explained above, two of the six CPTs presented here were seismic CPTs and thus, two shear wave velocity logs, identified as CPT26 and CPT27, were conducted through the target zone at the Phase III site (Iravani et al., 1995; after ConeTec, 1995). Detailed shear wave velocity logs are given in Appendix L. The shear wave velocity logs may contain some errors associated with conducting the tests at rather shallow depths.

Two geophysical logs, identified as GEO1 and GEO2, were conducted through the target zone at the Phase III site (Iravani et al., 1995; after Skirrow, 1995). Each geophysical hole was logged three times with each of two geophysical tools (9071A and 9036AA from Century Geophysics (Canada) Corporation). Readings were taken every 2 cm; however, in order to reduce "noise", the data were processed using a 5 point smoothing filter. The average interpreted void ratios from the three runs in each borehole were used in this report. It is important to note that the report by Skirrow (1995) concluded that "GEO1 may be said to be of lower quality than GEO 2" and that "for the most part both boreholes do not meet the criteria for high quality density logging results for liquefaction assessment application" due to "high compensation values" that "are likely due to excessive borehole rugosity, as indicated by the borehole caliper results, and probable filter cake build-up". Detailed geophysical logs for these runs are given in Appendix M.

Pressuremeter testing was also carried out in the target zone at Phase III (Hughes, 1996). A total of nineteen self-boring pressuremeter tests were conducted in three boreholes (SBPMT1, SBPMT2 and SBPMT3). The interpreted results for the nineteen pressuremeter tests are given in Appendix N. Thirteen of these tests (five from SBPMT1, five from SBPMT2, and all three from SBPMT3) were located at depths within the target zone. The interpretation of the pressuremeter results by Hughes (1996) suggests an average K_o of about 0.5, but there was some uncertainty in the interpretation. This report adopted an average K_o of 0.5 for interpretation of the Phase III site.

Two DMT soundings were also carried out in the Phase III target zone.

4.2 Estimation of In-situ State

a) Void ratio

i) Direct methods

Undisturbed samples

Successful ground freezing and sampling was carried out at the Phase III site (Hofmann and Sego, 1995), resulting in 6.9 m of 200 mm diameter undisturbed sandy soil core and 3.9 m of 100 mm diameter undisturbed sandy soil core (Hofmann, 1997). Samples of different dimensions were trimmed from these cores in order to produce samples for both triaxial testing and simple shear testing. The void ratio of each sample was calculated at the University of Alberta using volume calculations (Hofmann, 1995) prior to sending the samples out to the various laboratories to be tested.

Figure 37 summarizes the void ratios for each undisturbed frozen sample from Phase III. The solid dots represent the void ratios of the undisturbed frozen samples. The void ratios for the undisturbed samples are summarized in Table 7. Note that void ratio axis in Figure 37 has been plotted from 0.5 to 1.0, corresponding approximately to e_{min} and e_{max}

for the sand at the Phase III site (based on a fines content ranging from 10% to 40%; see Table 1). Thus approximate relative densities (D_r) for the soil samples can be computed directly from Figure 37. The thick solid horizontal lines at 3 m and 7 m in this figure and in subsequent figures indicate the extent of the target zone at Phase III.

For the undisturbed samples in Figure 37, the average void ratio is 0.762 (SD=0.053) ($D_r \approx 43\%$; SD=10%; based on e_{min} and e_{max} for FC = 10% to 40%, see Table 1). Some uncertainty exists in the values of relative density for these samples because the Phase III sand has different values of e_{min} and e_{max} depending on fines content (see Table 1). The thick semi-vertical line in Figure 37 represents void ratios corresponding to the Syncrude reference USL (see Figure 5 and Table 2) at the effective stresses present over the target zone, using a K_o of 0.5. This line corresponds to a relative density of approximately 23%. The undisturbed samples that were trimmed for testing have a wide range of void ratios, all less than the line (i.e. $D_r > 23\%$), except for one on the line (i.e. $D_r \approx 23\%$).

Figure 38 presents a comparison between the estimated in-situ void ratios calculated at U. of A. before sending the undisturbed samples out for testing (Hofmann, 1995) and those back-calculated by the testing laboratory (Vaid et al., 1996). In general, the Hofmann (1995) method appears to give similar values of void ratio for triaxial samples, but lower values of void ratio than the Vaid et al. (1996) method for simple shear samples and cyclic simple shear samples. For the remainder of this report, the void ratios calculated by Hofmann (1995) will be used as the estimated in-situ void ratios; however, these void ratios should be considered to be accurate to only approximately $\pm$ 0.01.

Geophysical logging

Figure 39 presents the results of the void ratio interpretation of the geophysical logs, as given by Skirrow (1995). Skirrow (1995) used G_s=2.63 for interpreting the geophysical logs. Superimposed on Figure 39 are the void ratios shown in Figure 37 for the undisturbed samples (G_s=2.62). The void ratio axis in Figure 39 has been plotted ranging

from 0.50 to 1.0, corresponding approximately to e_{min} and e_{max} for the sand at the Phase III site and the thick semi-vertical line represents the reference USL ($D_r \approx 23\%$).

The interpretation of the geophysical logs appears to slightly underpredict the average, but capture the range of void ratios from the frozen samples measured to date, predicting an average void ratio of 0.736 (SD=0.091) in the target zone. The geophysical logs (especially GEO1) predict a very rapid variation of void ratio. However, Skirrow (1993) reported that GEO1 was of poor quality due to "excessive borehole rugosity". Hence, based only on GEO2, the average void ratio is e = 0.721 (SD=0.068).

ii) Indirect methods

In-situ test profiles

Figure 40(a) to Figure 40(c) present the in-situ test signatures, corrected for effective overburden stress (and energy effects, in the case of the SPT profiles), for each of the SPTs, CPTs, and shear wave velocity logs at Phase III. In Figure 40(a), the SPT profiles are shown as discrete points with attached bars, corresponding to the midpoint and range, respectively, of the 30 cm over which the value of N was measured. In Figure 40(b), the CPT profiles are shown as continuous profiles, since measurements were taken every few centimetres. In Figure 40(c), the shear wave velocity profiles are shown as step functions, indicating that the shear wave velocity was measured (using a method of differences), as an average value over a given interval (typically about 1 m).

The two V_{s1} and six q_{c1} profiles are generally consistent with little scatter; however, CPT21 appears to indicate two zones in the target zone with higher tip resistances that are not evident in the other CPT profiles. The three $(N_1)_{60}$ profiles show some scatter. The CPT profiles do show some variability in the deposit. In the target zone, the average measured values are: V_{s1}=127.1 m/s (SD=3.0 m/s), q_{c1}=2.35 MPa (SD=1.53 MPa) (or 2.04 MPa (SD=0.79 MPa) if CPT21 is not included), and $(N_1)_{60}$= 3.4 (SD=2.0).

Figure 41(a) to Figure 41(d) present the estimated void ratio profiles at Phase III, based on D_r-based interpretations of the SPT and CPT, and interpretations of the shear wave velocity measurements. These interpretations are discussed in more detail below. The void ratios of the undisturbed frozen samples are superimposed on the plots for comparison. Again, the void ratio axes have been plotted from 0.50 to 1.0, corresponding approximately to e_{min} and e_{max} for the sand at Phase III, and the thick semi-vertical lines represent the reference USL ($D_r \approx 23\%$). Figure 41(d) presents the interpretations of the geophysical logs for comparison.

SPT

Figure 41(a) presents the results of the D_r-based void ratio interpretation of the SPT, based on the method by Skempton (1986), as outlined in the Introductory Data Review Report, using a value of 40 for the constant in the Skempton (1986) equation relating D_r to $(N_1)_{60}$. This should be reasonable for a loose sand with a relatively low fines content. In general, the D_r-based interpretation of the SPT at the Phase III site appears to overpredict the average of the undisturbed void ratios, but underpredict the overall range in void ratios, giving an overall average void ratio in the target zone of 0.816 (SD=0.041).

During the SPT investigation at the Phase III site, it was observed that the rate of penetration generally increased after the initial one or two blows. This indicated a possible high build-up of pore pressures due to the dynamic nature of the test.

CPT

Figure 41(b) presents the results of the D_r-based void ratio interpretation of the CPT, based on the method by Baldi et al. (1986), as outlined in the Introductory Data Review Report. In order to apply this method, it was assumed that the Phase III sand has grain characteristics similar enough to Ticino sand. Thus, the Ticino sand values for the material constants C_0, C_1, and C_2 could be used in the equation developed by Baldi et al.

(1986) relating tip resistance to D_r. This is not a very good assumption, based on the comparison between index parameters for Ticino sand and Phase III sand, as shown in Table 1. Consequently, the interpretations of void ratio based on the D_r-based method of interpreting the CPT at the Phase III site overpredict the average and do not capture the range of void ratios of the frozen samples. The overall predicted average void ratio in the target zone using this method is 0.893 (SD = 0.069).

Shear wave velocity

Figure 41(c) presents the results of the void ratio interpretation of the shear wave velocity, as outlined in the Introductory Data Review Report and the values of A and B for Phase III sand given in Table 2. The interpretations of void ratio from the shear wave velocity measurements at the Phase III site completely overpredict the void ratios for the frozen samples, predicting an average void ratio of 0.917 (SD=0.017) in the target zone.

Seismic CPT26 had shear wave velocity measurements made using a steel beam as a source, while seismic CPT27 had a steel auger embedded 2.2 m in the ground as a source. The individual profiles of shear wave velocity were corrected for the corresponding offsets. However, it is likely that the shear wave velocity profiles are not completely representative of the soil in-situ as a result of errors arising from conducting the tests at rather shallow depths (3 to 7 m in the target zone). This may at least partially explain the observed discrepancy between the measured and predicted void ratios in Figure 41(c). It is also possible that the shear wave velocity measurements may have been more influenced by the in-situ skeletal void ratio than the in-situ total void ratio.

iii) Correlations between in-situ tests

In order to compare the CPT and the SPT, the closest pairs of test types were determined by examining the detailed site plan (see Figure 36). SPT1 and CPT23 were paired together, SPT2 and CPT22 were paired together, and SPT3 and CPT20 were paired

together. Therefore, based on the comparisons between the three pairs of in-situ tests, Figure 42(a) shows that the value of $q_{c1}/(N_1)_{60}$ appears to be rather scattered in the target zone, with an average value of approximately 0.51 (SD=0.25). This average value is consistent with published values for a sand. The average $q_{c1}/(N_1)_{60}$ is slightly larger (and has more scatter) than the $q_{c1}/(N_1)_{60}$ of 0.44 (SD=0.15) at the Phase I site.

Comparing the CPT and shear wave velocity was straightforward because each CPT and shear wave velocity pair were conducted in the same hole and are directly comparable. However, no seismic CPTs were conducted in the detailed test area. Therefore, nearby seismic CPT26 and seismic CPT 27 were used in this analysis. In the target zone at the Phase III site, as shown in Figure 42(b), the value of Y was found to have an average value of 101.1 (SD=6.3) in the target zone, corresponding to a somewhat incompressible sand. This value of Y is larger than the value of 95.6 (SD=12.1) at the Phase I site.

In order to compare the SPT and shear wave velocity, the closest pairs of test types were determined by examining the detailed site plan (see Figure 36). SPT1 and seismic CPT26 were paired together and SPT2 and seismic CPT27 were paired together. It was felt that there was no seismic CPT close enough to SPT3 to make a direct comparison. In fact, since no seismic CPTs were conducted in the detailed test area, seismic CPT26 is fairly far from SPT1 and seismic CPT27 is fairly far from SPT2. Based on the comparison between these two pairs of in-situ tests, Figure 42(c) shows that the value of X was somewhat scattered, with an average value of 89.2 (SD=7.5) in the target zone. This value of X is higher than the value of 74.8 (SD=9.0) at the Phase I site.

Note that, as at Phase I, one would generally expect the values of $q_{c1}/(N_1)_{60}$ and X to be less reliable than the values of Y, since each profile of either $q_{c1}/(N_1)_{60}$ or X is determined from pairing an SPT borehole with a seismic CPT borehole, whereas each profile of Y is determined within a single seismic CPT borehole. However, because the shear wave velocity measurements themselves may be unreliable at Phase III, this may not be true.

iv) Shear wave velocity (V_s) based method of interpreting the SPT and CPT

Figure 43(a) to Figure 43(d) compare the V_s-based method of interpreting void ratio from the SPT and the CPT with the interpretations of void ratio from the shear wave velocity logs and the geophysical logs at the Phase III site. The V_s-based interpretations of both the SPT and CPT followed the methods outlined in the Introductory Data Review Report. Borehole-specific average values of X in the target zone were used to interpret the SPT profiles and borehole-specific values of Y in the target zone were used to interpret the CPT profiles. As a result, the void ratio estimations outside of the target zone are not reliable. However, it is only within the target zone that frozen samples are available for comparison. To be absolutely correct (particularly if applying this method for design purposes), values of X and Y that vary with depth should be used to interpret the CPT and SPT using the V_s-based method. However, this report has used average (although borehole-specific) values of both X and Y, for ease of calculation. The values of A and B that were used for the V_s-based interpretations of void ratio from the CPT and SPT at the Phase III site are given in Table 2. In Figure 43(a) to Figure 43(d), as in Figure 41(a) to Figure 41(d), the void ratios of the undisturbed frozen samples are shown, for comparison, and the reference USL ($D_r \approx 23\%$) is also indicated.

Comparing Figure 43(a) with Figure 41(a), it appears that the V_s-based method of interpreting the SPT gives results that agree less with the frozen samples, in terms of trend and range of void ratios, than the D_r-based method of interpretation. The poor agreement with the frozen samples is because interpretation of the shear wave velocity logs themselves does not result in a good prediction of the void ratios in-situ. The V_s-based method predicts an average void ratio in the target zone of 1.048 (SD = 0.275).

Comparing Figure 43(b) with Figure 41(b), it appears that the V_s-based method of interpreting the CPT also gives results that agree less with the frozen samples, in terms of trend and range of void ratios, than the D_r-based method of interpretation. The poor agreement with the frozen samples is because interpretation of the shear wave velocity logs themselves does not result in a good prediction of the void ratios in-situ. The

V_s-based method predicts an average void ratio in the target zone of 0.958 (SD = 0.085).

b) State parameter

i) Direct methods

CPT

Sladen and Hewitt (1989)

As explained previously for Phase I, based on values of e_{max}, e_{min}, G_s, average FC, D_{50} and D_{10} (see Table 1), Syncrude sand at Phase III initially appears to be somewhat similar to Nerlerk and Ukalerk (sometimes called Erksak; Sladen and Hewitt, 1989) sands (see soil descriptions in the Introductory Data Review Report). These sands were used to develop the field observation based relationship outlined in the Introductory Data Review Report that was proposed by Sladen and Hewitt (1989) to determine whether or not Nerlerk or Ukalerk (Erksak) sands were susceptible to flow liquefaction. Consequently, it would seem reasonable to apply the Sladen and Hewitt (1989) dividing line directly to the CPT data from the target zone at the Phase III site. However, as outlined in the Introductory Data Review Report, the best method of estimating if the response of two sands will be similar is to examine their USLs. As discussed earlier for the Phase I site, at low stresses (p'<200 kPa), although the USL for each sand has a similar slope, λ_{10} (0.0152 for Syncrude; 0.014 for Nerlerk; 0.013 for Ukalerk/Erksak), the value of Γ is quite different (0.919 for Syncrude; 0.885 for Nerlerk; 0.82 for Ukalerk/Erksak), with the result being that the Syncrude USL would be located at higher void ratios than either the Nerlerk or Ukalerk/Erksak USLs on an e-p' plot (see Figure 44(a)).

Based on a groundwater table at a depth of 0.5 m and unit weights of soil as given in Table 1, the Sladen and Hewitt (1989) relationship given in the Introductory Data Review Report can be converted to a liquefaction/non-liquefaction dividing line in terms of q_c versus depth. This dividing line is shown superimposed over CPT data from the target

zone at Phase III in Figure 44(b). In the target zone (3 to 7 m), the field observation method by Sladen and Hewitt (1989) for Nerlerk and Ukalerk (Erksak) sands, when applied directly, would predict that, on average, the material in the target zone at Phase III is susceptible to flow liquefaction. However, the USL for Syncrude sand is different that that for Nerlerk sand. Figure 44(a) clearly indicates that to move the Nerlerk USL or the Ukalerk/Erksak USL to the Syncrude USL on an e-p' plot would require an upward shift in void ratio. This would translate into a significant shift to the left in the Sladen and Hewitt (1989) dividing line shown in Figure 44(b), possibly resulting in a different evaluation of flow liquefaction potential in the Phase III target zone. However, the exact size of the corresponding shift is not clear at this point.

Been and Jefferies (1992)

Superimposed over CPT data from the target zone at the Phase III site, Figure 45 presents the dividing line (Ψ=0) determined for Syncrude sand using the method proposed by Been and Jefferies (1992). This method is based on correlating CPT results with state parameter for various soils, as outlined in the Introductory Data Review Report. The dividing line was determined using the equations given in the Introductory Data Review Report, assuming $B_q \approx 0$ in sandy deposits. The measured CPT profiles confirm that B_q was often small (see Appendix K). M was assigned a value of 1.4, the approximate average laboratory measured value for triaxial compression tests (M_C) on undisturbed samples from the Phase III site, as presented later in this report. The corresponding friction angle, ϕ' is approximately 34.7°, based on the equation relating M_C and ϕ' given in the Introductory Data Review Report. Since the range of stresses in the target zone at Phase III is low, the flatter part of the bi-linear USL can be used to estimate the state dividing line. This part of the USL has a λ_{10} of 0.0152 (see Table 2) which corresponds to a λ_{10g} of 0.035. Combining the five equations given in the Introductory Data Review Report, using the groundwater table depth and unit weights given in Table 1, and setting Ψ equal to zero results in the dividing line in terms of q_c versus depth as indicated in Figure 45. Also shown in Figure 45 are the lines for Ψ= - 0.05 and Ψ= -0.1.

In the target zone (3 to 7 m), the Been and Jefferies (1992) method would predict that the sand is on the borderline of being able to experience flow liquefaction because, in general, the entire deposit straddles the Ψ=0 dividing line. The sand appears to have greater potential for flow liquefaction at the top of the target zone than at the bottom of the target zone. The average predicted state is Ψ = + 0.010 (SD = 0.019). Based on the undisturbed samples from the Phase III site (see Table 7), the estimated mean in-situ state parameter is Ψ= -0.106 (SD=0.053), corresponding to a denser state than that predicted by the Been and Jefferies (1992) approach.

Plewes et al. (1992)

Figure 46 shows the CPT data from the target zone at the Phase III site plotted on the soil classification chart after Jefferies and Davies (1991), as proposed by Plewes et al. (1992) for estimating contours of state parameter. The method outlined in the Introductory Data Review Report with its associated assumptions was followed to produce the plot. On this soil classification chart, the material in the target zone (3 to 7 m) plots mostly in Zone 5 (silty sand to sandy silt) and Zone 6 (clean sand to silty sand), with some data falling in Zone 4 (clayey silt to silty clay) and Zone 7 (gravelly sands).

Figure 47 presents the Plewes et al. (1992) interpretation of the CPT data in the form of profiles of Ψ at the Phase III site. In order to produce the profiles of Ψ, M was assigned a value of 1.4, the approximate average laboratory measured value for triaxial compression tests (M_c) on undisturbed samples from Phase III. Note that this differs slightly from the M of 1.2 that Plewes et al. (1992) assumed in order to produce the contours of Ψ on their soil classification chart, as shown in Figure 46. Superimposed on Figure 47 is a thick vertical line representing the Ψ=0 state. By examining either Figure 46 or Figure 47, one can see that the method by Plewes et al. (1992) predicts an approximate average state of Ψ = - 0.069 (SD=0.035) in the Phase III target zone. This would suggest that the material is dense of ultimate state and would not be susceptible to flow liquefaction. This

conclusion does not agree with the prediction using the Been and Jefferies (1992). Application of the method by Plewes et al. (1992) allows for variability in compressiblity within the soil deposit (since the slope of the USL is estimated from F) whereas, in order to apply the method by Been and Jefferies (1992), a single USL slope needs to be assumed. The values of Ψ for the undisturbed frozen samples from the Phase III target zone are also shown on Figure 47 for comparison. The Plewes et al. (1992) based interpretation tends to overestimate the average, but underestimate the range of the Ψ of the undisturbed samples (having an average Ψ = - 0.106; SD=0.053). However, the Plewes et al. (1992) method matches the states of the undisturbed samples better than the Been and Jefferies (1992) method.

With vertical effective stresses ranging from approximately 35 kPa to 75 kPa and a K_o of 0.5, the Phase III target zone has an approximate range in mean normal effective stress, p', from 25 kPa to 50 kPa. Given that the reference USL in this stress range has been defined by Γ=0.919 and λ_{ln}=0.0152, the profiles of Ψ predicted using the method by Plewes et al. (1992) can be converted into profiles of void ratio, as shown in Figure 48. The void ratios of the undisturbed frozen samples are also shown for comparison. Comparing the void ratio profiles estimated from the in-situ tests with the void ratios of the undisturbed samples in Figure 48 is the same as comparing Ψ estimated from the in-situ tests with Ψ of the undisturbed samples in Figure 47, because the same relationship between Ψ and void ratio was used for both the in-situ testing and the undisturbed samples. The Plewes et al. (1992) interpretation predicts an average void ratio of 0.797 (SD=0.035), which slightly overestimates the average and underestimates the range of the void ratios of the undisturbed samples (average = 0.762; SD=0.053).

Self-boring pressuremeter

The results of the 13 self-boring pressuremeter tests in the target zone at the Phase III site could be used to estimate state parameter, following the methods by Yu (1994) and/or Yu et al. (1996), as described in the Introductory Data Review Report. An interpretation of

these pressuremeter tests using the method by Yu (1994) was not available.

Yu et al. (1996) proposed combining pressuremeter data and CPT data to estimate state parameter (see Figure 49(a)). The effective pressuremeter limit pressure from the 13 tests in the target zone at the Phase III site is approximately 190 kPa (see Appendix N). Note that in sandy soils, it is difficult to determine a limit pressure from a pressuremeter test, since the pressuremeter response curve does not always level off, but often continues to rise; therefore, for the analysis presented here, the end of the expansion part of the pressuremeter curve was taken as the pressure at 10% strain (essentially the limit pressure in all of the tests). The average measured cone tip resistance (q_c) associated with the depth ranges of the pressuremeter testing is approximately 1655 kPa. With the average initial pore pressure over the depth ranges of the pressuremeter testing being approximately 45 kPa, the average effective cone tip resistance is approximately 1610 kPa. Figure 49(b) shows that, when the effective pressuremeter and cone data are combined as a ratio (having a value of approximately 9.8), an average state parameter of Ψ = -0.204 is predicted. This underestimates the state of the frozen samples.

Appendix P includes a paper by Hughes et al. (1997) which provides a "broad-brush" interpretation of the state of the sand in the Phase III target zone based on the self-boring pressuremeter testing results. The paper concludes that "the sand at 4.5 m depth at J-pit is close to the critical state line and hence, would be very close to an unstable state".

ii) Indirect methods

When combined with the reference USL for Syncrude sand, at the appropriate stress level, any of the methods used above to estimate void ratio at the Phase III site can also be used to estimate state parameter. As explained above, with vertical effective stresses ranging from 35 kPa to 75 kPa and a K_o of 0.5, the Phase III site target zone has an approximate range in mean normal effective stress, p', from 25 kPa to 50 kPa. Given that the reference USL in this stress range has been defined by Γ=0.919 and λ_{ln}=0.0152, the

interpreted ranges in void ratio based on the SPT, CPT, V_s measurements and geophysical logs can be converted into ranges in state parameter.

Figure 50(a) to (d) present estimated profiles of state parameter in the target zone at the Phase III site from the D_r-based interpretations of void ratio from the SPT and CPT and the void ratio interpretations of the shear wave velocity and geophysical logs, as shown previously in Figure 43(a) to Figure 43(d). In the target zone, the D_r-based interpretation of the SPT predicts an average Ψ = -0.049 (SD=0.041). In the target zone, the D_r-based interpretation of the CPT predicts an average Ψ = 0.027 (SD=0.068), the interpretation of the shear wave velocity logs predicts an average Ψ = 0.051 (SD=0.019) and the interpretation of the geophysical logs predicts an average Ψ = -0.127 (SD=0.091).

Superimposed on Figure 50(a) to Figure 50(d) are the calculated values of state parameter for the undisturbed samples, based on the selected reference USL for Syncrude sand. The thick semi-vertical line represents the reference USL (i.e. Ψ=0). Comparing the Ψ profiles estimated from the in-situ tests with the Ψ of the undisturbed samples in Figure 50 is the same as comparing void ratios estimated from the in-situ tests with void ratios of the undisturbed samples in Figure 41, because void ratio was converted to Ψ using the same method for both in-situ testing and the undisturbed samples. Therefore, as for the void ratio comparison in Figure 41, the range in undisturbed sample Ψ seems to be captured best by the geophysical logging. Based on the undisturbed samples, the average estimated in-situ state parameter is Ψ= -0.106 (SD=0.053).

4.3 In-situ Response to Undrained Loading

a) Direct methods

Figure 51 presents an enlarged version of Figure 37. Different symbols have been used in Figure 51 for each undisturbed frozen sample (FS) indicating to which laboratory it was

sent (all Phase III samples that have been tested were sent to U.B.C.) and the type of test that was performed. The one loosest sample (i.e. with a void ratios on the reference USL) was subjected to a triaxial compression (TC) test. All other samples were denser than the USL. In addition, all of the samples experienced small changes in void ratio during thaw and consolidation. After thaw and consolidation, only one sample (one tested in triaxial extension) was looser than the reference USL. The changes in void ratio during thaw and consolidation will be discussed further later in this report.

The complete stress-strain response curves for all of the laboratory tests are presented in Appendix O. Results from triaxial (compression and extension) tests on undisturbed samples of Syncrude sand from the Phase III site are presented. No reconstituted samples of Phase III sand were tested.

i) Undisturbed triaxial samples

Table 8 summarizes the undrained triaxial compression and extension test results for undisturbed samples of Syncrude sand from the Phase III site. The individual tests are identified by the laboratory that conducted the testing as well as the sampling identification number assigned by Hofmann (1995). The results of testing each sample in undrained monotonic loading is broken down into the individual components of response, as outlined in the Introductory Data Review Report. Based on the definitions of response shown in the Introductory Data Review Report, each undrained TC and TE stress-strain curve (see Appendix O) has been divided into four main points: (A) initial state, (B) peak (or yield) state, (C) minimum state and (D) ultimate state.

Initial state

The initial state of each sample is defined by its void ratio after thaw and consolidation (e_c) and the vertical and horizontal effective stresses (σ'_{vi} and σ'_{hi}) placed on it. The values of e_c, σ'_{vi} and σ'_{hi} for the samples are those that were reported by the laboratory

(U.B.C.) that conducted the testing. For a given sample, the value of e_c is generally less than the void ratio in-situ (see Table 7), as estimated by Hofmann (1995), as a result of volume changes that occur during thaw and consolidation. The difference between the in-situ void ratio and e_c will be discussed later in this report.

Stress-strain response

None of the Phase III undisturbed samples that were tested strain-softened directly to their ultimate state during a triaxial test. All of the samples strain-hardened towards their ultimate state. However, three of the nine undisturbed samples that were subjected to triaxial extension and two of the ten undisturbed samples that were subjected to triaxial compression demonstrated limited strain-softening in that they strain-softened to a quasi-steady state (QSS) before eventually, at large enough strains, strain-hardening towards ultimate state (see Appendix O).

For samples that strain-hardened to their ultimate state without demonstrating any limited strain-softening (six of the triaxial extension tests and eight of the triaxial compression tests), the peak and minimum values of p' and q were taken as equal to the end-of-test values of p' and q. Consequently, the peak and minimum strengths were taken as equal to the end-of-test strength (which can be generally considered to be close to the ultimate state strength). These samples responded to undrained triaxial compression loading in a non-brittle manner and were assigned I_B=0 (see the Introductory Data Review Report). These samples were also assigned an axial strain at minimum strength of zero because there was no minimum condition during the stress-strain curve.

For the samples that were tested in triaxial extension, a QSS point occurred. The corresponding stress-strain curves (see Appendix O) had distinct peak, minimum and ultimate points since the samples demonstrated limited strain-softening. For each test, the values of p' and q (and, hence, the values of strength) were determined for each of the three individual points along the stress-strain curve. The values of I_B for the samples

tested in triaxial extension were still small (< 0.15) because the samples were anisotropically consolidated to approximate the level ground in-situ stress state and were therefore preloaded in compression. Significant unloading had to occur before the samples experienced limited strain-softening. One of the triaxial compression tests had an $I_B = 0.25$, but the other (sample FS5 C1B 2B from a depth of 3.6 m) was apparently infinitely brittle (i.e. strain-softened right away from the initial state, when loaded undrained) and was assigned an $I_B = 5$ in order to plot the datapoint. Axial strains that occurred while at the QSS point (i.e. at the point of minimum strength) were also fairly small, ranging from approximately 4% to 11%. The minimum strengths of these samples were significantly smaller than the end-of-test strengths ($S_{min} \approx 0.04$ to 0.35 of S_f).

ii) Reconstituted samples

No testing has been performed to date on reconstituted samples of sand specifically from the Phase III Site.

iii) Undisturbed simple shear samples

Simple shear testing was performed on seven undisturbed frozen samples of Phase III sand. The tests were all carried out by U.B.C. and the results are presented in Appendix O. However, cycles of shear loading reversal were carried out on all of the samples tested in monotonic simple shear (see Appendix O). Only two of the samples experienced slight temporary strain-softening (QSS) before strain-hardening towards ultimate state. Table 9 summarizes the undrained monotonic simple shear test results for the undisturbed samples of Syncrude sand from the Phase III site. The individual tests are identified by the sampling identification number assigned by Hofmann (1995). All of the samples were still dilating under the initial direction of loading when the loading was reversed. Consequently, it is difficult to assess the end-of-test state for each sample and, therefore, Table 9 remains incomplete.

b) Indirect methods

i) Self-boring pressuremeter tests (SBPMT)

Appendix P contains a copy of a paper by Roy et al. (1996). Included in this paper is a description of the application of computer aided modelling (CAM) techniques to pressuremeter data from the Phase III site. The computer aided modelling is used to first produce an acceptable match with pressuremeter test results; based on the model parameters required to produce an acceptable match, the in-situ response of the soil is then estimated and compared to laboratory results.

ii) Link with in-situ state

Void ratio

Figure 52 and Figure 53 present the various components of response of all of the undrained triaxial tests (with no loading reversal) on anisotropically consolidated undisturbed Phase III site samples tested to date in terms of the individual laboratory void ratio of each sample. In addition, Figure 52(a) presents the initial conditions of each sample relative to the selected Syncrude reference USL and Figure 53(a) presents the end-of-test conditions of each sample relative to the same USL. The undisturbed samples can be divided into two groups that were each tested over a different range in initial p'. The first range was from p'=25 kPa to p'=45 kPa (11 samples; average p'≈30 kPa), which is approximately equal to the range in-situ p' in the target zone (3 m to 7 m) at the Phase III site. The second range was from p'=55 kPa to p'=200 kPa (8 samples; average p'≈125 kPa), which is to simulate the stresses which would be imposed on the soil if the full-scale liquefaction test embankment were constructed above the detailed test area.

Figure 52(b) to Figure 52(d) and Figure 53(b) to Figure 53(d) present the components of response as follows: brittleness index (I_B), minimum strength ratio (S_{min}/p'_i), axial strain during minimum strength (ε_a), end-of-test strength ratio (S_f/p'_i), peak stress ratio (M_p) and

end-of-test stress ratio (M_f). Definitions of each of these terms are given in the Introductory Data Review Report. For a given direction of loading (i.e. TC or TE) each component of response appears to be generally a function of void ratio, but the relationships are not unique since the data are for a range in stress level. The trends suggested by Figure 52 and Figure 53 apply strictly to Phase III sand and are not applicable to all sands in general. This is due to the fact that different sands have different USLs and will respond in different ways, even when at the same void ratio.

Relative density

The graphs in Figure 52 and Figure 53 have been plotted with the laboratory void ratio axes ranging from 0.50 to 1.0, corresponding approximately to e_{min} and e_{max} for the sand at Phase III (see Table 1). Thus, approximate relative densities (D_r) can be computed directly from Figure 52 and Figure 53. Hence, similar conclusions can be drawn about the relationships between the various components of response and D_r as were drawn above about the relationships between the various components of response and void ratio. Although normalizing test data with respect to a soil's individual values of e_{min} and e_{max} may account for some of the differences between various soils with different USLs, the relationships between undrained response and relative density suggested Figure 52 and Figure 53 are not unique since the data are for a range in stress level.

State parameter

The graphs in Figure 52 and Figure 53 are replotted in Figure 54 and Figure 55 in terms of the individual laboratory state parameter of each sample. When examining response of samples in the laboratory, it is important to define Ψ for each sample based on e_c and the laboratory applied stresses. This combination defines the state of the sample immediately prior to testing and influences how it will respond to undrained loading. The value of Ψ is defined relative to the flat section of the bi-linear reference USL, since the initial values of p' for the samples all fall in the stress range corresponding to this portion of the USL.

For a given direction of loading (i.e. TC or TE), Ψ appears to provide a better link with each component of response than did void ratio. However, the relationship is still not unique because the data are for a range in stress level.

Reference state ratio (RSR)

Undrained triaxial response

The graphs in Figure 54 and Figure 55 are replotted in Figure 56 and Figure 57 in terms of the individual laboratory reference state ratio (RSR) of each sample. When examining the response of a sample in the laboratory, it is important to define RSR for the sample based on e_c and the laboratory applied stresses. This combination defines the state of the sample immediately prior to testing and influences how it will respond to undrained loading. RSR is defined relative to the appropriate section of the bi-linear reference USL shown in Figure 5 (see Table 2), depending on the value of e_c (i.e. whether it is greater than or less than the breakpoint void ratio of 0.979). For a given direction of loading (i.e. TC or TE) each component of response appears to be a function of RSR.

Note that Figure 55(d) presents the end-of-test values of M (which can be considered approximately equal to the ultimate values since the samples were generally all dilating towards ultimate state when the tests were stopped) versus RSR. Over a range of RSR, the ten triaxial compression tests on undisturbed samples all had similar values of M_C, with an average of 1.4 (SD=0.09). Likewise, over a similar range of RSR, the nine triaxial extension tests on undisturbed samples all had similar values of M_E, with an average of 0.95 (SD=0.10). The observed M_C correlates to an average friction angle, ϕ', of 34.7° (SD=2.0°). The observed M_E correlates to an average friction angle, ϕ', of 34.6° (SD=5.0°). Therefore, based on this limited test data, the triaxial compression and triaxial extension tests appear to have approximately the same ultimate state friction angle. Compared to the values for the undisturbed samples at the Phase I site, the value of M_C at the Phase III site is lower and the value of M_E is higher.

Undrained simple shear response

Cycles of shear loading reversal were carried out on each of the seven samples that was tested in monotonic simple shear (see Appendix O) and all of the samples were still dilating under the initial direction of loading when the loading was reversed. Consequently, it is difficult to produce complete plots of response versus state for these samples in a similar fashion as for the triaxial test data.

RSR profiles in-situ

Figure 58(a) to Figure 58(d) present estimated profiles of RSR based on the SPT, CPT, shear wave velocity measurements and geophysical logging. The RSR profiles from the SPT were estimated using the D_r-based method of estimating void ratio. The RSR profiles from the CPT were estimated using the void ratios calculated by combining the Plewes et al. (1992) method of estimating state parameter with the reference USL. The RSR profiles were determined by combining the void ratio profiles with the equations in the Introductory Data Review Report. These methods were selected for illustrative purposes only. Any method to estimate state (void ratio or state parameter) could be used; however, the methods selected here appear to be the best for estimating the state of the frozen samples. The value of RSR was referenced to either the flat or steep portion of the Syncrude reference USL in Figure 5 (see values of Γ and λ_{ln} in Table 2), depending on whether the estimated void ratio at any given depth was above or below the void ratio defining the breakpoint in the reference USL. RSR in Figure 58(a) to Figure 58(d) is plotted on a scale from 0.001 to 1000. Relative to the flat portion of the Syncrude reference USL (λ_{ln}=0.0152), this would correspond to a range in state parameter of Ψ= - 0.105 to Ψ= + 0.105. However, the estimated void ratio is often less than the breakpoint void ratio and therefore RSR is referenced to the steep portion of the USL.

Superimposed on Figure 58(a) to Figure 58(d) are solid dots representing the in-situ RSR

values of the undisturbed frozen samples obtained at the Phase III site (see Table 7). The RSR values of the samples were determined by combining the estimates of in-situ void ratio for each sample (Hofmann, 1995) with the estimated in-situ stresses and the reference USL. The values of RSR were referenced to either the flat or steep portion of the Syncrude reference USL shown in Figure 5 (see values of Γ and λ_{1n} in Table 2), depending on whether the estimated void ratio of a particular sample was above or below the void ratio defining the breakpoint in the reference USL.

Comparing RSR estimated from the in-situ tests with RSR of the undisturbed samples in Figure 58 is the same as comparing the void ratio estimated from the in-situ tests (using the same method of interpretation for each test as used to estimate RSR) with the void ratio of the undisturbed samples, because void ratio was converted to RSR using the same method for both in-situ testing and the undisturbed samples. When interpreted using the selected methods, as presented in Figure 58, all of the in-situ tests except shear wave velocity appear to estimate the average RSR of the undisturbed samples fairly well. The undisturbed samples that were trimmed for testing seem to indicate that over most of the target zone, RSR is generally less than one (i.e. dense of the USL). Although there are definitely regions in the target zone where higher values of RSR would be estimated (in particular, around a depth of 3.5 m), the undisturbed frozen samples that were trimmed for testing seem to indicate that over most of the target zone, the in-situ RSR ranges from approximately 0.02 to 0.2.

Link between field and laboratory data

As for Phase I, the proposed link between laboratory testing and in-situ testing for flow liquefaction considerations is the parameter RSR. The undrained response observed in the laboratory is linked to the RSR of the sample immediately prior to shearing; i.e. at the void ratio after thaw and consolidation and under the anisotropic stress state imposed in the laboratory. Based on the relationships between response and RSR in the laboratory, the true in-situ response at the depth from which the sample was obtained would only be

equal to the response of the sample if the in-situ RSR and the sample RSR were the same. Figure 59(a) compares the estimated in-situ void ratio of each sample (Hofmann, 1995) with the void ratio immediately before testing in the laboratory (as reported by each laboratory that tested samples). Figure 59(b) compares the estimated in-situ RSR of each sample with the RSR immediately before testing in the laboratory. The laboratory and field values of void ratio and RSR for each sample are summarized in Table 7.

Figure 59(a) shows that all of the undisturbed samples experienced small changes in void ratio during thaw and consolidation, with the void ratio immediately prior to testing (e_{lab}) generally being smaller than the estimated in-situ void ratio (e_{field}). All of the samples were tested by UBC; compared to the Phase I undisturbed samples tested by UBC (see Figure 34), the differences between e_{lab} and e_{field} are smaller at the Phase III site.

Figure 59(b) shows that for many of the undisturbed samples tested in monotonic triaxial loading under the in-situ stress conditions (solid dots), the RSR immediately prior to testing (RSR_{lab}) was similar to or slightly less than the estimated in-situ RSR (RSR_{field}). However, some of these undisturbed samples had values of RSR_{lab} more significantly higher or lower than RSR_{field}. Compared to the Phase I undisturbed samples tested by UBC (see Figure 34), the differences between RSR_{lab} and RSR_{field} (for the samples tested under the in-situ stress conditions) are generally smaller for Phase III. The group of samples tested under stresses to simulate the embankment loading appear to generally have values of RSR similar to those that would be calculated assuming no change in in-situ void ratio, but accounting for an increase in effective stresses (see dashed line in Figure 59(b)). However, some of these samples do not fit this trend.

Based on the above observations, it is reasonable to conclude that the response of the undisturbed samples in the laboratory tested under in-situ stresses would generally result in slightly less brittle behaviour, with slightly higher strength ratios than the in-situ material located at the same depths from which the undisturbed samples were obtained. Since there is generally a slight change in "state" between the in-situ condition of the

sample and the laboratory condition after thaw and consolidation, it can be difficult to conclude precisely the in-situ response to loading based only on the laboratory results. However, constitutive modelling, as described in the Introductory Data Review Report, can be used to interpolate and extrapolate the laboratory data into the in-situ range of soil state. This will be discussed in the final data review report. The response of the samples tested in the laboratory under higher stresses to simulate embankment loading can be expected to be generally similar to the behaviour of the in-situ material if the in-situ effective stresses were increased, with no change in void ratio.

4.4 Conclusions

Based on laboratory testing of undisturbed samples, Syncrude sand in the Phase III target zone initially appears to be generally strain-hardening in undrained triaxial compression and slightly strain-softening in undrained triaxial extension. In general, the sand strain-hardened to high strength ratios in undrained triaxial compression, but demonstrated limited strain-softening in undrained triaxial extension, reaching a low strength ratio temporarily before strain-hardening to a high strength ratio. Axial strains while at the low strength ratio (i.e. QSS) were about 7%, on average, and generally less than 11%. On average, the material appeared to have ultimate friction angles in the order of 35°. However, as a result of some void ratio changes during thaw and consolidation, it is reasonable to conclude that the response of the in-situ material would be slightly more brittle with slightly lower strength ratios than the undisturbed samples tested in the laboratory. The field void ratios of the undisturbed samples and the interpretation of the various in-situ tests at Phase III suggest the presence of some looser layers in the target zone. However, it is unlikely that these zones are continuous across the site.

If an embankment were constructed over the detailed test area, increasing the effective stresses (yet assuming no change in in-situ void ratio), the in-situ material would have a stronger state and respond in an even more stable manner when loaded undrained. If the increase in effective stresses would actually densify the soil and cause a decrease in void ratio as well, it is expected that the in-situ material would have an even stronger state.

5. CYCLIC SOFTENING – PHASE I SITE

5.1 Direct Methods

a) Undisturbed samples

To date, no undisturbed samples of Phase I Syncrude sand have been tested in cyclic simple shear. However, recently, five undisturbed samples of Phase I Syncrude sand have been tested in undrained cyclic triaxial loading at the University of Alberta. The results of this testing are presented in Appendix H.

a) Reconstituted samples

Table 6(a) summarizes the results of cyclic simple shear testing to date on reconstituted samples of Syncrude sand from the Phase I site. All of the testing was conducted at UBC. The detailed stress-strain curves are given in Appendix F. The state of each sample is defined by its void ratio after consolidation (e_c). Three samples have been tested to date, having an average e_c of 0.870 (SD=0.013), compared to an average in-situ void ratio, e, of 0.768 (SD=0.040), based on all of the undisturbed samples. The three samples were all subjected to an initial vertical effective stress of 400 kPa. This is less than the average in-situ vertical effective stress of approximately 500 kPa in the target zone at the Phase I site. Therefore, as a result of the combination of void ratio and effective stresses, the reconstituted samples have a significantly looser state than the in-situ Phase I material.

Table 6(a) summarizes the test results in terms of the applied cyclic stress ratio ($CSR=\tau_{cyc}/\sigma'_v$) and the measured number of cycles, N, required to cause uncontrolled deformations. Based on the method described in the Introductory Data Review Report, the equivalent earthquake magnitude, M, was calculated. The correction ($1/r_m$) proposed by Tokimatsu and Yoshimi (1983) for estimating the equivalent CSR for a Magnitude M=7.5 earthquake from the CSR for a given magnitude earthquake, based on the work by

Seed et al. (1985), was then calculated, using the method outlined in the Introductory Data Review Report. Multiplying the applied CSR by the appropriate correction factor gives the equivalent cyclic resistance ratio (CRR) for a Magnitude M=7.5 earthquake, considered to have N=15 uniform cycles of loading. The Phase I reconstituted samples of sand have a resulting average equivalent CRR for M=7.5 (or N=15 cycles) of 0.113 (SD=0.020). Since these reconstituted samples appear to have had a looser state than the in-situ Phase I material, one would expect that testing undisturbed samples would result in higher values of $CRR_{7.5}$.

b) Undisturbed samples

Table 6(b) summarizes the results of undrained cyclic triaxial testing on undisturbed samples of Syncrude sand from the Phase I site. All of the testing was conducted at the University of Alberta. The detailed stress-strain curves and interpretation of the results are given in Appendix H. The state of each sample is defined by its void ratio after thaw and consolidation (e_c). Five samples have been tested to date, having an average e_c of 0.703 (SD=0.042). However, one sample (FS5 C15A) had a very large change in void ratio during thaw and consolidation and was considered to be a poor quality test. If this sample is not included, the four remaining samples had an average e_c of 0.720 (SD=0.017). This is denser than the average in-situ void ratio, e, of 0.768 (SD=0.040), based on all of the undisturbed samples. These four samples were isotropically consolidated to effective stresses ranging from 311 kPa to 350 kPa (average of 328 kPa) in order to place similar mean normal effective stresses on each sample as those in-situ at the corresponding depths. For comparison, the average mean normal effective stress, p', in the Phase I target zone, is 330 kPa. As a result of the combination of void ratio and effective stresses, the undisturbed samples tested in the laboratory have a slightly denser state than the in-situ Phase I material.

Table 6(b) summarizes the test results in terms of the applied cyclic stress ratio ($CSR = \sigma'_d/[2\sigma'_3]$) and the measured number of cycles, N, required to cause uncontrolled

deformations. Based on the method described in the Introductory Data Review Report, the equivalent earthquake magnitude, M, was calculated. The correction ($1/r_m$) proposed by Tokimatsu and Yoshimi (1983) for estimating the equivalent CSR for a Magnitude M=7.5 earthquake from the CSR for a given magnitude earthquake, based on the work by Seed et al. (1985), was then calculated, using the method outlined in the Introductory Data Review Report. Multiplying the applied CSR by the appropriate correction factor gives the equivalent cyclic resistance ratio (CRR) for a Magnitude M=7.5 earthquake, considered to have N=15 uniform cycles of loading. The four reliable Phase I undisturbed samples have a resulting average equivalent triaxial cyclic resistance, CRR_{tx}, for M=7.5 (or N=15 cycles) of 0.323 (SD=0.112). However, previous experience (Seed, 1979) has shown that the triaxial cyclic resistance, CRR_{tx}, is different than the simple shear cyclic resistance, CRR_{ss}, and that the simple shear cyclic resistance best represents the cyclic resistance in the field. CRR_{tx} can be converted to CRR_{ss} by multiplying it by a correction factor, c_r. For K_o=0.5, a value of c_r of approximately 0.7 is appropriate (Seed, 1979). When this is done, the four reliable Phase I undisturbed samples have a resulting average equivalent simple shear ($\approx$ field) cyclic resistance, CRR_{ss}, for M=7.5 (or N=15 cycles) of 0.226 (SD=0.078).

However, several factors appear to influence the values of CRR_{ss}. First, the samples are all slightly denser than the in-situ conditions. This will be discussed in a subsequent section. Secondly, from back-calculations, it appears that the samples had varying degrees of saturation in-situ (see Appendix H). In order to test the samples as close to their in-situ condition as possible, the samples were not saturated prior to conducting the undrained cyclic testing. However, some change in degree of saturation was noted during the thaw and consolidation process for each sample; the estimated degree of saturation for each sample immediately prior to testing is given in Table 6 (b). It is likely that the range of degree of saturation of the samples is one factor contributing to the range in observed CSR_{ss} for the undisturbed samples.

5.2 Indirect Methods

a) SPT approach

The in-situ CRR can be estimated from the SPT data in the target zone at the Phase I site, following the methods outlined in the Introductory Data Review Report. The average $(N_1)_{60}$ in the target zone was 18.2 (SD=3.0). The estimated average fines content of 12 % (based on SPT soil samples; Hofmann, 1997) at Phase I is such that the sand would be classified as a silty sand (FC > 5%) by the Seed et al. (1985) methodology (i.e. a correction to the measured $(N_1)_{60}$ should be made). Using the Seed et al. (1985), based on an average fines content of 12%, a correction of $\Delta(N_1)_{60}$=3 should be added to the measured values of $(N_1)_{60}$ to obtain the clean sand equivalent values of $(N_1)_{60cs}$. As outlined in Robertson and Wride's (1997) recent contribution to the 1996 NCEER Workshop (circulated as a CANLEX report), the clean sand relationship between CRR and SPT $(N_1)_{60}$ by Seed et al. (1985), as shown in the Introductory Data Review Report, can be estimated using the following equation from Tom Blake (Youd, 1997):

$$y = \frac{a + cx + ex^2 + gx^3}{1 + bx + dx^2 + fx^3 + hx^4} \qquad [1]$$

where:

y	=	CRR	d	=	0.009578
x	=	$(N_1)_{60cs}$	e	=	0.0006136
a	=	0.04844	f	=	- 0.0003285
b	=	- 0.1248	g	=	- 1.673 E-05
c	=	- 0.004721	h	=	3.714 E-06

and $(N_1)_{60cs} < 30$.

Figure 60(a) illustrates the direct application of Equation 1 to the SPT results from the Phase I site. The interpretation predicts an overall average CRR of 0.244 (SD = 0.058).

However, this interpretation does not account for the high effective overburden stresses in the target zone. Figure 60(b) illustrates that if these high stresses are accounted for using the method proposed by the NCEER Workshop (1997), a lower overall average CRR of 0.166 (SD=0.041). Superimposed on Figure 60(a) and Figure 60(b) are the results of the four reliable undrained cyclic triaxial tests on undisturbed samples (in terms of CRR_{ss} equivalent values). Next to the dot representing each undisturbed sample is the estimated degree of saturation of the sample during the cyclic loading. Both the estimated profile of CRR and the undisturbed sample CRR values are for Magnitude M=7.5 earthquakes (N=15 cycles). The estimated profile of CRR assumes that the soil is completely saturated. Due to the variation in CRR of the undisturbed samples, and the various factors which may be affecting this variation (including degree of saturation) it is difficult to make any definite conclusions regarding the overburden correction factor, K_σ.

Based on the average $(N_1)_{60}$ of 18.2 in the target zone at Phase I, the chart by Fear and McRoberts (1995), as shown in the Introductory Data Review Report, would predict an average CRR of approximately 0.18 based on the conservative upper bound state line and CRR > 0.5 based on the upper bound state line for clean sand. However, these values are for low effective stresses. Since the target zone has high effective stresses, the predicted CRR would be lower, once normalized to account for the high stresses. Note that, as for the Seed et al. (1985) method, the standard deviation of 3.0 for $(N_1)_{60}$ measurements in the target zone translates to a large range in predicted CRR of at least ± 0.05.

b) Integrated CPT approach

The integrated CPT approach for estimating cyclic resistance ratio (CRR), as outlined in the Introductory Data Review Report, and updated and modified in Robertson and Wride's (1997) final contribution to the 1996 NCEER Workshop (modified from the version circulated as a CANLEX report), can be applied at the Phase I site in order to estimate the profile of CRR throughout the target zone. This profile can be compared to the results of the cyclic triaxial testing on undisturbed samples from Phase I.

Figure 61(a) presents the profiles of normalized CPT cone tip resistance, corrected for overburden stress (q_{c1N}). The profiles for CPT PI9402 to PI9405 are shown. Note that the overall average q_{c1N} in the target zone is 73.6 (SD=16.6). Figure 61(b) presents the profiles of normalized CPT sleeve friction (F). Again, the profiles for CPT PI9402 to PI9405 are shown. Note that, in general, the value of F is greater than 0.5% throughout the target zone, indicating that the target zone material is a silty sand. As mentioned previously, the average F in the Phase I target zone is 0.733 (SD=0.138).

At the beginning of the report, Figure 1(b) showed that interpreting all of the CPT profiles in the target zone using the soil classification chart by Robertson (1990) and the iterative procedure of normalization concluded that the target zone material is primarily a sand, ranging from a clean sand to a silty sand, with an average soil behaviour type index, I_c, of 1.942 (SD=0.105). This is also shown in Figure 61(c), which presents the profiles of I_c at Phase I, based on the relationship between I_c and the CPT results (in terms of q_{c1N} and F), as outlined in the Introductory Data Review Report. Some of the target zone material would be classified as a sand mixture, ranging from a silty sand to a sandy silt.

Using the relationship between I_c and apparent fines content (FC), as outlined in Robertson and Wride's (1997) final contribution to the 1996 NCEER Workshop[2], the profiles of I_c in Figure 61(c) can be used to estimate profiles of FC at the Phase I site, as shown in Figure 61(d). Most of these profiles predict a reasonably uniform apparent fines content over most of the target zone, having an average value of 11.5% (SD=2.8%), indicating a silty sand. Superimposed on Figure 61(d) are the fines contents corresponding to the undisturbed samples that were trimmed for testing. The undisturbed samples which had grain size tests conducted after shearing have an average fines content

[2] The relationship between I_c and apparent fines content (FC, in percent) has been slightly modified since the Introductory Data Review Report was produced, in order to increase the predicted FC for a given I_c. The revised relationship is as follows: $FC = 1.75\ I_c^{3.25} - 3.7$. Note that if $I_c<1.26$, FC should be set to zero and if $I_c>3.5$, FC should be set to 100. In addition, Robertson and Wride have recently added a further condition, so that clean loose sands are not mistaken for sands with fines, as follows: if $1.64 < I_c < 2.36$ and $F < 0.5$, then assume that FC is approximately equal to or less than 5%.

of 5.1% (SD=2.2%). Note that, as mentioned earlier, the samples obtained using the SPT sampler at the Phase I site had an average fines content of about 12%, which is higher than the average fines content of the undisturbed samples and more similar to the apparent fines content predicted by the CPT.

Robertson and Wride's (1997) final contribution to the 1996 NCEER Workshop updated the method for estimating the correction to normalized tip resistance in sandy soils containing fines[3]. Using the new relationships recommended by Robertson and Wride (1997), profiles of K_c for the Phase I site can be estimated. These profiles are presented in Figure 62(a). The estimated apparent fines content of approximately 11.5% on average in the target zone would lead to, in general, a small recommended correction factor of 1.25 (SD=0.24) (see Figure 62(a)) to be multiplied by the q_{c1N} profile to produce the clean sand equivalent profile of cone tip resistance, $(q_{c1N})_{cs}$, as shown in Figure 62(b). The resulting average $(q_{c1N})_{cs}$ in the target zone at the Phase I site is 90.2 (SD=13.5).

Using the resulting clean sand equivalent profile with the relationship between CRR and $(q_{c1N})_{cs}$, as recommended in Robertson and Wride's (1997) final contribution to the 1996 NCEER Workshop[4], leads to the estimated CRR profiles for Magnitude M=7.5 earthquakes (N=15 cycles), as shown in Figure 62(c). The average estimated CRR is 0.153 (SD=0.035). However, these estimated values do not include the effects of the high effective stresses present in the target zone at the Phase I site. Figure 62 (d) presents the

---

[3] The final updated method recommends correcting CPT results based on both penetration resistance and soil behaviour type index, I_c. The clean sand equivalent penetration resistance, $(q_{c1N})_{cs}$, can be calculated by multiplying the measured normalized tip resistance corrected for effective overburden pressure, q_{c1N}, by a correction factor, K_c. For $I_c > 1.64$, the correction factor K_c is a function of the soil behaviour type index, I_c, as given by the following equation: $K_c = -0.403\ I_c^4 + 5.581\ I_c^3 - 21.63\ I_c^2 + 33.75\ I_c - 17.88$. However, for $I_c \leq 1.64$, K_c should be set equal to 1.0.

[4] If $50 \leq (q_{c1N})_{cs} < 160$, the recommended relationship is as outlined in the CANLEX Introductory Data Review Report; i.e. $CRR = 93\left(\frac{(q_{c1N})_{cs}}{1000}\right)^3 + 0.08$. However, if $(q_{c1N})_{cs} < 50$, the recommended relationship has been modified to the following: $CRR = 0.833\left(\frac{(q_{c1N})_{cs}}{1000}\right) + 0.05$.

corresponding profiles of estimated CRR, accounting for the presence of high effective stresses, using the corrections recommended by the 1996 NCEER Workshop[5] (Youd, 1997). These profiles have an average predicted CRR of 0.104 (SD=0.024). Superimposed on Figure 62(c) and Figure 62(d) are the results of the four reliable undrained cyclic triaxial tests on undisturbed samples (in terms of CRR_{ss} equivalent values). Next to the dot representing each undisturbed sample is the estimated degree of saturation of the sample during the cyclic loading. Both the estimated profile of CRR and the undisturbed sample CRR values are for Magnitude M=7.5 earthquakes (N=15 cycles). The estimated profile of CRR assumes that the soil is completely saturated. Due to the variation in CRR of the undisturbed samples, and the various factors which may be affecting this variation (including degree of saturation) it is difficult to make any definite conclusions regarding the overburden correction factor, K_σ.

As outlined in the Introductory Data Review Report, Olsen and Koester (1995) and Suzuki et al. (1995) have also developed soil classification chart methods of predicting CRR from the CPT. Each soil classification chart normalizes cone tip resistance in a different manner; for vertical effective stresses close to the reference atmospheric pressure of 100 kPa, the two methods are very similar and similar to the method proposed here, as described earlier (see Figure 1). However, the Phase I site has very high vertical effective stresses (having an average value of about 500 kPa) and, therefore, the choice of normalization has a significant effect at this site (as illustrated earlier in Figure 1). As a result, it is difficult to directly apply either the Olsen and Koester (1995) or Suzuki et al. (1995) methods to the Phase I CPT data, for comparison.

c) Shear wave velocity approach

The shear wave velocity measurements in the target zone at the Phase I site can also be

[5] NCEER Workshop (1996) recommendations to account for high overburden stress in calculating CRR: multiply the predicted CRR by a factor K_σ, as first suggested by Seed et al. (1985). However, the values of K_σ recommended by the NCEER Workshop differ from Seed et al. (1985) and can be approximated by the following equation: $K_\sigma = 3.0945(\sigma'_o)^{-0.2443}$, where σ'_o is the effective overburden pressure.

used to estimate the in-situ CRR. The average V_{s1} in the target zone was 156.4 m/s (SD=20.1 m/s). The relationship between CRR and V_{s1} by Robertson et al. (1992) shown in the Introductory Data Review Report would predict an average CRR of approximately 0.16 based on the average V_{s1} of 156.4 m/s. However, the shear wave velocity correlation based on the recent NCEER Workshop (1996) discussions gives an estimated CRR in the order of 0.10. Neither one of these predictions accounts for the effects of high effective overburden stresses on the value of CRR. In both methods, the standard deviation of 20.1 m/s for V_{s1} measurements in the target zone translates into a fairly large range in predicted CRR.

c) Link between field and laboratory data

The undrained response to cyclic loading observed in the laboratory is linked to the state of a sample immediately prior to shearing. The true in-situ response at the depth at which a sample was obtained would only be equal to the response of the sample if the in-situ state were the same as the laboratory state of the sample. Figure 63 compares the estimated in-situ void ratio of each undisturbed sample that was subjected to cyclic loading (see Appendix H) with the void ratio immediately before testing in the laboratory (see Table 6 or Appendix H). Both the laboratory and estimated field values of void ratio for each sample are summarized in Table 3. Figure 63 shows that all of the undisturbed samples subjected to cyclic loading experienced changes in void ratio during thaw and consolidation, with the void ratio immediately prior to testing ($e_{lab} = e_c$) being smaller than the estimated in-situ void ratio (e_{field}). In general, Phase I samples tested in both monotonic loading by a variety of laboratories (see Figure 34) and triaxial cyclic loading by U. of A. experienced similar changes in void ratio due to thaw and consolidation.

5.3 Conclusions

For design purposes, an expected earthquake-induced cycle stress ratio (CSR) profile could be superimposed over Figure 62(c) to estimate zones in which cyclic liquefaction

would be predicted. If there were large zones over which CSR was significantly larger than CRR, potential deformations could be estimated using empirical methods to predict post cyclic liquefaction shear and volumetric strains using methods such as Ishihara (1993) or Tokimatsu and Seed (1987), as shown in the Introductory Data Review Report, although these methods are not necessarily applicable for such high effective overburden stresses. However, the Phase I site is located in a non-seismic region and, therefore, cyclic softening is generally not an issue, since CSR < 0.05.

Due to the variations in degree of saturation and the slightly denser state of the samples after thaw and consolidation, it is not possible to make clear conclusions regarding the overburden correction factor, K_σ.

6. CYCLIC SOFTENING – PHASE III SITE

6.1 Direct Methods

a) Undisturbed samples

Table 10 summarizes the results of cyclic simple shear testing to date on undisturbed samples of Syncrude sand from the Phase III site. All of the testing was conducted at UBC; the individual tests are identified by the sampling identification number assigned by Hofmann (1995). The detailed stress-strain curves are given in Appendix O. The state of each sample is defined by its void ratio after thaw and consolidation (e_c). As for the triaxial samples, the value of e_c is generally less than the void ratio of the sample in-situ, as estimated by Hofmann (1995), as a result of small volume changes that occur during thaw and consolidation. The difference between the in-situ void ratio and e_c will be discussed later in this report. It is the void ratio immediately prior to testing that will affect the response of the sample to undrained cyclic loading. The samples that have been tested to date had an average e_c of 0.754 (SD = 0.021), compared to an average in-situ void ratio, e, of 0.762 (SD=0.053) based on all of the undisturbed samples.

Table 10 summarizes the test results in terms of the applied cyclic stress ratio ($CSR=\tau_{cyc}/\sigma'_v$) and the measured number of cycles, N, required to cause uncontrolled deformations. Based on the method described in the Introductory Data Review Report, the equivalent earthquake magnitude, M, was calculated. The correction ($1/r_m$) proposed by Tokimatsu and Yoshimi (1983) for estimating the equivalent CSR for a Magnitude M=7.5 earthquake from the CSR for a given magnitude earthquake, based on the work by Seed et al. (1985), was then calculated, using the method outlined in the Introductory Data Review Report. Multiplying the applied CSR by the appropriate correction factor gives the equivalent cyclic resistance ratio (CRR) for a Magnitude M=7.5 earthquake, considered to have N=15 uniform cycles of loading. The Phase III samples have an resulting average equivalent CRR for M=7.5 (or N=15 cycles) of 0.082 (SD = 0.006).

6.2 Indirect Methods

a) SPT approach

The in-situ CRR can be estimated from the SPT data in the target zone at Phase III, following the methods outlined in the Introductory Data Review Report. The overall average $(N_1)_{60}$ in the target zone was 3.4 (SD=2.0). The estimated average fines content at Phase III of 10% (based on SPT soil samples; Hofmann, 1997) is such that the sand would be classified as a silty sand (FC > 5%) by the Seed et al. (1985) methodology (i.e. a correction to the measured $(N_1)_{60}$ should be made). Using the Seed et al. (1985) approach, based on an average fines content of 10%, a correction of $\Delta(N_1)_{60}$=2.5 should be added to the measured values of $(N_1)_{60}$ to obtain the clean sand equivalent values of $(N_1)_{60cs}$. As outlined for Phase I, Equation 1, as proposed by Tom Blake (Youd, 1997), approximates the Seed et al. (1985) relationship between CRR and $(N_1)_{60}$ in clean sand.

Figure 64(a) illustrates the direct application of Equation 1 to the SPT results from Phase III, making a correction of 2.5 to all values of $(N_1)_{60}$, based on the average FC at the site. The interpretation predicts an overall average CRR of 0.074 (SD = 0.014). Superimposed on Figure 64(a) are the results of cyclic simple shear tests on undisturbed samples from the Phase III target zone. Figure 64(b) shows the results of correcting each $(N_1)_{60}$ individually based on the specific FC for each SPT sample that had a grain size test performed, using the corrections suggested by Seed et al. (1985). This profile of estimated CRR has a similar average value of 0.076 (SD=0.021). Both estimated profiles of CRR and the undisturbed sample CRR values are for Magnitude M=7.5 earthquakes (N=15 cycles). Both estimated profiles of CRR slightly underestimate the CRR of the tested undisturbed samples, which have an average CRR of 0.082 (SD = 0.006).

Based on the overall average $(N_1)_{60}$ of 3.4 in the target zone at Phase III, the chart by Fear and McRoberts (1995), as shown in the Introductory Data Review Report, would predict

an average CRR of approximately 0.06 based on either the conservative upper bound state line or the upper bound state line for clean sand. Note that, as for the Seed et al. (1985) method, the overall standard deviation of 2.0 for $(N_1)_{60}$ measurements in the target zone translates to a range in predicted CRR of at least ± 0.05.

b) Integrated CPT approach

The integrated CPT approach for estimating cyclic resistance ratio (CRR), as outlined in the Introductory Data Review Report, and updated and modified in Robertson and Wride's (1997) final contribution to the 1996 NCEER Workshop (modified from the version circulated as a CANLEX report), can be applied at the Phase III site in order to estimate the profile of CRR throughout the target zone. This profile can be compared to the results of the cyclic simple shear testing on undisturbed samples from Phase III.

Figure 65(a) presents the profiles of normalized CPT cone tip resistance, corrected for overburden stress (q_{c1N}). The profiles for CPT20 to CPT23, CPT26 and CPT27 are shown. Note that the overall average q_{c1N} in the target zone is 24.2 (SD=14.8). Figure 65(b) presents the profiles of normalized CPT sleeve friction (F). Again, the profiles for CPT20 to CPT23, CPT26 and CPT27 are shown. Note that, in general, the value of F is greater than 0.5% throughout the target zone, indicating that the target zone material is a silty sand. The average F in the Phase III target zone is 0.872 (SD=0.331).

At the beginning of the report, Figure 2(b) showed that interpreting all of the CPT profiles in the target zone using the soil classification chart by Robertson (1990) and the iterative procedure of normalization concluded that the target zone material is primarily a sand mixture, ranging from a silty sand to a sandy silt, with an average soil behaviour index, I_c, of 2.421 (SD=0.228). This can also be seen in Figure 65(c), which presents profiles of I_c at the Phase III site, based on the relationship between I_c and the CPT results (in terms of q_{c1N} and F), as outlined in the Introductory Data Review Report. Some of the target zone material would be classified as a sand (ranging from a clean sand to a silty

sand), a silt mixture (ranging from a clayey silt to a silty clay), and a clay.

Using the relationship between I_c and apparent fines content (FC as outlined in Robertson and Wride's (1997) final contribution to the 1996 NCEER Workshop[6], the profiles of I_c in Figure 65(c) can be used to estimate profiles of FC at the Phase III site, as shown in Figure 65 (d). These profiles predict a fairly variable apparent fines content in the target zone (indicating a variety of soil behaviour types), with an average FC of 27.5% (SD=10.5%). Superimposed on Figure 65(d) are the fines contents corresponding to the undisturbed samples that were trimmed for testing. The undisturbed samples have an average fines content of 5.2% (SD=1.6%). Note that, as mentioned earlier, the samples obtained using the SPT sampler at the Phase III site had an average fines content of approximately 10%, which is higher than the average fines content of the undisturbed samples, but not as high as the average apparent FC predicted by the CPT.

Robertson and Wride's (1997) final contribution to the 1996 NCEER Workshop updated the method for estimating the correction to normalized tip resistance (Δq_{c1N}) in sandy soils containing fines[7]. Using the new relationships recommended by Robertson and Wride (1997), profiles of K_c for the Phase III site can be estimated. These profiles are presented in Figure 66(a). The estimated apparent fines content of approximately 27.5 % overall in the target zone would lead to, on average, a recommended correction of 2.63 (SD=1.04) (see Figure 66(a)) to be multiplied by the q_{c1N} profile to produce a clean sand equivalent profile of cone tip resistance, $(q_{c1N})_{cs}$, as shown in Figure 66(b). The average

[6] The relationship between I_c and apparent fines content (FC, in percent) has been slightly modified since the Introductory Data Review Report was produced, in order to increase the predicted FC for a given I_c. The revised relationship is as follows: $FC = 1.75\ I_c^{3.25} - 3.7$. Note that if $I_c<1.26$, FC should be set to zero and if $I_c>3.5$, FC should be set to 100. In addition, Robertson and Wride have recently added a further condition, so that clean loose sands are not mistaken for sands with fines, as follows: if $1.64 < I_c < 2.36$ and $F < 0.5$, then assume that FC is approximately equal to or less than 5%.

[7] The final updated method recommends correcting CPT results based on both penetration resistance and soil behaviour type index, I_c. The clean sand equivalent penetration resistance, $(q_{c1N})_{cs}$, can be calculated by multiplying the measured normalized tip resistance corrected for effective overburden pressure, q_{c1N}, by a correction factor, K_c. For $I_c > 1.64$, the correction factor K_c is a function of the soil behaviour type index, I_c, as given by the following equation: $K_c = - 0.403\ I_c^4 + 5.581\ I_c^3 - 21.63\ I_c^2 + 33.75\ I_c - 17.88$. However, for $I_c \leq 1.64$, K_c should be set equal to 1.0.

$(q_{c1N})_{cs}$ in the target zone at the Phase III site is 53.6 (SD=9.8).

Using the resulting clean sand equivalent profile with the relationship between CRR and $(q_{c1N})_{cs}$, as recommended in Robertson and Wride's (1997) final contribution to the 1996 NCEER Workshop[8], leads to the estimated CRR profiles, as shown in Figure 66(c). The average estimated CRR is 0.096 (SD=0.016). The solid dots superimposed on Figure 66(c) represent the results of the cyclic simple shear testing on undisturbed samples from the Phase III site target zone. Both the estimated profiles of CRR and the undisturbed sample CRR values are for Magnitude M=7.5 earthquakes (N=15 cycles). The estimated profiles of CRR slightly overestimate the results of the undisturbed samples that have been tested, which have an average CRR of 0.082 (SD=0.006).

As outlined in the Introductory Data Review Report, Olsen and Koester (1995) and Suzuki et al. (1995) have also developed soil classification chart methods of predicting CRR from the CPT. The Phase III site soil classification data presented at the beginning of the report in Figure 2 can be compared with the Olsen and Koester (1995) and Suzuki et al. (1995) soil classification chart methods of predicting CRR from the CPT. Each soil classification chart normalizes cone tip resistance in a different manner; for vertical effective stresses close to the reference atmospheric pressure of 100 kPa, the three methods are very similar. However, the vertical effective stress in the Phase III target zone ranges from approximately 35 kPa to 75 kPa, so some difference between the methods would be expected. Without taking any such difference into account, the Olsen and Koester (1995) method would predict a CRR of about 0.125, on average, in the Phase III site target zone. The Suzuki et al. (1995) method would predict an average

---

[8] If $50 \leq (q_{c1N})_{cs} < 160$, the recommended relationship is as outlined in the CANLEX Introductory Data Review Report; i.e. $CRR = 93\left(\frac{(q_{c1N})_{cs}}{1000}\right)^3 + 0.08$. However, if $(q_{c1N})_{cs} < 50$, the recommended relationship has been modified to the following: $CRR = 0.833\left(\frac{(q_{c1N})_{cs}}{1000}\right) + 0.05$.

CRR somewhat less than 0.15 in the target zone (only contours of CRR=0.15 and CRR=0.25 are given on the Suzuki et al. (1995) plots, so it is difficult to determine CRR using these plots).

c) Shear wave velocity approach

The shear wave velocity measurements in the target zone at the Phase III site can also be used to estimate the in-situ CRR. The average V_{s1} in the target zone was 127.1 m/s (SD=3.0 m/s). The relationship between CRR and V_{s1} by Robertson et al. (1992) shown in the Introductory Data Review Report would predict an average CRR of approximately 0.12 based on the average V_{s1} of 127.1 m/s; this is significantly higher that the results of laboratory testing on undisturbed samples, which have an average CRR of 0.082 (SD=0.006). However, the shear wave velocity correlation based on the recent NCEER Workshop (1996) discussions gives an estimated CRR of less than 0.10, close to the results of laboratory testing. The standard deviation of 3.0 m/s for V_{s1} measurements in the target zone translates into a small range in predicted CRR.

c) Link between field and laboratory data

The undrained response to cyclic loading observed in the laboratory is linked to the state of the sample immediately prior to shearing. The true in-situ response at the depth at which the sample was obtained would only be equal to the response of the sample if the in-situ state were the same as the laboratory state of the sample. Figure 67 compares the estimated in-situ void ratio of each undisturbed sample that was subjected to cyclic loading (Hofmann, 1995) with the void ratio immediately before testing in the laboratory (as reported by the UBC laboratory). Both the laboratory and estimated field values of void ratio for each sample are summarized in Table 7. Figure 67 shows that most of the undisturbed samples subjected to cyclic loading experienced a small change in void ratio during thaw and consolidation, with the void ratio immediately prior to testing ($e_{lab} = e_c$) being generally smaller than the estimated in-situ void ratio (e_{field}). In general, Phase III

samples tested by UBC in both triaxial loading (see Figure 59) and cyclic simple shear loading experienced similar changes in void ratio due to thaw and consolidation.

Based on Figure 51 and Table 7, it appears that two out of the five samples tested in cyclic simple shear were looser than the average in-situ state. When combined with the small change in void ratio due to thaw and consolidation (see Figure 67; Table 7), the average laboratory state immediately before testing is slightly denser than the average field state. Hence, the laboratory results probably slightly overestimate the average field conditions.

6.3 Conclusions

For design purposes, the expected earthquake-induced cycle stress ratio (CSR) profile could be superimposed over Figure 66(c) to estimate the zones where cyclic liquefaction is predicted. If there were large zones over which CSR is significantly larger than CRR, potential deformations should be estimated using empirical methods to predict post cyclic liquefaction shear and volumetric strains using methods such as Ishihara (1993) or Tokimatsu and Seed (1987), as shown in the Introductory Data Review Report. However, the Phase III site is located in a non-seismic region and, therefore, cyclic softening is generally not an issue, since CSR < 0.05.

7. DISCUSSION

7.1 Comparison of Phase I and Phase III Sites

a) Data review results

Table 11 compares the results of the data review at the Phase I and Phase III sites. These results will be compared with the results from the other phases of the CANLEX Project in subsequent CANLEX reports. All of the values in Table 11 are given as the overall average in the target zone at each site; for most parameters, the overall standard deviation in the target zone is also given. Index parameters for the two sites were given in Table 1. Grain characteristic parameters for the two sites were given in Table 2.

Overall, the target zone at the Phase I site had much higher average values of $(N_1)_{60}$, q_{c1}, and V_{s1} than the target zone at the Phase III site. This may be partially due to aging effects since the Phase I deposit is somewhat older than the Phase III deposit. The scatter in SPT and CPT data (as represented by the standard deviations) was similar at the two sites. However, the shear wave velocity data had much more scatter (as represented by the standard deviation) at the Phase I site than at the Phase III site. The average values of $q_{c1}/(N_1)_{60}$, X and Y were all slightly smaller at Phase I than at Phase III. However, the average void ratios of the frozen samples from the target zone at each site were similar.

The average void ratio predicted by the geophysical logs is slightly greater than the average of the undisturbed samples tested to date at the Phase I site. At the Phase III site, the borehole geophysical logging appears to slightly underpredict the average void ratio.

Using the integrated CPT method by Robertson and Wride (1997), a higher average apparent fines content was predicted at the Phase III site than at the Phase I site. At each site, the predicted apparent fines content is higher than the average fines content of the undisturbed samples for which grain size distributions have been performed. The average

fines contents of these undisturbed samples are similar at the two sites. The average fines content of samples obtained using the SPT sampler are similar at each site and are higher than those of the undisturbed samples. At the Phase I site, the average fines content predicted using the integrated CPT method is similar to the average fines content from the samples obtained using the SPT sampler. At the Phase III site, the integrated CPT method predicts a higher average fines content than the average fines content of the samples obtained using the SPT sampler. It is important to note that a large variation in fines content throughout the target zone is predicted by the CPT at the Phase III site.

b) Estimated response

i) Flow liquefaction

Table 11 summarizes the average state of Syncrude sand in the target zone at the Phase I and Phase III sites, based on the undisturbed samples available to date, in terms of void ratio, relative density, state parameter and RSR. Based on the results of the laboratory testing, samples with these average states should be generally strain-hardening in undrained triaxial compression and would possibly experience limited strain-softening in triaxial extension. Note, however, that both sites have a small number of samples that have loose in-situ states (i.e. RSR>1). These samples would be expected to respond to undrained shear in a slightly more brittle fashion.

Figure 68 presents a summarized plot of the end-of-test undrained strength ratio, S_f/p'_i, versus RSR for all of the triaxial and simple shear samples that were tested from both the Phase I and Phase III sites. For the triaxial tests, S_f is half of the end-of-test deviator stress and p'_i is the initial mean normal effective stress. For the simple shear tests, S_f is the end-of-test applied shear stress on the horizontal surface and p'_i is the initial mean normal effective stress calculated from the initial vertical effective stress, based on the assumption that the initial K_o=0.5. This plot suggests that ultimate undrained strength ratios are higher in triaxial compression than in triaxial extension, with simple shear results being somewhere in between the two. With the exception of a few samples,

Figure 68 also suggests that RSR (based on the selected reference USL) may be a good parameter for estimating the general undrained response of Syncrude sand under a given direction of loading.

ii) Cyclic softening

Interpretation of the SPT, CPT and shear wave velocity measurements at each of the Phase I and Phase III sites appear to give similar predictions of average CRR in the target zone. Most of the methods tend to slightly overpredict the CRR actually measured in the laboratory by testing undisturbed samples. Both sites appear to have a relatively constant CRR in the order of 0.10 in the target zone (generally greater than 0.10 at Phase I and less than 0.10 at Phase III). The potential for cyclic softening and the magnitude of any subsequent deformations at the sites is dependent on the size and duration of cyclic loading applied by an earthquake.

7.2 Summary

This report has synthesized and analyzed the large amounts of data from the CANLEX Phase I and Phase III sites at Syncrude Canada Ltd. (Mildred Lake and J-pit). Various methods of evaluating the potential for both flow liquefaction and cyclic softening (liquefaction) and estimating the associated undrained response have been applied.

Applying the various methods of evaluation to the Phase I and Phase III sites has led to the general conclusion that both sites would be, on average, essentially non-susceptible to flow liquefaction. If a suitable trigger resulted in undrained monotonic loading, it is likely that most of the target zone at each site would respond in a non-brittle, strain-hardening manner in triaxial compression and could exhibit a temporary loss in strength with small associated axial strains in triaxial extension before strain-hardening. Hence, the response to undrained loading would be a function of ground geometry, type of loading, and continuity of loose zones. Some further investigation would be required to evaluate the continuity of the looser layers.

When subjected to cyclic loading, much of the target zone at the Phase III site would have an average M=7.5 equivalent CRR in the order of 0.10. Cyclic liquefaction and subsequent deformations would occur if the earthquake induced CSR exceeded this resistance. It is difficult to make definite conclusions as to the magnitude of the cyclic resistance in the Phase I target zone, as a result of a variety of factors, including degree of saturation, playing a role in the cyclic resistance.

Table 1. Index parameters for Phase I and III CANLEX sites, Ticino sand and Nerlerk & Ukalerk sands

Parameter	Phase I (Mildred Lake)	Phase III (J-pit)	Ticino Sand*	Nerlerk & Ukalerk (Erksak) Sands #
Approx. age of deposit at time of site characterization	30 years	1 month	< 1 week	< 1 year
Target Zone Depth (m)	27 to 37	3 to 7	-	0 to 10
Average depth to GWT (m)	21	0.5	-	0
γ (kN/m^3) above GWT below GWT	 18.5 19.5	 18.5 19.5	-	-
Mineralogy (of silt size fraction of soil)	90% quartz 5 % feldspar 5% kaolinite	Assumed to be the same as for Phase I.	95% quartz 5% feldspar	75% quartz 12% chalcedony 10% amphiboles 3% feldspar (Ukalerk)
Grain Size C_U (D_{60}/D_{10})	2.22 (0.20/0.09)	Not presently available.	1.13 (0.65/0.40)	1.5 to 1.8 (Ukalerk)
Average FC (%) from SPT	12	10 (based on all SPTs) 15 (SPT1 & SPT3 only)	< 5	2 (Ukalerk) to 10 (Nerlerk)
e_{max} §	0.958	0.901 (FC = 4 - 10%) 0.986 (FC = 10 - 40%)	0.89	0.80 (Ukalerk)
e_{min} §	0.668	0.579 (FC = 4 - 10%) 0.461 (FC = 10 - 40%)	0.52	0.50 (Ukalerk)
G_s	2.66&	2.62&	2.67	2.66 (Ukalerk)
K_o***	$\approx$ 0.5	$\approx$ 0.5	0.45	0.4

Notes: * Calibration chamber studies (Baldi et al., 1986)
Sladen et al. (1985); Sladen and Hewitt (1989)
§ Values of e_{max} and e_{min} determined by U.B.C. for Phase I and by U. of A. for Phase III
*** Estimated from pressuremeter testing results
& Values calculated by U. of A.; U.B.C. used G_s=2.62 for Phase I and G_s=2.66 for Phase III; Laval used G_s=2.63 for Phase I; Skirrow (1995) used G_s=2.63 for Phase III

Table 2. Grain characteristic parameters for Phase I and Phase III CANLEX sites

Parameter	Phase I (Mildred Lake)	Phase III (J-pit)
Γ	0.919 (e>0.829) 1.92 (e<0.829)	Assumed same as for Phase I.
λ_{ln}	0.0152 (e>0.829) 0.182 (e<0.829)	Assumed same as for Phase I.
A*	311 (=311 + 0)	311 (=311 + 0)
B	188	188

Notes:

* a (= b + c), where: a = estimated value for the deposit in-situ; b = value determined from testing young reconstituted samples in the laboratory; c = correction to account for aging effects in-situ, based on the work by Robertson et al. (1995).

Table 3. Summary of data for Phase I frozen samples tested to date (N.B. continued on next page)

FROZEN SAMPLES	Sample No.	Specific Avg. Depth (m)	Specific Avg. Elevation (m)	Depth (m) Relative to Avg. Ground Elev. (352.29 m) at the site	Average σ'_v (kPa)	Void ratio as calculated by UofA (e_{sand})	Void ratio as backcalculated by testing labs (e_i)	Ψ based on e_{sand}	RSR based on e_{sand}	Lab sent to	T=triaxial (C,E) SS=simple shear CSS/CTX=cyclic SS/T	Fines Content (% passing No. 200 sieve)	Lab e (e_c)	Lab RSR
Quality I Core	FS1 C10B	34.54	317.76	34.53	519.8	Ayoubian did not document which of these two samples he tested				UofA - Ayoubian	One of these two samples		See previous comments	
Quality I Core	FS5 C17-3	36.19	316.10	36.20	535.8	what their calculated in-situ void ratios were				UofA - Ayoubian	was tested in TC		(to the left)	
Quality I Core	FS1 C10C	34.77	317.53	34.76	522.1	0.813	0.813			UofA - Hofmann				
Quality I Core	FS4 C12 B	34.75	317.53	34.76	521.9	0.730	0.730	-0.101	0.504	UofA - Hofmann				
Quality I Core	FS4 C13A	35.32	316.96	35.33	527.4	0.803	0.803	-0.029	0.758	UofA - Hofmann				
Quality I Core	FS4 C15A	36.71	315.58	36.72	540.8	0.725	0.725	-0.106	0.507	UofA - Hofmann				
Quality I Core	FS5 C11-1-2	33.15	319.14	33.16	506.3	0.836	0.836	0.004	1.325	UofA - Hofmann				
Quality I Core	FS1 C6C-1	31.49	320.79	31.50	490.3	0.714	0.714	-0.118	0.432	UofA - Hofmann	Samples used to develop			
Quality I Core	FS3 C14C	34.97	317.31	34.98	524.0	0.827	0.827	-0.004	0.860	UofA - Hofmann	thaw protocol and/or			
Quality I Core	FS5 C8B	31.51	320.77	31.52	490.4	0.807	0.807	-0.025	0.724	UofA - Hofmann	unsuccessful triaxial tests			
Quality I Core	FS5 C2	28.50	323.78	28.51	461.3	0.679	0.679	-0.154	0.335	UofA - Hofmann	(i.e. no data available)			
Quality I Core	FS4 C6C	31.12	321.16	31.13	486.7	0.748	0.748	-0.084	0.519	UofA - Hofmann				
Quality I Core	FS4 C11A	33.81	318.47	33.82	512.8	0.810	0.810	-0.022	0.765	UofA - Hofmann				
Quality I Core	FS1 C6E	31.85	320.43	31.86	493.7	0.723	0.723	-0.109	0.458	UofA - Hofmann				
Quality I Core	FS5 C10B	32.62	319.66	32.63	501.2	0.743	0.743	-0.089	0.520	UofA - Hofmann				
Quality I Core	FS5 C14	34.58	317.70	34.59	520.2	0.746	0.746	-0.085	0.549	UofA - Hofmann	TC		0.737	0.521
Quality I Core	FS4 C14A	35.99	316.29	36.00	533.9	0.847	0.847	0.017	3.008	UofA - Hofmann	TC		0.834	1.231
Quality I Core	FS3 C17B	37.66	314.62	37.67	550.1	0.777	0.777	-0.053	0.687	UofA - Hofmann	TC		0.734	0.542
Quality I Core	FS5 C10A	32.44	319.84	32.45	499.5	0.728	0.728	-0.104	0.475	UofA - Hofmann	TE		0.704	0.418
Quality I Core	FS4 C16-2	37.47	314.81	37.48	548.3	0.729	0.729	-0.102	0.525	UofA - Hofmann	TE		0.612	0.277
Quality II Core	FS1 C9B2	34.19	318.11	34.18	516.4	0.760	0.773	-0.071	0.587	UBC	TE - DRAINED	6.12		
Quality II Core	FS5 C13-2	33.97	318.31	33.98	514.3	0.747	0.748	-0.084	0.545	UBC	TE - DRAINED	5.66		
Quality II Core	FS4 C13A	35.27	317.01	35.28	526.9	0.785	0.802	-0.046	0.688	UBC	TE	5.39	0.718	0.476
Quality II Core	FS5 C18-2	36.49	315.79	36.50	538.8	0.746	0.766	-0.085	0.567	UBC	TE	4.98	0.691	0.419
Quality II Core	FS1 C9B1	33.99	318.31	33.98	514.5	0.730	0.759	-0.101	0.496	UBC	TC - DRAINED	6.05	0.684	
Quality II Core	FS5 C13-1	33.90	318.38	33.91	513.6	0.800	0.817	-0.031	0.728	UBC	TC - DRAINED	11.1	0.73	
Quality II Core	FS3 C7A	30.94	321.37	30.92	484.9	0.735	0.753	-0.097	0.481	UBC	TC	4.64	0.683	0.361
Quality II Core	FS5 C18-1	36.49	315.79	36.50	538.8	0.768	0.790	-0.063	0.640	UBC	TC	5.07	0.708	0.460
Quality II Core	FS1 C3B1	29.75	322.55	29.74	473.4	0.750	0.776	-0.083	0.510	UBC	SS	4.23	0.688	0.359
Quality II Core	FS1 C3B2	29.77	322.53	29.76	473.6	0.727	0.754	-0.106	0.449	UBC	SS	3.62	0.682	0.351
Quality II Core	FS1 C8B-1	32.95	319.35	32.94	504.4	0.766	0.793	-0.066	0.593	UBC	SS	6.01	0.727	0.479
Quality II Core	FS1 C8B-2	32.97	319.33	32.96	504.6	0.772	0.799	-0.060	0.613	UBC	SS	8.08	0.724	0.471
Quality II Core	FS3 C7B-1	31.18	321.13	31.16	487.2	0.830	0.858	-0.002	0.861	UBC	SS	2.56	0.777	0.608
Quality II Core	FS3 C7B-2	31.18	321.13	31.16	487.2	0.764	0.791	-0.068	0.566	UBC	SS	2.44	0.737	0.488
Quality II Core	FS1 C4A-1	30.64	321.66	30.63	482.0	0.746	0.773	-0.086	0.508	UBC	SS	1.8	0.720	0.440
Quality II Core	FS1 C4A-2	30.64	321.66	30.63	482.0	0.723	0.749	-0.109	0.447	UBC	SS	4.18	0.709	0.414
Quality I Core	FS3 C5A	29.95	322.36	29.93	475.3	0.798		-0.034	0.667	UBC				
Quality I Core	FS3 C14B-1	34.77	317.55	34.75	522.0	0.815		-0.016	0.804	UBC				
Quality I Core	FS3 C14B-2	34.81	317.50	34.79	522.5	0.899		0.067	88.802	UBC				
Quality I Core	FS5 C6-1A	30.27	322.02	30.28	478.4	0.783		-0.049	0.618	UBC				
Quality II Core	FS1 C6B	31.36	320.94	31.35	489.0	0.769		-0.063	0.584	UBC				

N.B. Void ratios by U.B.C. are based on G_s=2.62, by Laval are based on G_s=2.63, by Klohn-Crippen are based on G_s=2.65, and by U. of A. are based on G_s=2.66.

Table 3 (continued).

FROZEN SAMPLES	Sample No.	Specific Avg. Depth (m)	Specific Avg. Elevation (m)	Depth (m) Relative to Avg. Ground Elev. (352.29 m) at the site	Average σ'_v (kPa)	Void ratio as calculated by UofA (e_{sat})	Void ratio as backcalculated by testing labs (e_i)	Ψ based on e_{sat}	RSR based on e_{sat}	Lab sent to	T=triaxial (C,E) SS=simple shear CSS/CTX=cyclic SS/T	Fines Content (% passing No. 200 sieve)	Lab e (e_c)	Lab RSR
Quality I Core	FS5 C12B1	33.39	318.89	33.40	508.7	0.753		-0.078	0.558	Laval				
Quality I Core	FS5 C8A	31.19	321.10	31.20	487.3	0.760		-0.072	0.555	Laval				
Quality II Core	FS1 C8B	33.19	319.11	33.18	506.7	0.756	0.729	-0.076	0.563	Laval - FM42	TC		0.695	0.403
Quality II Core	FS1 C4	30.64	321.66	30.63	482.0	0.799	0.78	-0.034	0.677	Laval - FM43	TC		0.699	0.392
Quality II Core	FS5 C5C	29.93	322.35	29.94	475.1	0.731	0.71	-0.102	0.460	Laval - FM44	TC		0.674	0.337
Quality II Core	FS3 C11A	33.16	319.14	33.15	506.5	0.760	0.733	-0.071	0.577	Laval - FM45	TC		0.664	0.340
Quality II Core	FS3 C10	32.91	319.40	32.89	504.0	0.745	0.719	-0.086	0.529	Laval - FM46	TC		0.671	0.352
Quality II Core	FS1 C7	32.53	319.77	32.52	500.3	0.769	0.7425	-0.063	0.598	Laval - FM47	TC		0.657	0.323
Quality II Core	FS3 C9	32.45	319.86	32.43	499.6	0.756	0.7298	-0.076	0.556	Laval - FM48	TC		0.693	0.393
Quality I Core	FS4 C15B-1	36.87	315.41	36.88	542.4	0.800	0.7559	-0.031	0.768	Laval - FM55	TC		0.7	0.444
Quality I Core	FS5 C9-1	31.80	320.49	31.81	493.2	0.788	0.806	-0.044	0.655	Klohn Crippen	TC		0.749	0.528
Quality I Core	FS5 C12B2	33.65	318.64	33.66	511.2	0.783		-0.049	0.659	Klohn Crippen	no data			
Quality I Core	FS3 C5B-1	30.15	322.17	30.13	477.2	0.746	0.768	-0.086	0.503	Klohn Crippen	TC		0.708	0.408
Quality III Core	FS4 C3A	29.78	322.50	29.79	473.7	0.734	0.734	-0.099	0.467	U of A	CTX		0.704	0.396
Quality III Core	FS4 C3B	29.62	322.67	29.63	472.1	0.685	0.685	-0.148	0.356	U of A	CTX; no data			
Quality III Core	FS1 C5	30.90	321.40	30.89	484.5	0.786	0.786	-0.046	0.636	U of A	CTX		0.737	0.486
Quality III Core	FS5 C15A	34.93	317.35	34.94	523.6	0.755	0.755	-0.076	0.579	U of A	CTX		0.632	0.295
Quality III Core	FS5 C15B	35.07	317.22	35.08	524.9	0.770	0.770	-0.061	0.631	U of A	CTX; no data			
Quality III Core	FS1 C11A	30.15	322.13	30.16	477.3	0.732	0.732	-0.101	0.465	U of A	not tested (dense)			
Quality III Core	FS4 C8A-1	31.73	320.55	31.74	492.6	0.723	0.723	-0.109	0.457	U of A	not tested (dense)			
Quality III Core	FS4 C8A-2	31.89	320.40	31.90	494.1	0.692	0.692	-0.140	0.387	U of A	not tested (dense)			
Quality III Core	FS4 C6A	30.82	321.46	30.83	483.8	0.779	0.779	-0.053	0.611	U of A	CTX		0.708	0.413
Quality III Core	FS1 C3B	29.89	322.39	29.90	474.7	0.717	0.717	-0.116	0.426	U of A	not tested (poor quality)			
Quality III Core	FS5 C16B	35.70	316.58	35.71	531.1	0.792	0.792	-0.039	0.720	U of A	CTX		0.732	0.518
Quality III Core	FS4 C5C	30.25	322.03	30.26	478.2	0.807	0.807	-0.026	0.704	U of A	not tested (poor quality)			
Quality III Core	FS4 C3B	29.41	322.87	29.42	470.1	0.757	0.757	-0.076	0.526	U of A	not tested (poor quality)			

N.B. Void ratios by U.B.C. are based on G_s=2.62, by Laval are based on G_s=2.63, by Klohn-Crippen are based on G_s=2.65, and by U. of A. are based on G_s=2.66.

Table 4. Summary of undrained monotonic triaxial testing results for Phase I (N.B. continued on next page)

Laboratory	Test No.	INITIAL STATE										PEAK STATE				
		e_c	σ'_{vi} (kPa)	σ'_{hi} (kPa)	p'_i (kPa)	q_i (kPa)	S_i (kPa)	e_{cs}	p'_{cs} (kPa)	Ψ $e_c - e_{cs}$	RSR p'_i/p'_{cs}	q_p (kPa)	S_p (kPa)	p'_p (kPa)	Mp $(q/p')_p$	Peak ϕ'
UBC - Undisturbed TC	FS3-C7A	0.683	510	255	340	255.0	127.5	0.830	902.7	-0.147	0.377	1337.7	668.9	885	1.51	37.1
UBC - Undisturbed TC	FS5-C18-1	0.708	570	285	380	285.0	142.5	0.840	786.8	-0.132	0.483	1073.2	536.6	848.9	1.26	31.5
UBC - Undisturbed TE	FS5-C18-2	0.691	570	285	380	285.0	142.5	0.840	863.9	-0.149	0.440	84.6	42.3	144.7	0.58	18.9
UBC - Undisturbed TE	FS4-C13A	0.718	550	275	366.7	275.0	137.5	0.829	744.7	-0.111	0.492	49.4	24.7	121.4	0.41	12.6
LAVAL - Undisturbed TC	42	0.695	546.6	272.5	363.9	274.1	137.05	0.829	845.1	-0.134	0.431	1184.7	592.4	746.3	1.59	38.9
LAVAL - Undisturbed TC	43	0.699	470.7	232.1	311.6	238.6	119.3	0.832	826.7	-0.133	0.377	1122.4	561.2	657.6	1.71	41.6
LAVAL - Undisturbed TC	44	0.674	334.1	105.5	181.7	228.6	114.3	0.840	948.6	-0.166	0.192	1393.2	696.6	798.8	1.74	42.5
LAVAL - Undisturbed TC	45	0.664	553.8	269.9	364.5	283.9	141.95	0.829	1002.2	-0.165	0.364	1129.0	564.5	711	1.59	38.9
LAVAL - Undisturbed TC	46	0.671	542.0	268.7	359.8	273.3	136.65	0.830	964.3	-0.159	0.373	1401.4	700.7	826.5	1.70	41.4
LAVAL - Undisturbed TC	47	0.657	540.6	264.3	356.4	276.3	138.15	0.830	1041.5	-0.173	0.342	1270.6	635.3	788	1.61	39.5
LAVAL - Undisturbed TC	48	0.693	535.7	268.0	357.2	267.7	133.85	0.830	854.4	-0.137	0.418	1315.9	658.0	819.7	1.61	39.3
LAVAL - Undisturbed TC	55	0.700	535.1	273.1	360.4	262.0	131	0.830	822.2	-0.130	0.438	2422.9	1211.5	1450.2	1.67	40.8
U of A - Undisturbed TC	SS-UT-TC-A	0.778	498.5	272.4	347.8	226.1	113.05	0.830	535.3	-0.052	0.650	1150.0	575.0	710	1.62	39.6
U of A - Undisturbed TC	FS5C14	0.737	469	235	313	234.0	117	0.832	670.8	-0.095	0.467	1458	729	859	1.70	41.4
U of A - Undisturbed TC	FS4C14A	0.834	480	240	320	240.0	120	0.831	268.3	0.003	1.193	934	467	632	1.48	36.4
U of A - Undisturbed TC	FS3C17B	0.734	495	248	330.33333	247.0	123.5	0.831	681.9	-0.097	0.484	2014	1007	1350	1.49	36.7
U of A - Undisturbed TE	FS5C10A	0.704	450	225	300	225.0	112.5	0.832	804.3	-0.128	0.373	250	125	230	1.09	41.6
U of A - Undisturbed TE	FS4C162	0.612	494	247	329.33333	247.0	123.5	0.831	1334.1	-0.219	0.247	283	141.5	334	0.85	29.6
U of A - Reconstituted TC	SS-MT-TC-A (T5)	0.879	488.7	257	334.23333	231.7	115.85	0.831	13.9	0.048	24.054	282.1	141.1	340	0.83	21.4
U of A - Reconstitued TE	SS-MT-TE-A (T6)	0.889	484	241.2	322.13333	242.8	121.4	0.831	7.2	0.058	44.760	61.3	30.7	120	0.51	16.2
UBC - Reconstituted TC	σ'_3=400;K_c=2 (Test 16)	0.81	800	400	533.33333	400.0	200	0.779	448.9	0.031	1.188	487.6	243.8	490.1	0.99	25.3
UBC - Reconstituted TC	σ'_3=200;K_c=2 (Test 14)	0.788	400	200	266.66667	200.0	100	0.834	506.7	-0.046	0.526	252.1	126.1	227.9	1.11	27.8
UBC - Reconstituted TC	σ'_3=100;K_c=2 (Test 12)	0.777	200	100	133.33333	100.0	50	0.845	538.3	-0.068	0.248	1350.0	675.0	790.0	1.71	41.7
UBC - Reconstituted TC	σ'_3=50;K_c=2 (Test 10)	0.815	100	50	66.666667	50.0	25	0.855	436.7	-0.040	0.153	800.0	400.0	600.0	1.33	33.1
UBC - Reconstituted TE	σ'_3=400;K_c=1.5 (Test 9)	0.801	600	400	466.66667	200.0	100	0.803	471.7	-0.002	0.989	123.5	61.8	239.7	0.52	16.4
UBC - Reconstituted TE	σ'_3=400;K_c=2 (Test 17)	0.782	800	400	533.33333	400.0	200	0.779	523.7	0.003	1.018	118.5	59.3	238.6	0.50	15.7
UBC - Reconstituted TE	σ'_3=200;K_c=2 (Test 15)	0.765	400	200	266.66667	200.0	100	0.834	575.0	-0.069	0.464	70.6	35.3	117.7	0.60	19.5
UBC - Reconstituted TE	σ'_3=100;K_c=2 (Test 13)	0.781	200	100	133.33333	100.0	50	0.845	526.6	-0.064	0.253	25.2	12.6	60.4	0.42	13.0
UBC - Reconstituted TE	σ'_3=50;K_c=2 (Test 11)	0.803	100	50	66.666667	50.0	25	0.855	466.5	-0.052	0.143	15.0	7.5	32.3	0.46	14.6

Table 4 (continued).

Laboratory	Test No.	MINIMUM STATE						ULTIMATE (End of test) STATE					
		q_{min} (kPa)	S_{min} (kPa)	S_{min}/p'_i	p'_{min} (kPa)	% axial strain, ε_a during S_{min}	I_B	q_f (kPa)	S_f (kPa)	S_f/p'_i	p'_f (kPa)	M_f $(q/p')_f$	End-of-test ϕ'
UBC - Undisturbed TC	FS3-C7A	1337.7	668.9	1.967	885	0	0.00	1337.7	668.9	1.967	885	1.51	37.1
UBC - Undisturbed TC	FS5-C18-1	1073.2	536.6	1.412	848.9	0	0.00	1073.2	536.6	1.412	848.9	1.26	31.5
UBC - Undisturbed TE	FS5-C18-2	77.0	38.5	0.101	94.3	3	0.02	242.4	121.2	0.319	310.5	0.78	26.7
UBC - Undisturbed TE	FS4-C13A	31.8	15.9	0.043	40.4	5	0.05	243.6	121.8	0.332	266.9	0.91	32.6
LAVAL - Undisturbed TC	42	1184.7	592.4	1.628	746.3	0	0.00	1184.7	592.4	1.628	746.3	1.59	38.9
LAVAL - Undisturbed TC	43	1122.4	561.2	1.801	657.6	0	0.00	1122.4	561.2	1.801	657.6	1.71	41.6
LAVAL - Undisturbed TC	44	1393.2	696.6	3.834	798.8	0	0.00	1393.2	696.6	3.834	798.8	1.74	42.5
LAVAL - Undisturbed TC	45	1129.0	564.5	1.549	711	0	0.00	1129.0	564.5	1.549	711	1.59	38.9
LAVAL - Undisturbed TC	46	1401.4	700.7	1.947	826.5	0	0.00	1401.4	700.7	1.947	826.5	1.70	41.4
LAVAL - Undisturbed TC	47	1270.6	635.3	1.783	788	0	0.00	1270.6	635.3	1.783	788	1.61	39.5
LAVAL - Undisturbed TC	48	1315.9	658.0	1.842	819.7	0	0.00	1315.9	658.0	1.842	819.7	1.61	39.3
LAVAL - Undisturbed TC	55	2422.9	1211.5	3.361	1450.2	0	0.00	2422.9	1211.5	3.361	1450.2	1.67	40.8
U of A - Undisturbed TC	SS-UT-TC-A	1150.0	575.0	1.653	710.0	0	0.00	1150.0	575.0	1.653	710	1.62	39.6
U of A - Undisturbed TC	FS5C14	1458	729	2.329	859	0	0	1458	729	2.329	859	1.70	41.4
U of A - Undisturbed TC	FS4C14A	934	467	1.459	632	0	0	934	467	1.459	632	1.48	36.4
U of A - Undisturbed TC	FS3C17B	2014	1007	3.048	1350	0	0	2014	1007	3.048	1350	1.49	36.7
U of A - Undisturbed TE	FS5C10A	250	125	0.417	230	0	0	250	125	0.417	230	1.09	41.6
U of A - Undisturbed TE	FS4C16Z	283	141.5	0.430	334	0	0	283	141.5	0.430	334	0.85	29.6
U of A - Reconstituted TC	SS-MT-TC-A (T5)	12.9	6.5	0.019	5.0	25	5.34	12.9	6.5	0.019	5	2.58	64.4
U of A - Reconstituted TE	SS-MT-TE-A (T6)	1.3	0.7	0.002	1.0	18	0.20	1.3	0.7	0.002	1	1.30	56.1
UBC - Reconstituted TC	σ'_3=400;K_c=2 (Test 16)	400.0	200.0	0.375	317.7	3.5	1.000	1712.4	856.2	1.605	1014.6	1.7	41.19
UBC - Reconstituted TC	σ'_3=200;K_c=2 (Test 14)	221.8	110.9	0.416	169.3	3.5	0.582	1250.0	625.0	2.344	747.3	1.7	40.85
UBC - Reconstituted TC	σ'_3=100;K_c=2 (Test 12)	1350.0	675.0	5.063	790	0	0.000	1350.0	675.0	5.063	790.0	1.7	41.68
UBC - Reconstituted TC	σ'_3=50;K_c=2 (Test 10)	800.0	400.0	6.000	600	0	0.000	800.0	400.0	6.000	600.0	1.3	33.06
UBC - Reconstituted TE	σ'_3=400;K_c=1.5 (Test 9)	68.1	34.1	0.073	77.6	3.5	0.171	155.0	77.5	0.166	221.4	0.7	23.35
UBC - Reconstituted TE	σ'_3=400;K_c=2 (Test 17)	58.0	29.0	0.054	66.2	3.7	0.117	160.0	80.0	0.150	236.7	0.7	22.39
UBC - Reconstituted TE	σ'_3=200;K_c=2 (Test 15)	50.4	25.2	0.095	57.2	3.5	0.075	140.0	70.0	0.263	230.4	0.6	19.76
UBC - Reconstituted TE	σ'_3=100;K_c=2 (Test 13)	12.4	6.2	0.047	16.2	4.5	0.102	71.8	35.9	0.269	126.8	0.6	18.22
UBC - Reconstituted TE	σ'_3=50;K_c=2 (Test 11)	10.0	5.0	0.075	11.5	5	0.077	55.0	27.5	0.413	81.1	0.7	22.48

N.B. Void ratios calculated by U.B.C. are based on G_s=2.62 (Vaid et al., 1996); void ratios calculated by Laval are based on G_s=2.63; void ratios calculated by U. of A. are based on G_s=2.66 (Hofmann, 1995).

Table 5. Summary of undrained monotonic simple shear testing results for Phase I

Laboratory	Test No.	INITIAL STATE e_c	σ'_{vi} (kPa)	σ'_{hi} (kPa)	p'_i (kPa)	τ_i (kPa)	e_{us}	p'_{us} (kPa)	Ψ $e_c - e_{us}$	RSR p'_i/p'_{us}	PEAK STATE τ_p (kPa)	σ'_{vp} (kPa)	τ_p/σ'_{vp}	Peak ϕ' $\tan^{-1}(\tau_p/\sigma'_{vp})$
			$K_o = 0.500$											
UBC	FS1 C3B1	0.686	510	255	340.0	0	0.830	888.0	-0.144	0.383	79.6	267.3	0.30	16.58
UBC	FS1 C3B2	0.682	510	255	340.0	0	0.830	907.7	-0.148	0.375	200.0	350	0.57	29.74
UBC	FS3 C7B1	0.777	520	260	346.7	0	0.830	538.3	-0.053	0.644	75.0	316.7	0.24	13.32
UBC	FS3 C7B2	0.737	520	260	346.7	0	0.830	670.8	-0.093	0.517	87.0	305.6	0.28	15.89
UBC	FS1 C8B1	0.727	540	270	360.0	0	0.830	708.7	-0.103	0.508	226.8	422.2	0.54	28.24
UBC	FS1 C8B2	0.724	540	270	360.0	0	0.830	720.5	-0.106	0.500	196.3	372	0.53	27.82
UBC	FS4 C4A1	0.72	510	255	340.0	0	0.830	736.5	-0.110	0.462	255.6	471.3	0.54	28.47
UBC	FS4 C4A2	0.709	510	255	340.0	0	0.830	782.4	-0.121	0.435	270.4	500	0.54	28.40

Laboratory	Test No.	MINIMUM STATE τ_{min} (kPa)	τ_{min}/σ'_{vi}	τ_{min}/p'_i	σ'_{vmin} (kPa)	% shear strain at τ_{min}	I_B $\frac{(\tau_p - \tau_{min})}{(\tau_p - \tau_i)}$	ULTIMATE (End of test) STATE τ_f (kPa)	τ_f/σ'_{vi}	τ_f/p'_i	σ'_{vf}	τ_f/σ'_{vf}
UBC	FS1 C3B1	77.8	0.153	0.229	193.5	3.8	0.023	159.8	0.313	0.470	288.70	0.55
UBC	FS1 C3B2	200.0	0.392	0.588	350	0	0.000	200.0	0.392	0.588	350.00	0.57
UBC	FS3 C7B1	50.0	0.096	0.144	116.7	5	0.333	57.4	0.110	0.166	113.00	0.51
UBC	FS3 C7B2	83.3	0.160	0.240	210.3	3.2	0.043	153.7	0.296	0.443	282.20	0.54
UBC	FS1 C8B1	226.8	0.420	0.630	422.2	0	0.000	226.8	0.420	0.630	422.20	0.54
UBC	FS1 C8B2	196.3	0.364	0.545	372	0	0.000	196.3	0.364	0.545	372.00	0.53
UBC	FS4 C4A1	255.6	0.501	0.752	471.3	0	0.000	255.6	0.501	0.752	471.30	0.54
UBC	FS4 C4A2	270.4	0.530	0.795	500	0	0.000	270.4	0.530	0.795	500.00	0.54

Notes: Assumed that the initial K_o=0.5 in order to calculate σ'_{hi} and p'_i from σ'_{vi}.
Brittleness index is defined relative to the applied shear stresses, τ.

N.B. Void ratios calculated by U.B.C. are based on G_s=2.62 (Vaid et al., 1996).

Table 6. Summary of cyclic testing results for Phase I

(a) Reconstituted samples tested in cyclic simple shear

Sample No.	e_c	σ'_{vc}	τ_{cy}/σ'_{vc}	N	M*	Correction $\frac{CRR_M}{CRR_{M=7.5}}$	CRR (M=7.5)
S11	0.884	400	0.117	35	8.71	0.844	0.139
S13	0.868	400	0.16	2	5.177	1.556	0.103
S14	0.859	400	0.141	4	5.619	1.407	0.100

(b) Undisturbed samples tested in cyclic triaxial loading

Depth (m)	Sample No.	e_c	σ'_3, σ'_1 (kPa)	S_r (%)	Triaxial CSR $\sigma'_d/(2\sigma'_3)$	N	M*	Correction $\frac{CRR_M}{CRR_{M=7.5}}$	CRR_{tx} (M=7.5)	CRR_{ss} (M=7.5) (= $0.7CRR_{tx}$)
29.78	FS4 C3A	0.704	311	77.4	0.32	55	9.33	0.78	0.410	0.287
34.93	FS5 C15A **	0.632	346	92.6	0.361	1	4.94	1.65	0.219	0.153
35.065	FS1 C5	0.737	324	95.6	0.185	11	6.93	1.10	0.169	0.118
35.75	FS5 C16B	0.732	350	84.2	0.36	22	8.24	0.90	0.401	0.281
30.82	FS4 C6A	0.708	325	101.4	0.231	76	9.78	0.74	0.312	0.218

Notes: * To calculate the equivalent earthquake magnitude, M, from the number of cycles of uniform loading, N, the following equations were used: for $N \leq 35$, $M = -0.0038\ N^2 + 0.2442\ N + 4.7034$ (the equation given in the Introductory Data Review Report); for $N > 30$, $M = 1.3831 ln(N) + 3.7876$ (a different formula which gives better results for high values of N). Note that for $2 < N < 30$, the two formulae give similar values of M for a given value of N.

** Poor quality test; results likely unreliable.

Table 7. Summary of data for Phase III frozen samples tested to date

Sample No.	Average Depth (m)	Average σ'_v (kPa)	Void ratio as calculated by UofA (e_{sent})	Void ratio as backcalculated by testing lab (e_i)	Ψ based on e_{sent}	RSR based on e_{sent}	Lab sent to	T=triaxial (C,E) SS=simple shear CSS=cyclic SS	Fines Content (% passing No. 200 sieve)	Lab e	Lab σ'_v (kPa) Applied	Lab RSR
FS52 C6B-3	6.72	69.6	0.7759	0.787	-0.085	0.086	UBC	TC	5.16	0.772	66	0.080
FS52 C4A-1	4.58	48.8	0.7172	0.711	-0.149	0.044	UBC	TC		0.714	48	0.042
FS52 C4A-2	4.71	50.1	0.7386	0.726	-0.127	0.051	UBC	TC	5.42	0.725	48	0.045
FS5 C1B-2B	3.585	39.2	0.87	0.881	0.001	1.040	UBC	TC		0.847	42	0.245
FS5 C1B-3-2	3.735	40.6	0.8253	0.827	-0.044	0.066	UBC	TC	8.43	0.804	44	0.063
FS 6 C2B-2-4	3.035	33.8	0.6889	0.696	-0.183	0.026	UBC	TC		0.68	48	0.035
FS26 C2-1-2	3.305	36.5	0.7183	0.706	-0.152	0.033	UBC	TC	4.92	0.691	40	0.031
FS5 C1B-3-3*	3.735	40.6	0.8194	0.824	-0.049	0.064	UBC	TC		0.811	204	0.305
FS 6 C2B-2-2*	3.035	33.8	0.6943	0.698	-0.177	0.027	UBC	TC	6.29	0.682	194	0.142
FS26 C2-1-3*	3.305	36.5	0.7217	0.727	-0.149	0.034	UBC	TC		0.703	196	0.162
FS26 C3-1A	4.53	48.3	0.8371		-0.029	0.147	UBC	sample collapsed **				
FS4 C1-3A	3.78	41.1	0.8151		-0.054	0.063	UBC	sample collapsed **				
FS4 C1-3B	3.78	41.1	0.8094		-0.059	0.061	UBC	sample collapsed **	5.26			
FS5 C1B-2A*	3.585	39.2	0.8552	0.877	-0.014	0.393	UBC	TE	8.67	0.827	80	0.130
FS5 C1B-2C	3.585	39.2	0.8479	0.845	-0.022	0.243	UBC	TE		0.833	42	0.098
FS5 C1B-3-1	3.735	40.6	0.8257	0.833	-0.043	0.066	UBC	TE	5.68	0.811	44	0.066
FS 6 C2B-2-3	3.035	33.8	0.7105	0.727	-0.161	0.029	UBC	TE		0.722	48	0.044
FS26 C2-1-1	3.305	36.5	0.7113	0.72	-0.159	0.032	UBC	TE		0.708	40	0.034
FS26 C3-1B*	4.53	48.3	0.8402	0.882	-0.026	0.181	UBC	TE		0.868	112	2.606
FS5 C1B-3-4*	3.735	40.6	0.8223	0.822	-0.047	0.065	UBC	TE		0.796	204	0.280
FS 6 C2B-2-1*	3.035	33.8	0.6809	0.673	-0.191	0.025	UBC	TE	5.03	0.657	294	0.188
FS26 C2-1-4*	3.305	36.5	0.729	0.7	-0.142	0.035	UBC	TE		0.698	196	0.157
FS26 C2-2-3*	3.455	37.9	0.7562	0.764	-0.114	0.042	UBC	TE/C		0.749	196	0.208
FS26 C54 3	6.85	70.8	0.7818	0.771	-0.079	0.091	UBC	TE/E		0.745	68	0.071
FS26 C42 2*	5.63	59.0	0.7257	0.743	-0.137	0.056	UBC	TE/C		0.734	100	0.098
FS26 C42 3*	5.63	59.0	0.7294	0.746	-0.134	0.057	UBC	TE/C		0.741	100	0.102
FS52 C6A-1	6.17	64.2	0.7004		-0.161	0.053	Laval					
FS52 C6B-1	6.48	67.3	0.6608		-0.200	0.044	Laval					
FS52 C6B-2	6.6	68.4	0.6889		-0.172	0.053	Laval					
FS52 C5D	6.07	63.3	0.7034		-0.159	0.053	Laval					
FS5 C1B-2D	3.585	39.2	0.8535		-0.016	0.351	UofA					
FS26 C2-2-1A*	3.4	37.4	0.7389	0.776	-0.131	0.038	UBC	SS	3.4	0.737	100	0.099
FS26 C2-2-1B*	3.42	37.6	0.7527	0.79	-0.117	0.041	UBC	SS	5	0.735	100	0.098
FS26 C2-2-1C*	3.45	37.9	0.7555	0.791	-0.114	0.042	UBC	SS	3.5	0.733	100	0.097
FS26 C2-2-1D*	3.48	38.2	0.7537	0.797	-0.116	0.042	UBC	SS	5.1	0.738	100	0 100
FS26 C2-2-2A*	3.4	37.4	0.7305	0.766	-0.140	0.036	UBC	SS	5	0.716	100	0.089
FS26 C2-2-2B*	3.42	37.6	0.7474	0.779	-0.123	0.040	UBC	SS	3.3	0.727	100	0.094
FS26 C2-2-2C*	3.46	38.0	0.7577	0.777	-0.112	0.043	UBC	SS	5.1	0.714	100	0.088
FS26 C2-2-2D*	3.48	38.2	0.7513	0.783	-0.119	0.041	UBC	SS	5	0.721	100	0.091
FS26 C42 1A	5.57	58.4	0.7401	0.772	-0.123	0.060	UBC	CSS		0.716		
FS26 C42 1B	5.59	58.6	0.7322	0.78	-0.131	0.057	UBC	CSS	3.6	0.725		
FS26 C42 1C	5.65	59.2	0.7456	0.812	-0.118	0.062	UBC	CSS	8	0.741		
FS26 C42 1D	5.67	59.4	0.779	0.801	-0.084	0.075	UBC	CSS	5	0.729		
FS26 C54 1A	6.79	70.3	0.774	0.792	-0.087	0.086	UBC	CSS	2.5	0.077		
FS26 C54 1B	6.81	70.5	0.7914		-0.069	0.095	UBC					
FS26 C54 1C	6.87	71.0	0.7949		-0.065	0.098	UBC					
FS26 C54 1D	6.89	71.2	0.8054		-0.055	0.104	UBC					

Notes: 1. * Samples which were tested in the laboratory under effective stresses higher than those in-situ, in order to simulate embankment loading.

2. ** Samples collapsed while applying differential vacuum.

3. Void ratios by U.B.C. are based on G_s=2.66 (Vaid et al., 1996); however, void ratios by U. of A. are based on G_s=2.62 (Hofmann, 1995).

4. TE/C indicates samples loaded in TE followed by TC; TE/E indicates samples loaded in TE, unloaded, and reloaded in TE (see Appendix O).

Table 8. Summary of undrained monotonic triaxial testing results for Phase III (N.B. continued on next page).

Laboratory	Test No.	INITIAL STATE										PEAK STATE				
		e_c	σ'_{vi} (kPa)	σ'_{hi} (kPa)	p'_i (kPa)	q_i (kPa)	S_i (kPa)	e_{ss}	p'_{ss} (kPa)	Ψ $e_c - e_{ss}$	RSR p'_i/p'_{ss}	q_p (kPa)	S_p (kPa)	p'_p (kPa)	Mp $(q/p')_p$	Peak ϕ'
UBC	FS5 C1B 2B (TC)	0.847	42	21	28.00	21	10.5	0.868	114.1	-0.021	0.245	21	10.5	28	0.75	19.5
UBC	FS 52 C4A1 (TC)	0.714	48	24	32.00	24	12	0.866	761.2	-0.152	0.042	417.6	208.8	283	1.48	36.3
UBC	FS 52 C4A2 (TC)	0.725	48	24	32.00	24	12	0.866	716.5	-0.141	0.045	400	200	277.1	1.44	35.6
UBC	FS 52 C6B3 (TC)	0.772	66	33	44.00	33	16.5	0.861	553.3	-0.089	0.080	501.8	250.9	351.5	1.43	35.2
UBC	FS5 C1B3 2 (TC)	0.804	44	22	29.33	22	11	0.868	464.0	-0.064	0.063	150	75	118	1.27	31.6
UBC	FS5 C1B3 3 (TC)*	0.811	204	102	136.00	102	51	0.844	446.5	-0.033	0.305	129.8	64.9	124	1.05	26.5
UBC	FS6 C2B2 2 (TC)*	0.682	194	97	129.33	97	48.5	0.845	907.7	-0.163	0.142	438	219	314.7	1.39	34.4
UBC	FS6 C2B2 4 (TC)	0.68	48	24	32.00	24	12	0.866	917.8	-0.186	0.035	375	187.5	244.5	1.53	37.6
UBC	FS26 C21 2 (TC)	0.691	40	20	26.67	20	10	0.869	863.9	-0.178	0.031	339.2	169.6	227.7	1.49	36.6
UBC	FS26 C21 3 (TC)*	0.703	196	98	130.67	98	49	0.845	808.7	-0.142	0.162	428.6	214.3	311	1.38	34.1
UBC	FS26 C3-1 (B) (TE)*	0.868	112	56	74.67	56	28	0.853	28.7	0.015	2.606	8.4	4.2	24.9	0.34	10.3
UBC	FS5 C1B 2C (TE)	0.833	42	21	28.00	21	10.5	0.868	286.5	-0.035	0.098	56.8	28.4	58.8	0.97	35.1
UBC	FS5 C1B 2A (TE)*	0.827	80	40	53.33	40	20	0.859	408.8	-0.032	0.130	66.6	33.3	76.7	0.87	30.5
UBC	FS5 C1B3 1 (TE)	0.811	44	22	29.33	22	11	0.868	446.5	-0.057	0.066	4.2	2.1	13.5	0.31	9.4
UBC	FS5 C1B3 4 (TE)*	0.796	204	102	136.00	102	51	0.844	484.9	-0.048	0.280	26.4	13.2	54.4	0.49	15.3
UBC	FS6 C2B2 1 (TE)*	0.657	294	147	196.00	147	73.5	0.839	1041.5	-0.182	0.188	393	196.5	374.3	1.05	39.5
UBC	FS6 C2B2 3 (TE)	0.722	48	24	32.00	24	12	0.866	728.4	-0.144	0.044	68.6	34.3	68.4	1.00	37.0
UBC	FS26 C21 1 (TE)	0.708	40	20	26.67	20	10	0.869	786.8	-0.161	0.034	105.2	52.6	99.9	1.05	39.7
UBC	FS26 C21 4 (TE)*	0.698	196	98	130.67	98	49	0.845	831.3	-0.147	0.157	115.8	57.9	107	1.08	41.3
UBC	FS26 C22 3 (TE/C)*	0.749	196	98	130.67	98	49	0.845	627.9	-0.096	0.208					
UBC	FS 26 C54 3 (TE/E)	0.745	68	34	45.33	34	17	0.861	641.9	-0.116	0.071					
UBC	FS26 C42 2 (TE/C)*	0.734	100	50	66.67	50	25	0.855	681.9	-0.121	0.098					
UBC	FS26 C42 3 (TE/C)*	0.741	100	50	66.67	50	25	0.855	656.2	-0.114	0.102					

Notes: 1. * Samples which were tested in the laboratory under effective stresses higher than those in-situ, in order to simulate embankment loading.
2. Void ratios calculated by U.B.C. are based on G_s=2.66 (Vaid et al., 1996).
3. TE/C indicates samples loaded in TE followed by TC; TE/E indicates samples loaded in TE, unloaded, and reloaded in TE (see Appendix O).

Table 8 (continued).

Laboratory	Test No.	MINIMUM STATE						ULTIMATE (End of test) STATE					
		q_{min} (kPa)	S_{min} (kPa)	S_{min}/p'_i	p'_{min} (kPa)	% axial strain, ε_a during S_{min}	I_B	q_f (kPa)	S_f (kPa)	S_f/p'_i	p'_f (kPa)	M_f $(q/p')_f$	End-of-test ϕ'
							(actually infinity)						
UBC	FS5 C1B 2B (TC)	16.4	8.2	0.29	13.6	7	5	116.6	58.3	2.08	87.6	1.33	33.0
UBC	FS 52 C4A1 (TC)	417.6	208.8	6.53	283	0	0	417.6	208.8	6.53	283	1.48	36.3
UBC	FS 52 C4A2 (TC)	400	200	6.25	277.1	0	0	400	200	6.25	277.1	1.44	35.6
UBC	FS 52 C6B3 (TC)	501.8	250.9	5.70	351.5	0	0	501.8	250.9	5.70	351.5	1.43	35.2
UBC	FS5 C1B3 2 (TC)	150	75	2.56	118	0	0	150	75	2.56	118	1.27	31.6
UBC	FS5 C1B3 3 (TC)*	122.8	61.4	0.45	95.3	4.4	0.25	350.8	175.4	1.29	271.3	1.29	32.1
UBC	FS6 C2B2 2 (TC)*	438	219	1.69	314.7	0	0	438	219	1.69	314.7	1.39	34.4
UBC	FS6 C2B2 4 (TC)	375	187.5	5.86	244.5	0	0	375	187.5	5.86	244.5	1.53	37.6
UBC	FS26 C21 2 (TC)	339.2	169.6	6.36	227.7	0	0	339.2	169.6	6.36	227.7	1.49	36.6
UBC	FS26 C21 3 (TC)*	428.6	214.3	1.64	311	0	0	428.6	214.3	1.64	311	1.38	34.1
UBC	FS26 C3-1 (B) (TE)*	3.8	1.9	0.03	4.8	7.4	0.07	49.2	24.6	0.33	58.6	0.84	29.2
UBC	FS5 C1B 2C (TE)	56.8	28.4	1.01	58.8	7.4	0.00	56.8	28.4	1.01	58.8	0.97	35.1
UBC	FS5 C1B 2A (TE)*	66.6	33.3	0.62	76.7	0	0.00	66.6	33.3	0.62	76.7	0.87	30.5
UBC	FS5 C1B3 1 (TE)	0.4	0.2	0.01	1.7	10.6	0.15	9.8	4.9	0.17	11.8	0.83	28.8
UBC	FS5 C1B3 4 (TE)*	15.8	7.9	0.06	19.3	4.7	0.08	52.6	26.3	0.19	61.4	0.86	30.0
UBC	FS6 C2B2 1 (TE)*	393	196.5	1.00	374.3	0	0	393	196.5	1.00	374.3	1.05	39.5
UBC	FS6 C2B2 3 (TE)	68.6	34.3	1.07	68.4	0	0	68.6	34.3	1.07	68.4	1.00	37.0
UBC	FS26 C21 1 (TE)	105.2	52.6	1.97	99.9	0	0	105.2	52.6	1.97	99.9	1.05	39.7
UBC	FS26 C21 4 (TE)*	115.8	57.9	0.44	107	0	0	115.8	57.9	0.44	107	1.08	41.3
UBC	FS26 C22 3 (TE/C)*												
UBC	FS 26 C5-1 3 (TE/E)												
UBC	FS26 C42 2 (TE/C)*												
UBC	FS26 C42 3 (TE/C)*												

* Samples which were tested in the laboratory under effective stresses higher than those in-situ, in order to simulate embankment loading.

N.B. Void ratios calculated by U.B.C. are based on G_s=2.66 (Vaid et al., 1996).

Table 9. Summary of undrained monotonic simple shear testing results for Phase III

Laboratory	Test No.	INITIAL STATE e_c	σ'_{vi} (kPa)	σ'_{hi} (kPa)	p'_i (kPa)	τ_i (kPa)	e_{us}	p'_{us} (kPa)	Ψ $e_c - e_{us}$	RSR p'_i/p'_{us}	PEAK STATE τ_p (kPa)	σ'_{vp} (kPa)	τ_p/σ'_{vp}	Peak ϕ' $\tan^{-1}(\tau_p/\sigma'_{vp})$
				Ko = 0.500										
UBC	FS26 C22 1A	0.737	100	50	66.7	0	0.855	670.8	-0.118	0.099	13	56	0.23	13.07
UBC	FS26 C22 1B	0.735	100	50	66.7	0	0.855	678.2	-0.120	0.098				
UBC	FS26 C22 1C	0.733	100	50	66.7	0	0.855	685.7	-0.122	0.097				
UBC	FS26 C22 1D	0.738	100	50	66.7	0	0.855	667.1	-0.117	0.100				
UBC	FS26 C22 2A	0.716	100	50	66.7	0	0.855	752.9	-0.139	0.089				
UBC	FS26 C22 2B	0.727	100	50	66.7	0	0.855	708.7	-0.128	0.094	13	59	0.22	12.43
UBC	FS26 C22 2C	0.714	100	50	66.7	0	0.855	761.2	-0.141	0.088				
UBC	FS26 C22 2D	0.721	100	50	66.7	0	0.855	732.5	-0.134	0.091				

Laboratory	Test No.	MINIMUM STATE τ_{min} (kPa)	τ_{min}/σ'_{vi}	τ_{min}/p'_i	σ'_{vmin} (kPa)	% shear strain at τ_{min}	I_B $\frac{(\tau_p - \tau_{min})}{(\tau_p - \tau_i)}$	ULTIMATE (End of test) STATE τ_f (kPa)	τ_f/σ'_{vi}	τ_f/p'_i	σ'_{vf}	τ_f/σ'_{vf}
UBC	FS26 C22 1A	11	0.110	0.165	32		0.154					
UBC	FS26 C22 1B											
UBC	FS26 C22 1C											
UBC	FS26 C22 1D											
UBC	FS26 C22 2A											
UBC	FS26 C22 2B	11	0.110	0.165	26		0.154					
UBC	FS26 C22 2C											
UBC	FS26 C22 2D											

Notes: Assumed that the initial K_o=0.5 in order to calculate σ'_{hi} and p'_i from σ'_{vi}.
Brittleness index is defined relative to the applied shear stresses, τ.

N.B. Void ratios calculated by U.B.C. are based on G_s=2.66 (Vaid et al., 1996)

Table 10. Summary of cyclic simple shear testing results for Phase III

Depth (m)	Sample No.	e_c	τ_{cy}/σ'_{vc}	N	M	Correction $\frac{CRR_M}{CRR_{M=7.5}}$	CRR (M=7.5)
5.56	FS26 C42 1A	0.716	0.116	4	5.62	1.41	0.08
5.58	FS26 C42 1B	0.725	0.101	8	6.41	1.20	0.08
5.64	FS26 C42 1C	0.741	0.082	12	7.09	1.07	0.08
5.66	FS26 C42 1D*	0.729	0.066	87	9.96	0.73	0.09
6.78	FS26 C54 1A	0.712	0.08	13	7.24	1.04	0.08

Notes:
1. Void ratios calculated by U.B.C. are based on G_s=2.66 (Vaid et al., 1996)
2. * Since the number of cycles was so high (i.e. N =87), a different formula was used to estimate M from N for this sample than for the other samples. For this sample, the formula $M = 1.3831 \ln(N) + 3.7876$ was used. For the other samples, the formula given in the Introductory Data Review Report was used (i.e. $M = -0.0038 N^2 + 0.2442 N + 4.7034$). Note that for $2 < N < 30$, the two formulae give similar values of M for a given value of N.

Table 11. Summarized results of data review: average values of soil parameters in the target zones of the Phase I and Phase III CANLEX sites

Parameter	Phase I (Mildred Lake)	Phase III (J-pit)
Site conditions:		
Target zone depth (m)	27 to 37	3 to 7
GWT(m)	21	0.5
Unit weight of soil (assumed; kN/m^3)	18.5 (above GWT) 19.5 (below GWT)	18.5 (above GWT) 19.5 (below GWT)
in-situ σ'_{vi} (kPa)	495.2	52.9
in-situ K_o	0.5	0.5
in-situ σ'_{hi} (kPa)	247.6	26.4
in-situ p'_i (kPa)	330.1	35.3
in-situ q_i (kPa)	247.6	26.4
In-situ testing results:		
$(N_1)_{60}$	18.2 (SD=3.0)	3.4 (SD=2.0)
FC (%) of SPT samples	12	10
q_{c1} (MPa)	7.38 (SD=1.67)	2.35 (SD=1.53) 2.04 (SD=0.79)[&]
q_{c1N}	73.8 (SD=16.7)	25.5 (SD=16.5)
Q	32.0 (SD=7.8)	31.0 (SD=23.9)
F	0.727 (SD=0.150)	0.872 (SD=0.331)
I_c (based on q_{c1N} and F)	1.942 (SD=0.105)	2.431 (SD=0.369)
Soil behaviour type based on CPT	clean sand to silty sand	silty sand to sandy silt
FC (%) predicted by CPT	11.5 (SD=2.8)	27.5 (SD=10.5)
V_{s1} (m/s)	156.4 (SD=20.1)	127.1 (SD=3.0)
Y	95.6 (SD=12.1)	101.1 (SD=6.3)
X	74.8 (SD=9.0)	89.2 (SD=7.5)
$q_{c1}/(N_1)_{60}$	0.44 (SD=0.15)	0.51 (SD=0.25)
e (predicted by geophysical)	0.788 (SD=0.053)	0.721 (SD=0.068)[$]
Frozen samples tested to date:		
FC (%)	5.1 (SD=2.2)	5.2 (SD=1.6)
e	0.768 (SD=0.040)	0.762 (SD=0.053)
D_r (%) *	66.0 (SD=15.2)	43.0 (SD=10.0)
Ψ**	-0.064 (SD=0.040)	-0.106 (SD=0.053)
RSR[#]	0.588	0.061

Notes:

Parameter values are shown as the average in the target zone (SD = standard deviation) *calculated using e_{max} and e_{min} (Table 1); **relative to the flat portion of reference USL (Table 2); [#]relative to reference USL (Table 2); calculated from average e of frozen samples and average estimated p' in target zone; [&]not including CPT21; [$]GEO2 only.

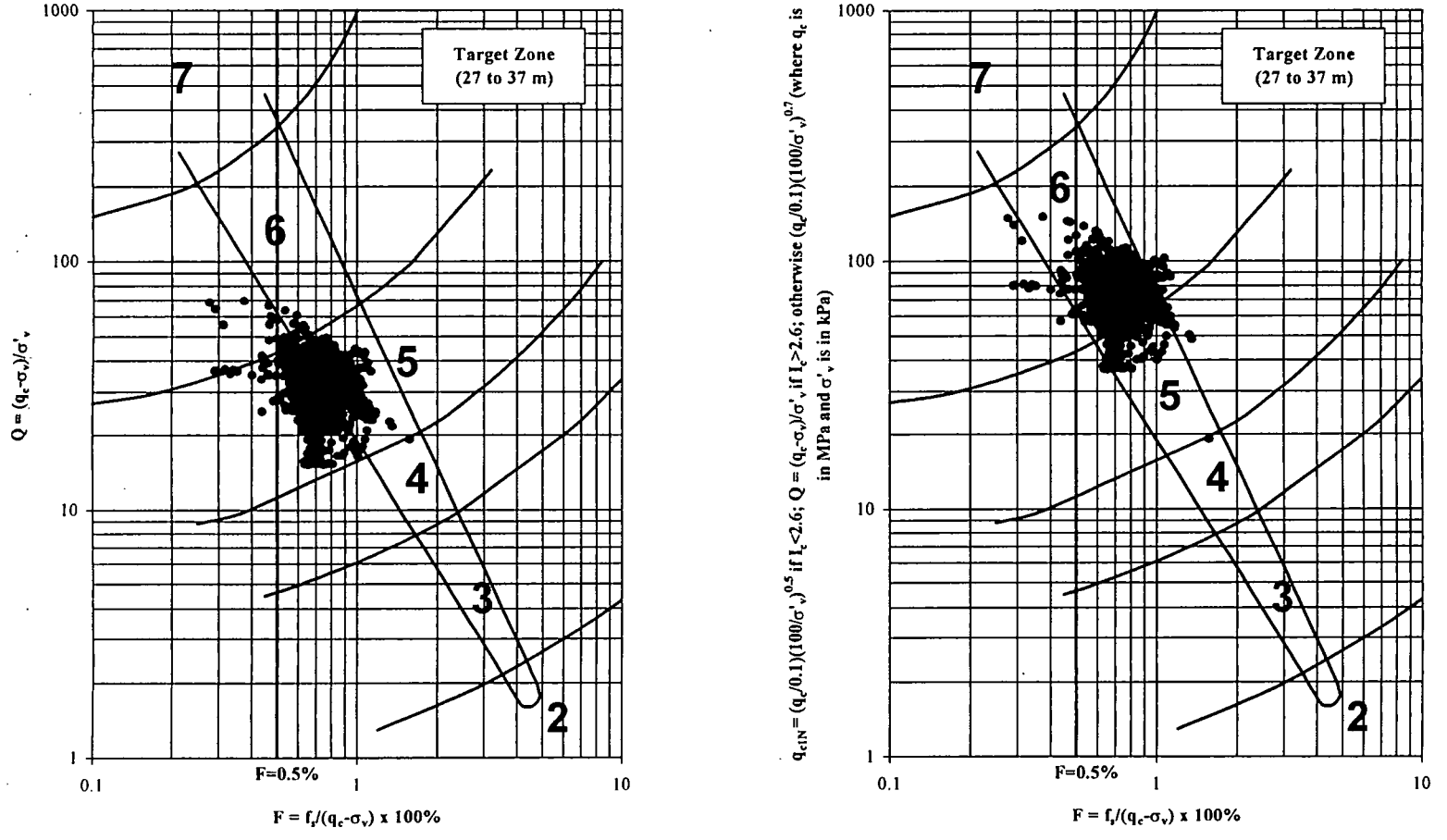

Figure 1. **CPT-based soil classification of the Phase I Site: (a) using the method by Robertson (1990); (b) using the revised method described in this report.**

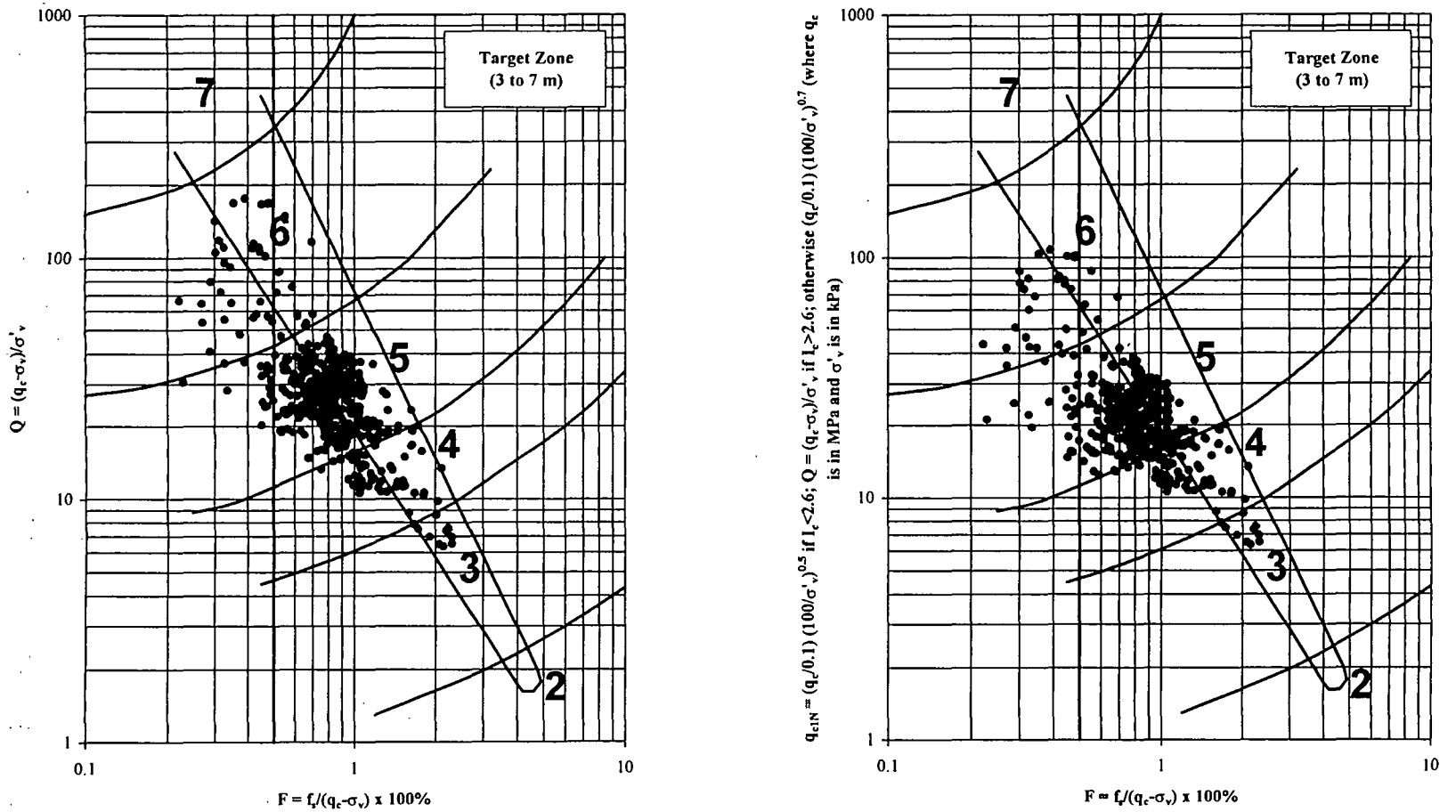

Figure 2. **CPT-based soil classification of the Phase III site: (a) using the method by Robertson (1990); (b) using the revised method described in this report.**

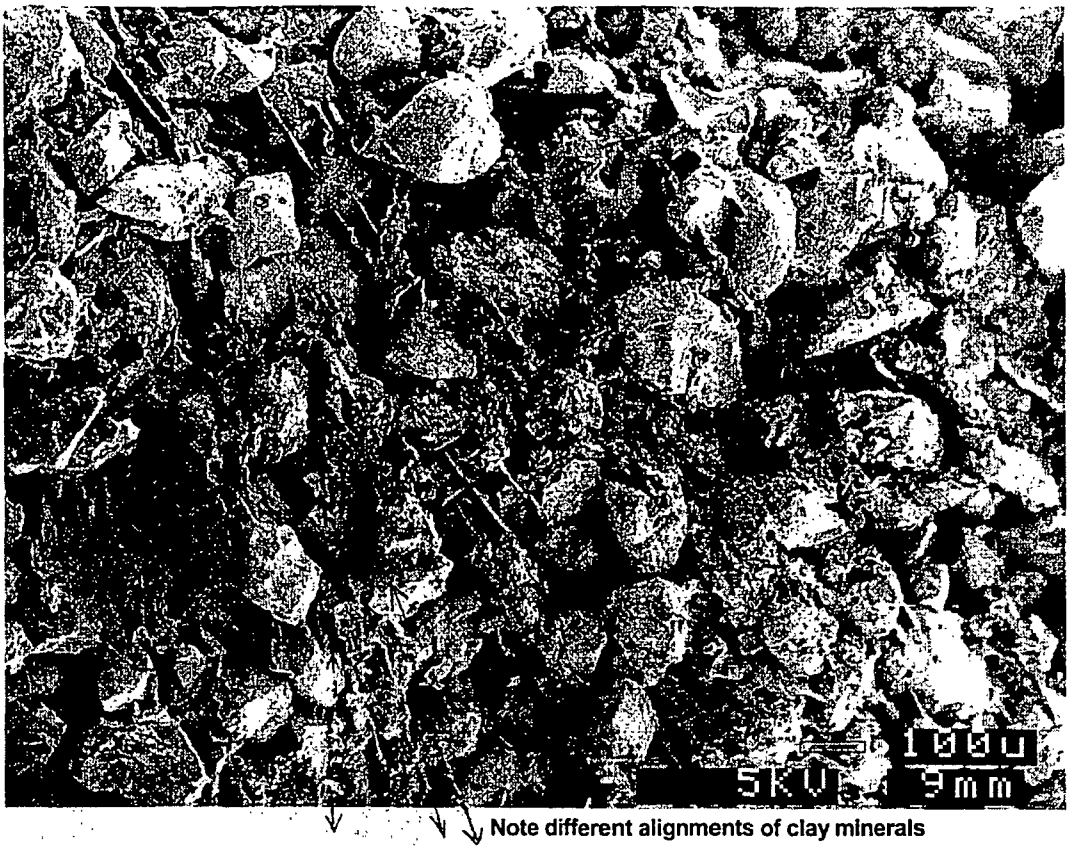

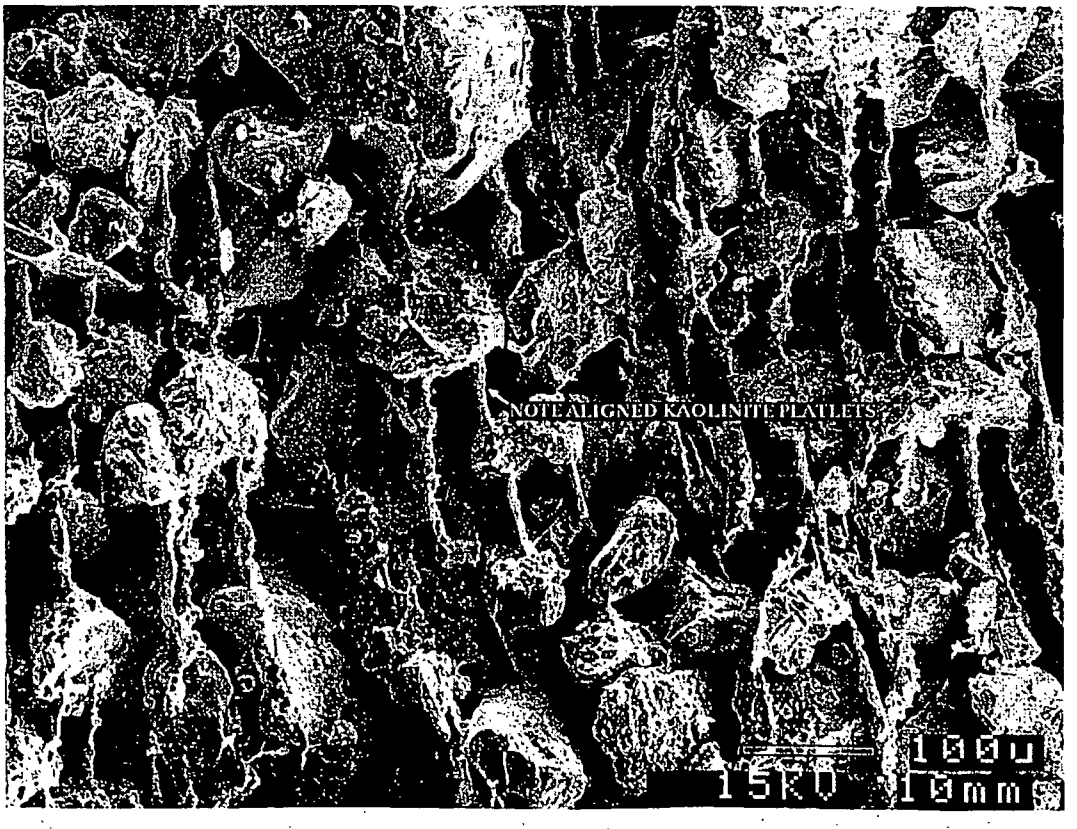

Figure 3. Scanning electron microscope (SEM) photos of in-situ frozen soil samples from (a) the Phase I site target zone, and (b) the Phase III site target zone.

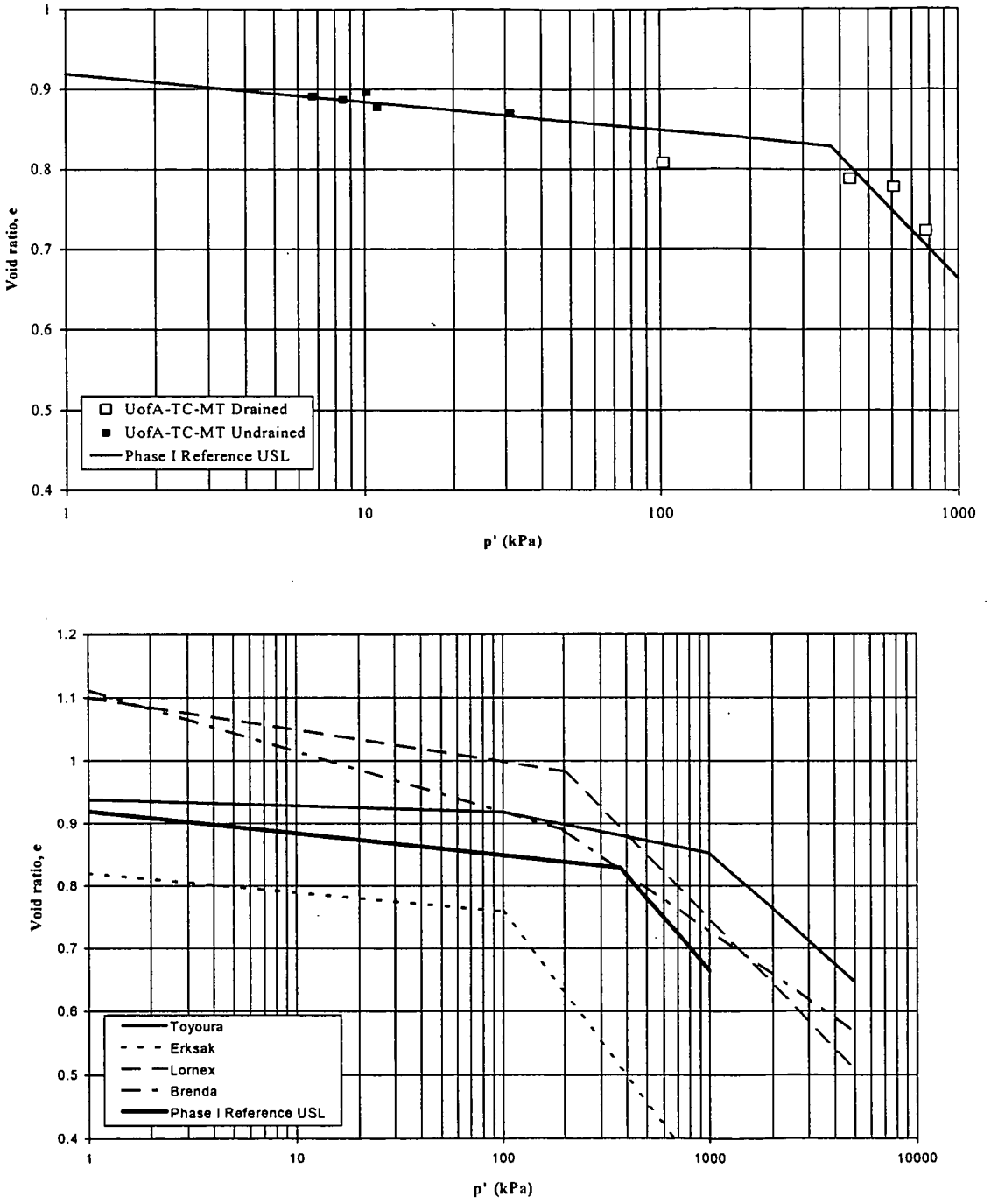

Figure 4. **(a) Reference USL based on triaxial compression testing of reconstituted isotropically consolidated Syncrude Phase I sand (after Cunning, 1994); (b) comparison of the selected Phase I USL with USLs for other sands, as summarized by Sasitharan et al. (1994) and shown in the Introductory Data Review Report.**

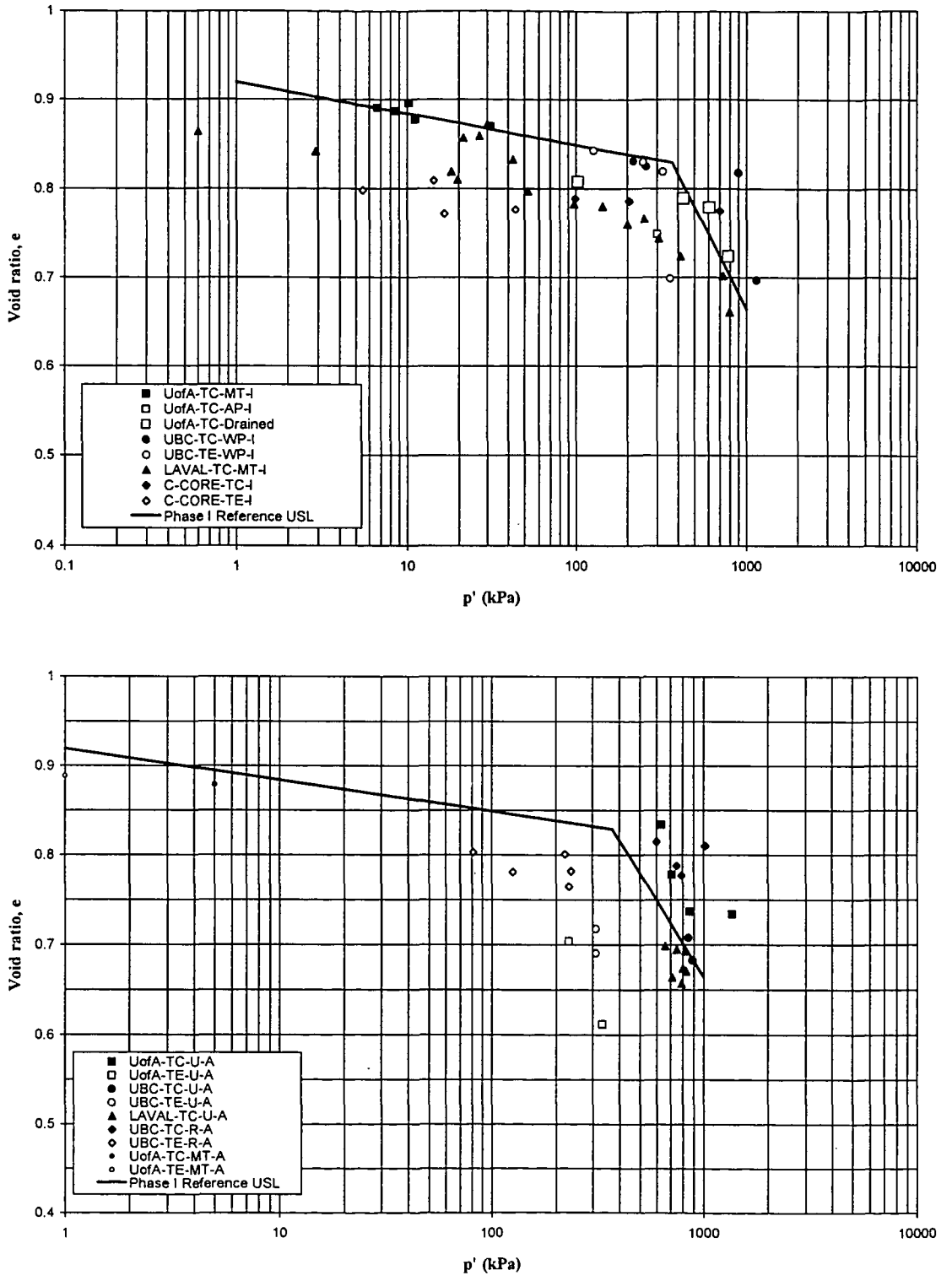

Figure 5. Comparison of selected Phase I reference USL with end-of-test points for Phase I tests on (a) reconstituted, isotropically consolidated samples; (b) reconstituted and undisturbed anisotropically consolidated samples.

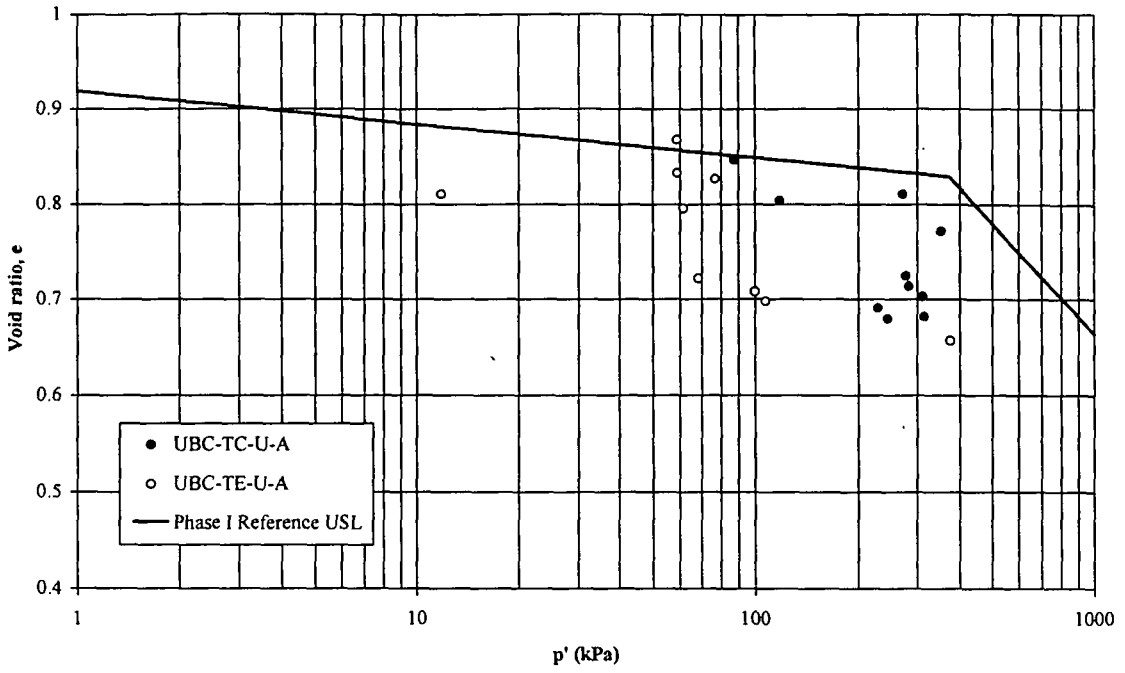

Figure 6. Comparison of selected Phase I reference USL with end-of-test points of tests on undisturbed anistropically consolidated Phase III samples.

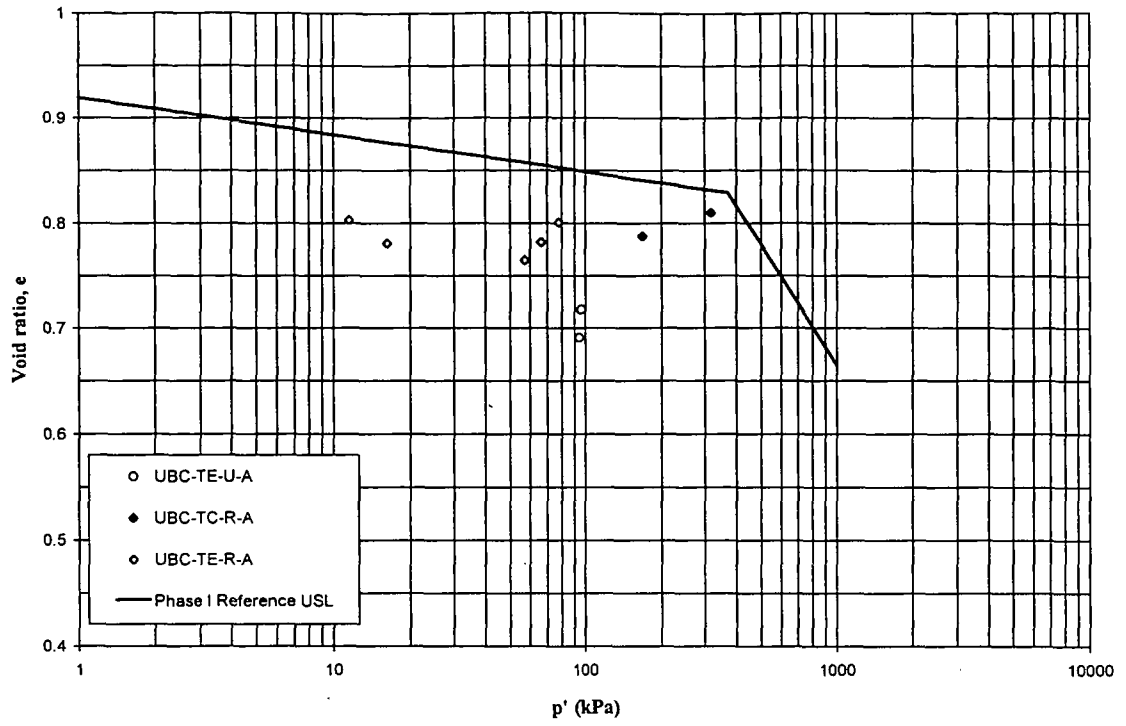

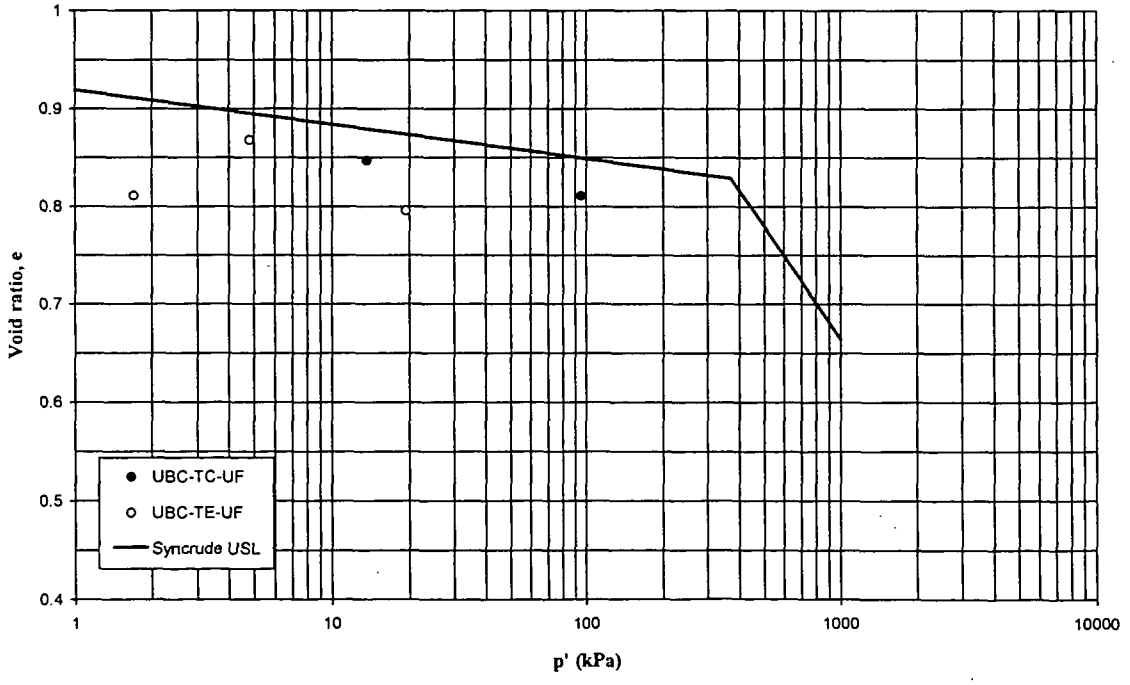

Figure 7. Quasi-steady-states (QSS) of (a) Phase I reconstituted and undisturbed anisotropically consolidated samples and (b) Phase III undisturbed anisotropically consolidated samples.

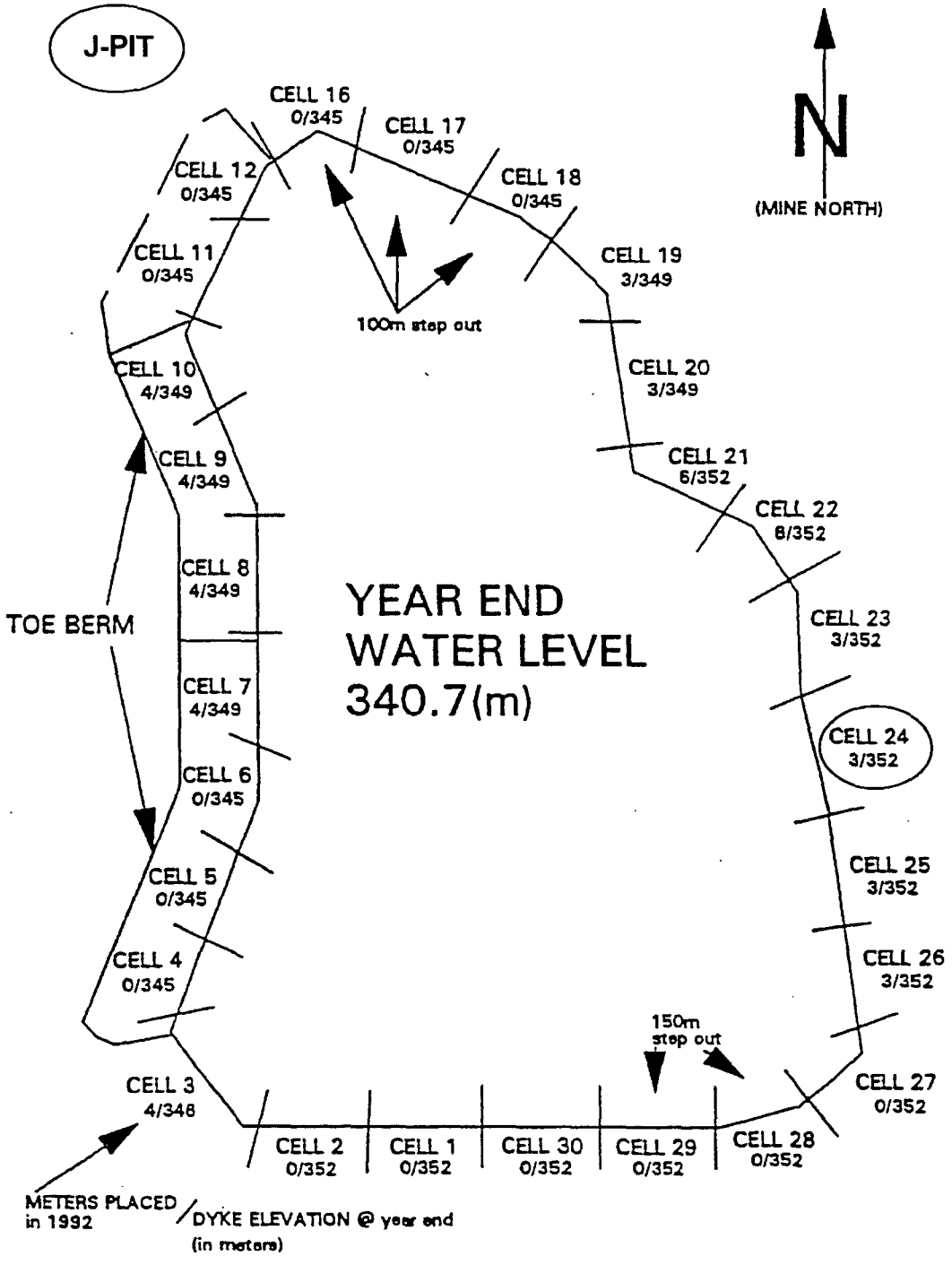

Figure 8. **Phase I site, located, as indicated, in Cell 24 of Mildred Lake Settling Basin at Syncrude Canada Ltd.; also indicated is the approximate location of J-pit, the Phase III site (after Robertson et al., 1993).**

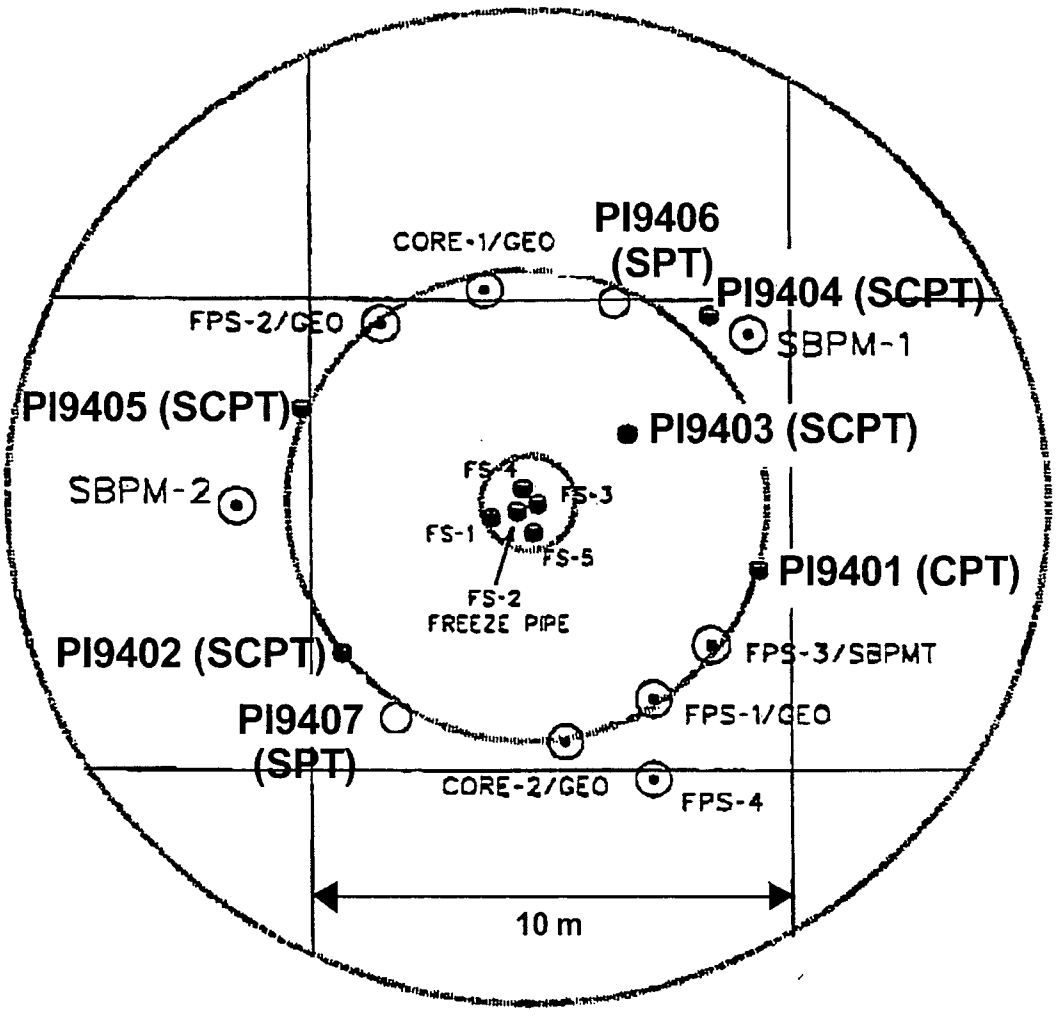

Figure 9. **Detailed site plan of the in-situ testing area at the Phase I Site (after Campanella, 1994).**

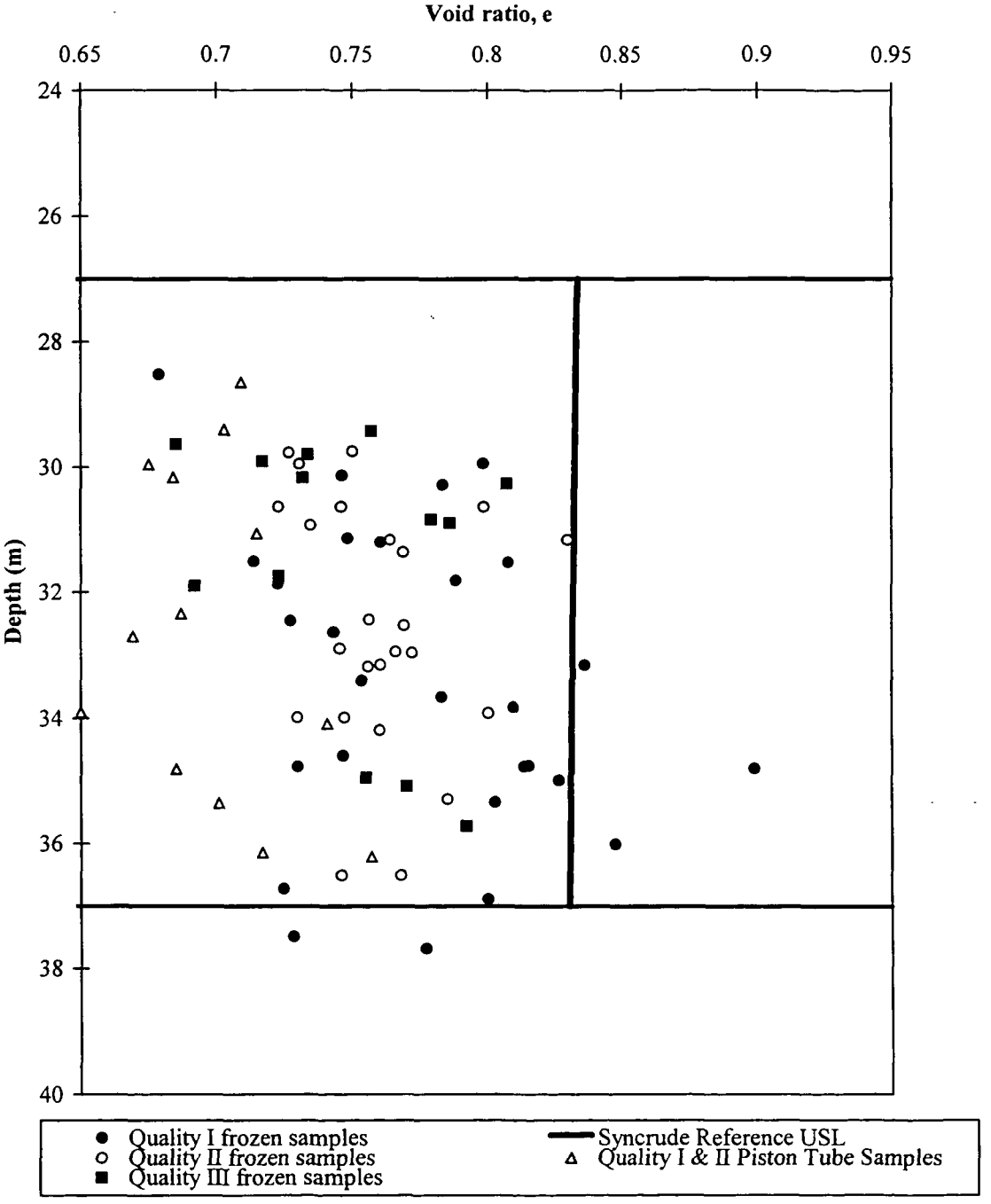

Figure 10. Void ratios of undisturbed frozen samples and piston tube samples obtained at the Phase I site.

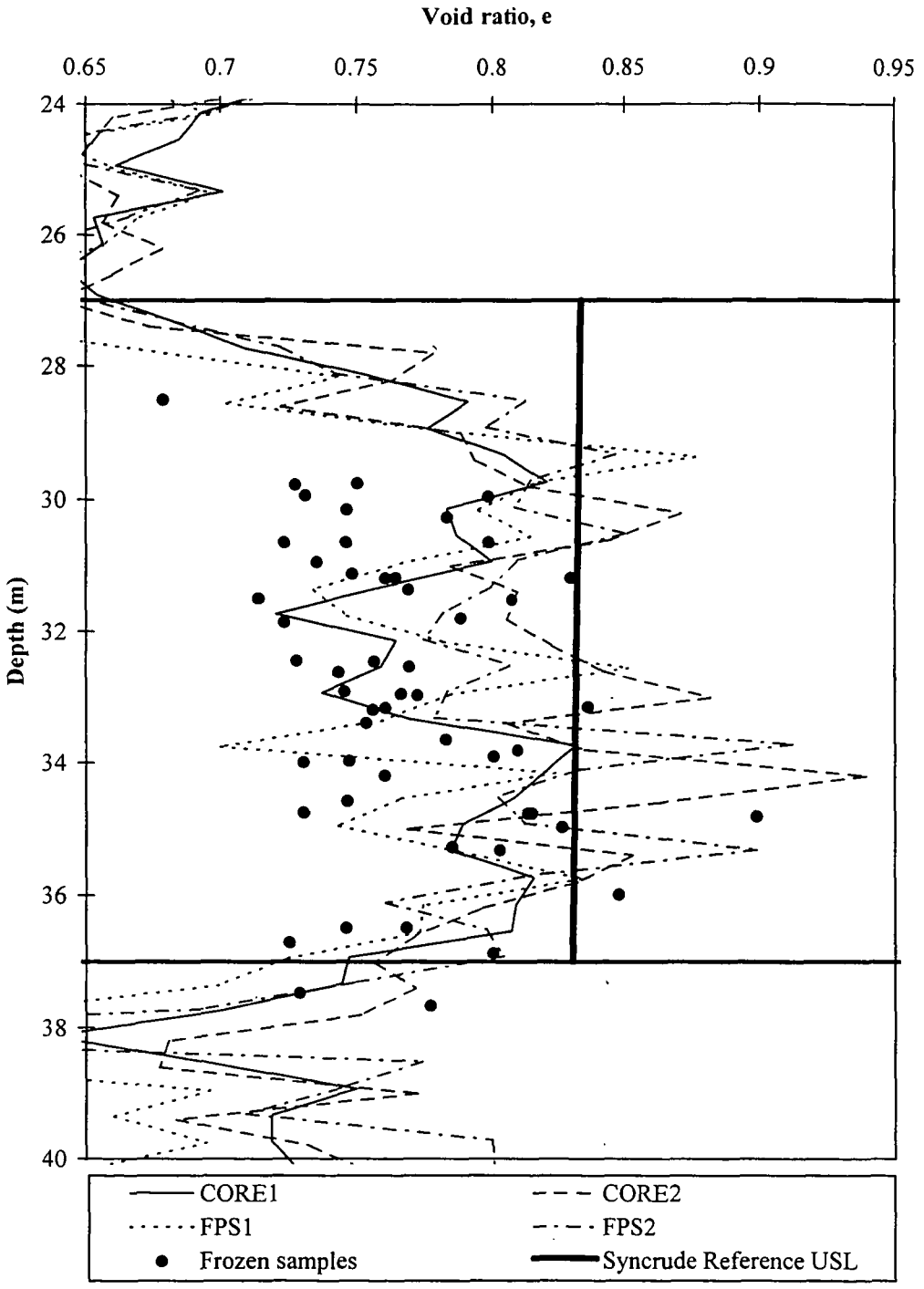

Figure 12. Comparison of geophysical logging predictions of void ratio (G_s=2.63) at the Phase I site with undisturbed samples (G_s=2.66).

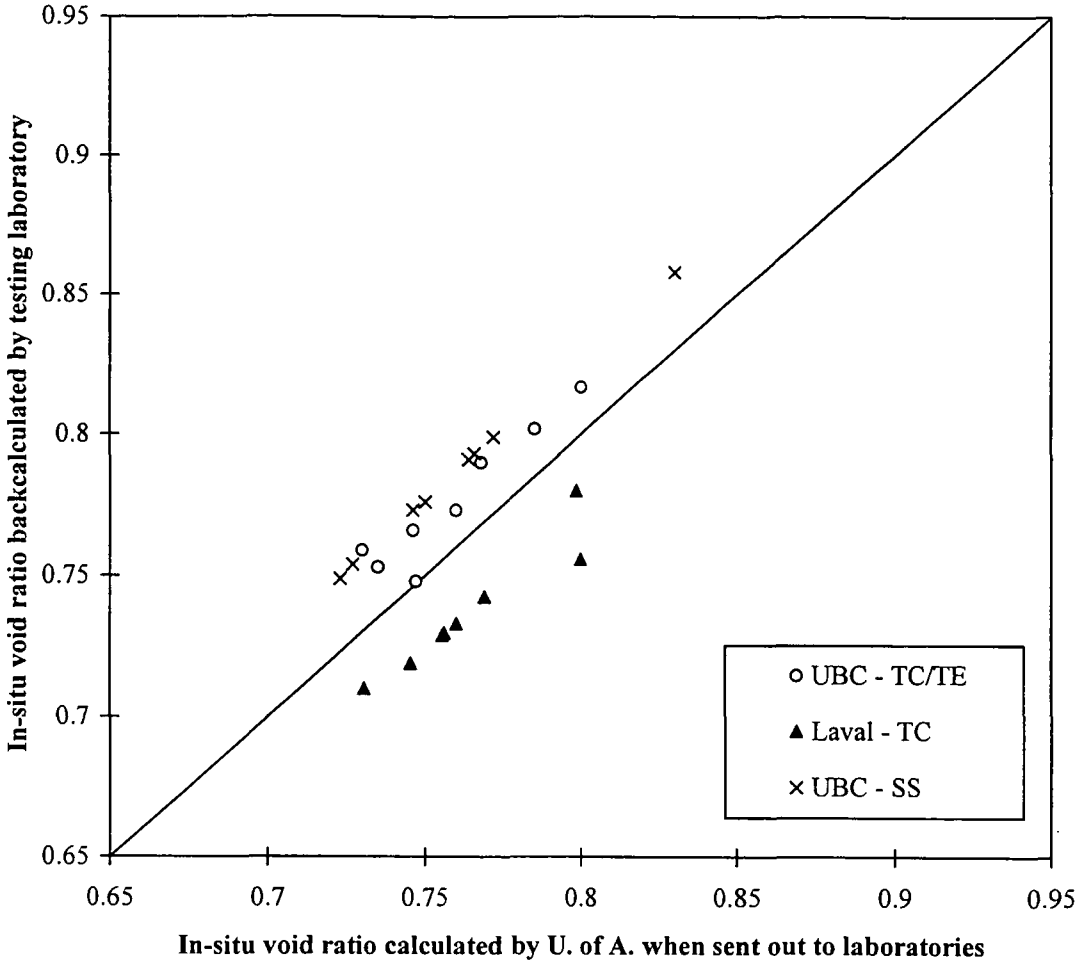

Figure 11. Comparison of different methods of calculation of in-situ void ratio for undisturbed samples from the Phase I site (N.B. U. of A. used G_s=2.66; U.B.C. used G_s=2.62; Laval used G_s=2.63).

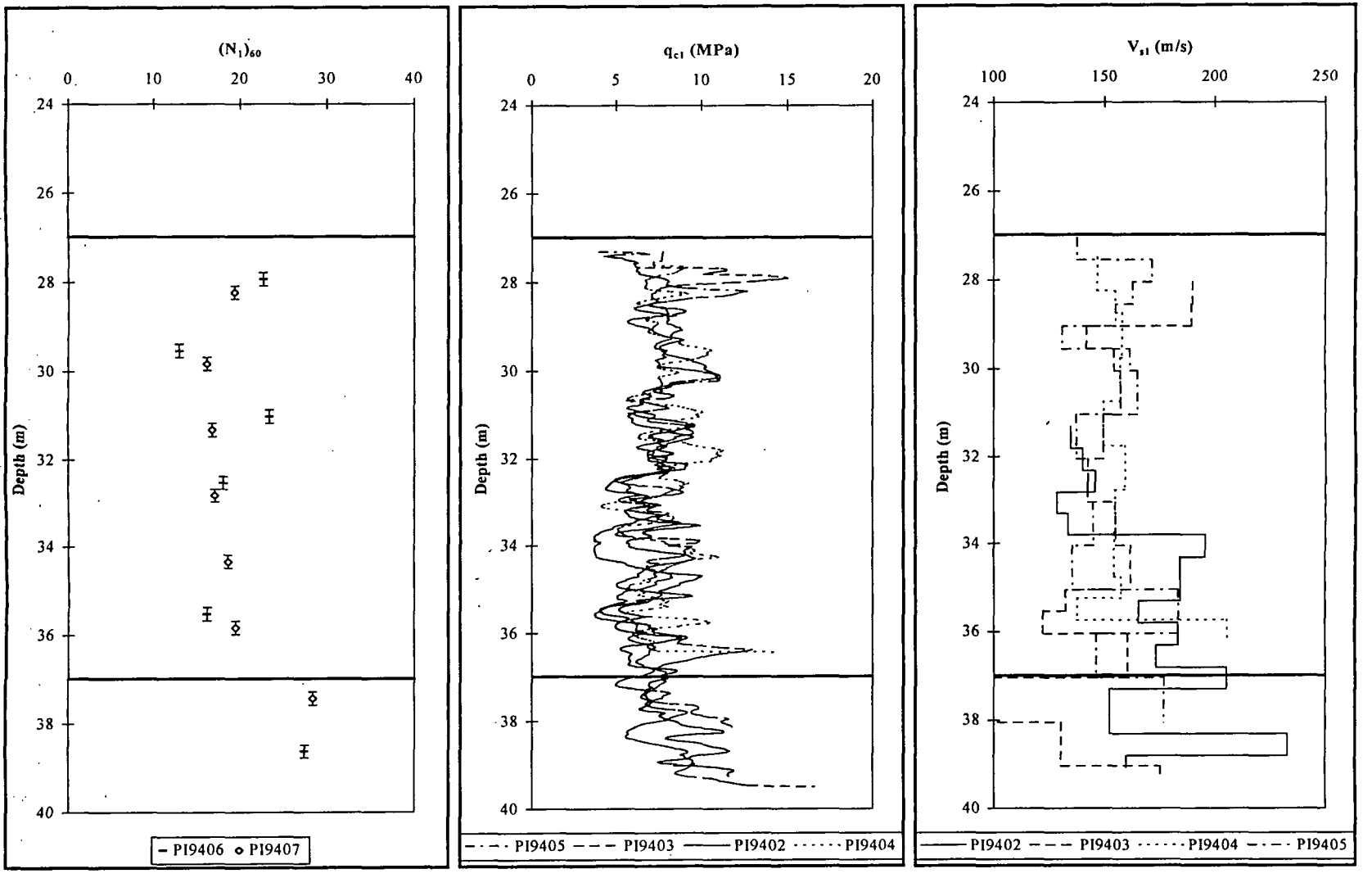

Figure 13. Corrected (a) SPT, (b) CPT and (c) V_s profiles at the Phase I site.

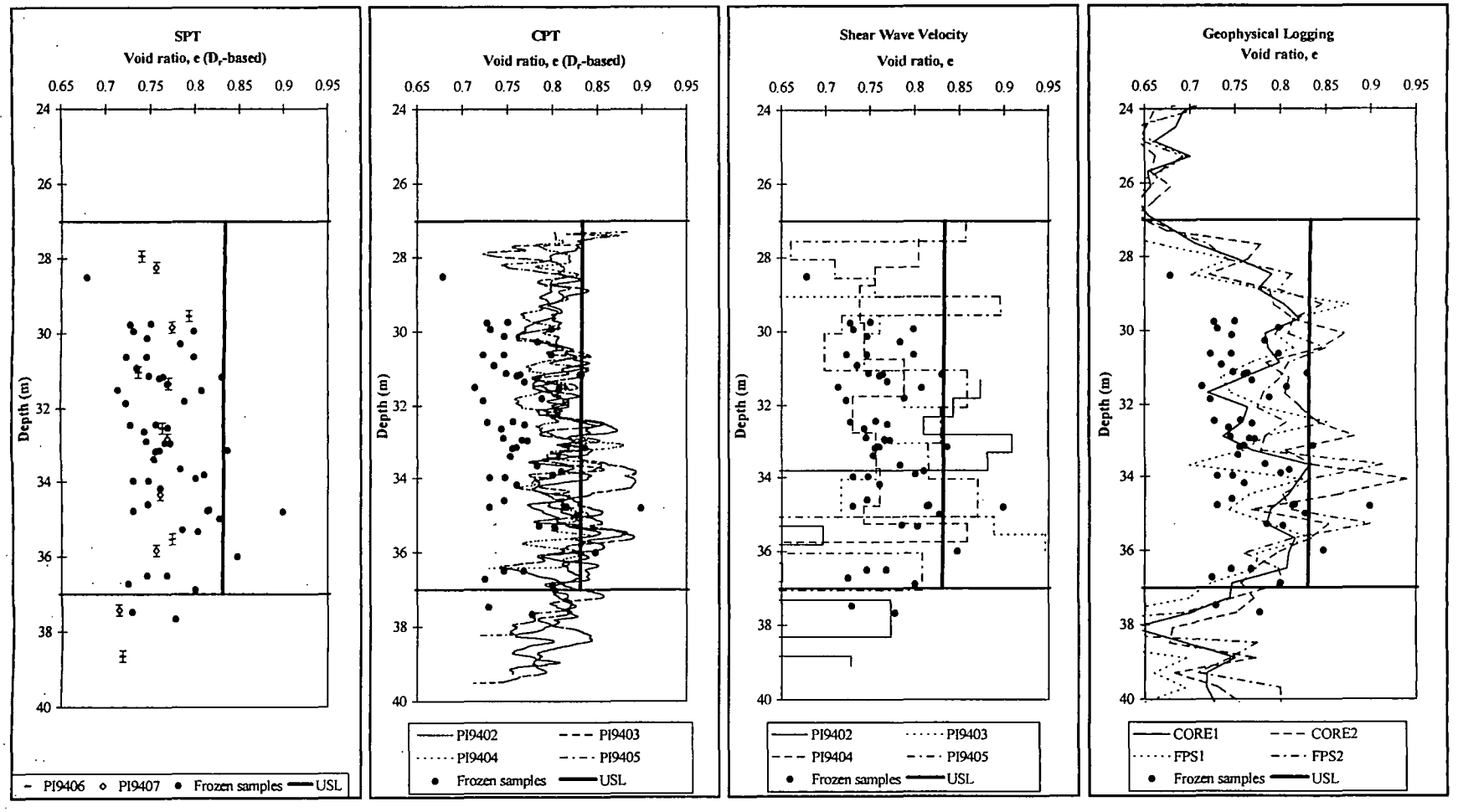

Figure 14. Estimated void ratio profiles in the target zone at the Phase I site from D_r-based interpretations of (a) SPT and (b) CPT, and interpretation of (c) V_s, and (d) geophysical logs.

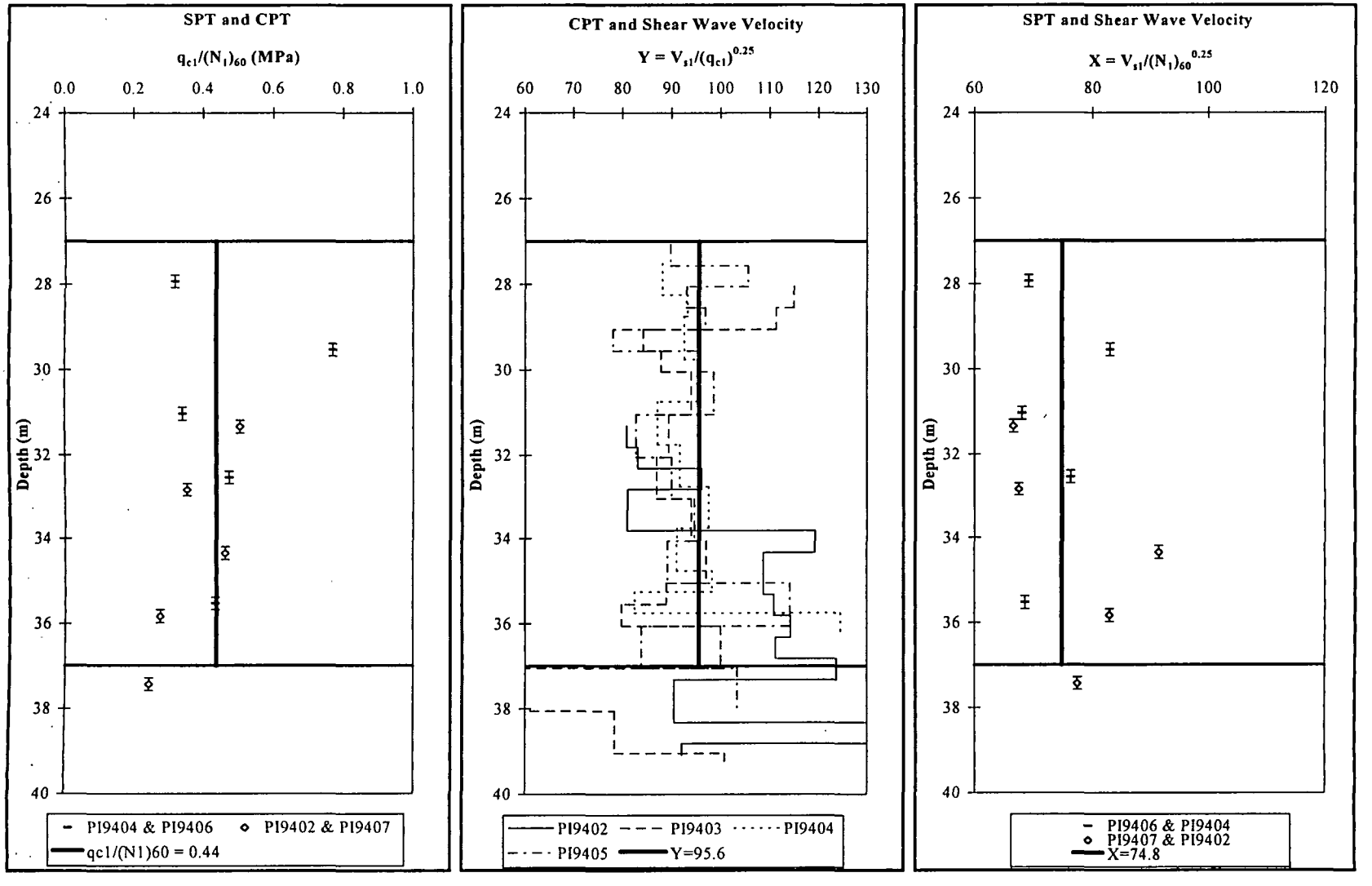

Figure 15. Plots of (a) $q_{c1}/(N_1)_{60}$, (b) Y and (c) X versus depth at the Phase I site.

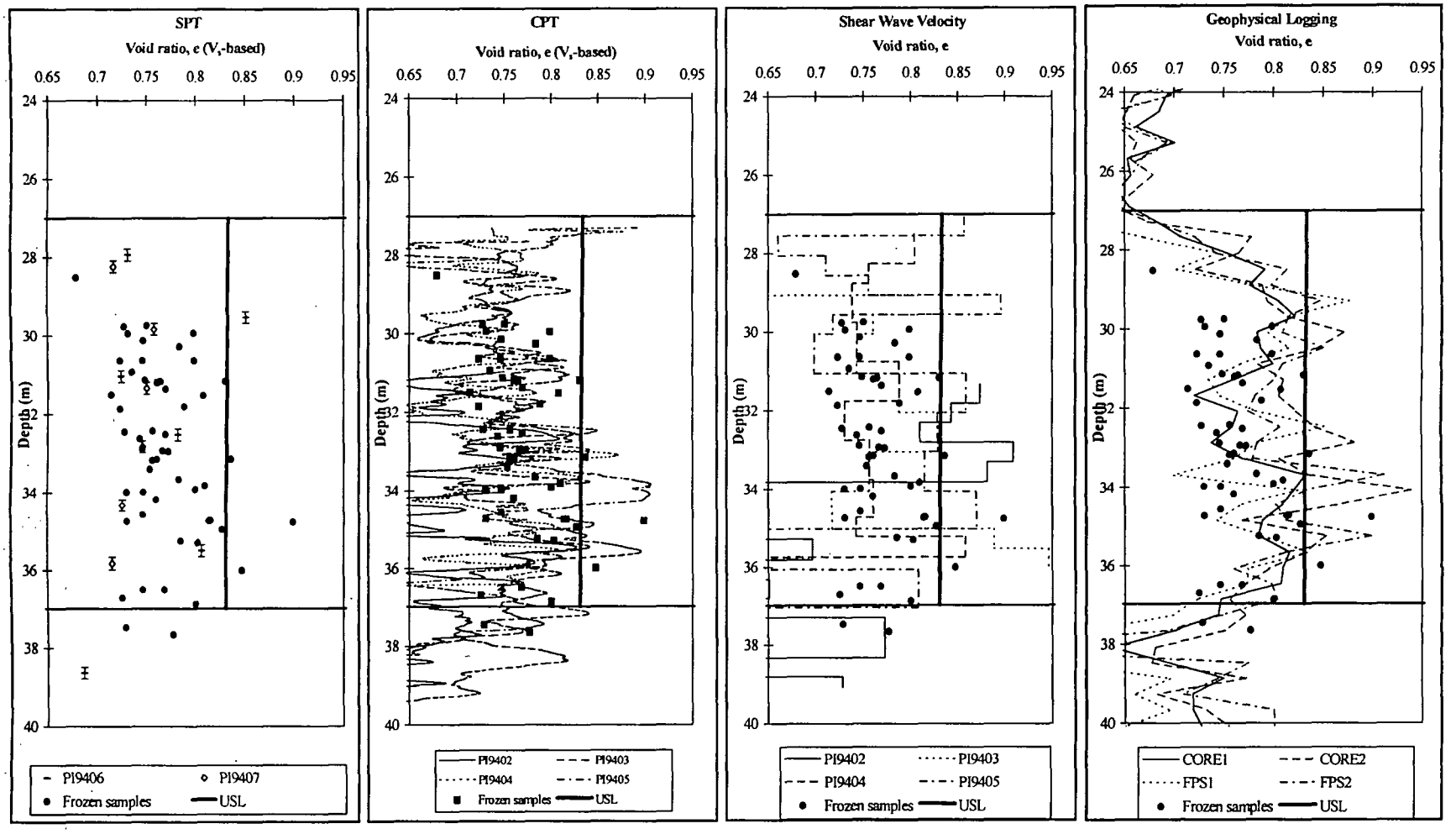

Figure 16. Estimated void ratio profiles in the target zone at the Phase I site from V_s-based interpretations of (a) SPT and (b) CPT, and interpretation of (c) V_s, and (d) geophysical logs.

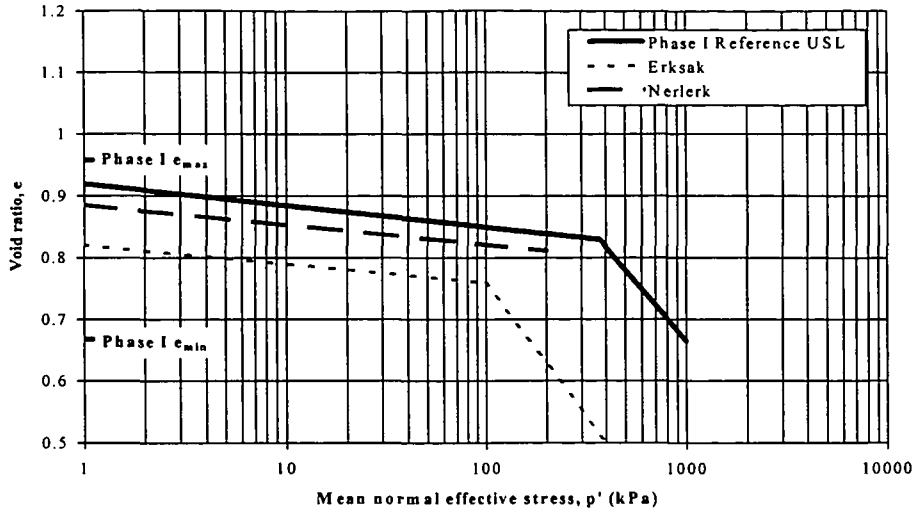

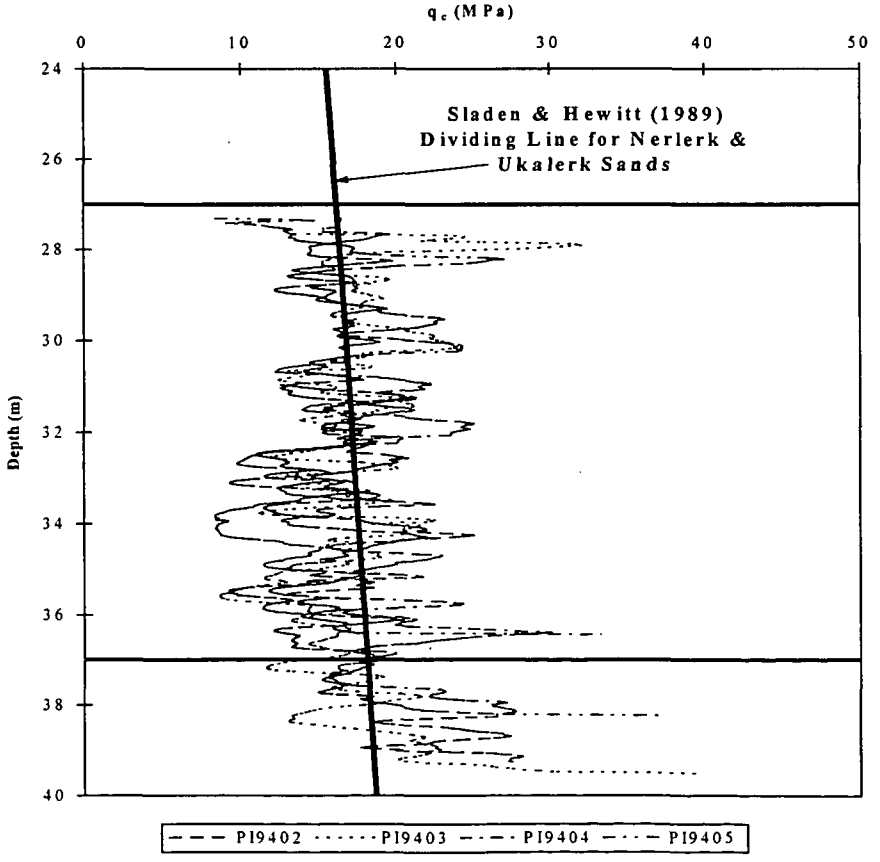

Figure 17. (a) Comparison of the reference USL for Syncrude Sand with the USLs for Nerlerk and Ukalerk (Erksak) sands; (b) estimation of flow liquefaction potential at the Phase I site from CPT results based on the method for Nerlerk and Ukalerk sands by Sladen & Hewitt (1989).

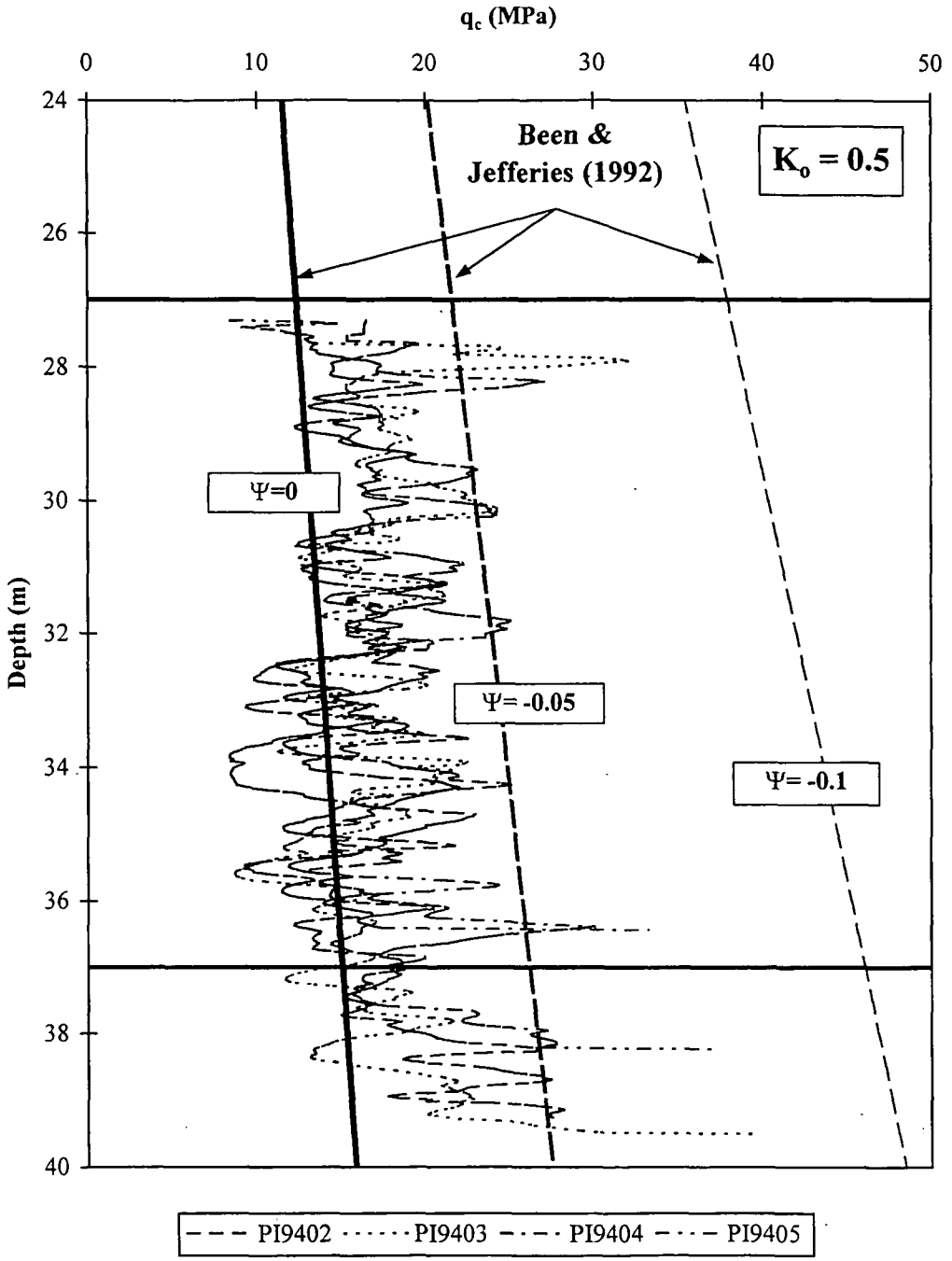

Figure 18. Estimating flow liquefaction potential at the Phase I site from CPT results based on the method by Been & Jefferies (1992).

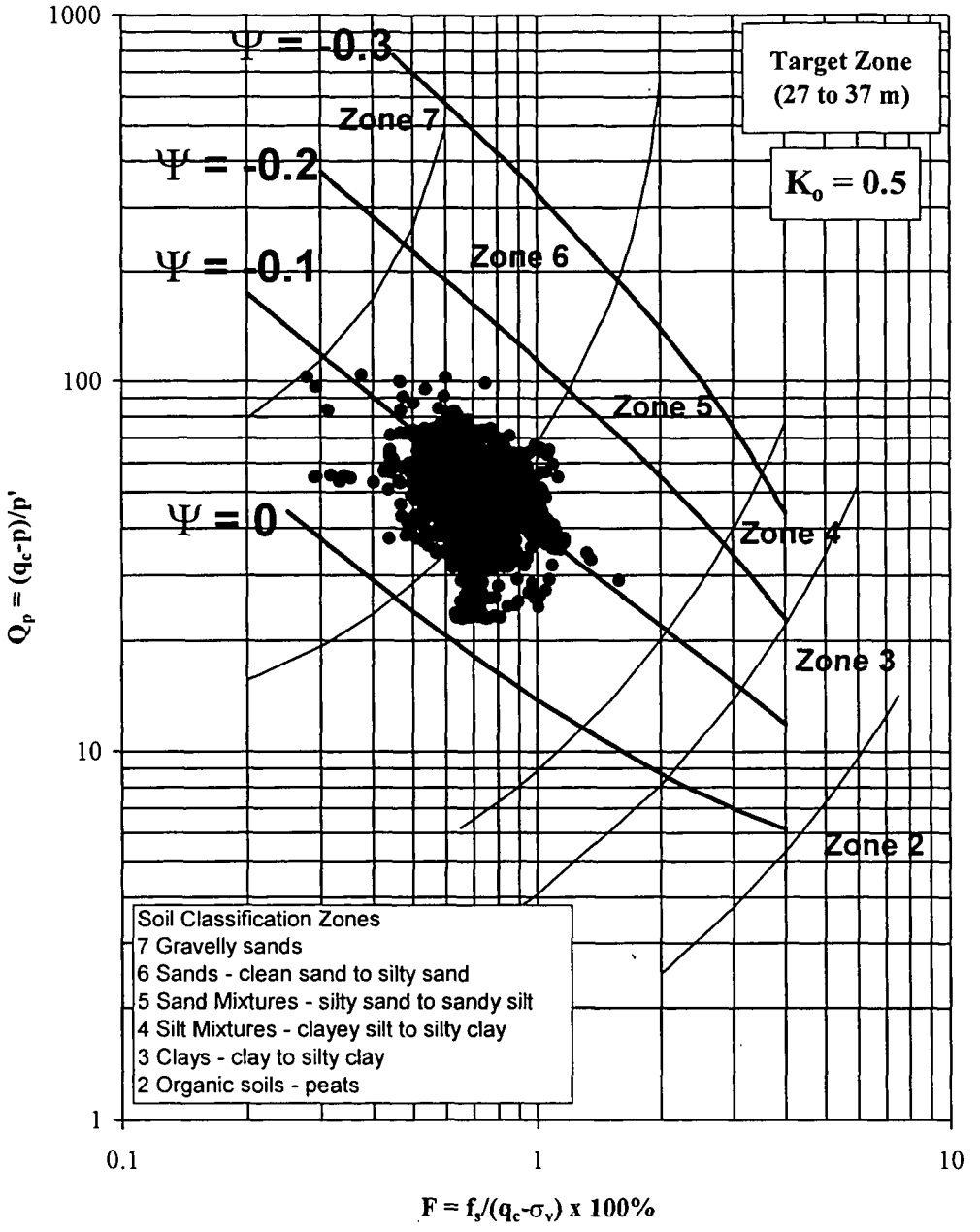

Figure 19. Estimating state at the Phase I site from CPT results based on the method by Plewes et al. (1992).

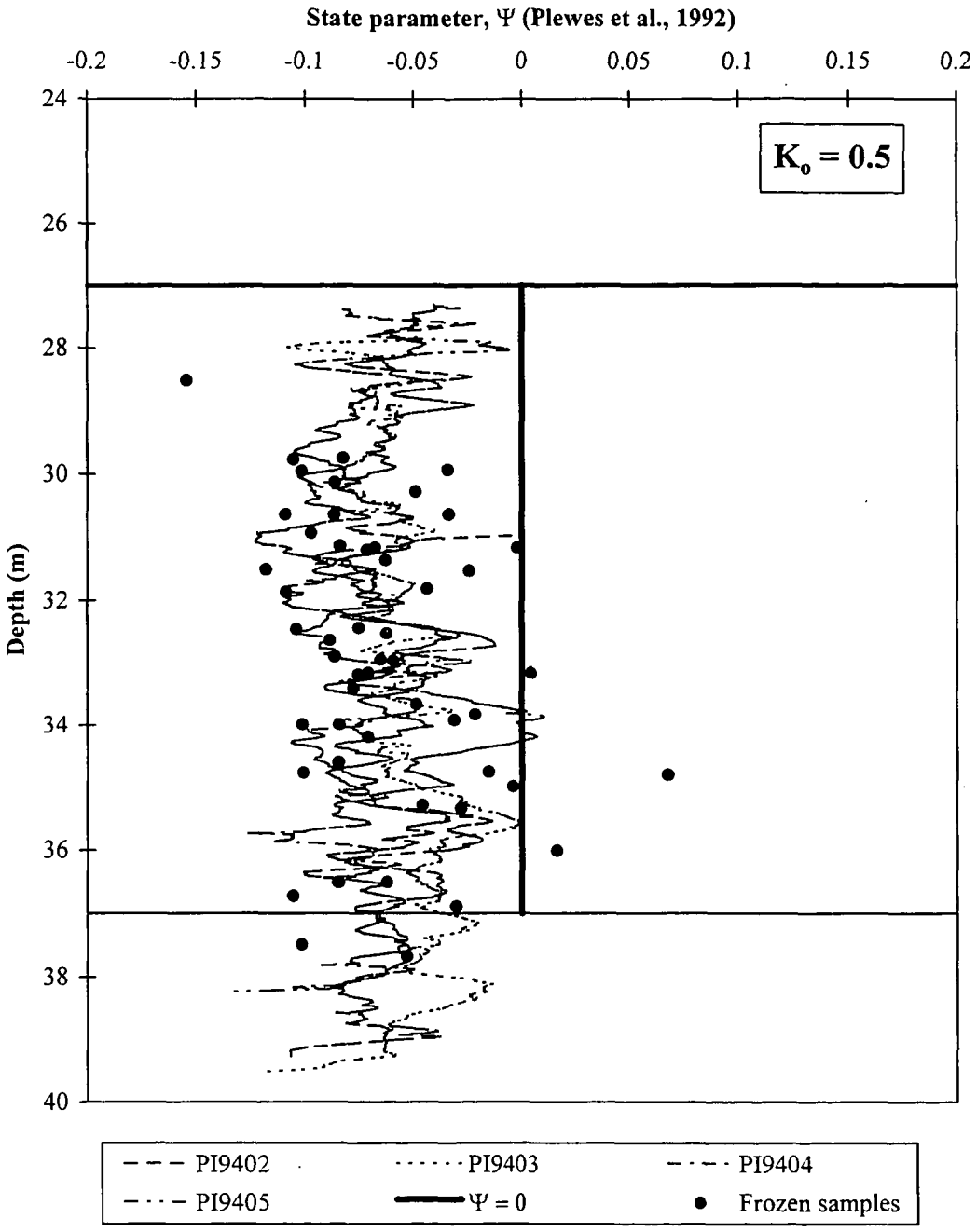

Figure 20. Estimated profiles of state parameter at the Phase I site from CPT results based on the method by Plewes et al. (1992).

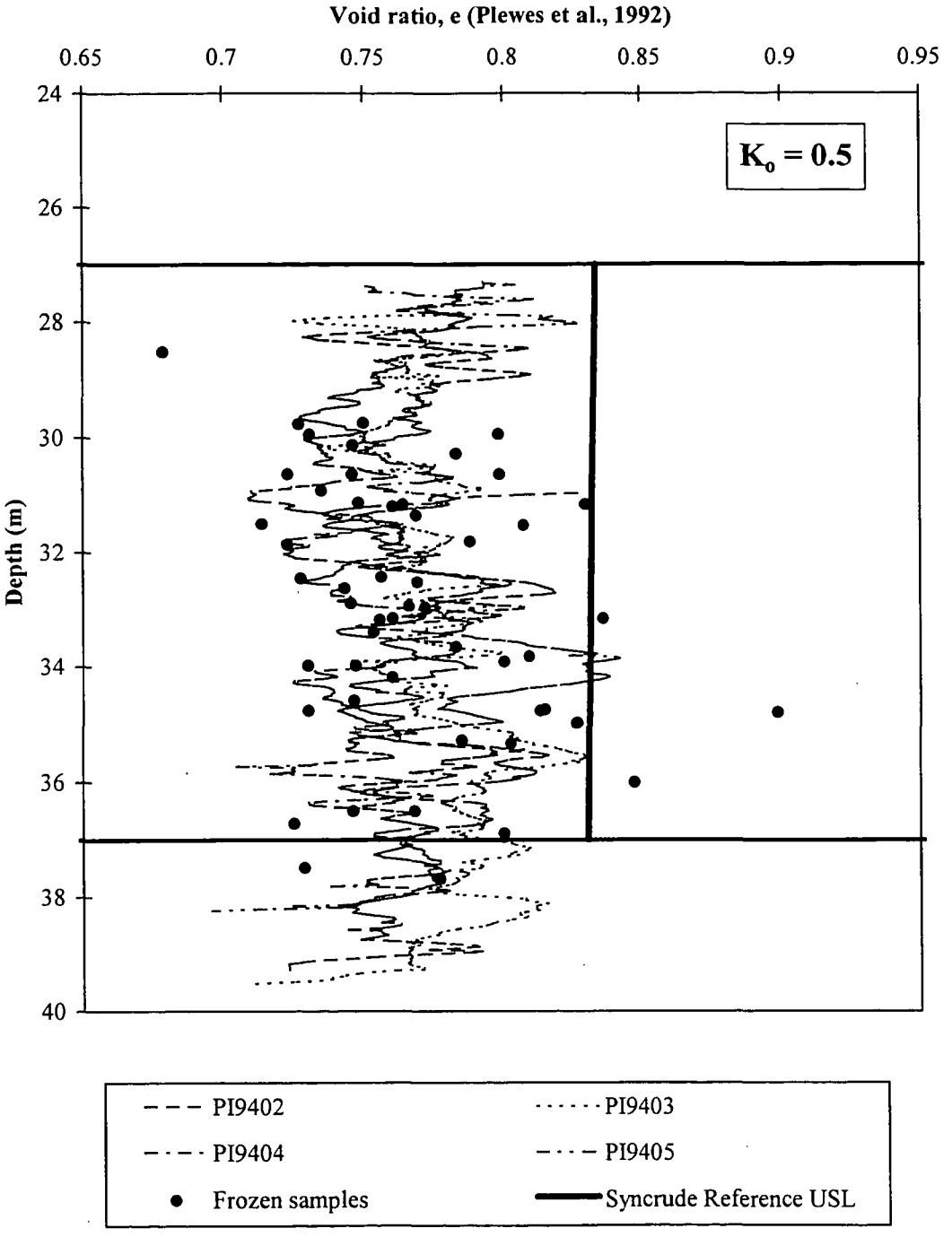

Figure 21. Estimated profiles of void ratio at the Phase I site from CPT results based on the method by Plewes et al. (1992).

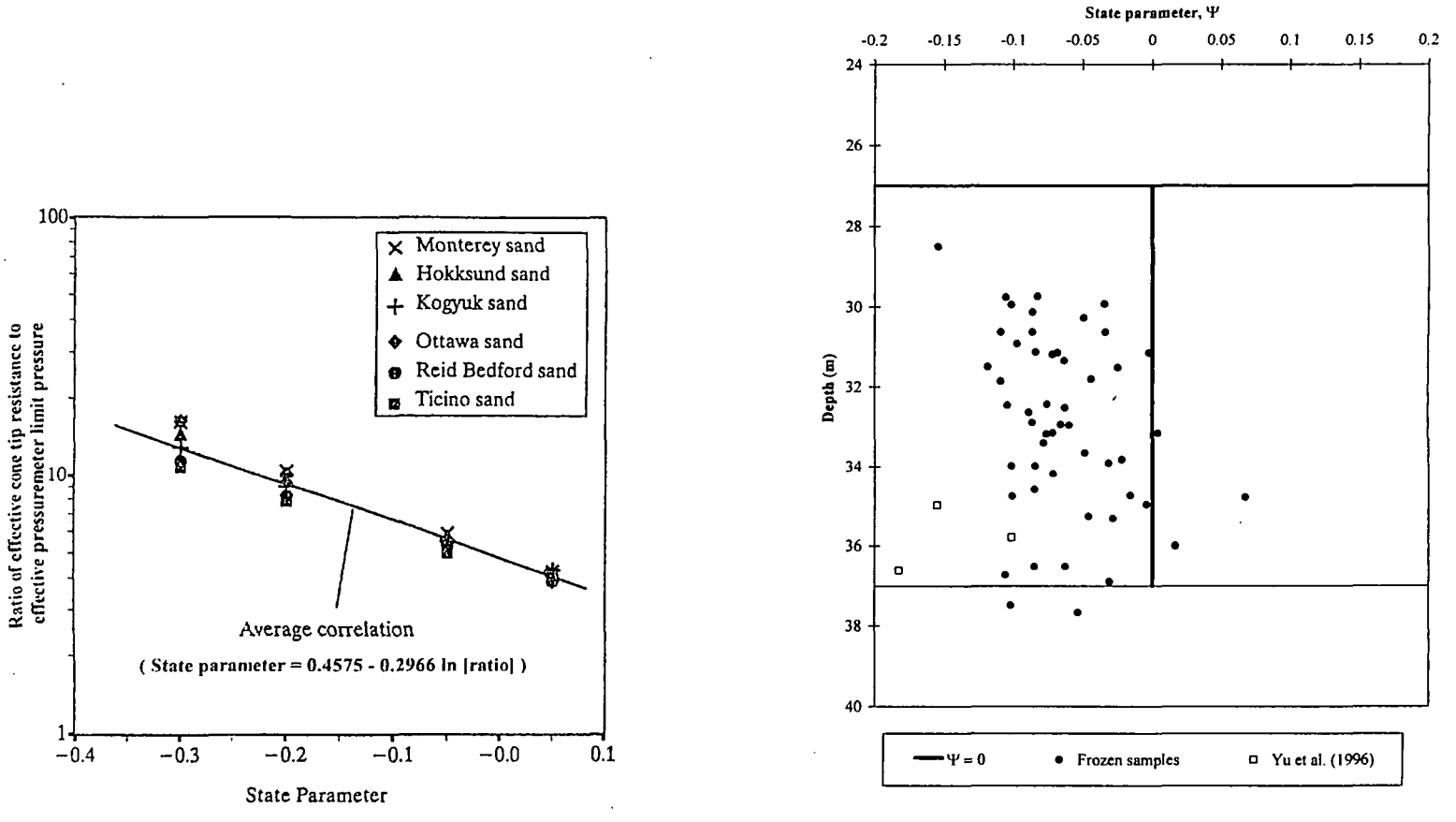

Figure 22. (a) The method by Yu et al. (1996), and (b) estimating state parameter in the Phase I site target zone from pressuremeter results based on the method by Yu et al. (1996).

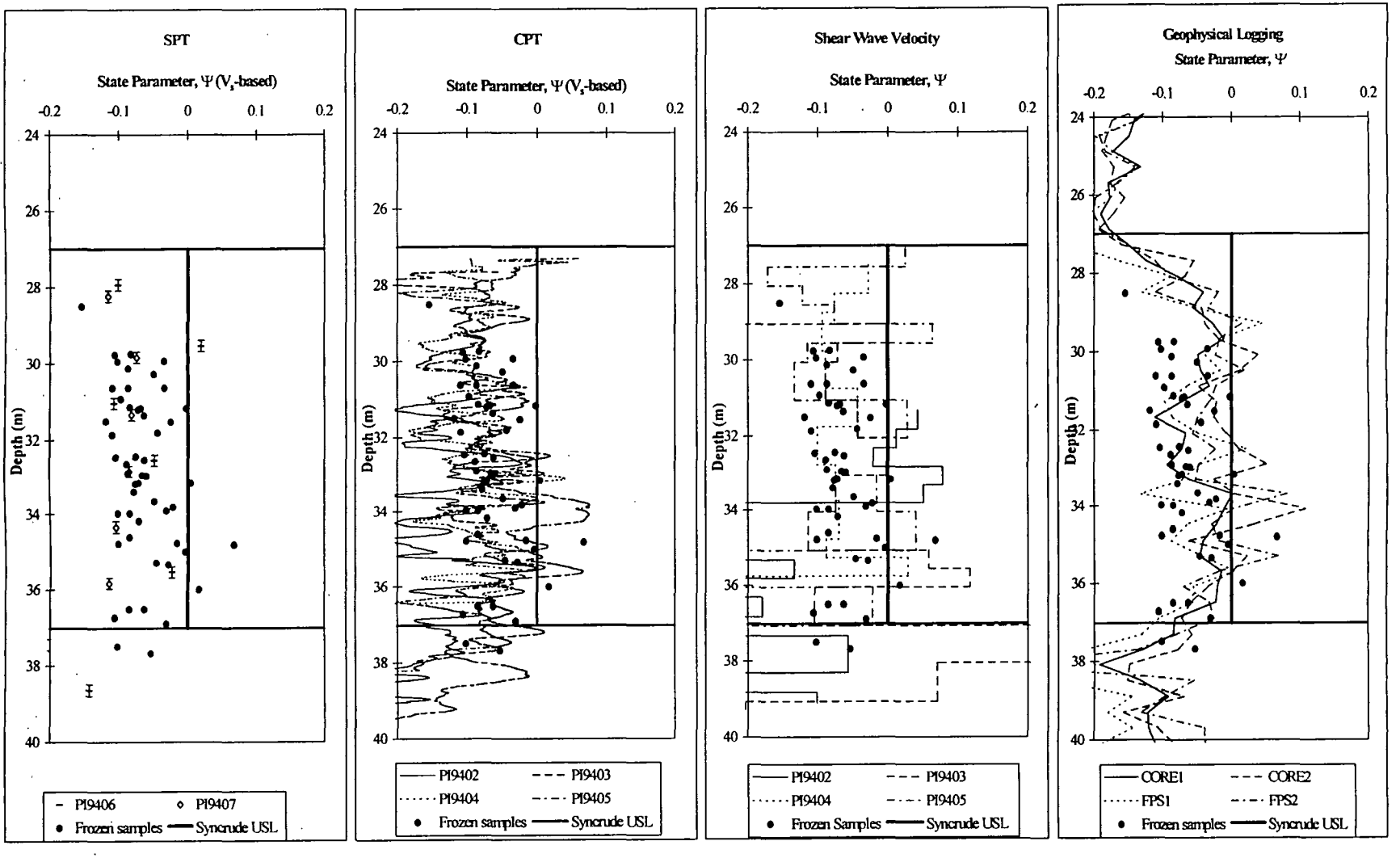

Figure 23. Estimated profiles of state parameter at the Phase I site from the V_s-based interpretations of void ratio from (a) SPT and (b) CPT and void ratio interpretations of (c) V_s and (d) geophysical logs.

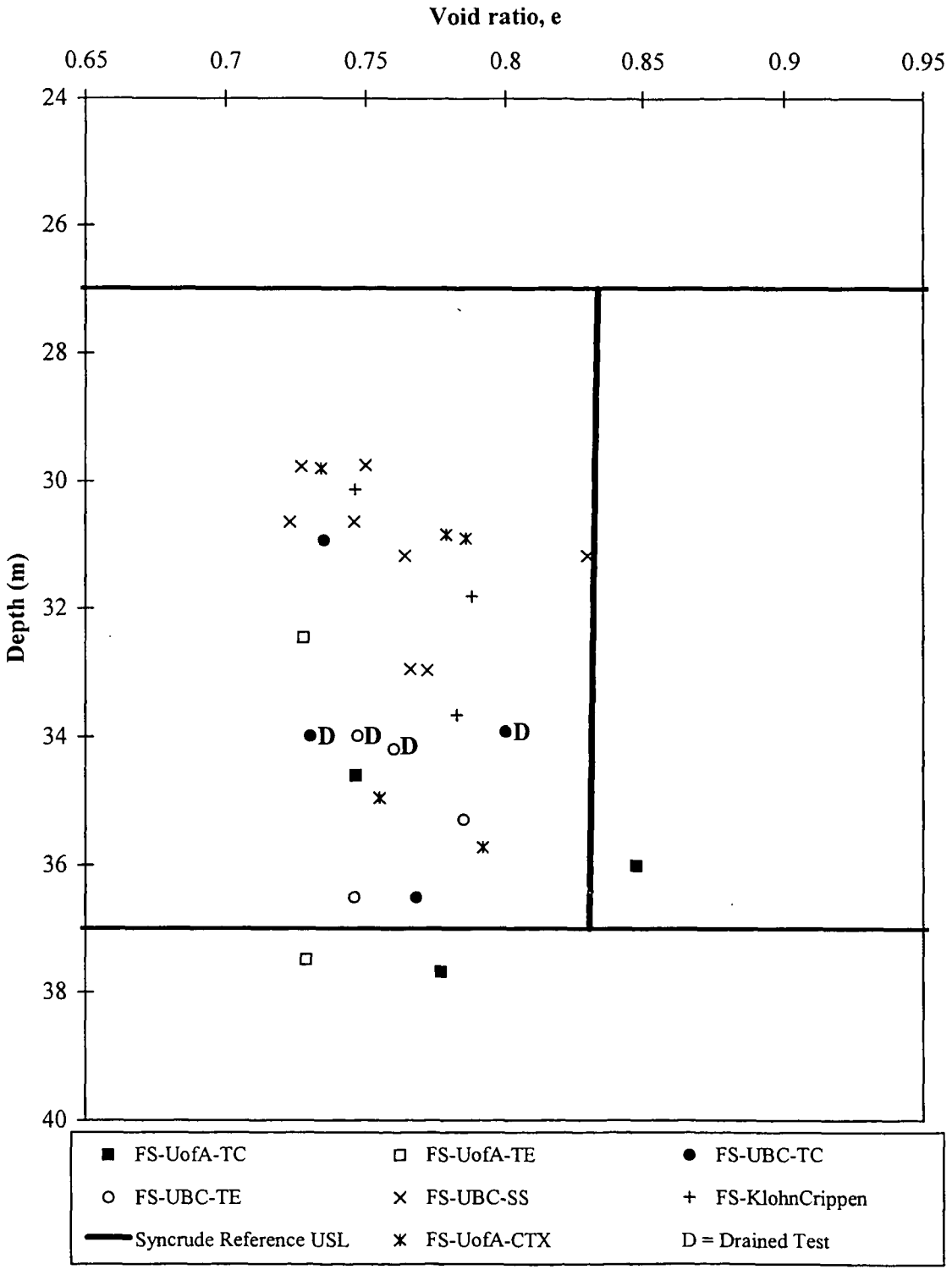

Figure 24. Enlarged plot of void ratios from the Phase I site undisturbed frozen samples (FS), illustrating the type of tests conducted on the samples.

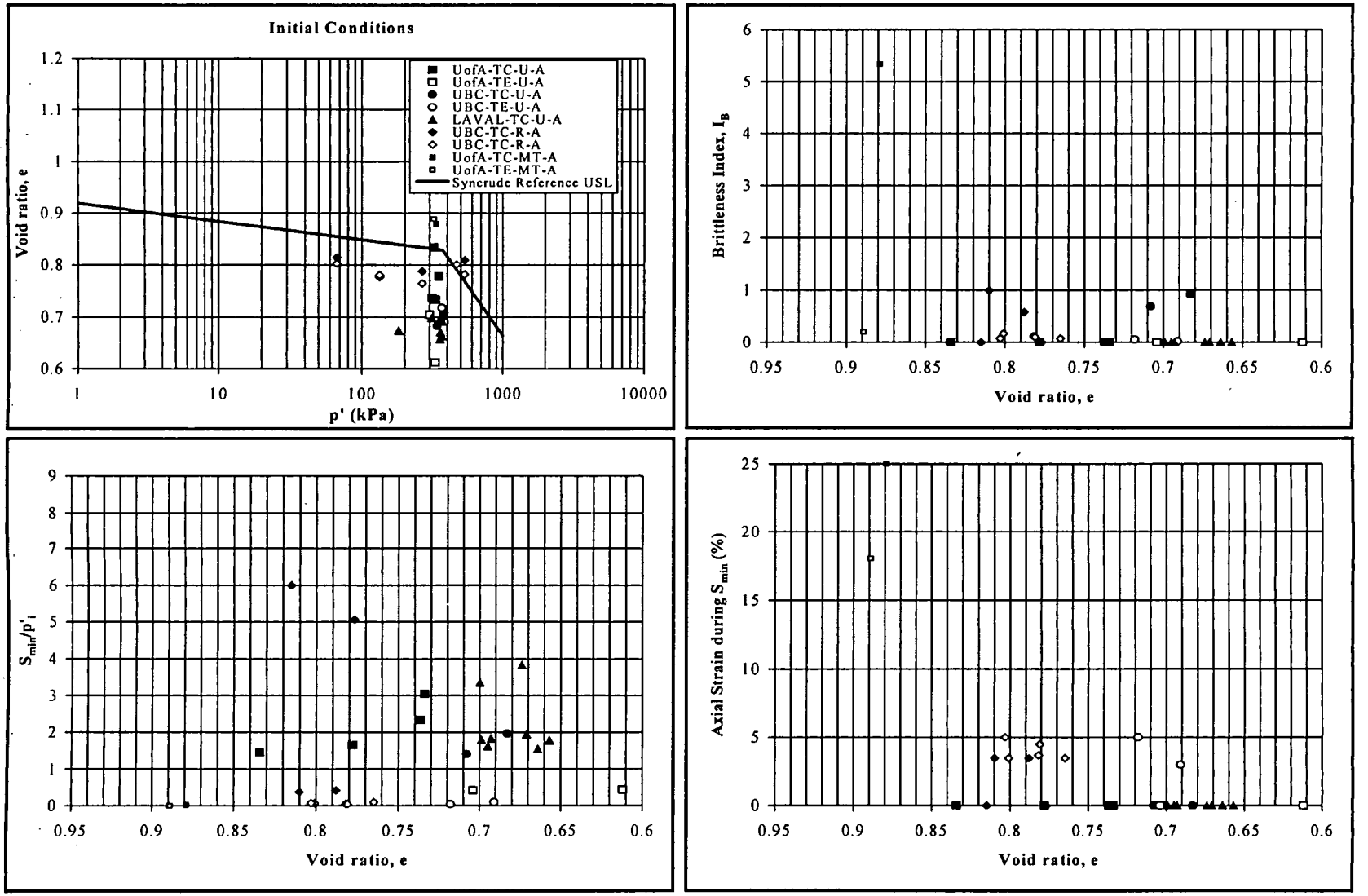

Figure 25. Relationship between void ratio (e) and undrained monotonic response of anisotropically consolidated undisturbed triaxial samples from the Phase I site: (a) initial conditions, (b) brittleness index (I_B), (c) minimum strength ratio (S_{min}/p'_i), and (d) axial strain (ε_a) during minimum strength.

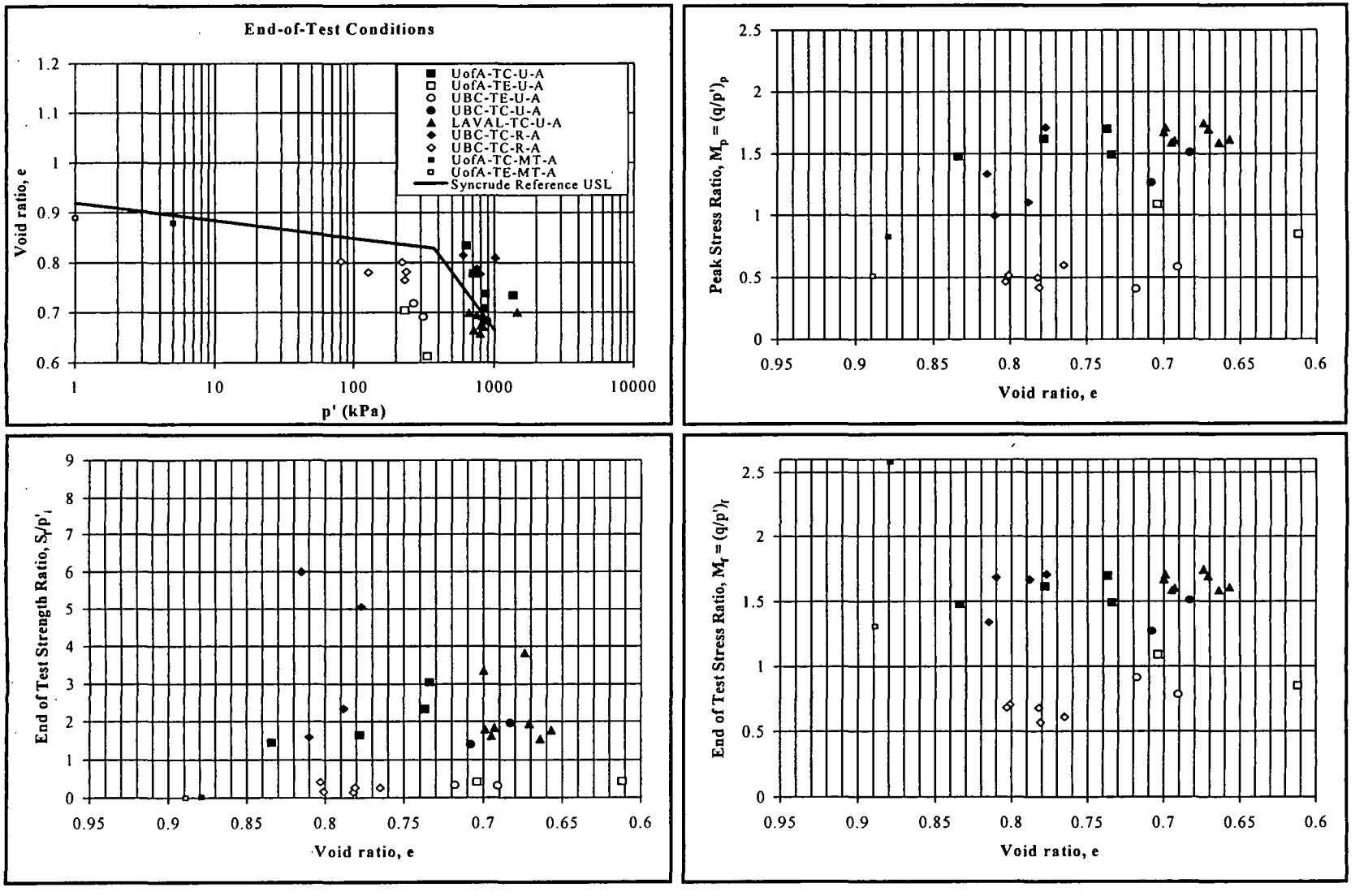

Figure 26. Relationship between void ratio (e) and undrained monotonic response of anisotropically consolidated undisturbed triaxial samples from the Phase I site: (a) end-of-test conditions, (b) end-of-test strength ratio (S_f/p'_i), (c) peak stress ratio (M_p), and (d) end-of-test stress ratio (M_f).

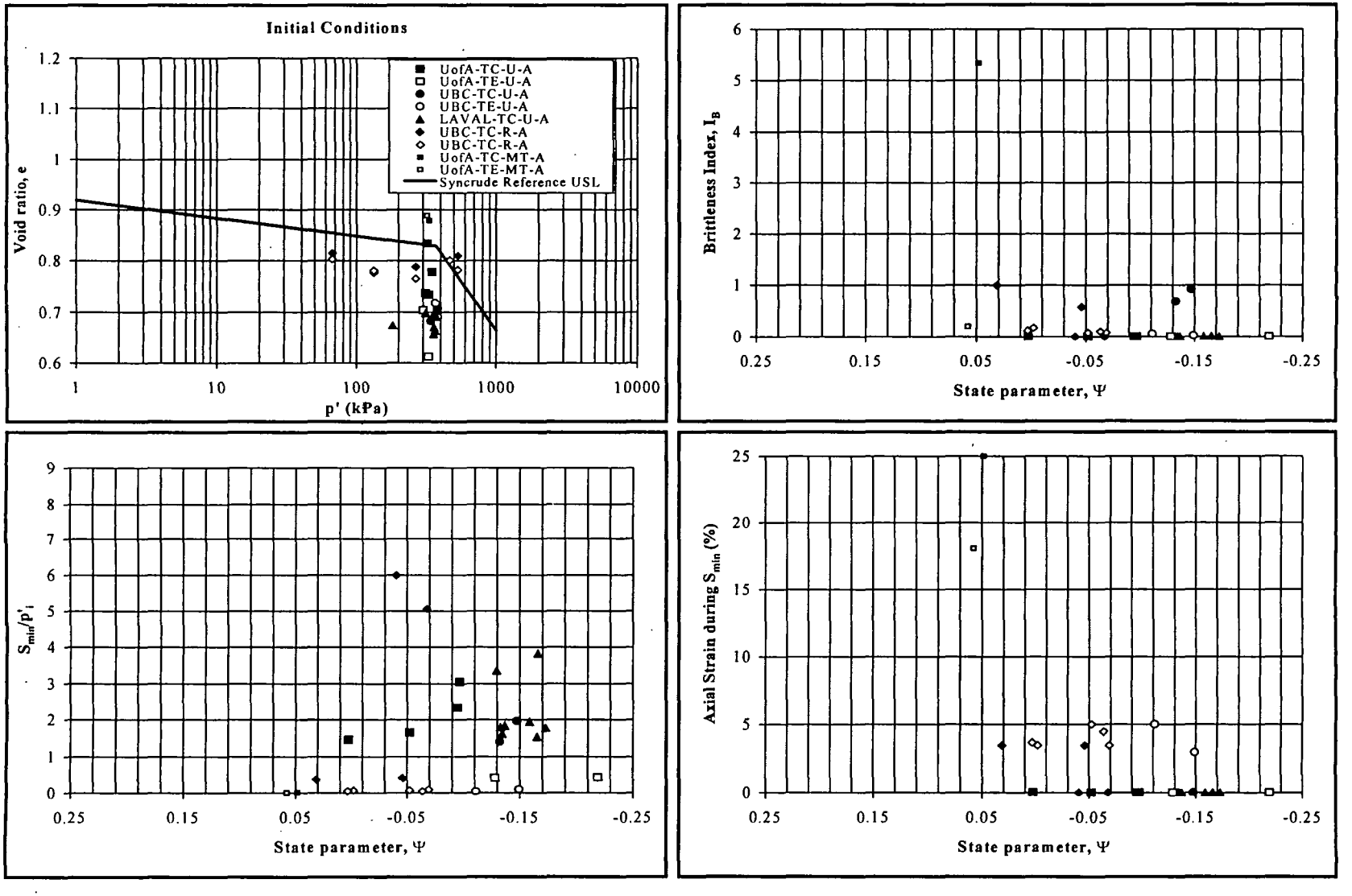

Figure 27. Relationship between state parameter (Ψ) and undrained monotonic response of anisotropically consolidated undisturbed triaxial samples from the Phase I site: (a) initial conditions, (b) brittleness index (I_B), (c) minimum strength ratio (S_{min}/p'_i), and (d) axial strain (ε_a) during minimum strength.

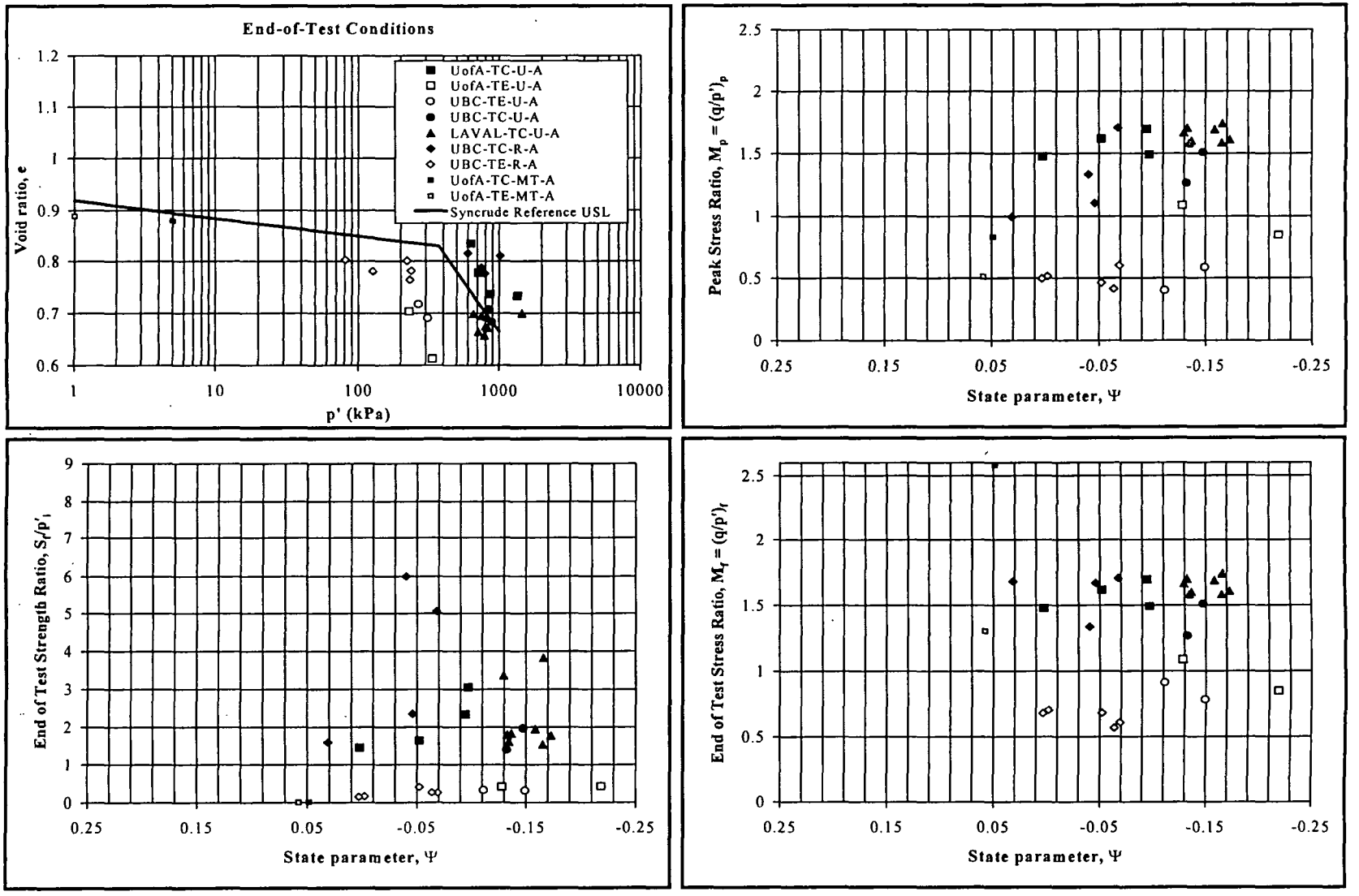

Figure 28. Relationship between state parameter (Ψ) and undrained monotonic response of anisotropically consolidated undisturbed triaxial samples from the Phase I site: (a) end-of-test conditions, (b) end-of-test strength ratio (S_f/p'_i), (c) peak stress ratio (M_p), and (d) end-of-test stress ratio (M_f).

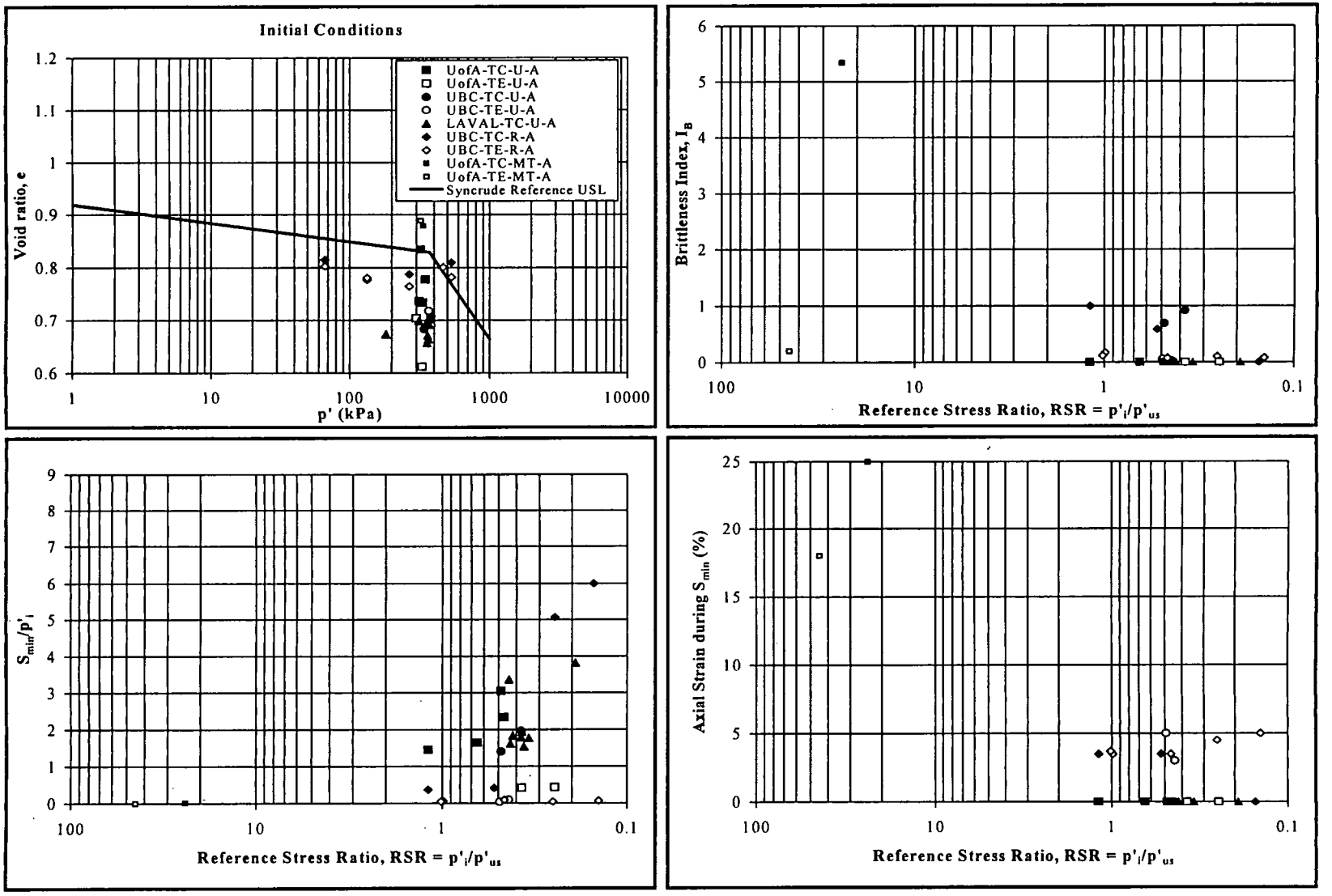

Figure 29. Relationship between reference state ratio (RSR) and undrained monotonic response of anisotropically consolidated undisturbed triaxial samples from the Phase I site: (a) initial conditions, (b) brittleness index (I_B), (c) minimum strength ratio (S_{min}/p'_i), and (d) axial strain (ε_a) during minimum strength.

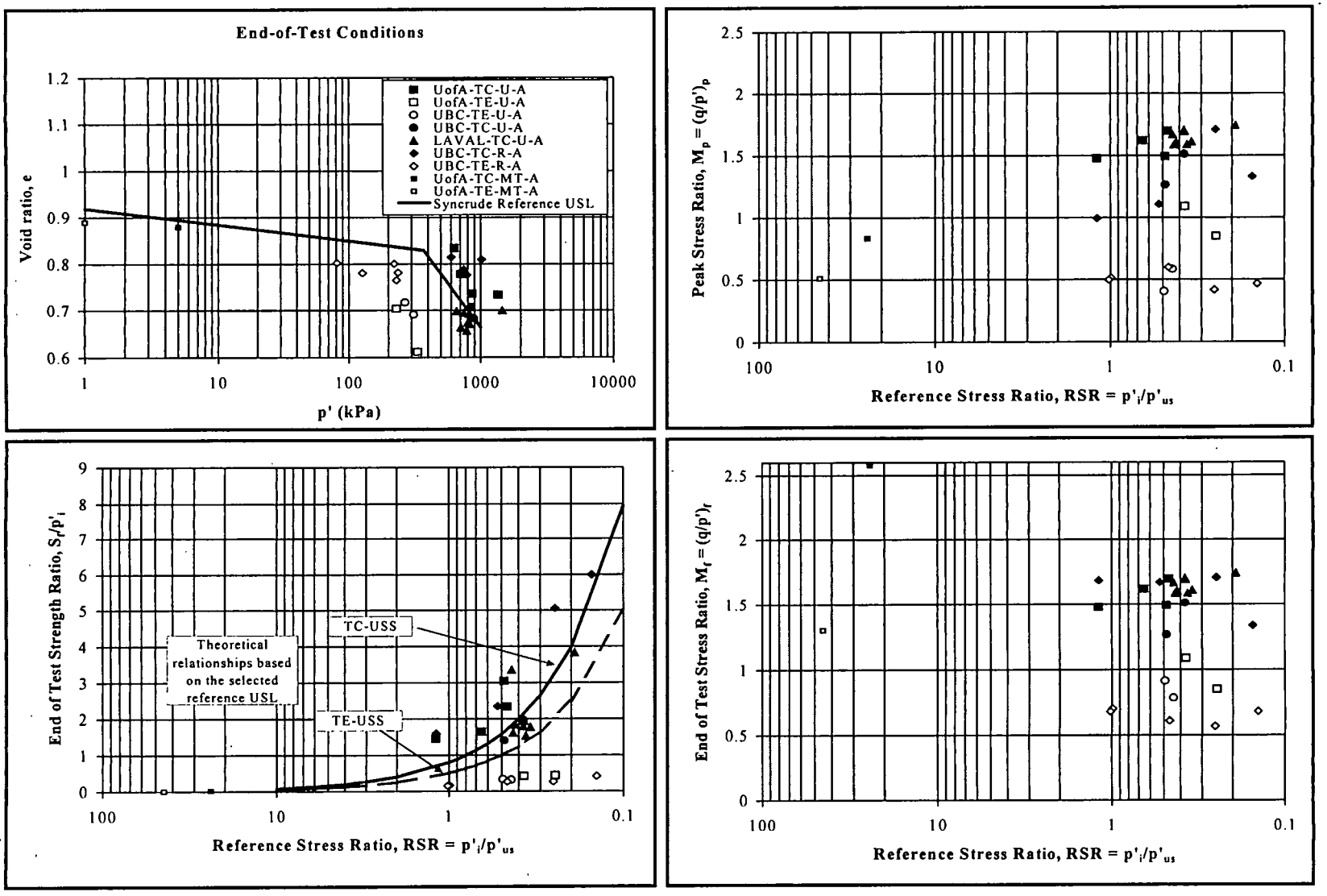

Figure 30. **Relationship between reference state ratio (RSR) and undrained monotonic laboratory response of anisotropically consolidated undisturbed triaxial samples from the Phase I site: (a) end-of-test conditions, (b) end-of-test strength ratio (S_f/p'_i), (c) peak stress ratio (M_p), and (d) end-of-test stress ratio (M_f).**

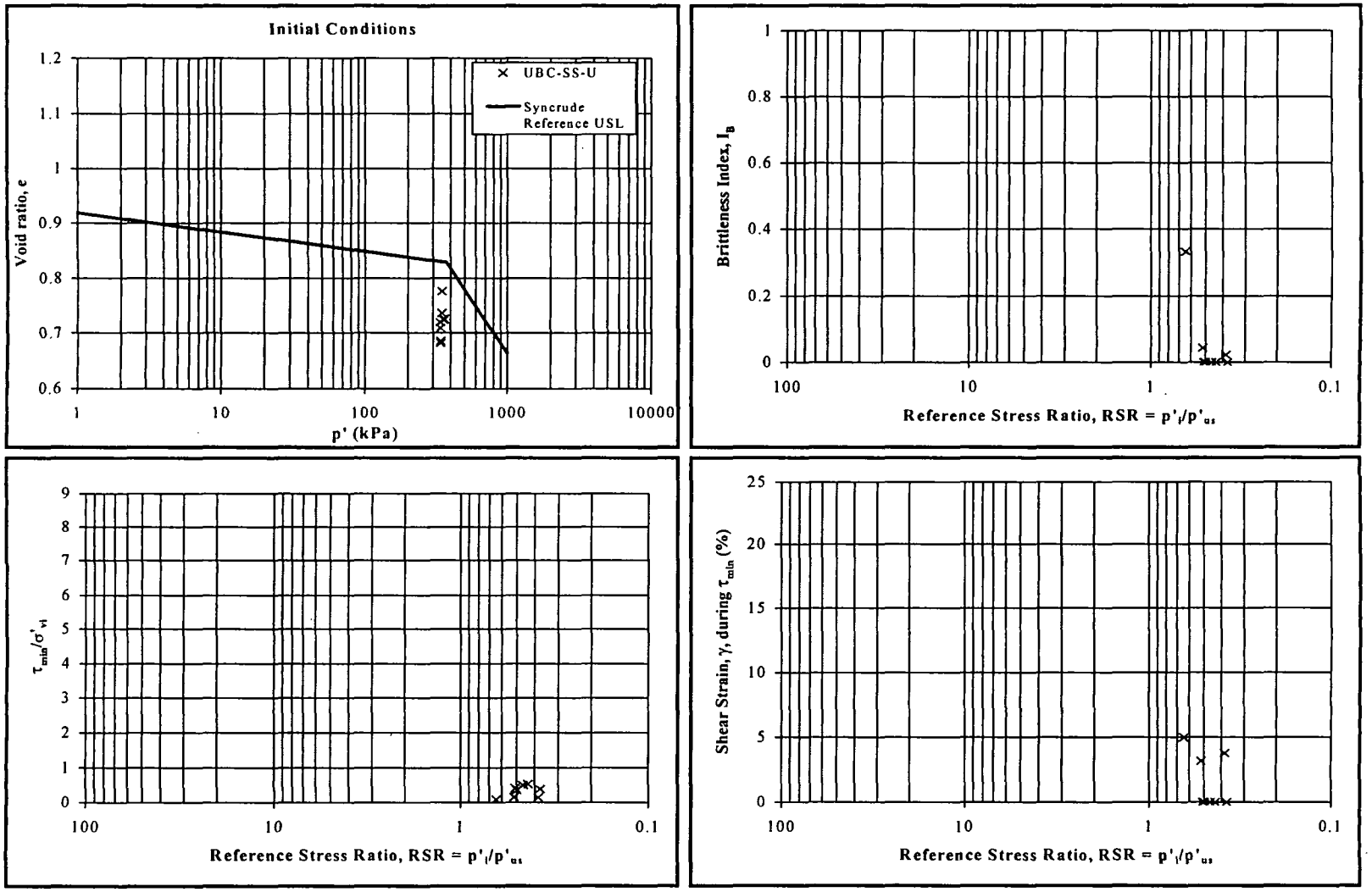

Figure 31. Relationship between reference state ratio (RSR) and undrained monotonic response of undisturbed simple shear samples from the Phase I site: (a) initial conditions, (b) brittleness index (I_B), (c) minimum strength ratio (τ_{min}/σ'_{vi}), and (d) shear strain (γ) during minimum strength.

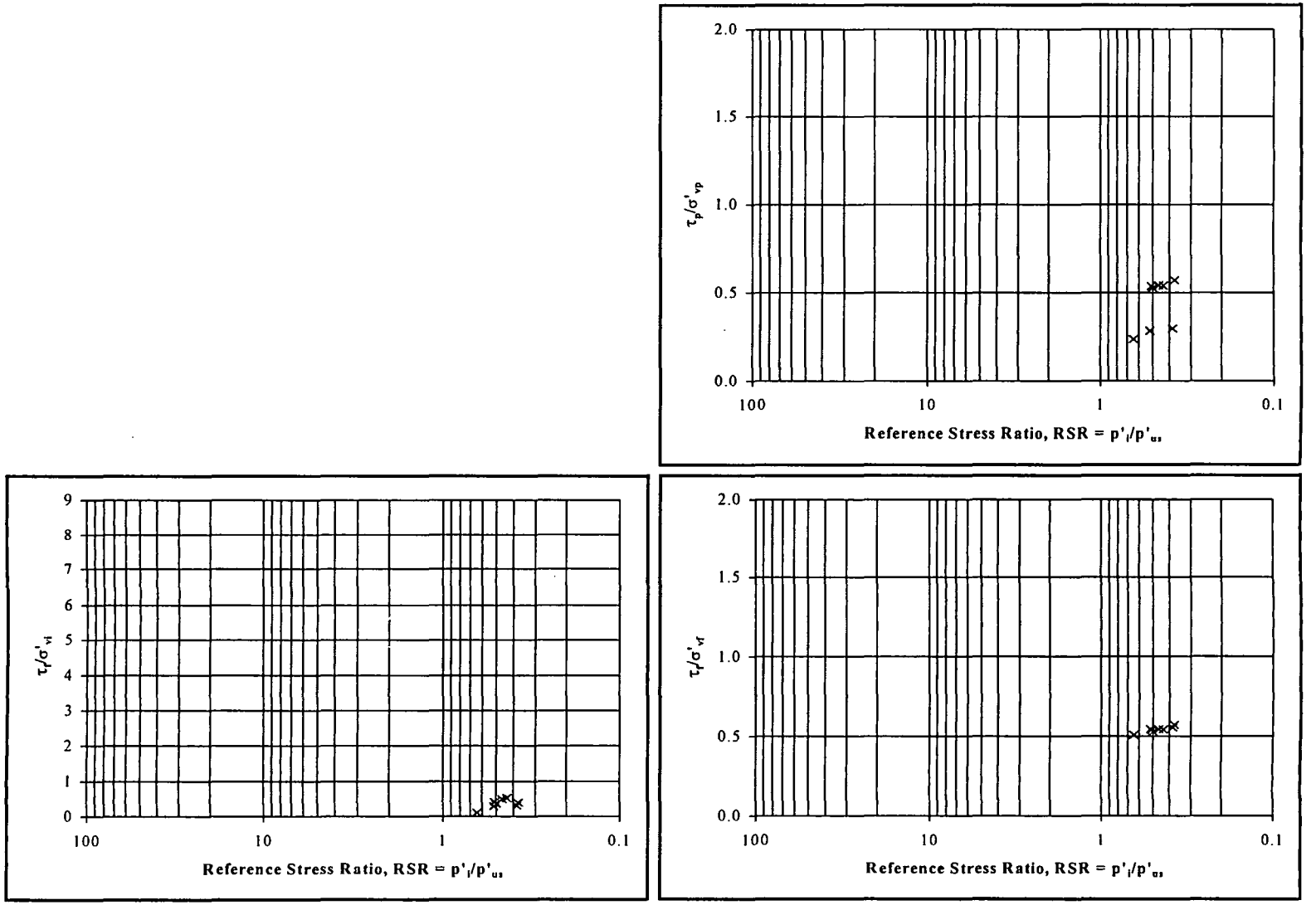

Figure 32. **Relationship between reference state ratio (RSR) and undrained monotonic laboratory response of undisturbed simple shear samples from the Phase I site: (a) end-of-test strength ratio (τ_f/σ'_{vi}), (b) peak stress ratio (τ_p/σ'_p), and (c) end-of-test stress ratio (τ_f/σ'_{vf}).**

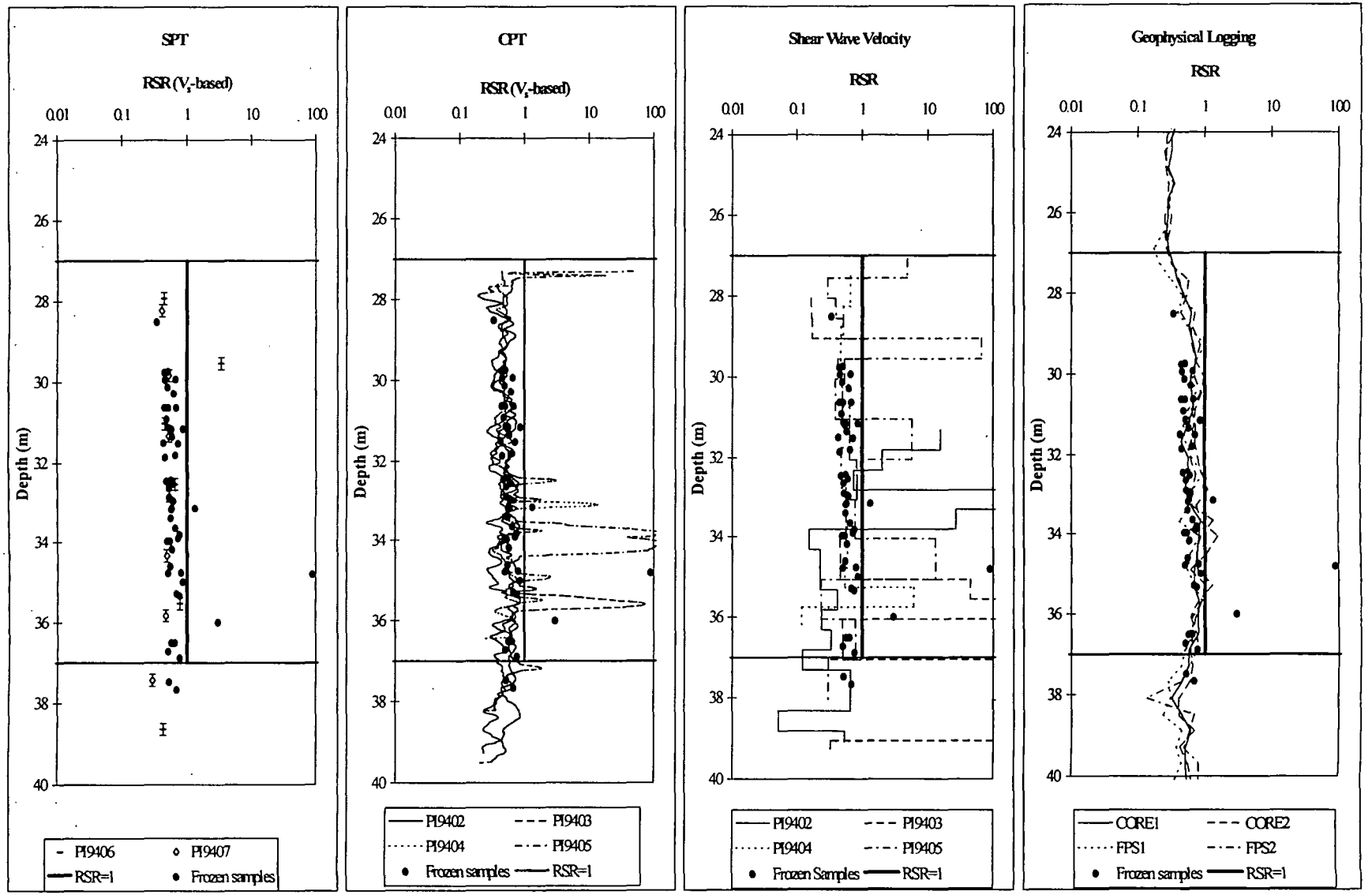

Figure 33. Profiles of estimated RSR at the Phase I site for (a) SPT, (b) CPT, (c) V_s, and (d) geophysical logs.

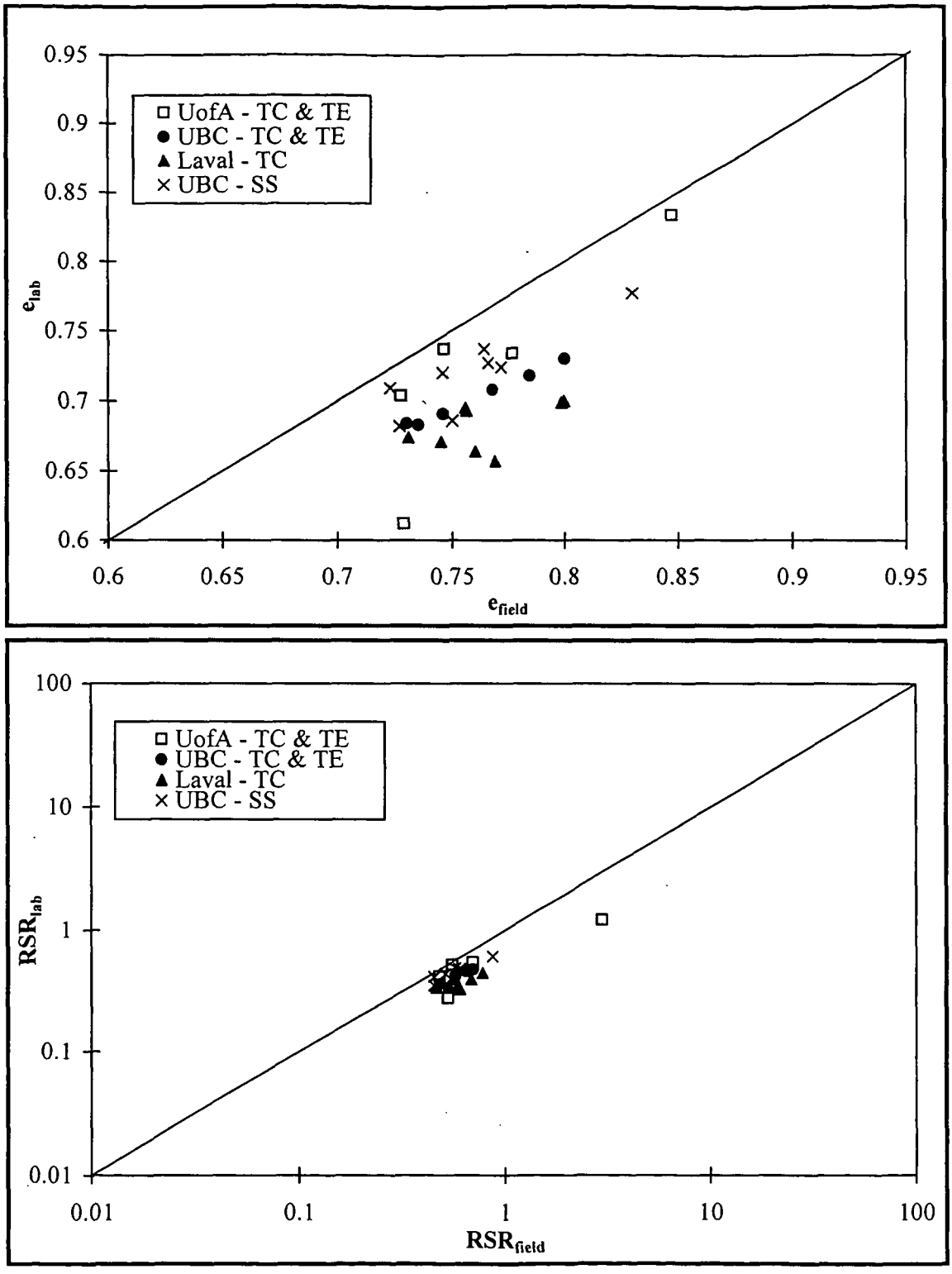

Figure 34. Comparison at the Phase I site of (a) void ratio and (b) RSR in the laboratory and in the field for samples tested under monotonic loading; N.B. e_{field} is based on G_s=2.66; e_{lab} is based on G_s=2.66 for U. of A., G_s=2.62 for U.B.C. and G_s=2.63 for Laval.

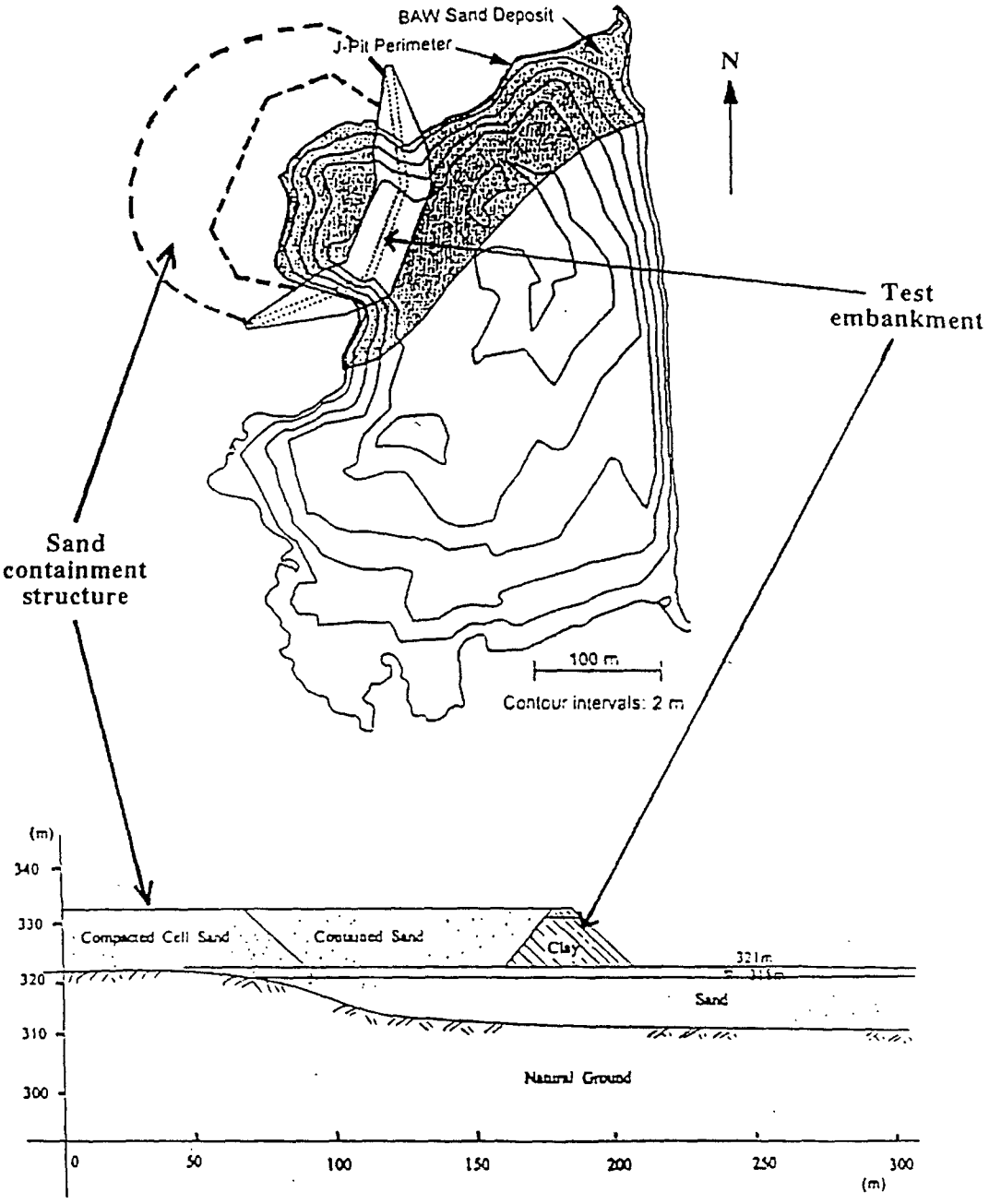

Figure 35. Phase III Site at Syncrude Canada Ltd. (after Iravani et al., 1995).

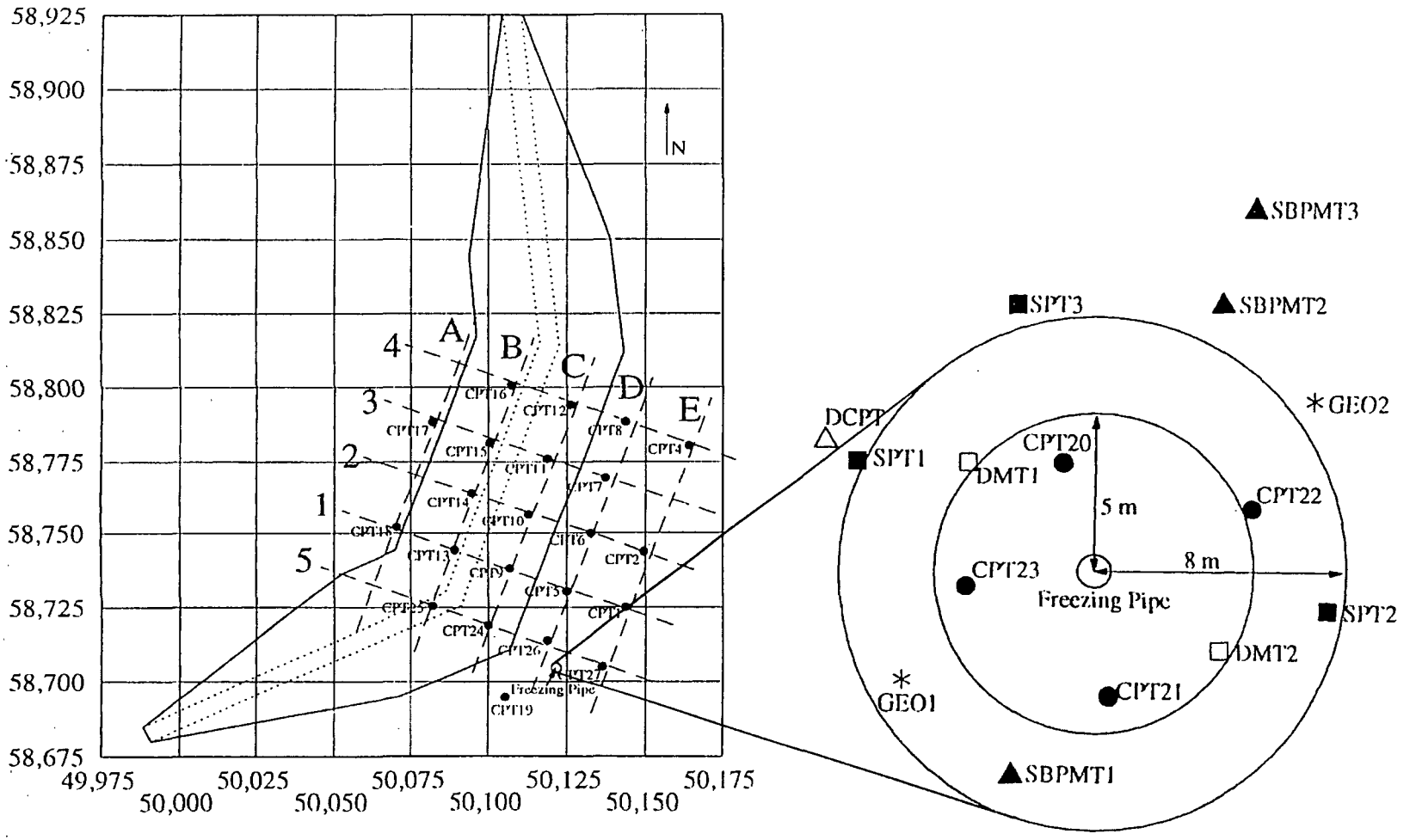

Figure 36. Detailed site plan of the testing area at the Phase III Site (after Iravani et al., 1995): (a) location relative to the embankment for the full-scale liquefaction test and the rest of the CPTs across the site (in particular, note the relative locations of CPT26 and CPT27); (b) layout of the in-situ tests in the detailed testing area.

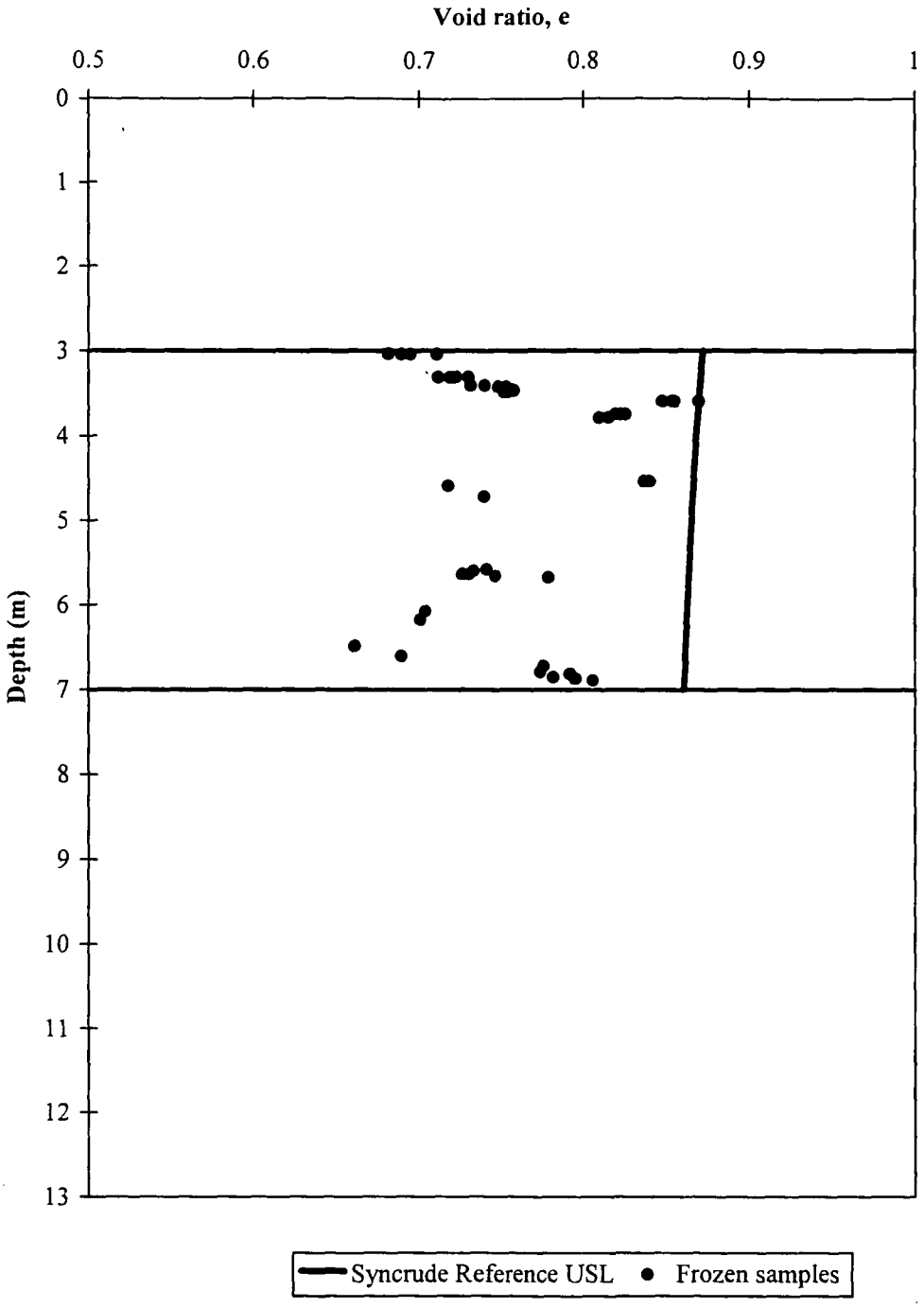

Figure 37. Void ratios from undisturbed frozen samples at the Phase III site.

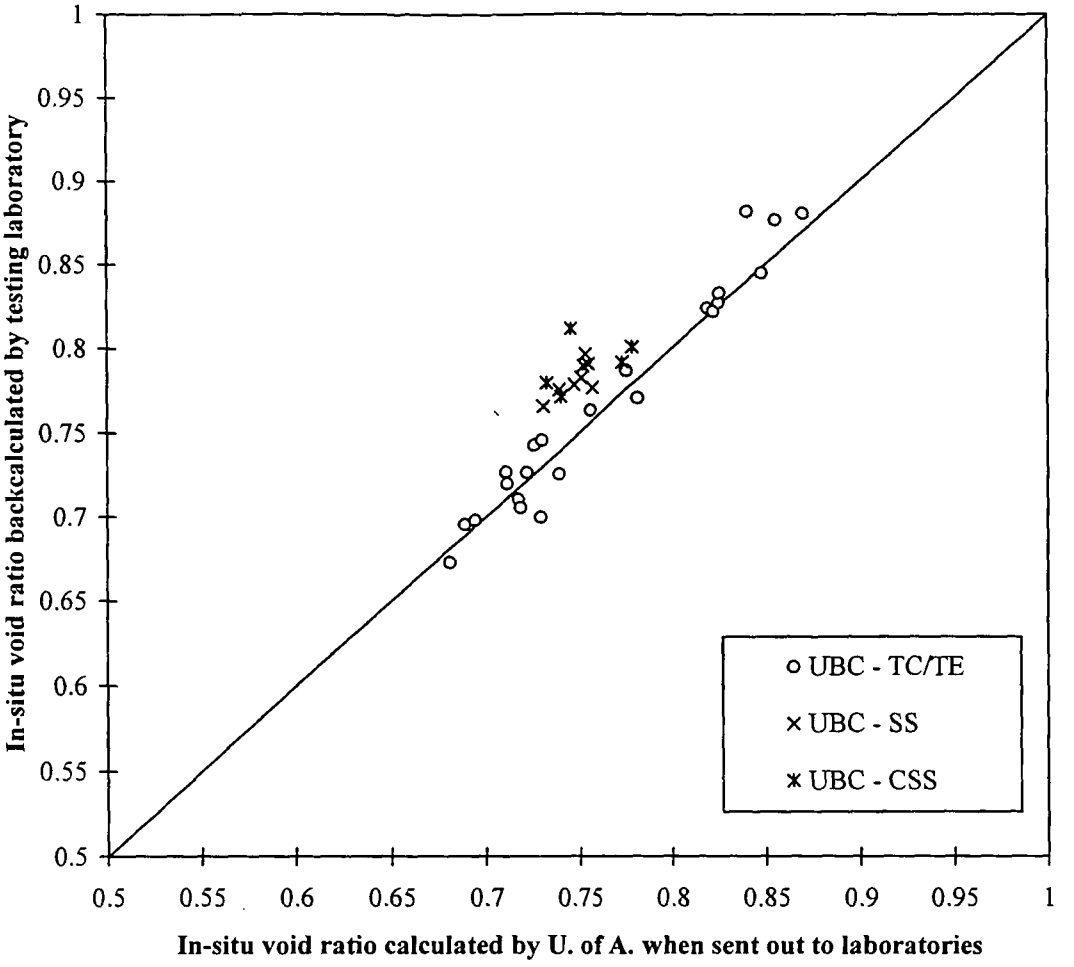

Figure 38. Comparison of different methods of calculation of in-situ void ratio for undisturbed samples from the Phase III site (N.B. U. of A. void ratios are based on G_s=2.62; U.B.C. void ratios are based on G_s=2.66).

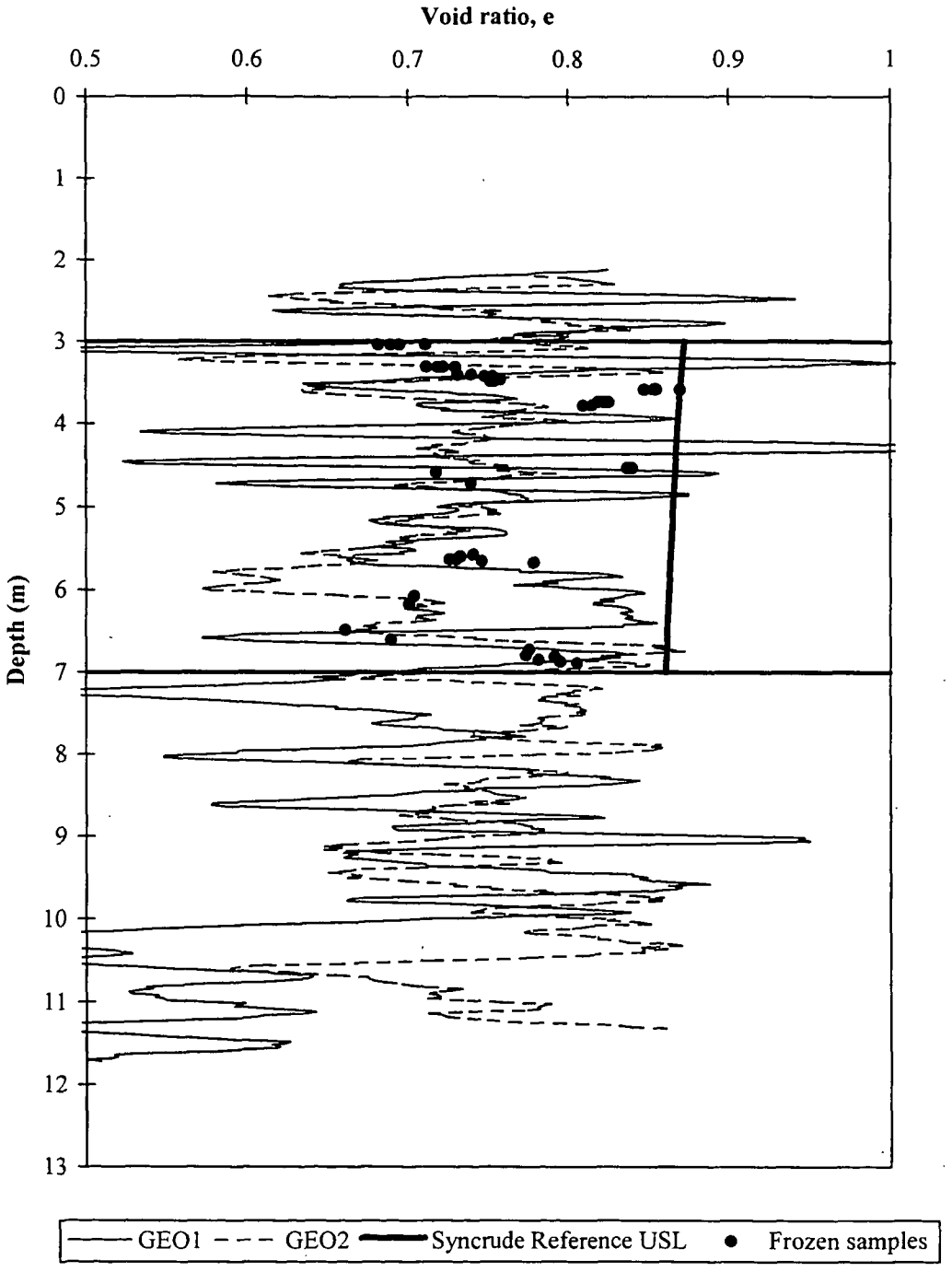

Figure 39. Comparison of geophysical logging predictions of void ratio at the Phase III site with undisturbed samples.

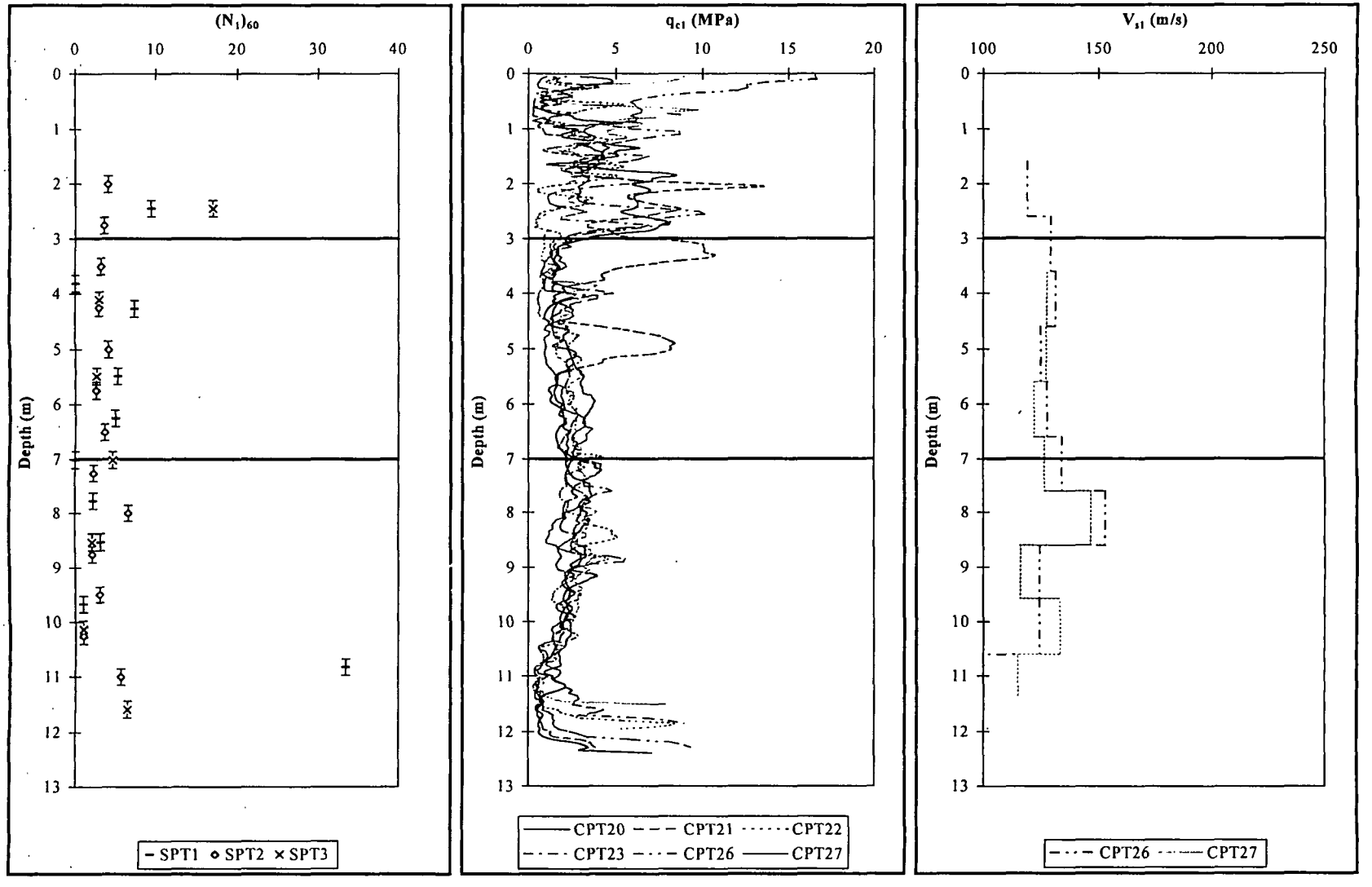

Figure 40. Corrected (a) SPT, (b) CPT and (c) V_s profiles at the Phase III Site.

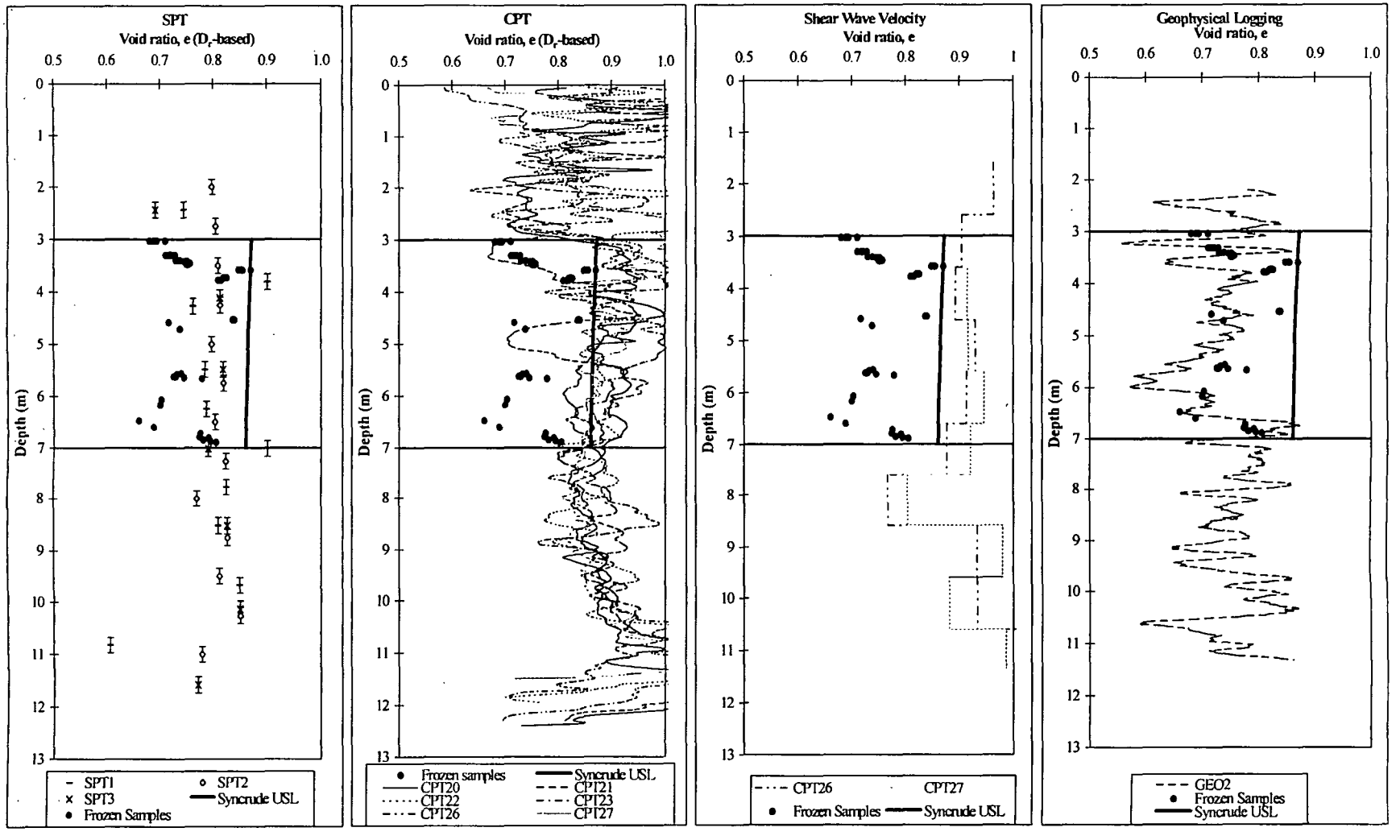

Figure 41. Estimated void ratio profiles in the target zone at the Phase III site from D_r-based interpretations of (a) SPT and (b) CPT, and interpretation of (c) V_s, and (d) geophysical logs.

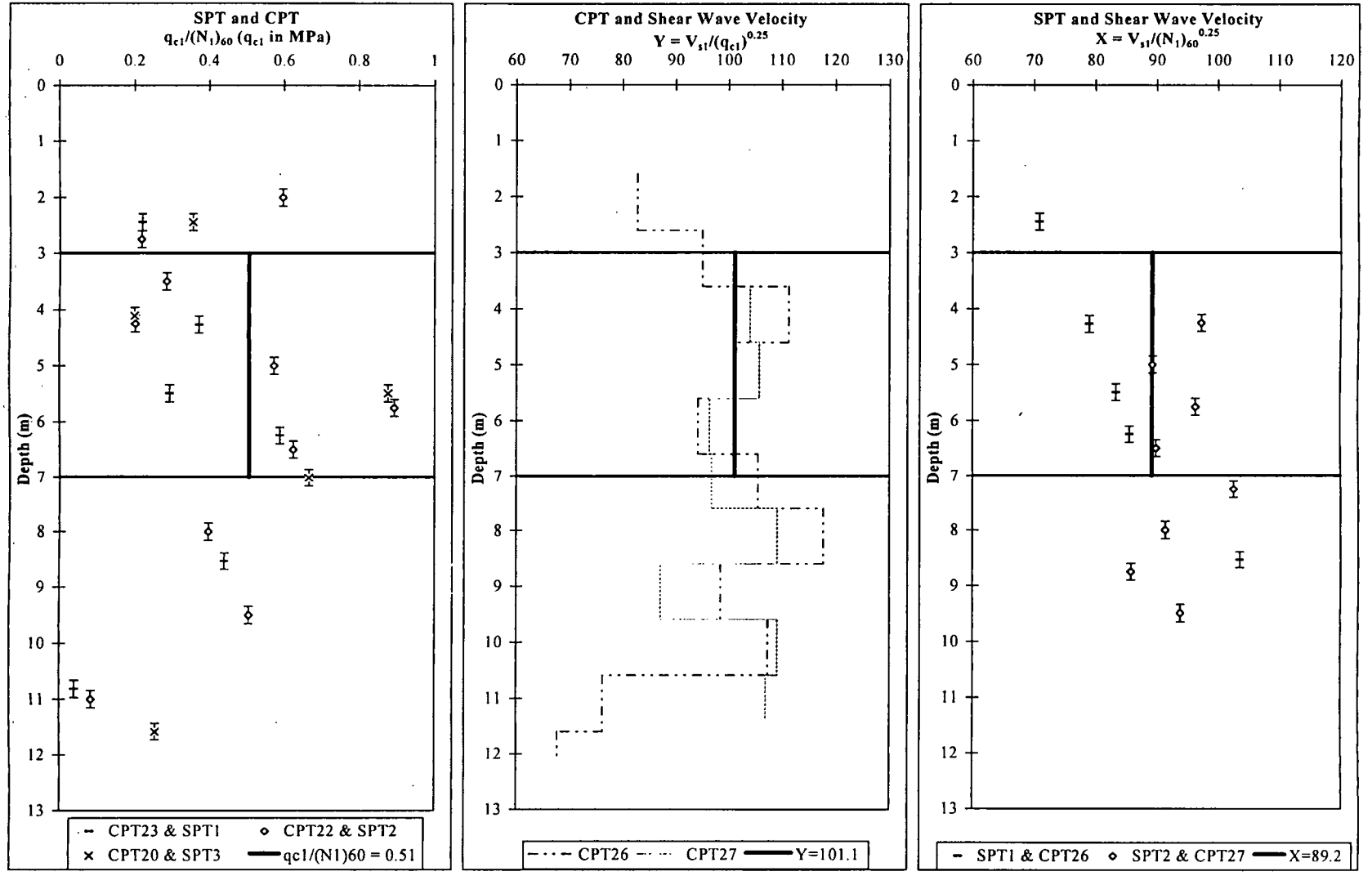

Figure 42. Plots of (a) $q_{c1}/(N_1)_{60}$, (b) Y and (c) X versus depth at the Phase III Site.

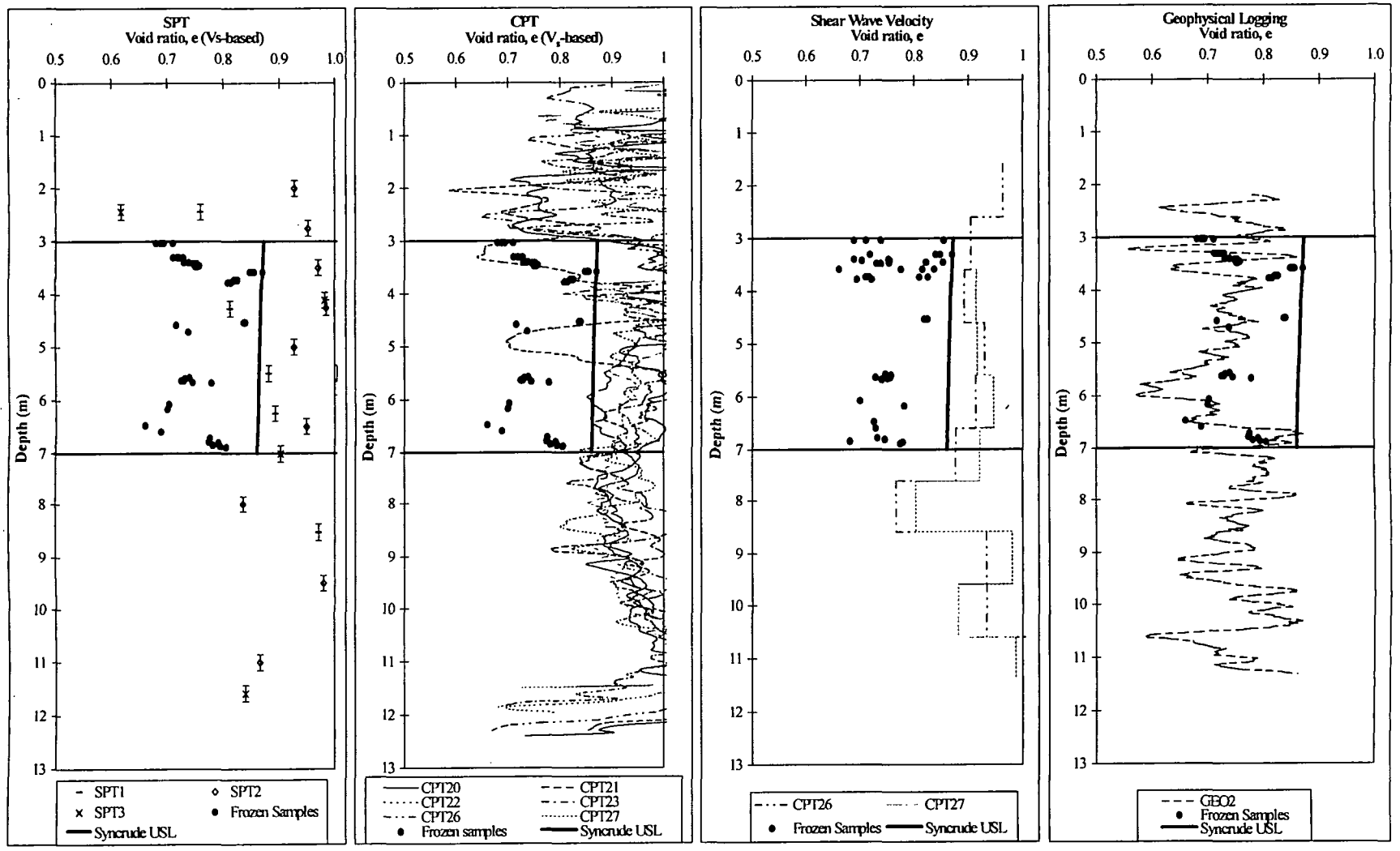

Figure 43. Estimated void ratio profiles in the target zone at the Phase III site from V_s-based interpretations of (a) SPT and (b) CPT, and interpretation of (c) V_s, and (d) geophysical logs.

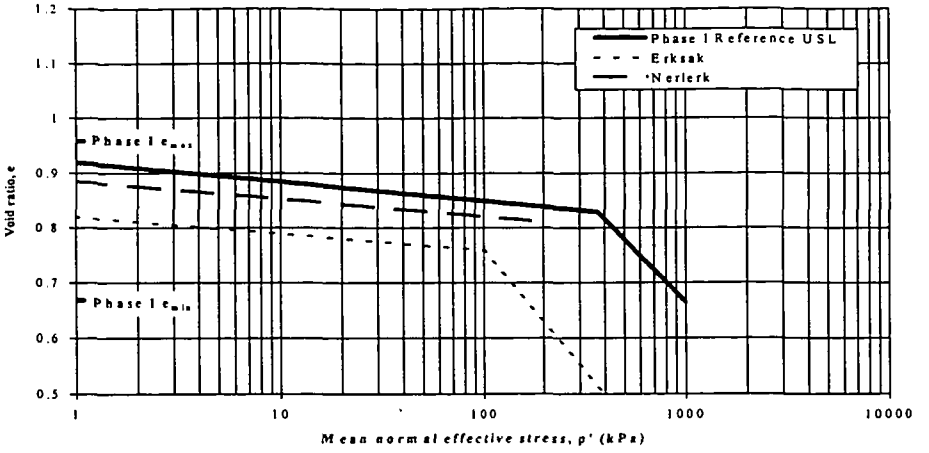

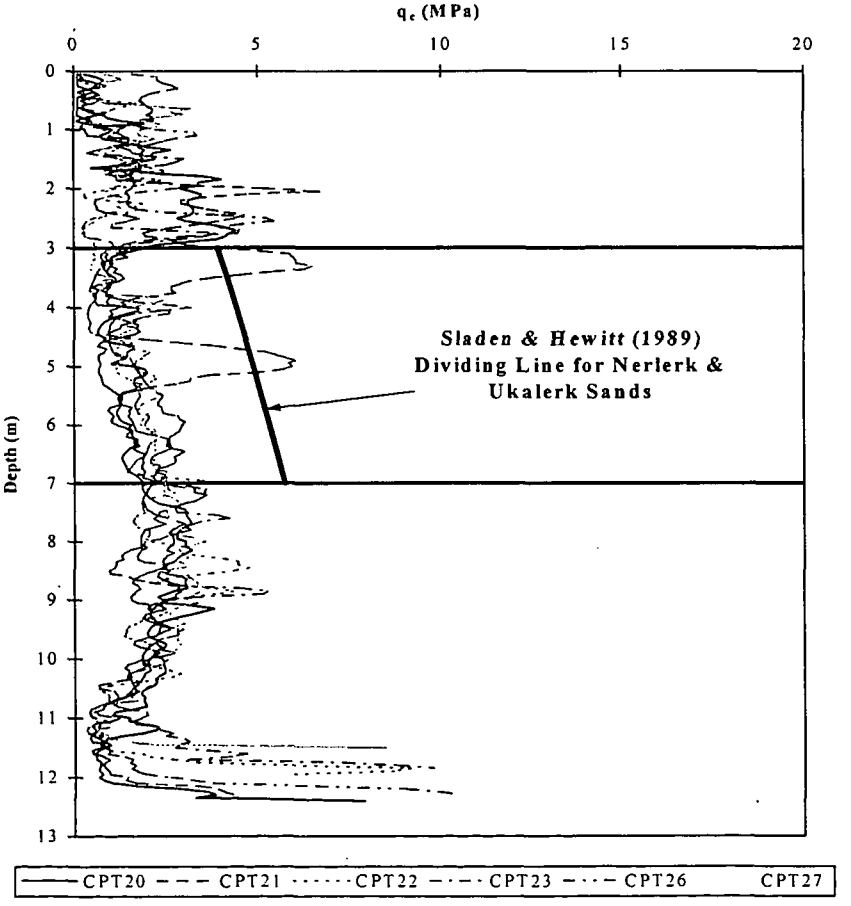

Figure 44. (a) Comparison of the reference USL for Syncrude Sand with the USLs for Nerlerk and Ukalerk (Erksak) sands; (b) estimation of flow liquefaction potential at the Phase III site from CPT results based on the method for Nerlerk and Ukalerk sands by Sladen & Hewitt (1989).

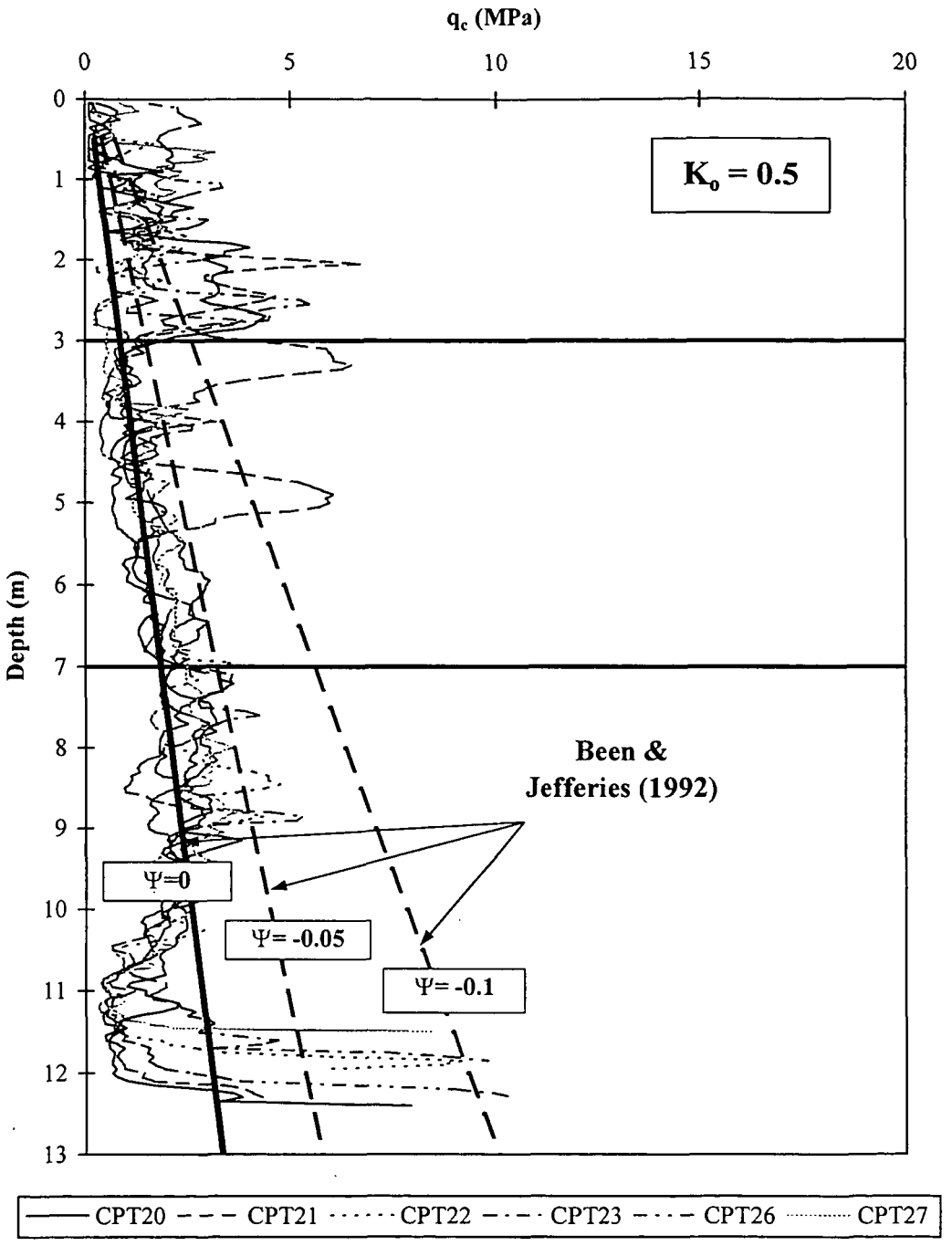

Figure 45. Estimating flow liquefaction potential at the Phase III site from CPT results based on the method by Been and Jefferies (1992).

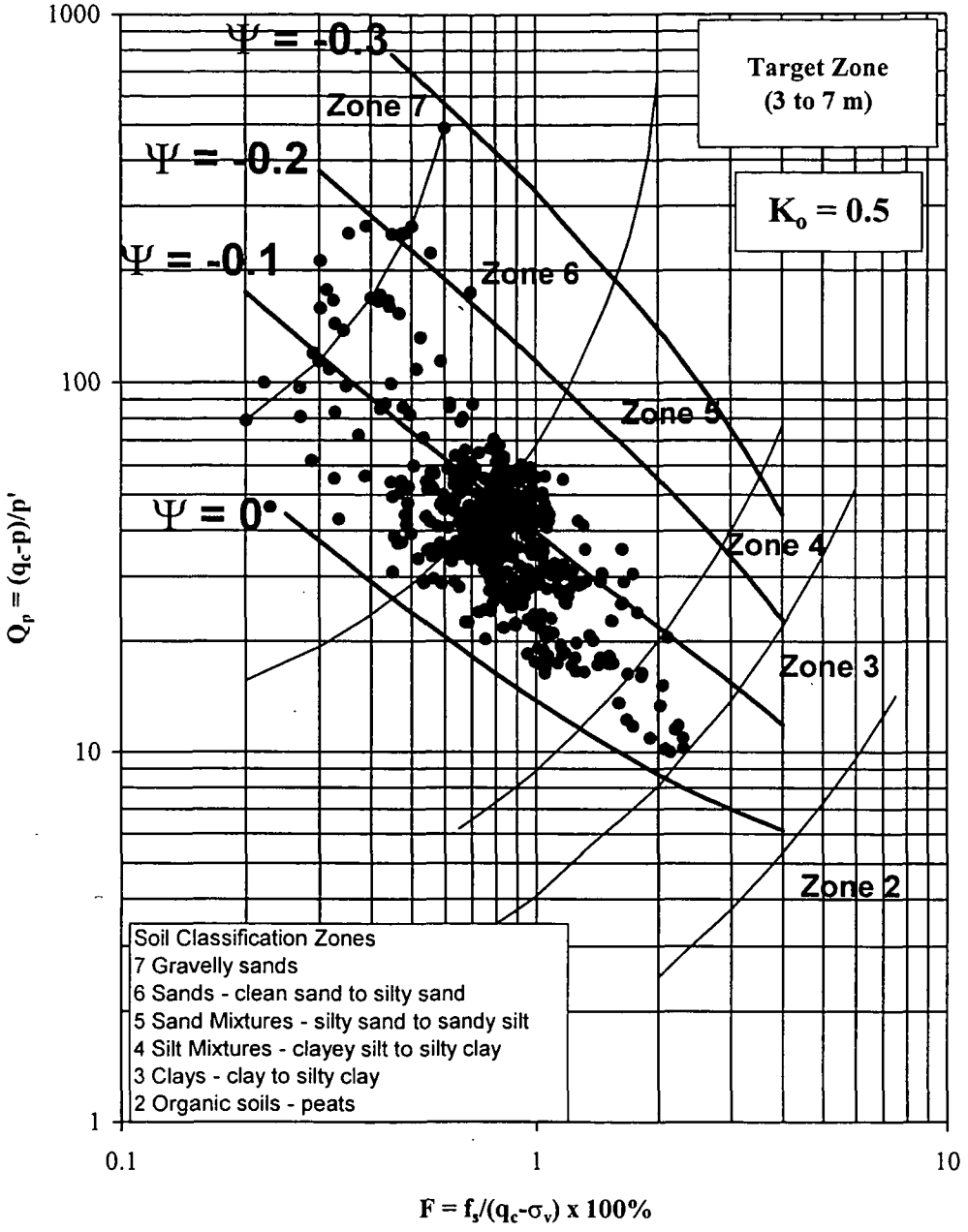

Figure 46. Estimating state at the Phase III site from CPT results based on the method by Plewes et al. (1992).

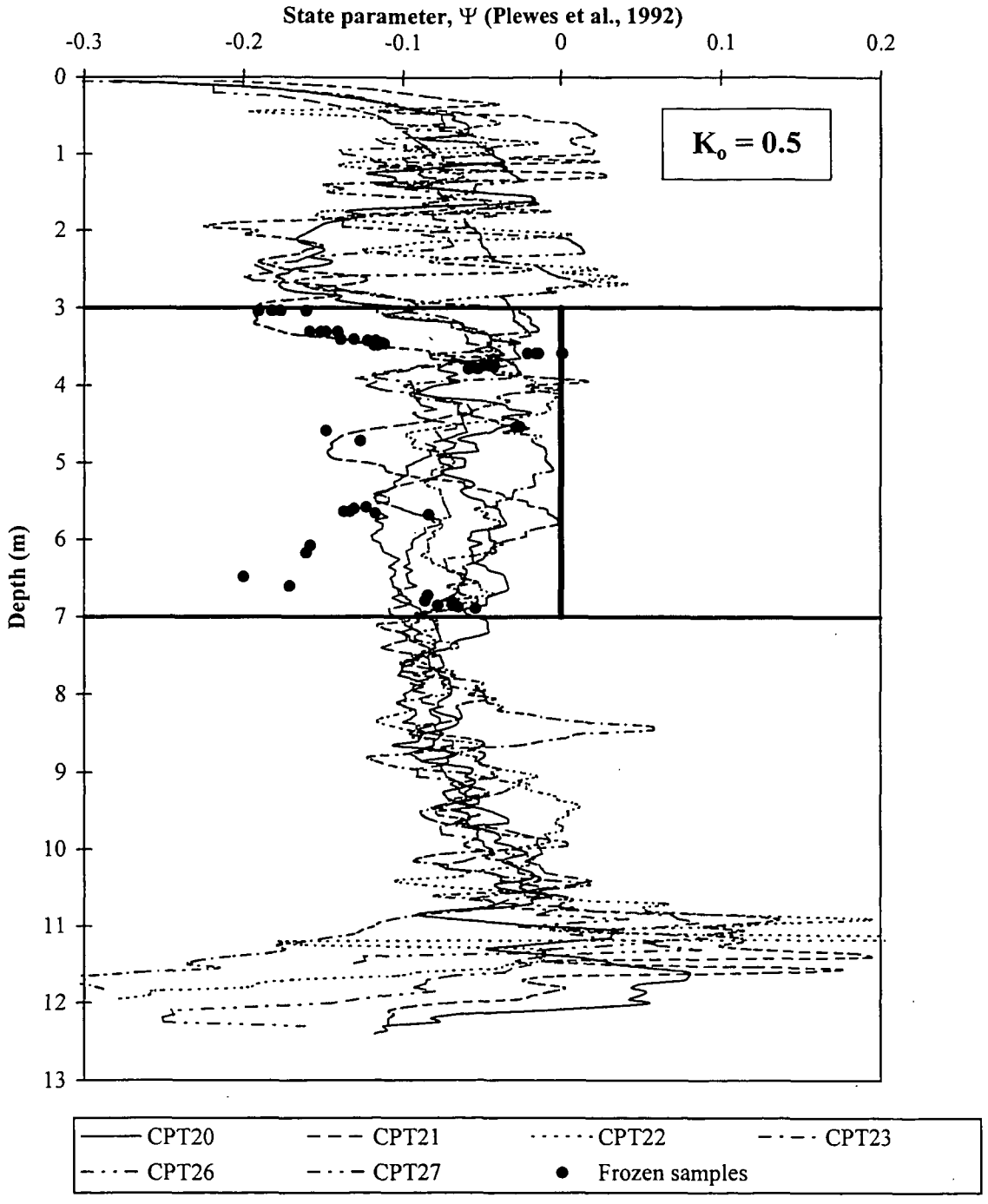

Figure 47. Estimated profiles of state parameter at the Phase III site from CPT results based on the method by Plewes et al. (1992).

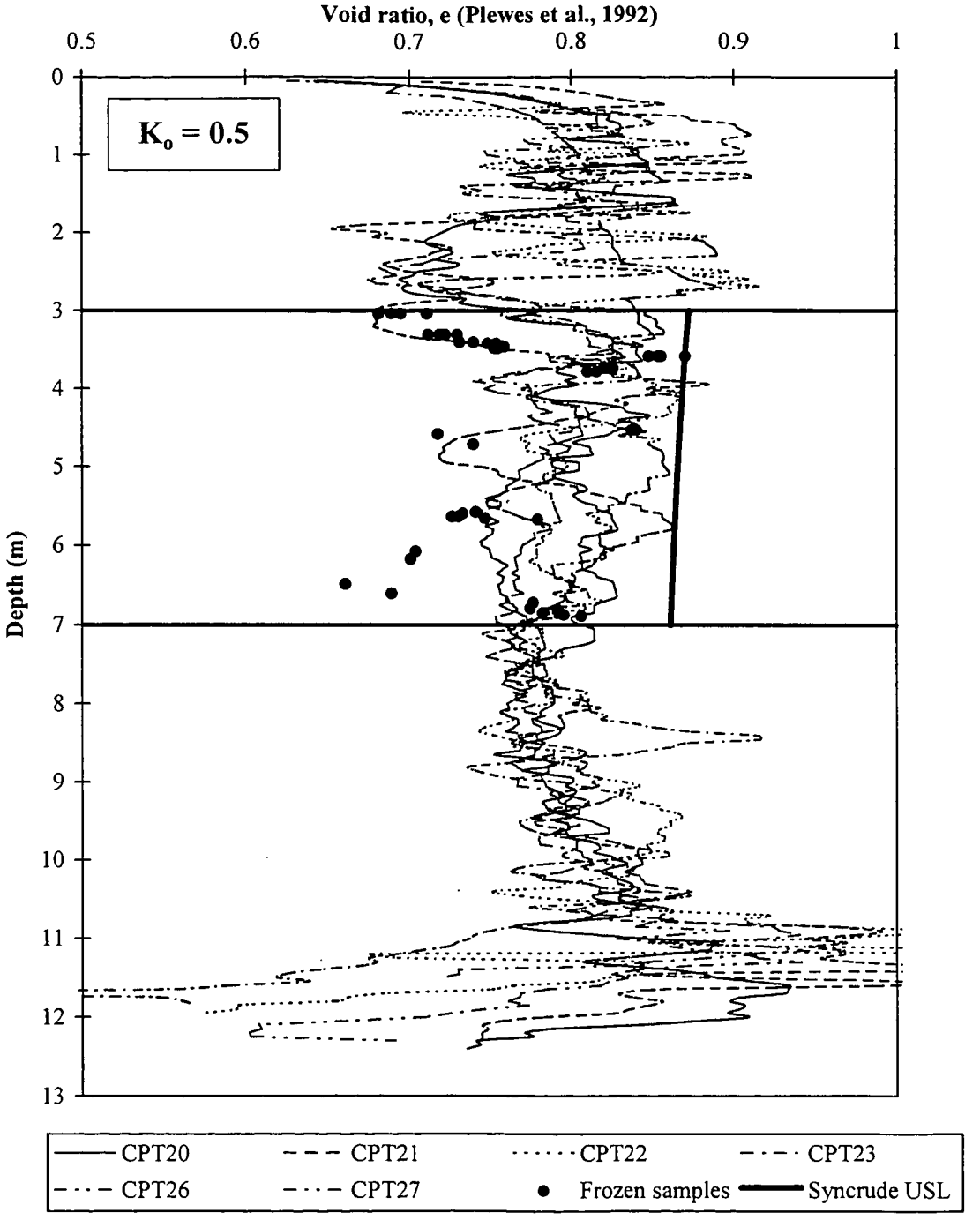

Figure 48. Estimated profiles of void ratio at the Phase III site from CPT results based on the method by Plewes et al. (1992).

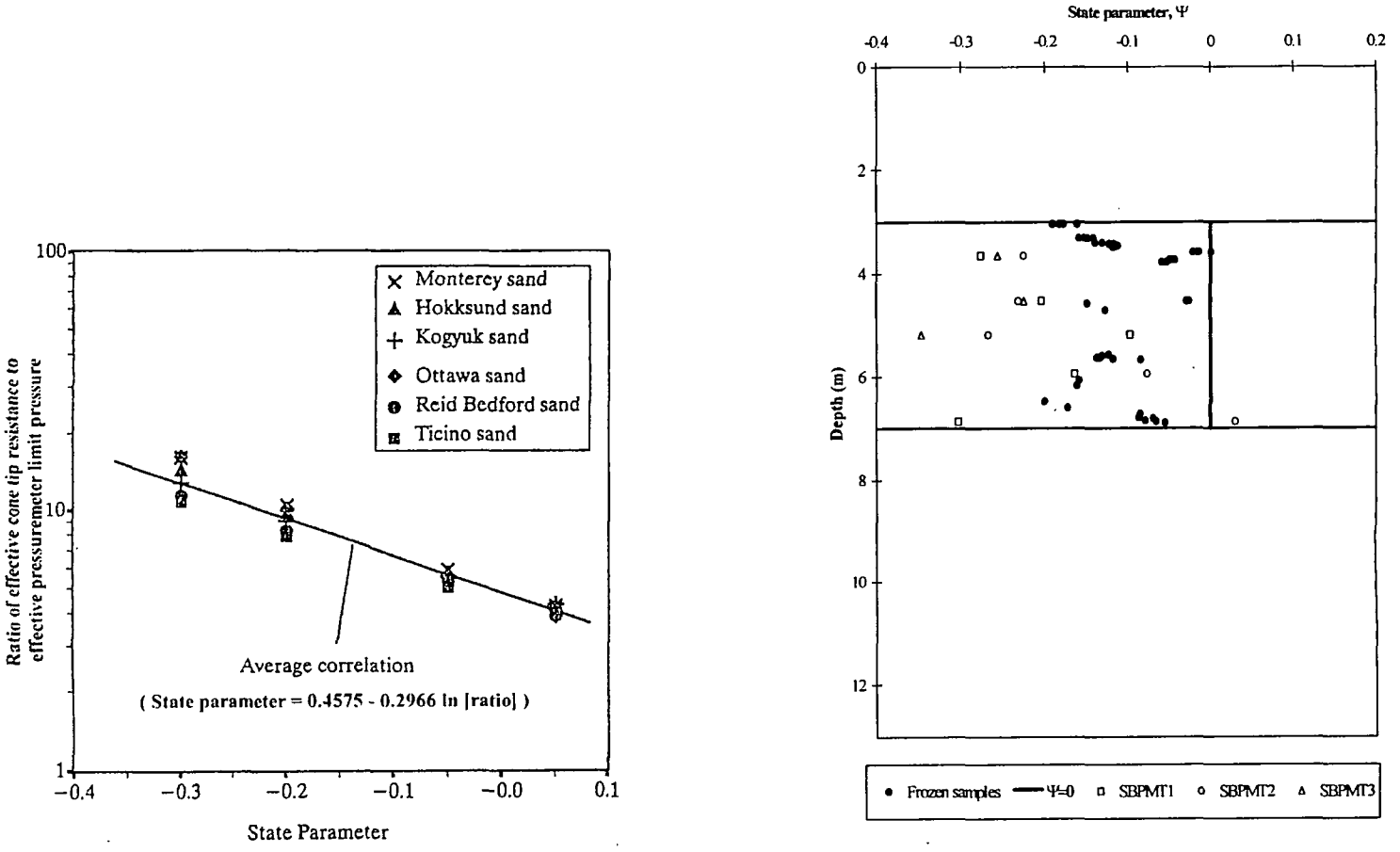

Figure 49. (a) The method by Yu et al. (1996), and (b) estimating state parameter in the Phase III site target zone from pressuremeter results based on the method by Yu et al. (1996).

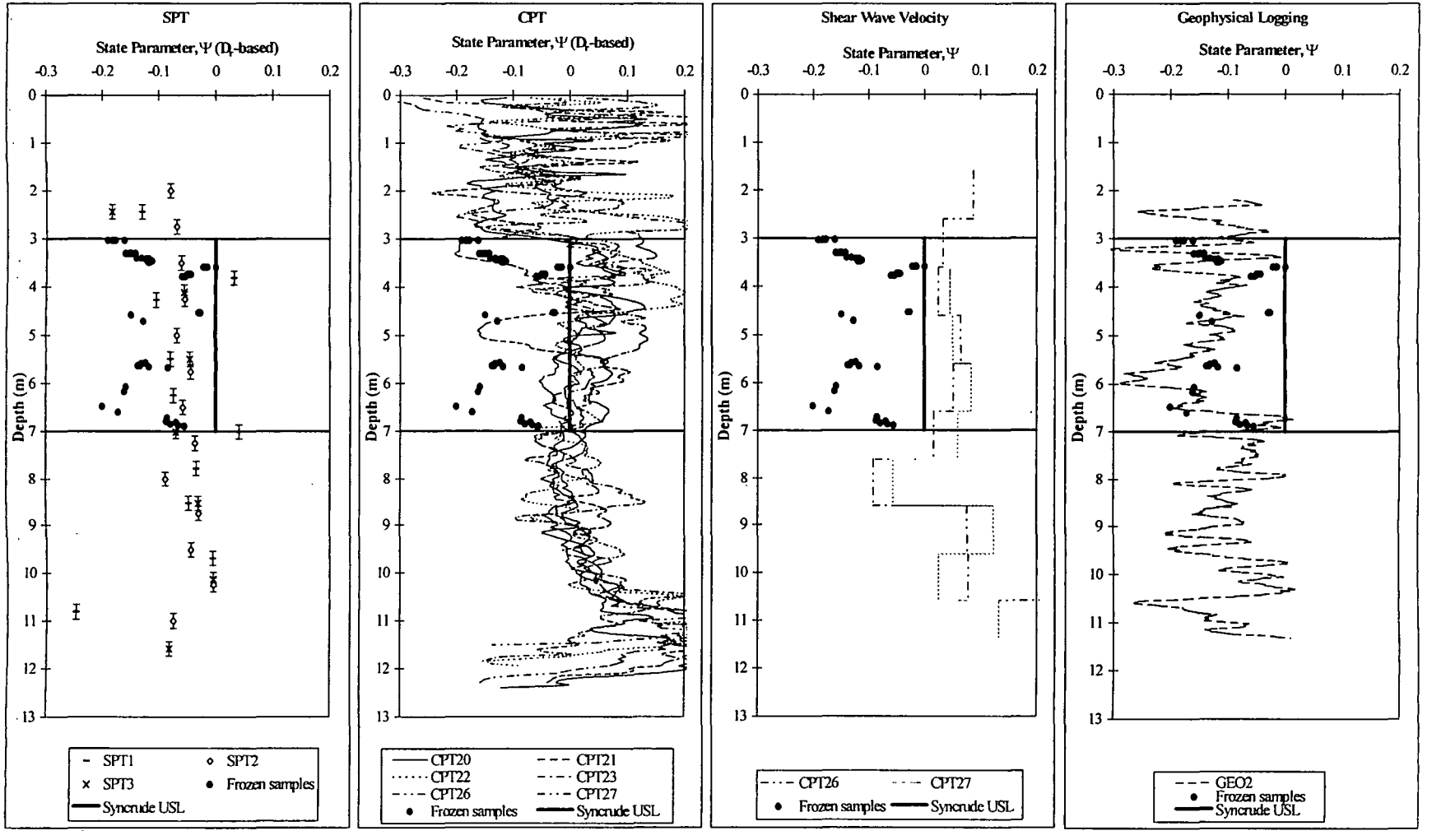

Figure 50. Estimated profiles of state parameter at the Phase III site from the D_r-based interpretations of void ratio from (a) SPT and (b) CPT and void ratio interpretations of (c) V_s and (d) geophysical logs.

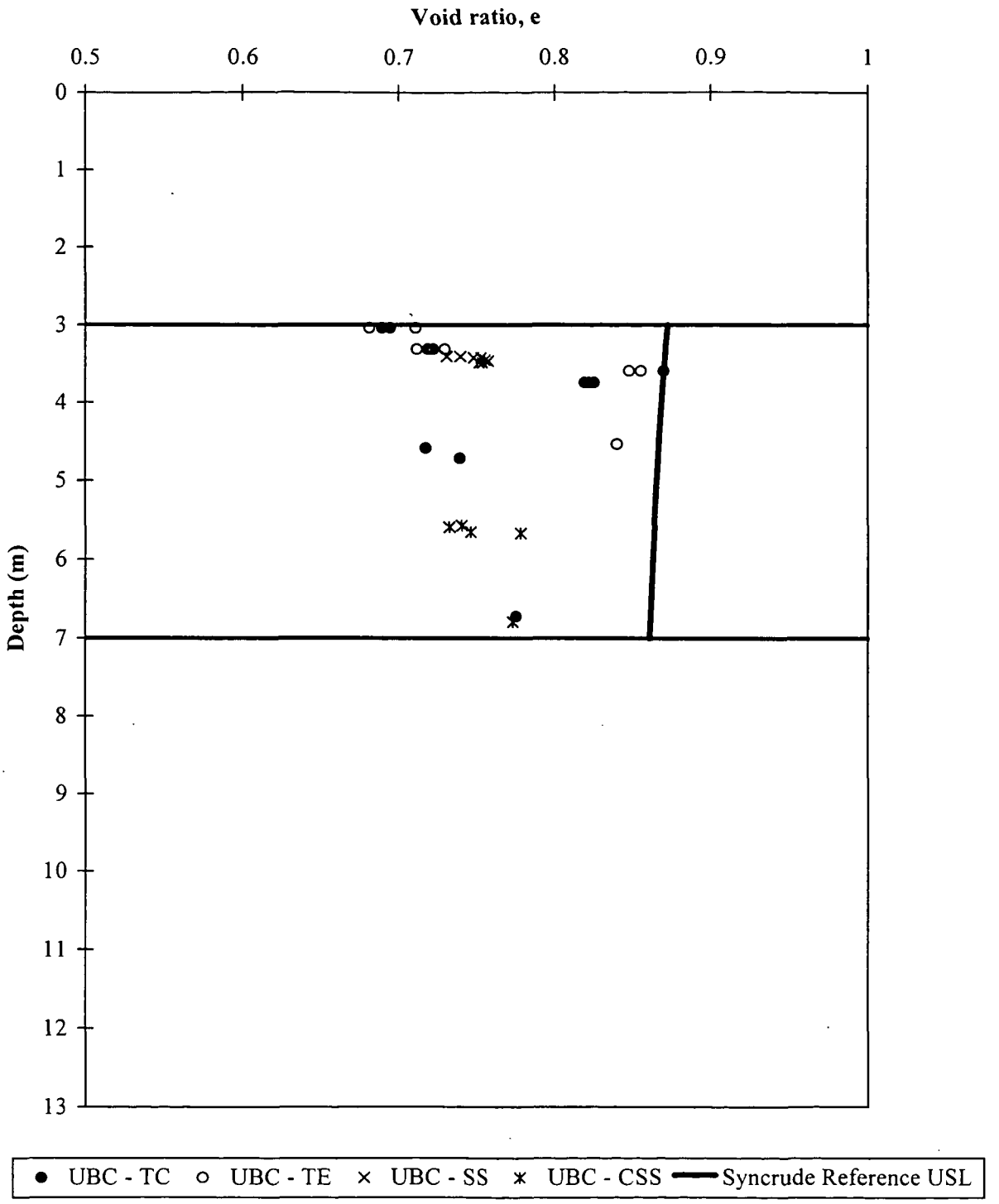

Figure 51. Enlarged plot of void ratios for the Phase III site undisturbed frozen samples, illustrating the type of tests that were conducted on the samples.

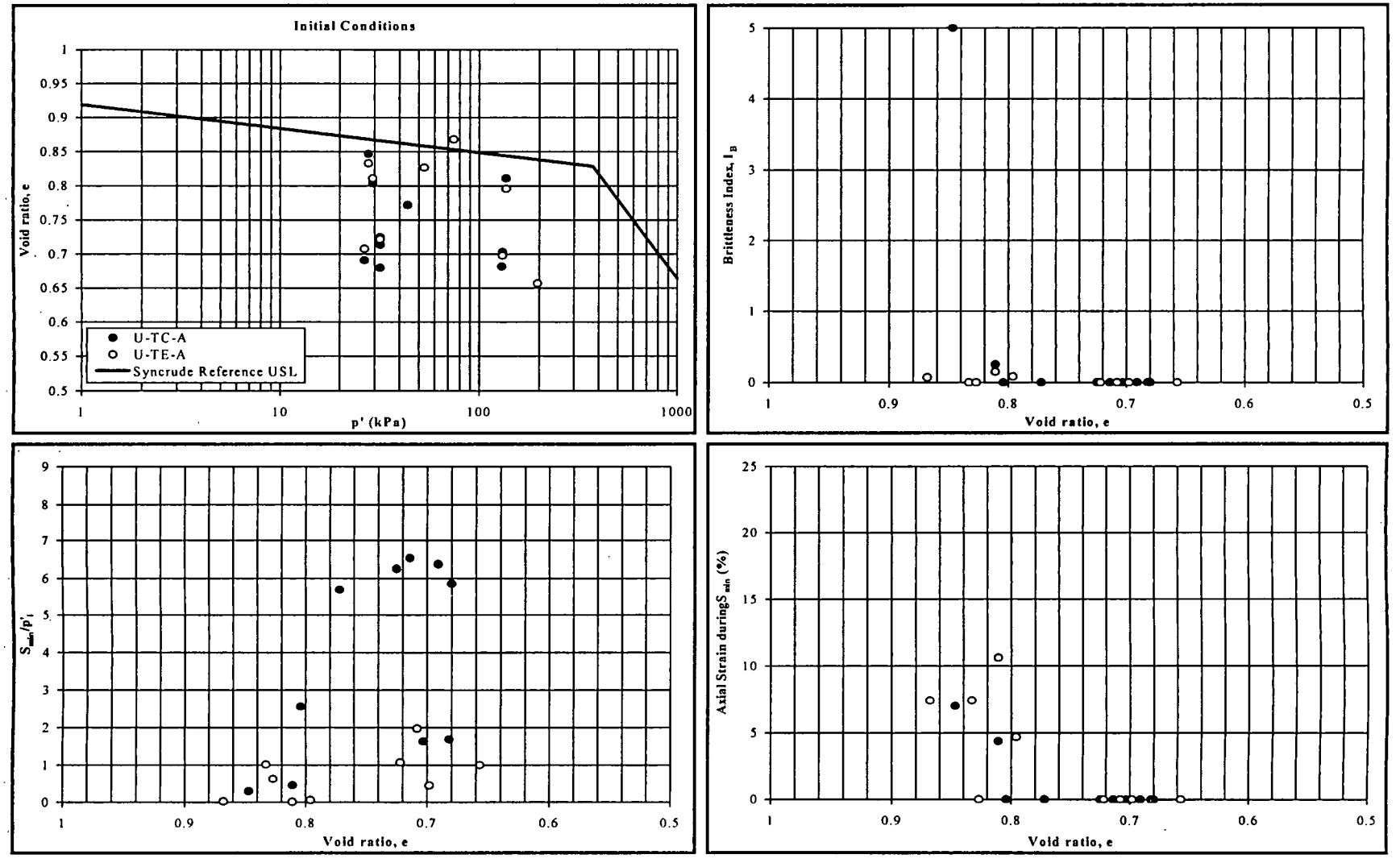

Figure 52. Relationship between void ratio (e) and undrained monotonic laboratory response of anisotropically consolidated undisturbed triaxial samples from the Phase III site: (a) initial conditions, (b) brittleness index (I_B), (c) minimum strength ratio (S_{min}/p'_i), and (d) axial strain (ε_a) during minimum strength.

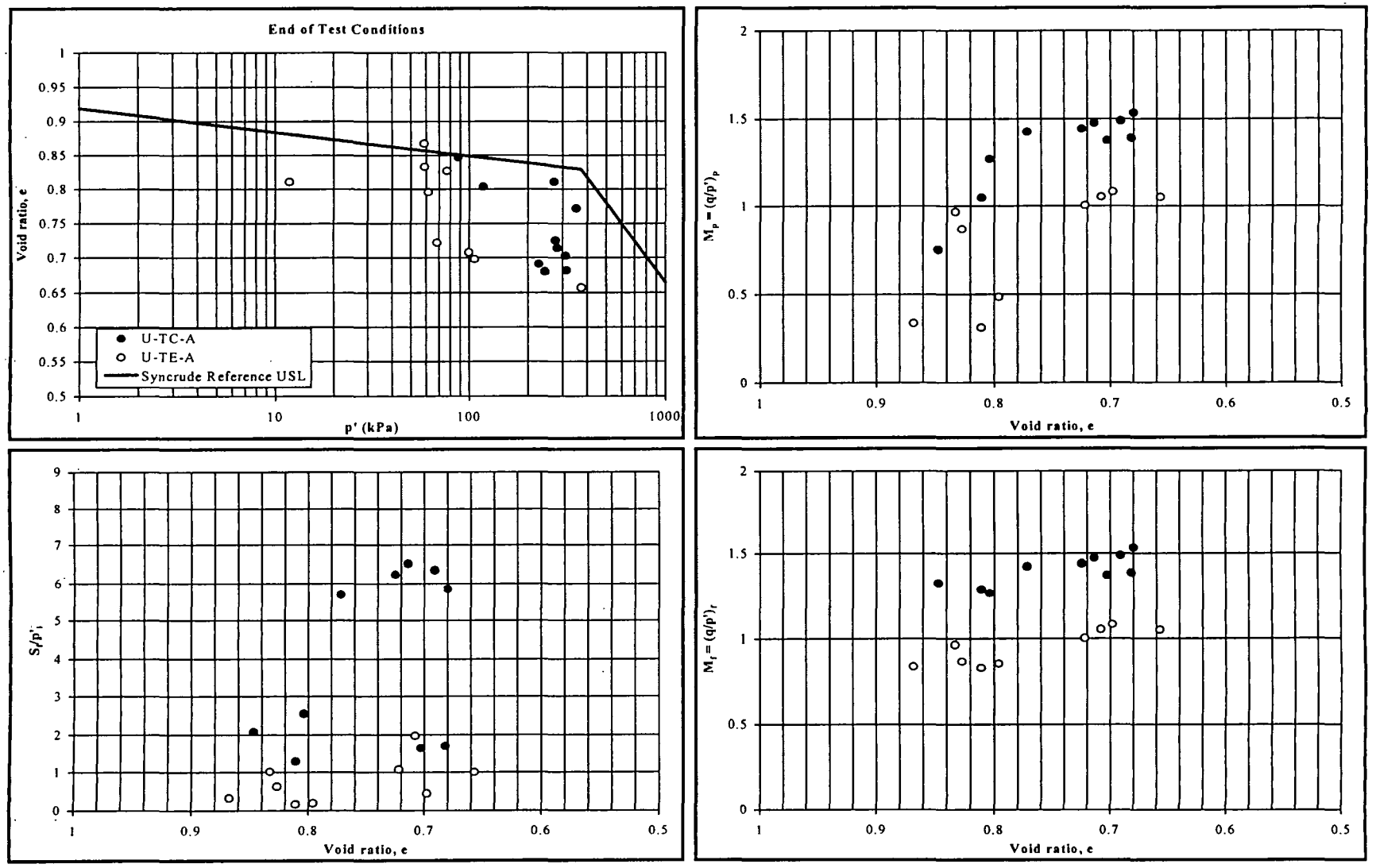

Figure 53. Relationship between void ratio (e) and undrained monotonic response of anisotropically consolidated undisturbed triaxial samples from the Phase III site: (a) end-of-test conditions, (b) end-of-test strength ratio (S_f/p'_i), (c) peak stress ratio (M_p), and (d) end-of-test stress ratio (M_f).

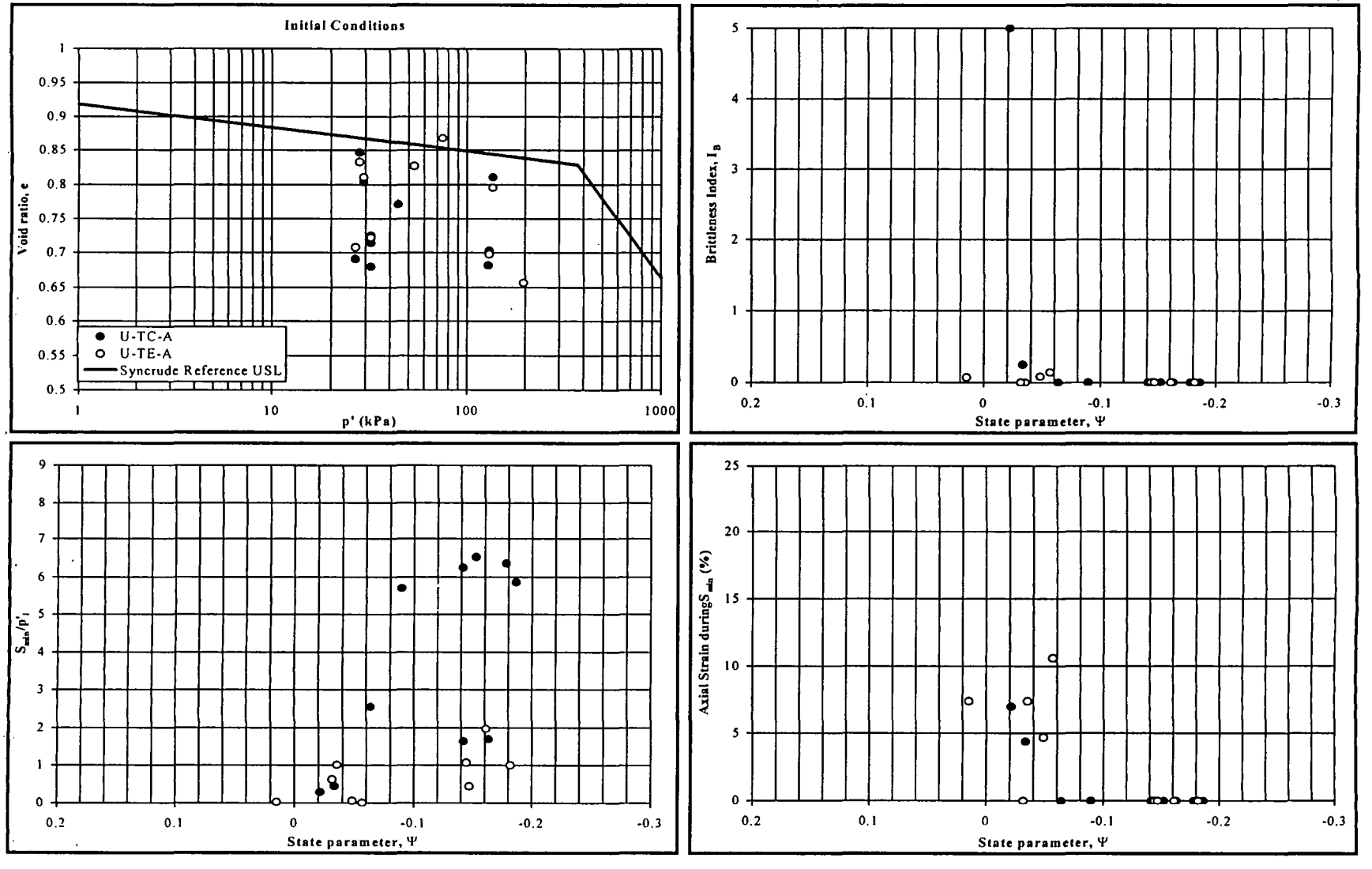

Figure 54. Relationship between state parameter (Ψ) and undrained monotonic response of anisotropically consolidated undisturbed triaxial samples from the Phase III site: (a) initial conditions, (b) brittleness index (I_B), (c) minimum strength ratio (S_{min}/p'_i), and (d)axial strain (ε_a) during minimum strength.

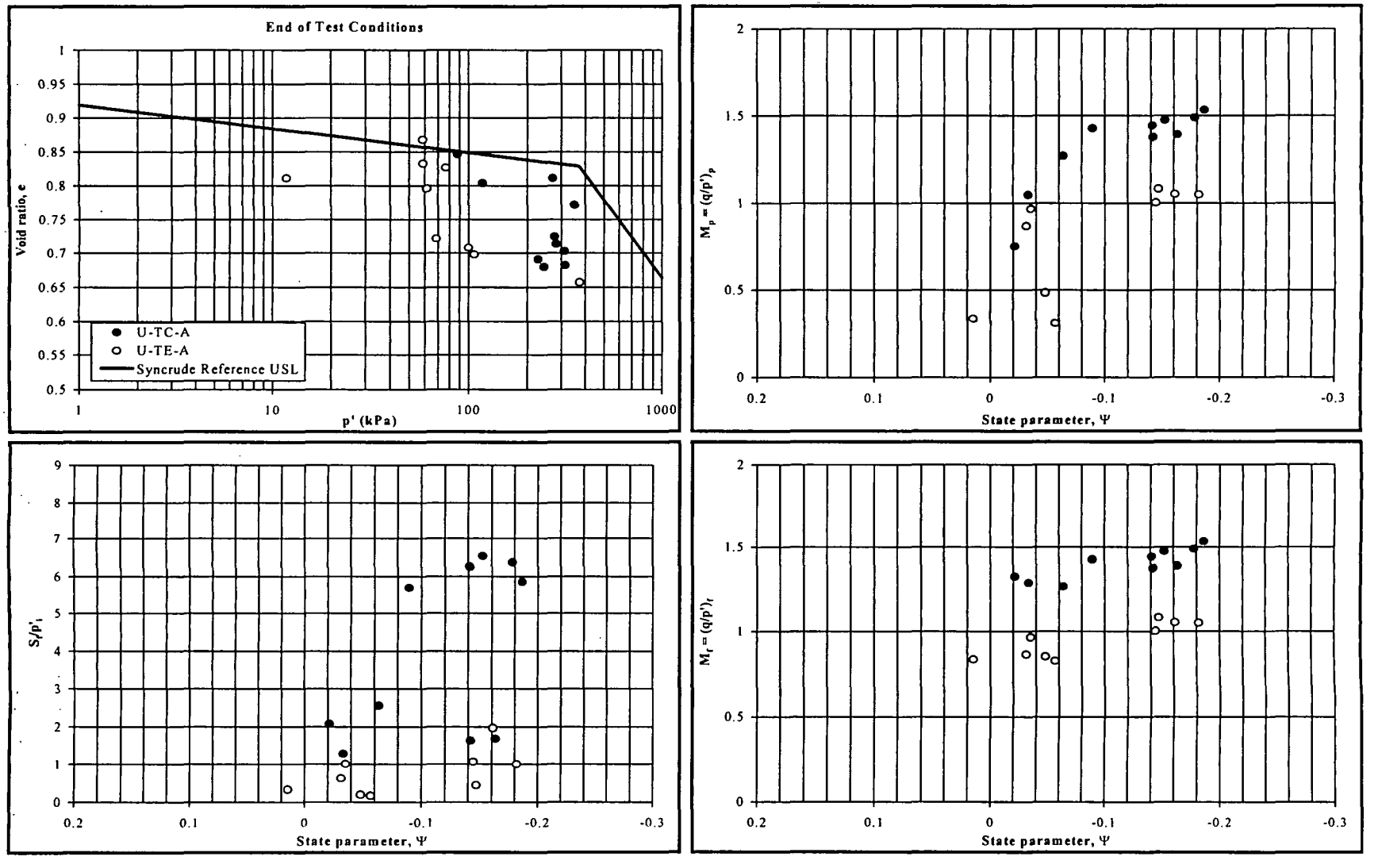

Figure 55. Relationship between state parameter (Ψ) and undrained monotonic response of anisotropically consolidated undisturbed triaxial samples from the Phase III site: (a) end-of-test conditions, (b) end-of-test strength ratio (S_f/p'_i), (c) peak stress ratio (M_p), and (d) end-of-test stress ratio (M_f).

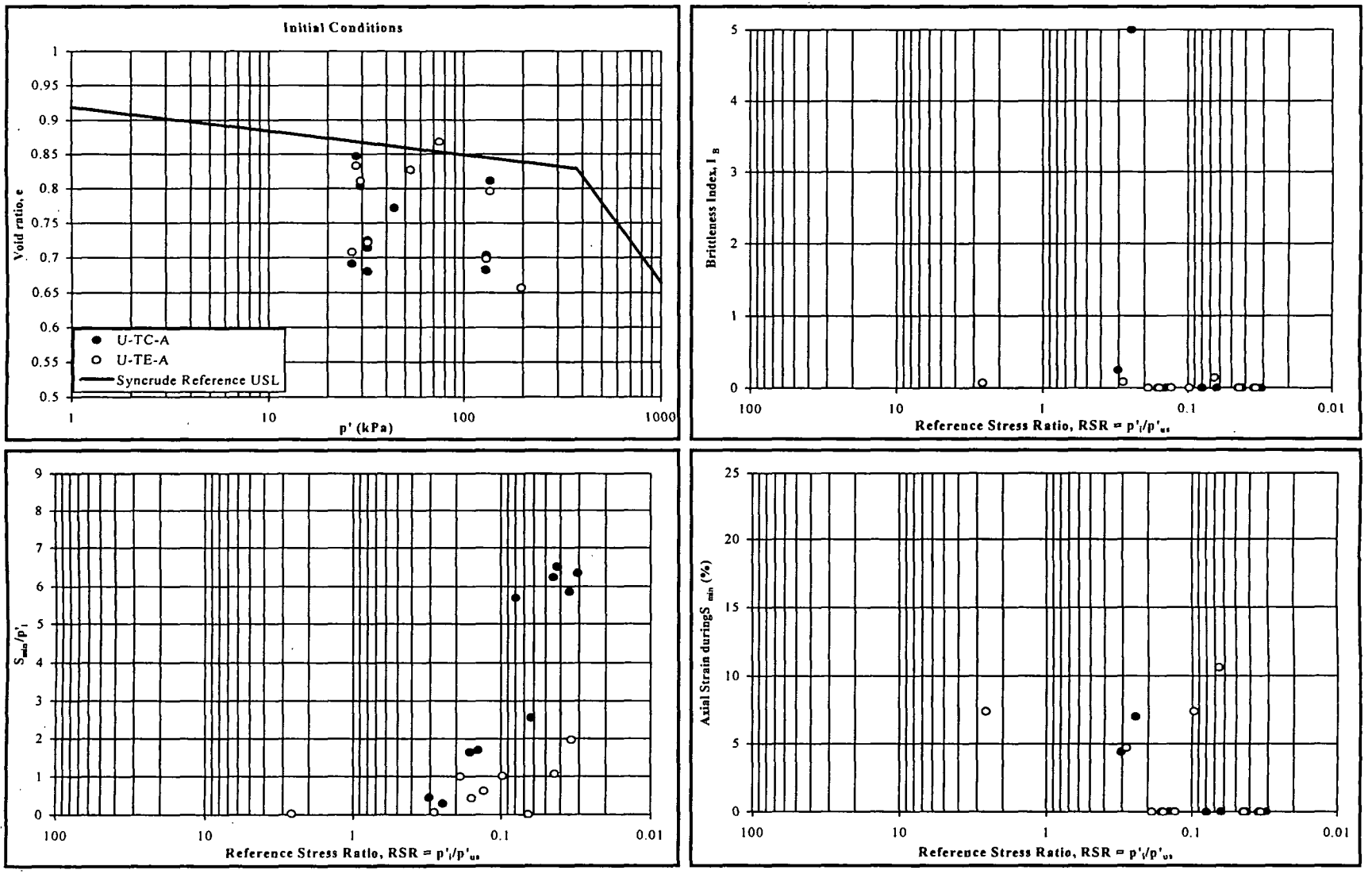

Figure 56. Relationship between reference state ratio (RSR) and undrained monotonic response of anisotropically consolidated undisturbed triaxial samples from the Phase III site: (a) initial conditions, (b) brittleness index (I_B), (c) minimum strength ratio (S_{min}/p'_i), and (d) axial strain (ε_a) during minimum strength.

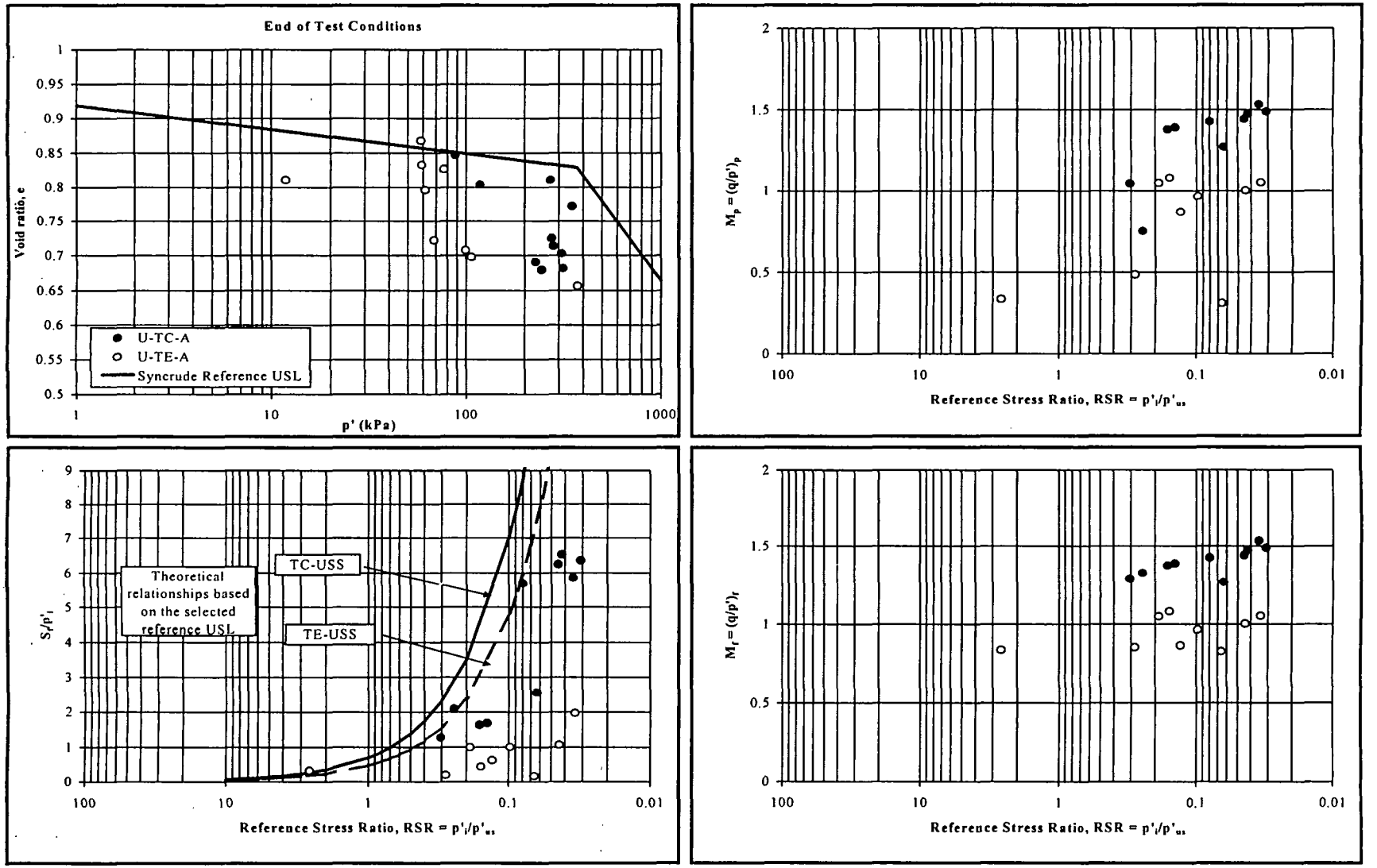

Figure 57. Relationship between reference state ratio (RSR) and undrained monotonic response of anisotropically consolidated undisturbed triaxial samples from the Phase III site: (a) end-of-test conditions, (b) end-of-test strength ratio (S_f/p'_i), (c) peak stress ratio (M_p), and (d) end-of-test stress ratio (M_f).

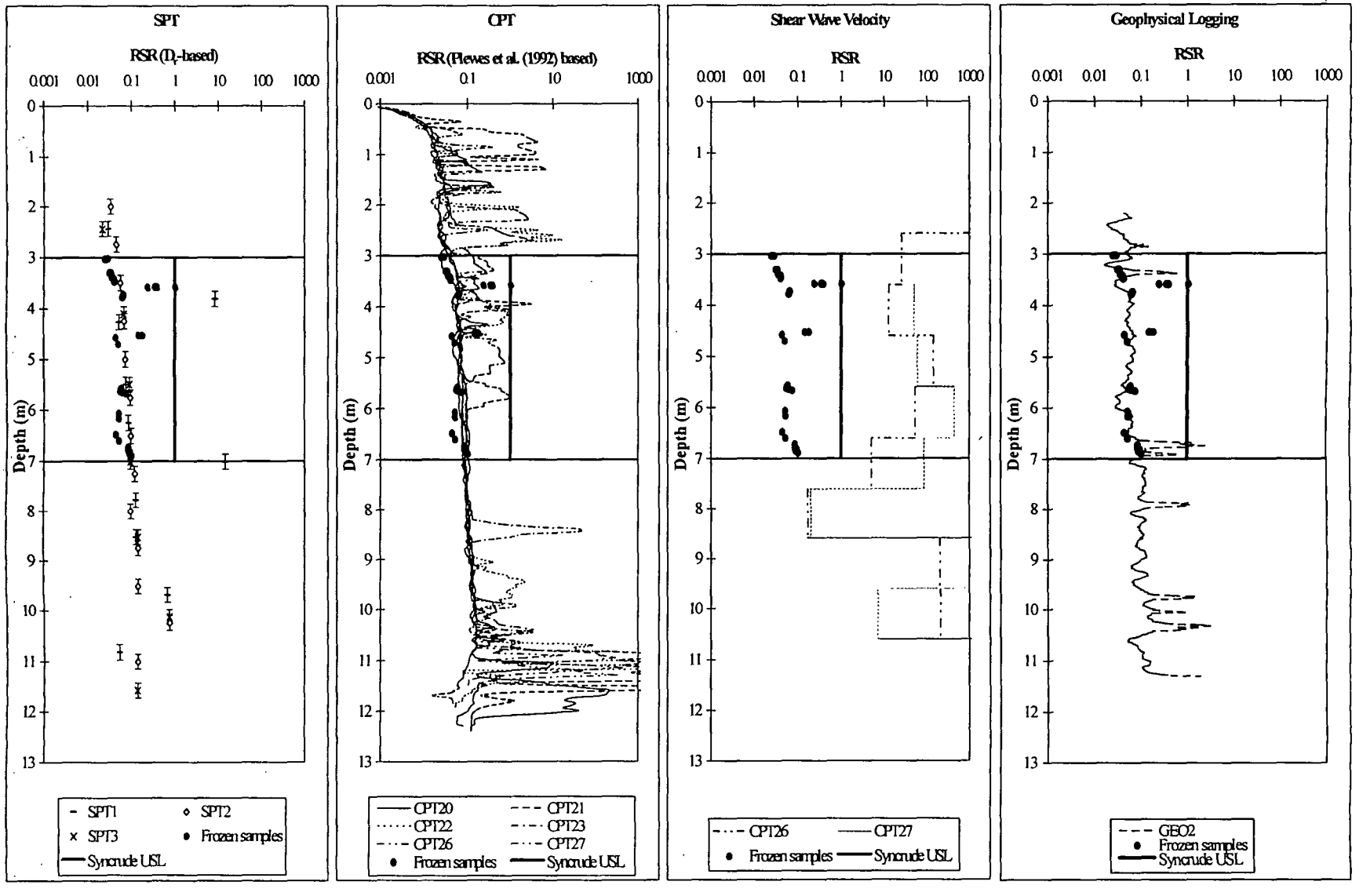

Figure 58. Profiles of estimated RSR at the Phase III site for (a) SPT, (b) CPT, (c) V_s, and (d) geophysical logs.

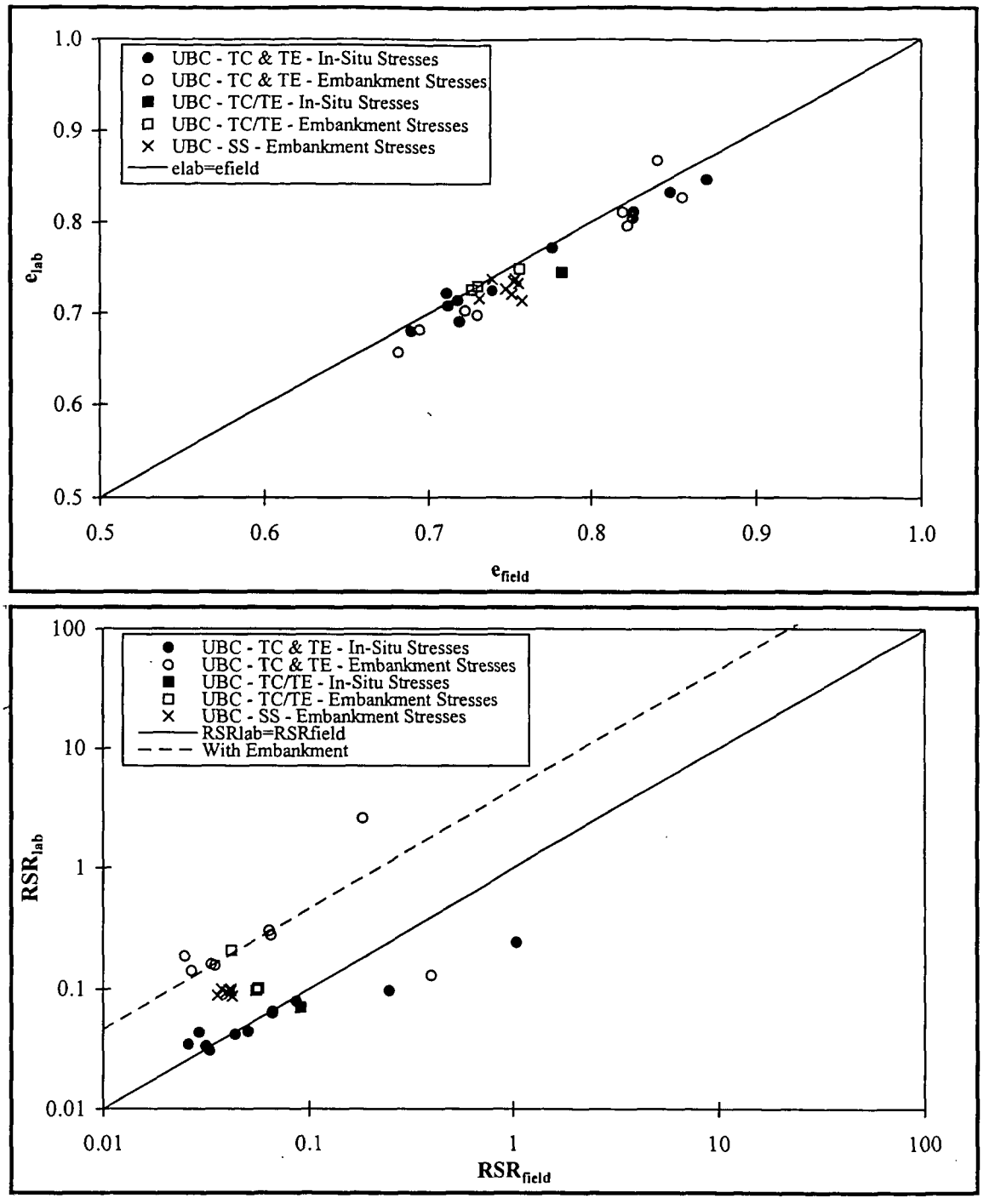

Figure 59. Comparison at the Phase III site of (a) void ratio and (b) RSR in the laboratory and in the field for samples tested under monotonic loading; note that some samples were tested under higher initial stresses than those in-situ, in order to simulate the stresses beneath the full-scale liquefaction event embankment, once it was constructed.

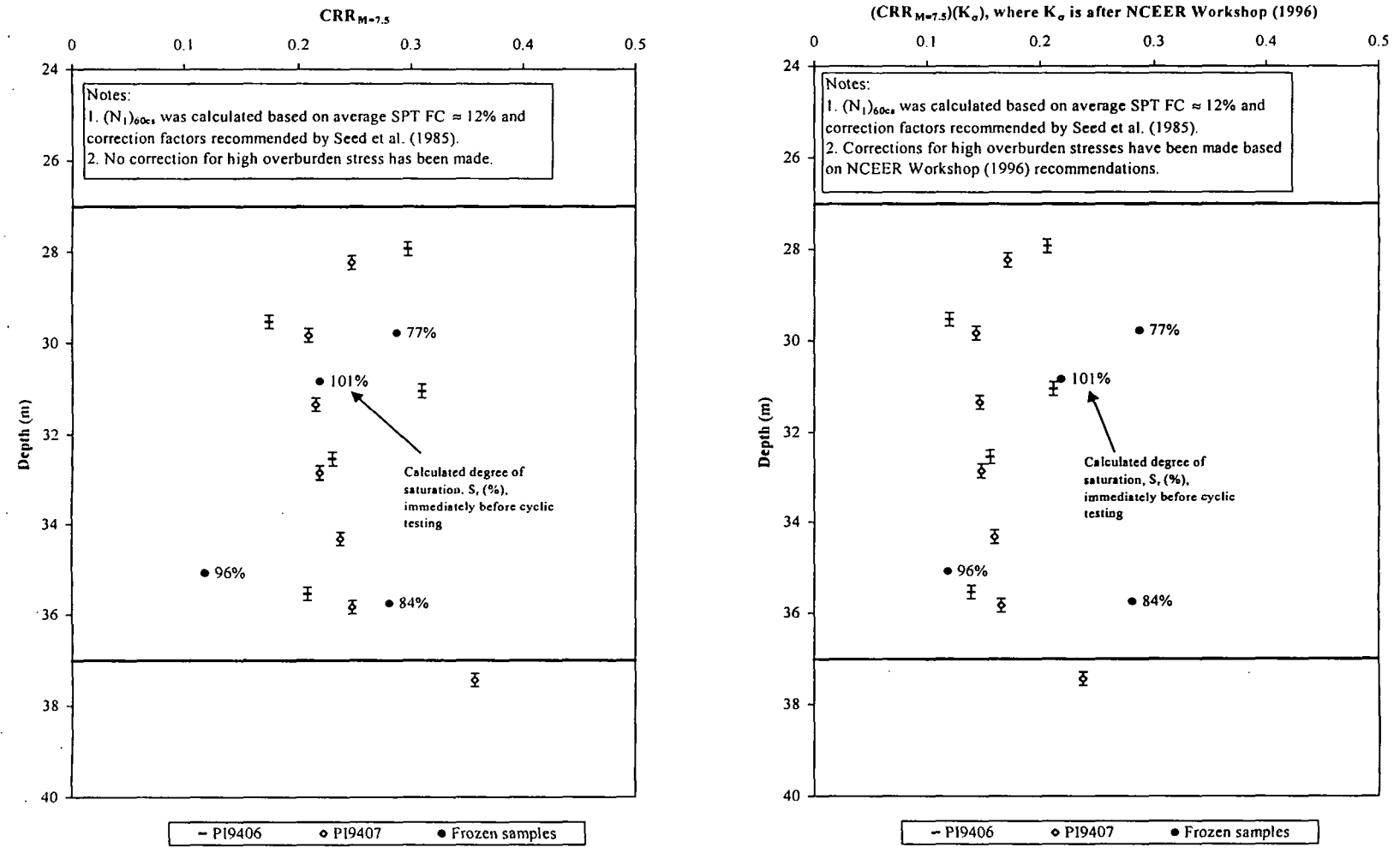

Figure 60. CRR predicted by interpreting SPT results at Phase I using the method by Seed et al. (1985): (a) not accounting for effect of high overburden stresses, and (b) accounting for effect of high overburden stresses; note that undrained cyclic triaxial test results on frozen samples are shown for comparison.

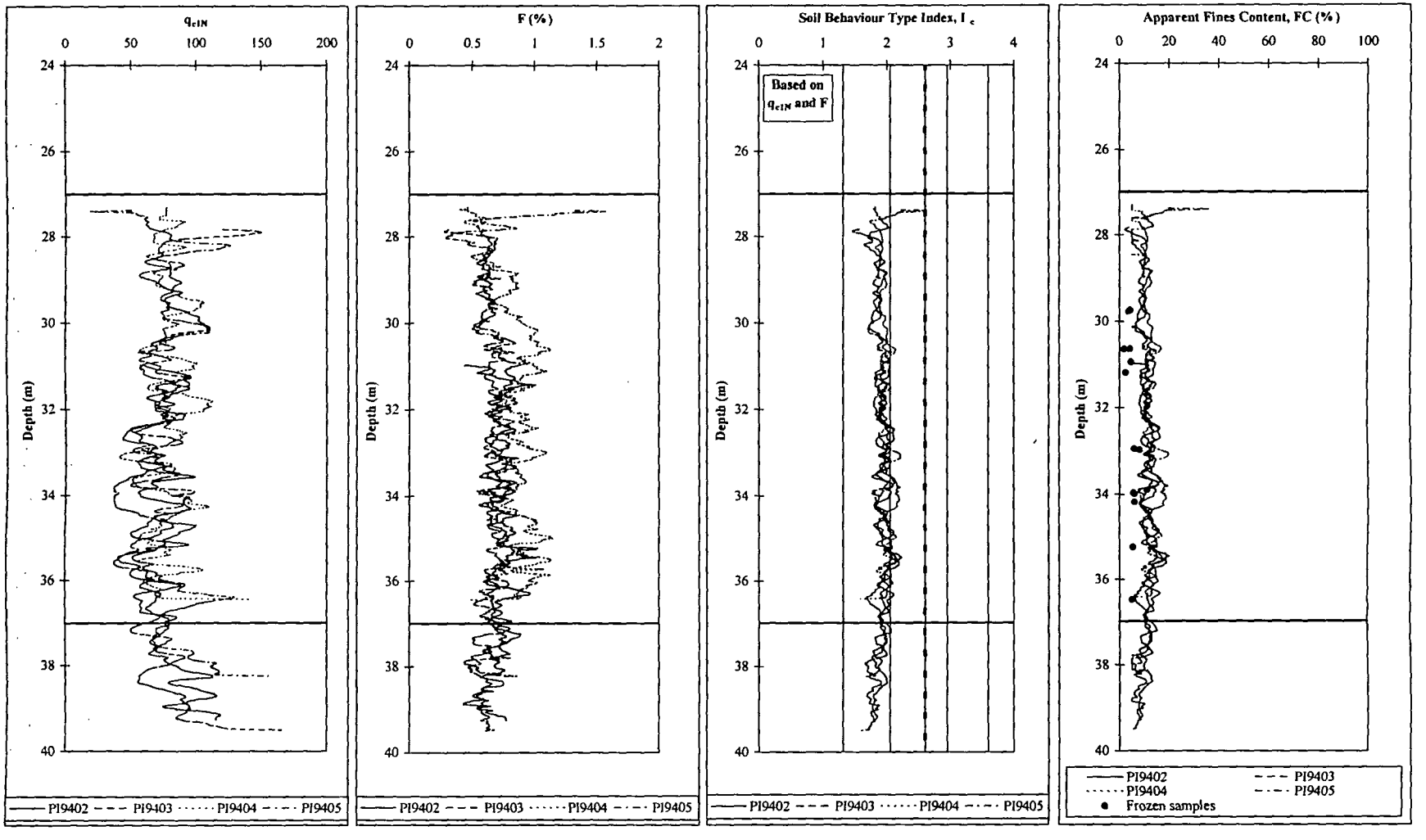

Figure 61. Estimating cyclic softening potential at the Phase I site, Part I: profiles of (a) q_{c1N}, (b) F, (c) soil behaviour index (I_c), and (d) CPT predicted apparent fines content (FC).

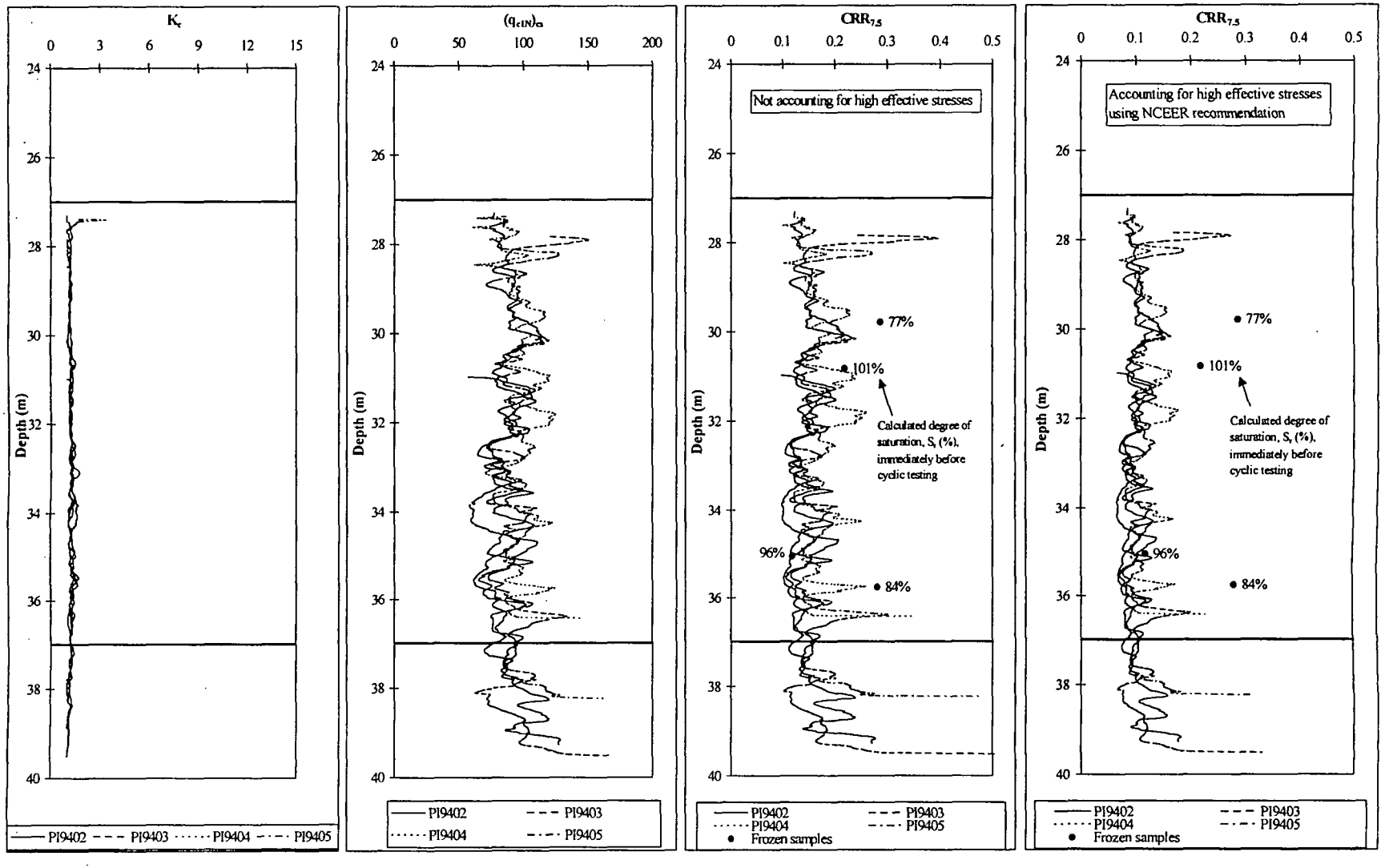

Figure 62. Estimating cyclic softening potential at the Phase I site, Part II: profiles of (a) CPT correction factor for grain characteristics (K_c), (b) $(q_{c1N})_{cs}$, (c) CPT predicted CRR without correction for high overburden stresses, and (d) CPT predicted CRR including correction for high overburden stresses; note that undrained cyclic triaxial test results on frozen samples are shown for comparison.

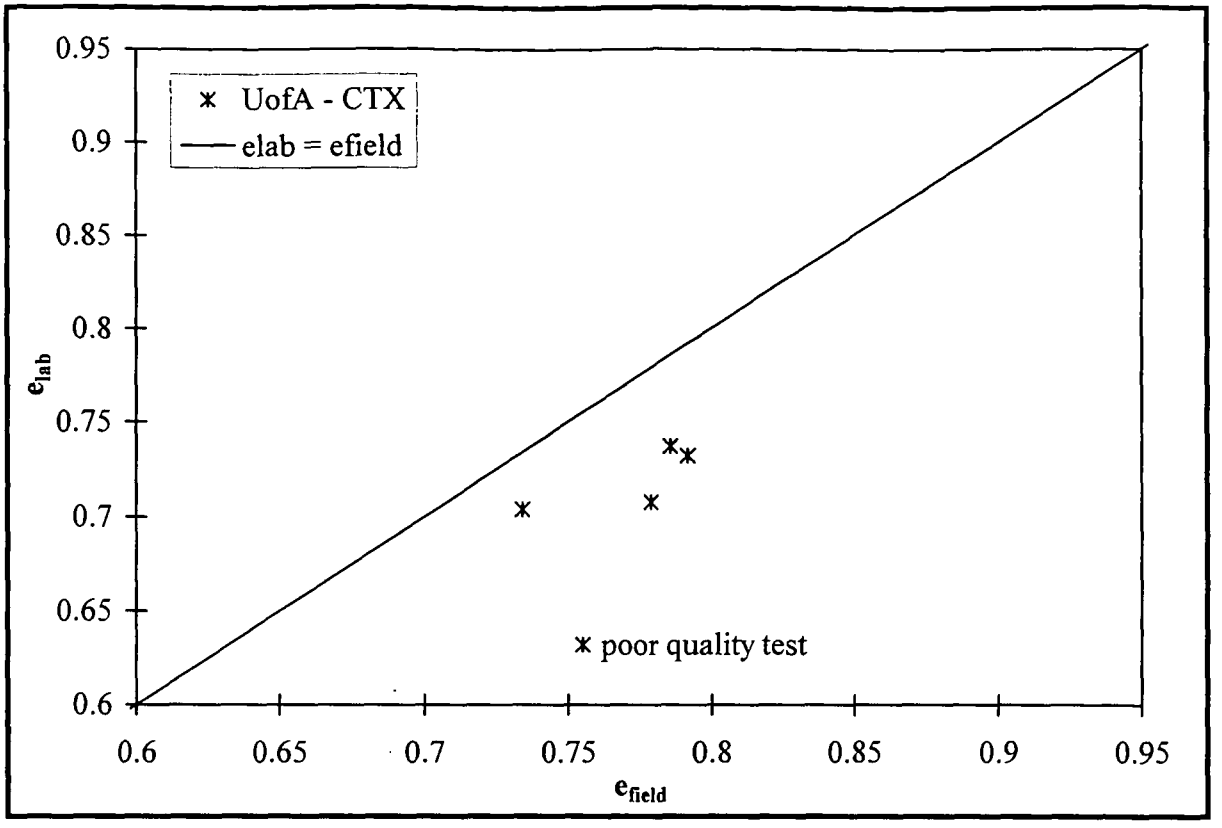

Figure 63. Comparison at the Phase I site of void ratio in the laboratory and in the field for samples tested under cyclic loading.

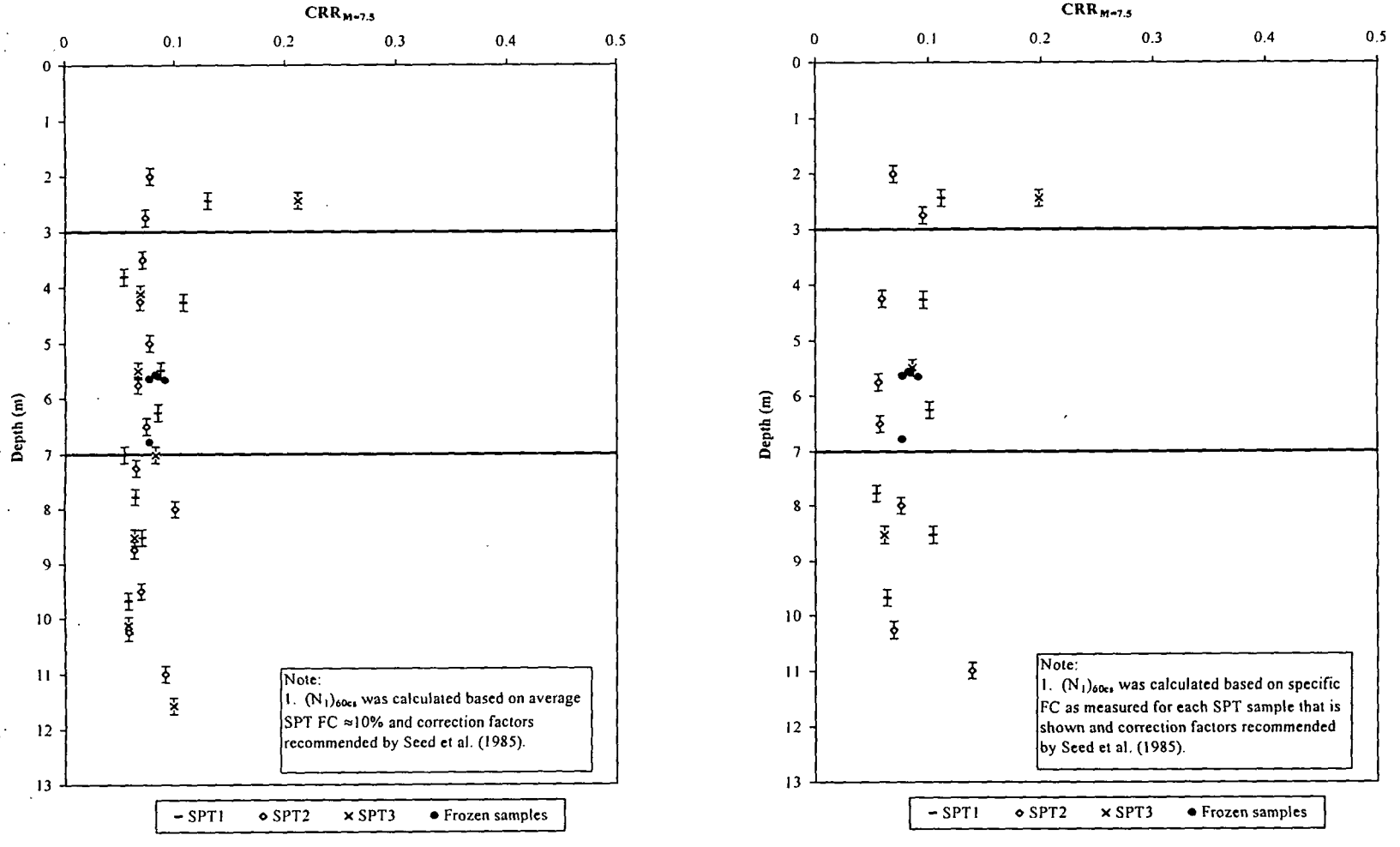

Figure 64. Comparison of CRR predicted by interpreting SPT results at the Phase III site using the method by Seed et al. (1985) and CRR measured in the laboratory from testing undisturbed samples: correction for fines based on (a) average FC of approximately 10% and (b) specific FC as measured for each SPT sample that is shown.

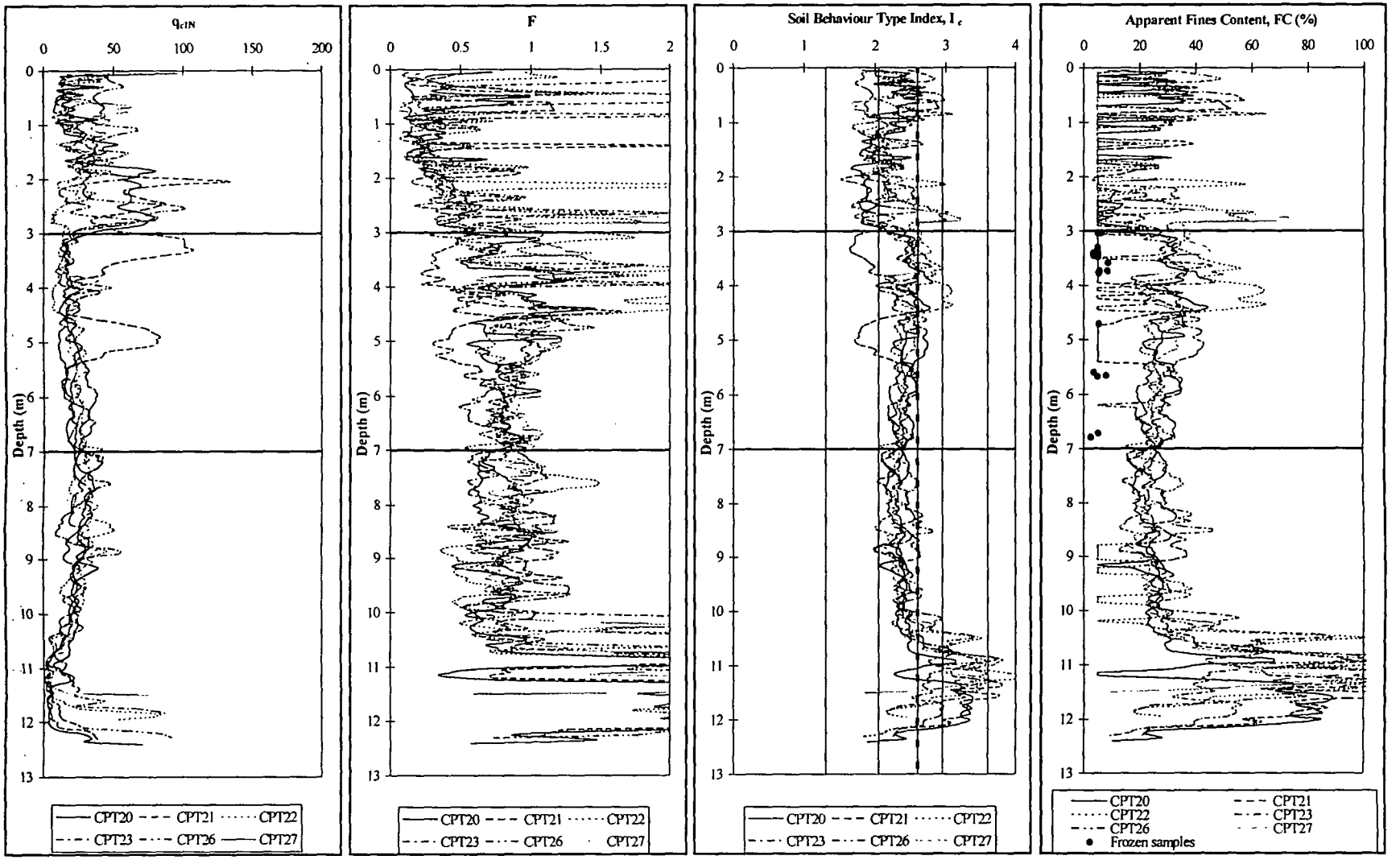

Figure 65. Estimating cyclic softening potential at the Phase III site, Part I: profiles of (a) q_{c1N}, (b) F, (c) soil behaviour index (I_c), and (d) CPT predicted apparent fines content (FC).

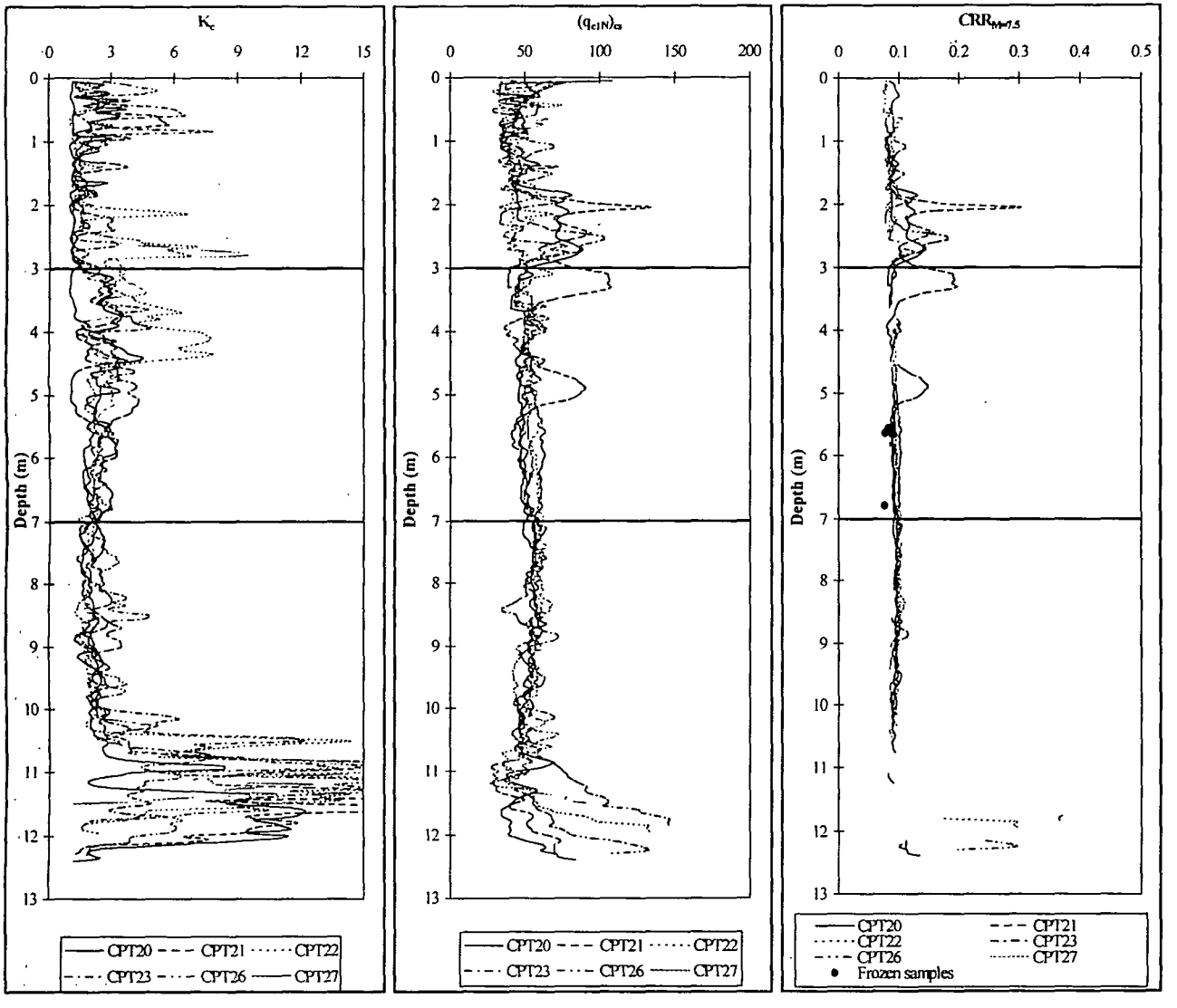

Figure 66. Estimating cyclic softening potential at the Phase III site, Part II: profiles of (a) CPT correction factor for grain characteristics (K_c), (b) $(q_{c1N})_{cs}$, and (c) CPT predicted CRR compared to frozen samples.

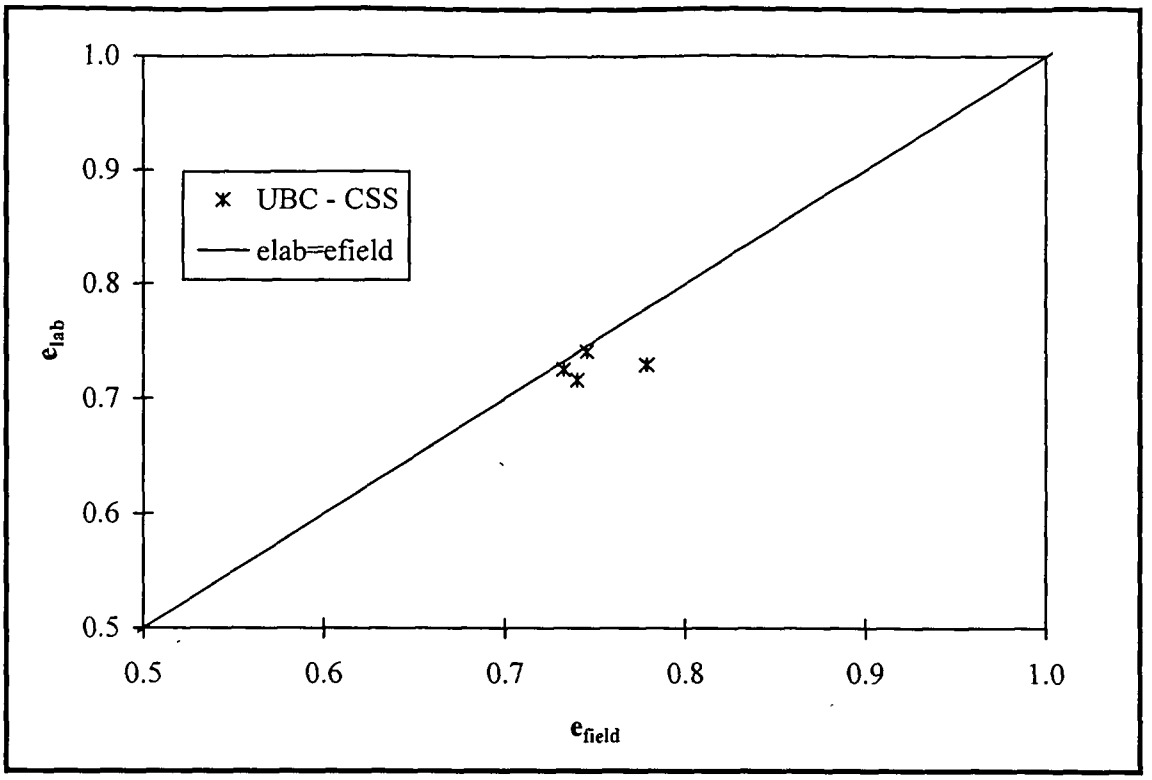

Figure 67. Comparison at the Phase III site of void ratio in the laboratory and in the field for samples tested under cyclic loading.

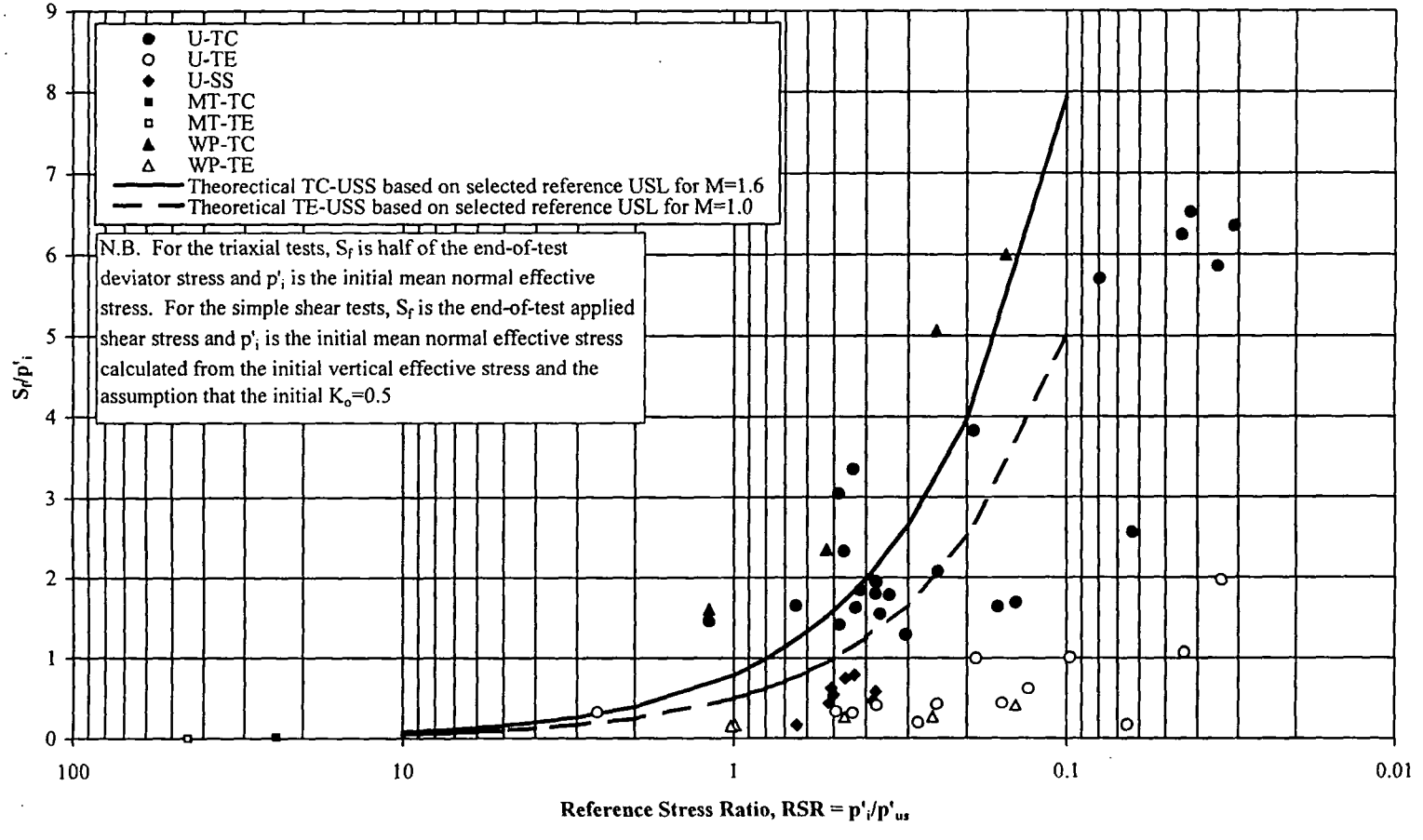

Figure 68. Summary of end-of-test undrained strength results for all Phase I and Phase III undisturbed and reconstituted samples.

REFERENCES

Ayoubian, A. 1996. Triaxial testing on very loose sands for flow liquefaction analyses. M.Sc. Thesis, U. of Alberta, Canada.

Baldi, G. et al. 1986. Interpretation of CPT's and CPTU's. II Part: Drained penetration on sands. Proc. IV Int. Geotech. Seminar on Field Instrumentation and In Situ Measurements, Nanyang Tech. Inst., Singapore.

Been, K., and Jefferies, M.G. 1992. Towards systematic CPT interpretation, Proc. of the Wroth Symposium, 44-55.

Byrne, P.M., Robertson, P.K., List, B.R., and Tan, S. 1994. CANLEX event planning, CANLEX Phase I Activity 6 Technical Report.

Campanella, R.G. 1994. General site characterization – Cell 24 – Mildred Lake Tailings, CANLEX Phase I Activity 3A Report, In-situ Testing Group, U.B.C., Canada.

ConeTec 1995. ConeTec field report prepared for the U. of Alberta, CANLEX In-situ testing program, Syncrude Canada Ltd. (Phase III test site).

Cunning, J.C. 1994. Shear wave velocity measurement of cohesionless soils for evaluation of in-situ state, M.Sc. Thesis, U. of Alberta, Canada.

Fear, C.E., and McRoberts, E.C. 1995. Reconsideration of initiation of liquefaction in sandy soils, Journal of Geotechnical Engineering, ASCE **121**(3): 249-261.

Hofmann, B.A. 1995. Personal communication.

Hofmann, B.A., 1997. In-situ ground freezing to obtain undisturbed samples of loose sand for liquefaction assessment, Ph.D. Thesis, U. of Alberta, Canada.

Hofmann, B.A., and Sego, D.C. 1994. In-situ ground freezing and sampling at the Phase I test site, CANLEX Technical Report, Phase I, Activity 4B, U. of Alberta.

Hofmann, B.A., and Sego, D.C. 1995. In-situ ground freezing and sampling at the Phase III event site, CANLEX Technical Report, Phase III, Activity 4B, U. of Alberta.

Hofmann, B.A., Robertson, P.K., Sego, D.C., Fear, C.E., Lefebvre, M., Natarajan, S., Cyre, G., Woeller, D., Hughes, J. and Gräpel, C.K. 1996a. CANLEX Phase III full scale liquefaction test: site characterization, Proc. of the 49th Can. Geotech. Conf., St. John's, Nfld., **2**, 579-586.

Hofmann, B.A., Robertson, P.K., Gräpel, C.K., Cyre, G., Lefebvre, M. and Natarajan, S. 1996b. CANLEX Phase III full scale liquefaction test: instrumentation and construction, Proc. of the 49th Can. Geotech. Conf., St. John's, Nfld., **2**, 587-595.

Hughes, J. M.O. 1994. Pressuremeter testing at Syncrude for the CANLEX project - data summary and preliminary analysis, CANLEX Technical Report, Phase I, Activity 3A, Hughes In-Situ Engineering Inc.

Hughes, J.M.O. 1996. Pressuremeter investigation - data summary and preliminary interpretation - CANLEX Stage III liquefaction event at Syncrude Canada Ltd., CANLEX Technical Report, Phase III, Hughes In-Situ Engineering Inc.

Hughes, J.M.O. 1997. A simple understanding of the liquefaction potential of sands from self-boring pressuremeter tests, Proc. of the 14th Int. Conf. on Soil Mech. and Found. Eng., Hamburg, Germany, **1**, 515-518.

Iravani, S., Hofmann, B.A., Fear, C., Cyre, G., Lefebvre, M.E., Natarajan, S., Stahl, R.P., and Robertson, P.K. 1995. General site characterization – J-pit site – Syncrude Canada Ltd., CANLEX Technical Report, Phase III, Activity 3A, U. of Alberta.

Ishihara, K. 1993. Liquefaction and flow failure during earthquakes. The 33rd Rankine Lecture, Géotechnique, **43**(3): 351-415.

Jefferies, M.G. and Davies, M.P. 1991. Discussion on soil classification by the cone penetration test. Can. Geotech. J., 28(1): 173-176.

Konrad, J.-M., and Saint-Laurent, S. 1995. Laboratory testing of reconstituted and in-situ frozen specimens – Syncrude tailings sand, CANLEX Technical Report, Phase I, Activity 8C, Université Laval.

Küpper, A. 1994. Geophysical logging of Phase I site, CANLEX Phase I Activity 3B Report, AGRA Earth & Environmental Limited.

NCEER Workshop 1996 (in progress). Proceedings of the 1996 NCEER Workshop on Liquefaction Resistance of Soils, T.L. Youd (Chair).

Olsen R.S. and Koester J.P., 1995. Prediction of Liquefaction Resistance using the CPT. Proc. of the Int. Symposium on Cone Penetration Testing, CPT'95. Linkoping, Sweden, 2: 251-256.

Olsen, R.S., and Malone, P.G. 1988. Soil classification and site characterization using the cone penetrometer test. Penetration Testing 1988, ISOPT-1, *Edited by* De Ruiter, Balkema, Rotterdam, Vol. 2, pp. 887-893.

Plewes, H.D., Davies, M.P, and Jefferies, M.G. 1992. CPT based screening procedure for evaluating liquefaction susceptibility, Proc. of the 45th Can. Geotech. Conf., Toronto, Ont., 4:1-4:9.

Plewes, H.D. 1993. Conventional sampling summary report, CANLEX Technical Report, Phase I, Activity 4A, Klohn-Crippen Consultants, Ltd.

Puebla, H., Byrne, P.M., and Phillips, R. 1996. Analysis of CANLEX liquefaction embankments: prototype and centrifuge models, Proc. of the 49th Can. Geotech. Conf., St. John's, **2**, Nfld., 597-604.

Robertson, P.K. 1990. Soil classification using the CPT, Can. Geotech. J., 27(1):151-158.

Robertson, P.K., and Wride (née Fear), C.E. 1997. Cyclic liquefaction and its evaluation based on SPT and CPT, final contribution to the Proceedings of the 1996 NCEER Workshop on Liquefaction Resistance of Soils, T.L. Youd (Chair).

Robertson, P.K., Fear, C.E., Woeller, D.J., and Weemees, I. 1995. Estimation of sand compressibility from seismic CPT, Proc. of the 48th Can. Geotech. Conf., Vancouver, B.C., 1, 441-448.

Robertson, P.K., List, B., Hofmann, B., and Cone Tec Investigations Ltd., 1993. Site location selection (Phase I), initial CPT screening, CANLEX technical report, Phase I, Activity 2.

Robertson, P.K., Woeller, D.J., and Finn, W.D.L. 1992. Seismic cone penetration test for evaluating liquefaction potential under cyclic loading. Can. Geotech. J., 29: 686-695.

Robertson, P.K., Sego, D.C., Chan, D., Morgenstern, N.R., Fear, C.E., Hofmann, B., Soroush, A., Byrne, P.M., Vaid, Y.P., Plewes, H.D., Cathro, D.C., Gu, W.H., and List, B.R. 1996. CANLEX Phase III full scale flow liquefaction test: planning,

objectives and conclusions, Proc. of the 49th Can. Geotech. Conf., St. John's, Nfld., **2**, 567-578.

Roy, D., Campanella, R.G., Byrne, P.M., and Hughes, J.M.O. 1996. Strain level and uncertainty of liquefaction related index tests, in Uncertainty in the Geologic Environment - from Theory to Practice, Shackleford, C.D., Nelson, P.P., and Roth, M.J.S. (eds.), Geotechnical Special Publication No. 58, ASCE 2: 1149-1162.

Sasitharan, S., Robertson, P.K., Sego, D.C., and Morgenstern, N.R. 1994. State boundary surface for very loose sand and its practical implications. Can. Geotech. J., **31**(3): 321-334.

Seed, H.B. 1979. Soil liquefaction and cyclic mobility evaluation for level ground during earthquakes, J. of the Geotech. Eng. Div., ASCE, 105 (GT2): 201-255.

Seed, H.B., Tokimatsu, K., Harder, L.F., and Chung, R. 1985. Influence of SPT procedures in soil liquefaction resistance evaluations, J. of Geotech. Eng., ASCE 111(12): 1425-1445.

Skempton, A.W. 1986. Standard penetration test procedures and the effects in sands of overburden pressure, relative density, particle size, aging and overconsolidation. Géotechnique, **36**(3): 425-447.

Skirrow, R.K. 1995. Site characterization of Phase III site - geophysical logging, Report submitted to the U. of Alberta, Phase III, Activity 3, AGRA Earth & Environmental Limited.

Sladen, J.A., D'Hollander, R.D., and Krahn, J. 1985. The liquefaction of sands, a collapse surface approach. Can. Geotech. J., **22**: 564-578.

Sladen, J.A., and Hewitt, K.J. 1989. Influence of placement method on the in situ density of hydraulic sand fills, Can. Geotech. J., 26: 453-466.

Soroush, A., Chan, D. and Morgenstern, N.R. 1996. Numerical analysis of the CANLEX Phase III field event, Proc. of 49th Can. Geotech. Conf., St. John's, Nfld, **2**, 605-614.

Suzuki, Y., Tokimatsu, K., Koyamada, K., Taya, Y., and Kubota, Y. 1995b. Field correlation of soil liquefaction based on CPT data. *Proc. of the Int. Symposium on Cone Penetration Testing*, CPT'95. Linkoping, Sweden, 2: 583-588.

Tokimatsu, K. and Seed, H.B. 1987. Evaluation of settlements in sands due to earthquake shaking, J. of Geotech. Eng., ASCE 113(GT8): 861-878.

Tokimatsu, K., and Yoshimi, Y. 1983. Empirical correlation of soil liquefaction based on SPT N-value and fines content, Soil and Foundations, 23(4): 56-74.

Vaid, Y.P., Sivathayalan, S., Eliadorani, A., and Uthayakumar, M. 1996. Laboratory testing at U.B.C., CANLEX technical report (N.B. consists of a main report, plus a separate addendum).

Wride (née Fear) C.E., and Robertson, P.K. 1997. CANLEX introductory data review report. CANLEX technical report.

Youd, T.L. 1997. Personal communication.

Yu., H.S. 1994. State parameter from self-boring pressuremeter tests in sand. J. of Geotech. Eng., ASCE 120(12): 2118-2135.

Yu, H. S. 1996. Interpretation of pressuremeter unloading tests in sands. Géotechnique 46(1): 17-31.

Yu, H.S., Schnaid, F., and Collins, I.F. 1996. Analysis of cone pressuremeter tests in sands. J. of Geotech. Eng., ASCE 122(8): 623-632.